5-2018

Measuring and Predicting Hydroxyl Radical Generation From Irradiated TiO2 Nanoparticles Under Simulated Environmental Conditions and Correlations to *Daphnia magna* Toxicity

Jason Alan Coral
Clemson University, jcoral629@gmail.com

MEASURING AND PREDICTING HYDROXYL RADICAL GENERATION FROM IRRADIATED TiO_2 NANOPARTICLES UNDER SIMULATED ENVIRONMENTAL CONDITIONS AND CORRELATIONS TO *Daphnia magna* TOXICITY

A Dissertation
Presented to
the Graduate School of
Clemson University

In Partial Fulfillment
of the Requirements for the Degree
Doctor of Philosophy
Environmental Toxicology

---

by
Jason Alan Coral
May 2018

Accepted by:
Dr. Christopher L. Kitchens, Committee Chair
Dr. Stephen J. Klaine
Dr. Julia Brumaghim
Dr. Elizabeth Carraway
Dr. Aaron Roberts

ABSTRACT

Interest in inclusion of titanium dioxide nanoparticles in a multitude of industrial and personal products has driven production over the past two decades. Concurrent with increases in nanoparticle production, an increase in nanoparticle movement from use to environment can be expected. Particular concern is focused on TiO_2 nanoparticles moving to freshwater compartments. Inherent photocatalytic nanoparticle properties generate reactive oxygen species upon exposure to water, oxygen, and ultraviolet light. While this particular feature is utilized for surface-cleaning and pollution mitigating applications, it poses a significant risk to organisms exposed to these nanoparticles. This risk can be difficult to quantify, exhibited by the variation in toxicity reports from various labs. These variations are a result of differing conditions. Environmental factors such as presence of natural organic matter (NOM), intensity of ultraviolet (UV) light, and the wavelengths of UV light exposure will affect toxicity as well as physical characteristics of the nanoparticle, including size and crystallinity. These variations impart uncertainty to toxicity measurements creating a knowledge gap regarding conditional effects acting on TiO_2 to modulate toxicity.

The goal of the present research was to develop a comprehensive understanding of the effects that environmentally relevant conditions have on TiO_2 radical generation and correlate these conditionally affected rate changes to toxicity measurements. To accomplish these goals, a systematic approach of a full factorial exposure design to quantify the interacting effects of simulated environmental conditions on irradiated TiO_2 nanoparticles at eight TiO_2 concentrations, five NOM concentrations (measured as

dissolved organic carbon), and four UV-A intensities was utilized. Radicals generated by irradiated TiO_2 were characterized as hydroxyl radicals using Electron Paramagnetic Resonance spectroscopy. The exposure conditions were characterized and compared to existing literature and natural conditions. The changes in hydroxyl radical generation rates were monitored using fluorescence spectroscopy. Linear regression techniques were used to determine how the conditional effects regulated hydroxyl generation rate.

A number of trends were well correlated with conditions. Rate of hydroxyl generation was positively correlated with concentration of TiO_2 nanoparticles as a result of increased total available surfaces for photon impingement. Increases in light intensity were likewise positively correlated to increases in hydroxyl generation rate, a result of a greater number of photons interacting with the nanoparticle surface. The reciprocal interaction of these conditions demonstrates classic phototoxic behavior wherein a low concentration of TiO_2 and a high intensity of UV-A generates an equivalent response compared to high concentrations of TiO_2 and low intensities of UV-A. This reciprocal effect is complicated by the addition of NOM. Increasing total amounts of NOM to suspensions results in decreased hydroxyl generation rate. Decreased generation rates are related to the large number of oxidizable functionalities that exist within the NOM conglomeration of molecules. Readily available functionalities can competitively quench radicals, resulting in the attenuated hydroxyl generation rate measurements. Additional rate reduction as a result of coating effects and aggregation/agglomeration to reduce available surface area may also occur.

These rates were compiled and AICc linear regression techniques were used to model the relationship between TiO_2 nanoparticle concentration, NOM concentration, UV-A intensity, and their effect on hydroxyl generation rate. Two models were generated, one from only TiO_2 and UV_i data, and one from TiO_2, DOC and UV_i. The predictions produced by the models describe the effects from the data well (R^2 = 0.970, 0.948 respectively). The models were validated by comparing predicted hydroxyl radical concentration to literature measured hydroxyl radicals. Comparison of residuals and literature measured hydroxyl radical concentrations show that the models perform well in conditions that are under and close to experimental bounds but becomes less reliable as model bounds are exceeded.

Correlations of changes in conditions to the changes in toxicity of TiO_2 to *D. magna* were assessed using standard 48-hour acute bioassays. The trends associated with hydroxyl generation rates were well conserved in the bioassays. Compared to conditions with no UV light, toxicity increased multiple orders of magnitude when *D. magna* were co-exposed to TiO_2 and UV-A radiation. Addition of NOM to exposures at the same TiO_2 concentration and UV-A intensity resulted in significant toxicity attenuation. Properties of reciprocity were also demonstrated within the bioassays. Using fluorescence spectroscopy, radical generation was directly correlated to toxicity. Considering that TiO_2 is the vector that generates the toxicant hydroxyl radical under particular conditions, drawing a link between changes in exposure condition to radical generation will help to more accurately describe organism toxicity from irradiated TiO_2. By correlating TiO_2 toxicity to hydroxyl radical concentration, biological examination directly linking the rate

of hydroxyl generation to organism response, via both morphological examination and identifying changes in oxidative stress markers can be completed.

Relative to each bioassay, it was found that higher concentrations of hydroxyl radicals result in higher percent mortalities. These lethal concentrations of radicals were dependent on the conditions through which they were produced. Conditions with no DOC resulted in equivalent lethal concentrations of hydroxyl radicals, regardless of light intensity. However, as NOM concentration increased, tolerance for increases in hydroxyl radicals occurred. This tolerance could be a result of a number of mechanisms, including competitive quenching from oxidative functionalities, or coating of nanoparticles resulting in overall decreased production. Likely, it is a combination of both, resulting in the increased ability of the organism to repair of oxidative damage over time, as a result of slower radical generation. Energy resource allocation to anti-oxidative functions and damage repair could decrease overall fitness and reproductive ability under long-term exposure conditions.

Overall, the results of this work indicate there is a significant correlation between exposure conditions, such as intensity of UV-A light, presence of NOM, and concentration of nanoparticles, and hydroxyl generation rate. The models estimate hydroxyl generation rates as a result of these interactions, and provides a viable tool for TiO_2 risk assessment, and can be used to better focus TiO_2 nanoparticle disposal regulations. This stochastic model represents an upper-bound estimate of hydroxyl radical generation by describing all TiO_2 nanoparticles as anatase crystallinity under low UV-A light in Suwanee River water natural organic matter. The correlations between

toxicity and rate of hydroxyl generation provide a means to explain the protective effect of natural organic matter through competitive radical quenching by oxidizable functionalities.

The model does not account for specific wavelengths within the UV-A spectra, variation of nanoparticle size or crystallinity, or the mechanistic interactions between NOM and the nanoparticle surface. Additional insight on the effect these components have on rate generation and toxicity should improve the overall function of the model. Future focus on model improvement by including mechanistic interactions between nanoparticles and the environment, and investigations into the biological effects of short-term and long-term exposure to TiO_2 in terms of energy allocation, fitness, and morphological impact of hydroxyl radical damage to organisms is suggested.

DEDICATION

This dissertation is dedicated to the ever-present love, support and attention from my family. I would not be here without Amy, Glen, Jon, and Stacey Coral. To my grandparents, Lloyd and Betsy Yoder, the investment you made in me all those years ago got me through college and almost the entirety of Graduate School, and I am forever grateful for that. Barbara "Old Spice", thank you for the engaging and delightful conversations we've had over breaks and vacations that pushed me forward. Art and Marilynn, thank you as well. To Gina Depper, your love and support through the 4 years I've known you here has been second to none. I can say, completely and with utmost gravity that this dissertation would not be possible without you. To my dog, Bloo, I know you can't read, but coming home every day to your excitement and enthusiasm always made me forget about any struggle I was having, if only for a minute. Thank you for reminding me to always stop and smell the roses along the way, and then roll in them.

I also dedicate this dissertation to any young and vibrant student interested in research. I wish you more success than I have had, and pledge to support you in any way I possibly can. Just as this work would not be possible without those that mentored me, I only hope that I can fulfill a similar role for you.

Finally, this work is dedicated to the everlasting memory of Dr. Stephen J. Klaine. You've shaped me as a researcher, a person, and taught me things I'd never thought I'd learn. Thank you for all you've done for me.

ACKNOWLEDGMENTS

This dissertation would not be possible without the consistent support, insight, and constructive criticism of my Committee Members: Dr. Chris Kitchens, Dr. Julia Brumaghim, Dr. Elizabeth Carraway, and Dr. Aaron Roberts. Thank you all for the time you've dedicated to me during my journey. A special thank you specifically to Chris, for taking me on as a graduate student upon Steve's passing. The journey to this point has been a long and strange trip and would not have been possible without you. Thank you.

I have been very lucky to have an incredible group of lab mates and cohorts spanning across multiple labs. In the Klaine Lab, many thanks are due, to all of my lab mates, who all had a hand in helping me grow as a researcher and been some of my closest cohorts and friends. In the Kitchens Lab, thank you guys, for treating me as brother. To the Brumaghim Lab, thank you for helping me get my project off the ground.

To Benardo Dargan, your insight and expertise during my time as a Graduate Student leader has meant the world to me. Thank you for all you've done. To my roommates, Eric Riddell and Evan Apanovitch, thank you for being sounding boards for ideas, keeping me grounded, and sources of inspiration and good times. And to all my friends I've met here at Clemson, you have all helped to shape an incredible five years of my life. Thank you all for being a part of this.

TABLE OF CONTENTS

Page

Table of Contents (Continued)

Page

Table of Contents (Continued)

Page

Table of Contents (Continued)

Page

Table of Contents (Continued)

LIST OF TABLES

List of Tables (Continued)

Table Page

LIST OF FIGURES

LIST OF FIGURES (Continued)

Figure Page

CHAPTER 1

BACKGROUND AND INTRODUCTION

According to the American Society for Testing Materials, and the British Standards Institution, and the Science Committee on Emerging and Newly-Identified Health Risks, nanoparticles are defined as materials of roughly spherical shape with at least two dimensions between 1 and 100 nm[1]. Materials at the nanoscale commonly exhibit behaviors and properties (such as changes in conductivity, optical properties or surface reactivity), that are different from their bulk (micro- and macro-scale) counterparts; these property changes are often quite advantageous from a usage prospective. Within the past few decades, the advent of more sensitive analytical techniques has identified many of these of property changes. The result is inclusion into materials based on nanoparticle properties[1].

Titanium dioxide (TiO_2) is a well-known, much used photocatalyst. Within the past 50 years (since about 1972), a significant amount of research has been dedicated specifically to the uses of TiO_2 nanomaterials[2]. Applications of titanium dioxide nanoparticles (TiO_2 NPs) span across multiple fields, into many products, both common-use and industrial. TiO_2 NPs are most commonly found in paints[3], cosmetics[4], solar cells[2], and surfacing materials including ceramic tiles and concretes[2,5,6]. The photocatalytic properties of TiO_2 NPs generate reactive oxygen species (ROS) in the presence of ultraviolet light, making the use TiO_2 materials attractive for anti-microbial and anti-biofouling[7] uses, water pollution remediation[8] and air pollution control[9,10].

There are a number of methods to produce these nanomaterials in large amounts, such as sol-gel, sol, physical/chemical vapor deposition, electrodeposition, and hydro/solvo-thermal methods, to name a few[11]. Differing methods will produce different shapes of particles, sizes, and crystallinities, allowing for materials to be relatively finely tuned to usage.

Titanium Dioxide (TiO_2) Production Methods

Sol-gel methods generally refer to polymerization/hydrolysis reactions that form colloids from inorganic metals salts or metal alkoxides. These reactions are adept at producing a variety of structures, dependent on reaction parameters. Amines are used as shape controllers, generating particles with shapes ranging from cuboidal to ellipsoidal, driven by amine identity and pH. Size of NPs range from 7 nm-50 nm. Nanorods, nanotubes, and nanowires can be produced via reactions with sol-gel methodology and anodic alumina membrane templates[2].

Sol methods are similar to sol-gel methods, although generally sol methodology forgoes hydrolysis. Sol methods can produce NPs in the 10 nm and below range, depending on the nucleophilicity of the halide associated with the Ti precursor used during the initial reaction (TiF_4 generating 9.2 nm anatase crystals, TiI_4 generating 3.8 nm anatase crystals) [11]. As with sol-gel methods, surfactants can aid the shaping and size of the particles [2].

The hydrothermal method produces nanoparticles by precisely controlling temperature and pressure within autoclaves. By elevating the temperature above the boiling point of water, pressure can be adjusted to reach vapor saturation points. Depending on the co-solvents and concentration of Ti precursor, nanoparticles ranging in size from 7-25nm can be produced. [2]. Nanorods, nanotubes, and nanowires can also be produced, depending on the conditions, and whether the reaction is stirred[2]. Solvothermal methodology closely compares to hydrothermal methodology, with the exception that all solvents are non-aqueous. In this way, temperatures can

reach much higher levels without a high amount of pressure, resulting in superior control of shape and size distribution of the nanoparticles[2].

Titanium dioxide nanomaterials can also be produced by the direct oxidation of titanium metals. Specifically, nanorods and nanotubes are generated with a high degree of crystallinity. Inorganic salts of sodium, NaX (X= F^-, SO_4^{2-}, Cl^-) are used to drive the formation of crystals: F^- and SO_4^{2-}using results in the precipitation of pure anatase nanorod crystals, while addition of Cl^- will form rutile nanorods. Length of tubes and rods can be controlled by application of electric potential[2].

Vapor deposition describes a coating technique in which Ti materials in a vapor state condense to form a solid-phase material. Reactions occur within a vacuum chamber, and will generally occur in one of two different processes, chemical or physical. Chemical vapor deposition (CVD) occurs as thermal energy heats gases and drives deposition reactions, allowing both phase and morphology to be tuned to the process. CVD processes include but are not limited to electrostatic spray hydrolysis, diffusion flame hydrolysis, thermal plasma hydrolysis, and laser-induced pyrolysis[2].

Physical vapor deposition (PVD) occurs simply by evaporating pure titanium metal and then condensing it to form solid materials. Nanowires can be constructed in this fashion. Intense heat is required to evaporate titanium metal; methods using PVD include sputtering, thermal deposition, ion plating (and implantation), laser vaporization, and laser alloying[2].

Physical Properties of TiO_2

There are three major crystalline structures of TiO_2 NPs, anatase, rutile, and brookite, each slightly different in atomic configuration. Each particular configuration has slight physical differences, resulting in different inherent behaviors at the nano-scale[1]. Crystallinity is

generally controlled by the temperature and methodology at which these particles are annealed[2]. Due to the general obscurity of brookite in industrial process, and its lack of bearing on this dissertation, it will not be discussed.

Rutile's lattice structure consists of a Ti^{4+} surrounded by six O^{2-} ions, arranged in a slightly distorted orthorhombic fashion, with positive uniaxicality. This configuration allows each octahedron to be in contact with 10 neighbor octahedrons, two sharing oxygen pairs on the edge, and eight sharing corner oxygen atoms. The Ti-Ti atomic distances in rutile are 3.57 and 2.96 Å, with Ti-O distances measuring 1.949 and 1.980 Å[12].

Anatase is also an octahedron lattice, although significantly more distorted, and less symmetrical than its rutile counterpart. The anatase octahedron shares four edges and four corners, for a total of eight neighbors. Ti-Ti distances are 3.79 and 3.04 Å and Ti-O distances are 1.934 and 1.980 Å. These lattice structure differences result in physical differences, such as anatase having lower specific gravity compared to rutile (3.9 vs 4.2), and being less hard compared to rutile (5.5-6.0 Mohs vs 6.0-6.5 Mohs). More importantly, in terms of photoactivity, the electronic band gaps differ, 3.28 eV for anatase, and 3.00 eV for rutile[12].

Photocatalysis and Radical Generation from Irradiated TiO2

Photocatalysis describes the catalysis of a photochemical reaction at the surface of a semiconductor, involving 2 simultaneous reactions: a reduction reaction initiated by photogenerated electrons in the conductance band, and an oxidation reaction from photogenerated holes in the valance band. [13]. Titanium dioxide is a well-known photocatalyst.. Both major crystalline configurations respond electrochemically to irradiant wavelengths in the UV range; anatase to UV-A and below, and rutile to UVB and below[14,15] The photocatalytic

activity of brookite is relatively unknown, due to the difficulty of obtaining the crystals in pure-phase[16].

The TiO_2 process of electron excitement and transfer is detailed in Figure 1.1. High intensity light irradiation (3.28 eV for anatase, 3.00 eV for rutile) excites electrons from the lower energy valance band to the high energy conductance band [13,17,18]. The promotion results in a positively charged area referred to as a 'hole' (h_{vb}); some of these holes will become trapped within the lattice surface (h_{tr}) [19]. Trapped holes can be shallow, with similar reactivity and mobility to free (surface) holes, while deeper trapped holes are rather unreactive, and will only react slowly with mobile physisorbed substances, as these substances move across the lattice[13].

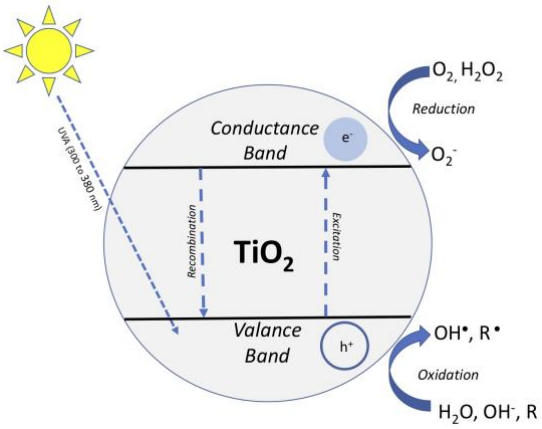

Figure 1.1 Photocatalytic generation of ROS by Ultraviolet-A (UV-A) Irradiation TiO_2 Nanoparticles. UV-A irradiation of TiO_2 nanoparticles results in photocatalytic excitation of electrons, generating free electrons and 'holes'. This results in the generation of various radical species.

While electron/hole recombination can occur, electrons are scavenged from a surrounding molecule of water, generating multiple radical species: hydroxyl radicals ($OH^{\bullet}$)[13,19-21], superoxide ($O_2^{\bullet-}$)[13,19,22], singlet oxygen ($^1O_2$) [13,22,23]. The high-energy

promoted electron will most commonly transfer to an oxygen atom, generating superoxide anions[13,19]. The promotion process occurs within a time scale of picoseconds, while electron transfer occurs within nanoseconds[18]. These superoxide radicals can react with other species, or undergo disproportionation reactions and generate hydrogen peroxide[13].

$TiO_2 + h\nu \rightarrow e_{cb}^- + h_{vb}^+$ (1)

$h_{vb}^+ \rightarrow h_{tr}^+$ (2)

$O_2 + e^- \rightarrow O_2^{\bullet -}$ (3)

$O_2^{\bullet -} + O_2^{\bullet -} + 2H^+ \rightarrow H_2O_2 + O_2$ (4)

$O_2 + 2e^- + 2H^+ \rightarrow H_2O_2$ (5)

Hydroxyl radicals can be generated through a number of mechanisms. Oxidation of water or hydroxide ions by valance band holes(h_{vb}^+) will result in hydroxyl radical generation. Additionally, there are several reactions that will reduce, or split hydrogen peroxide to hydroxyl radicals[13,19].

$h_{vb}^+ + H_2O \rightarrow OH^{\bullet}$ (6)

$OH^- + h_{vb}^+ \rightarrow OH^{\bullet}$ (7)

$H_2O_2 + e_{cb}^- \rightarrow OH^{\bullet} + OH^-$ (8)

$H_2O_2 + O_2^{\bullet -} \rightarrow OH^{\bullet} + OH^- + O_2$ (9)

$H_2O_2 + h\nu \rightarrow OH^{\bullet} + OH^{\bullet}$ (10)

Holes and electrons, radicals, and radicals and trapped holes (h_{tr}^+) can also react together through recombination, effectively neutralizing the threat of oxidation. Products from the neutralization reactions can then be oxidized or reduced by holes or electrons respectively, as shown above, creating a radical cycling chain[19].

$O_2^{\bullet -} + h_{tr}^+ \rightarrow O_2$ (11)

$OH^{\bullet} + OH^{\bullet} \rightarrow H_2O_2$ (12)

$h^{+}_{vb} + e^{-} \rightarrow$ Recombination (13)

The recombination of these electron/hole pairs drives the limitations of photocatalyst, resulting in the release of heat energy. Non-radiative recombination can be measured using time-resolved photoacoustic spectroscopy (TRPAS). Leytnar and Hupp (2000) measured the amount of heat generated from the recombination of these electron/hole pairs and the time it took for recombination. The results of the analysis indicated conduction band trapping, trapped electron-hole recombination, as well as a slower recombination step. Approximately 60% of trapped electrons recombined on a timescale of close to 25ns [24]. The recombination rate implies that electron transfer to generate radicals must happen within this timescale; further, reactant molecules must be in extraordinarily close proximity, within nanometers[20].

Radiative recombination will occur, measurable as visible light in the photoluminescence (PL) band[18,25]. Knorr et al. (2008), ascertain exactly this by observing the PL emissions of anatase nanoparticles under multiple solvent conditions. They observed both the recombination of trapped electrons with mobile holes, and the recombination of mobile holes with the valance band with trapped electrons[25].

Characterizing and Quantifying Radical Generation from Irradiated TiO_2

As the radicals produced by TiO_2 ultraviolet irradiation are extraordinarily short lived, with half-lives on the scale of nanoseconds[13], identification and measurement of these radicals can be difficult. Characterization and short-term measurement can be accomplished using electron paramagnetic resonance techniques, while longer term quantitation (and some identification) often requires fluorescence spectroscopy[26]. Both of these techniques utilize

specialized probe molecules called spin traps to bind radical species, extending half-lives to allow for qualitative and quantitative measurements.

Electron Paramagnetic Resonance (EPR) utilizes magnetic fields and microwave power to elevate electrons to higher energy levels. EPR spectroscopy utilizes the electron magnetic moment to orient electron spins parallel or antiparallel to a magnetic field. This forced alignment (called field-for-resonance) creates two distinct energy levels of electrons. Electrons with spins aligned parallel to the field are at a lower energy, whilst antiparallel electrons exist at higher energies [27]. Microwaves are passed across the field-for-resonance to excite electrons to the upper energy level. Microwave sources that produce variable frequencies having sufficient amplitude and frequency stability are incredibly difficult to create. Therefore, the microwave frequency is held constant, and the magnetic field (corresponding to the energy field) is increased[28]. When the strength of separation of the field-for-energy matches the microwave frequency, electrons aligning parallel to the magnetic field are forced anti-parallel, "jumping" to the higher energy level. The movement of the electrons to the upper energy level results in a distinct spectrum[27,28].

Due to the short lifetime of radicals, a separate molecule known as a 'spin trap' often must be used to detect them. This spin trap reacts with the radical of interest, forming a more stable radical adduct. The spectrum obtained by use of a spin trap in EPR spectroscopy, therefore, is not from the radical itself, but rather the radical-adduct[29]. Spin traps can be organized into two different categories, nitroso or nitrone compounds. Nitroso-containing spin traps are excellent for biological studies, due to the extreme reactivity of the C-nitroso group; they will not be discussed here. Nitrone-containing spin traps, however, are very common in studies of TiO_2.

Spin traps can be very specific for the radicals they detect. For example, 2,2,6,6-tetramethyl-4-piperdone (TEMP) and 4-oxo-2,2,6,6-tetramethyl-2-piperdone (4-oxo-TEMP) detect singlet oxygen[29]. Common spin traps to identify radicals produced in a TiO_2 system include 5,5-dimethyl-1-pyrroline (DMPO)[29-32], α-phenyl-*N*-tert-butylnitrone (PBN)[29] and α-(4-pyridyl-1-oxide)-*N*-tert-butylnitrone (POBN) [29,30]. 4-Carboxy-2,2,6,6-tetramethyl-2-piperdone (TEMPOL), 3-carboxy-2,2,5,5-tetramethyl-1-pyrrolidine-1-oxyl (CTPO)[21,31], and 3-carboxy-2,2,5,5-tetramethylpiperdine-1-oxyl (CTMPO) are also utilized[21,30]. These spin traps are used to detect hydroxyl and superoxide radicals, and have varying trapping efficiencies. Trapping efficiency is an important factor when determining short-term radical generation. Some of these spin traps will react with and detect multiple radical species, or even photogenerated holes[30,32] (such as DMPO), although addition of specific radical scavengers (such as for superoxide dismutase or mannitol) allow measurements of singular radical species, even in the presence of multiple radical types[29,32].

Although these spin traps extend the half-lives of radical species, they still have relatively short lifetimes, and EPR spectroscopy will only allow for 'snapshots' of radicals generated at a single point in time; this is a static measurement system. The process for tuning the EPR cavity to prepare for measurements is also time consuming, so for longer-term and more extensive measurements, fluorescence spectroscopy is utilized.

According to fluorescence theory, molecules exist at ground level energy, the lowest vibrational level of ground electronic state, also known as highest occupied molecular orbital (HOMO). As these molecules absorb high energy photons, they are elevated to higher singlet S_1 states (paired electrons with opposite spin), in the lowest unoccupied molecular orbital (LUMO).

For absorption bands in the visible region, this energy gap is about 40 to 80 kcal/mol[33]. Further excitation with photons will elevate the molecules to higher S_n states.

Molecules will rid themselves of this excess energy through number of different pathways. Energy can be released through non-radiative means, such as internal conversion or intersystem crossing. Internal conversion occurs between two states of the same multiplicity (singlet-singlet or triplet-triplet), whereas intersystem crossing is movement from one state of multiplicity to another (singlet to triplet)[33,34]. This process is depicted in a classic Jablonski diagram in Figure 1.2.

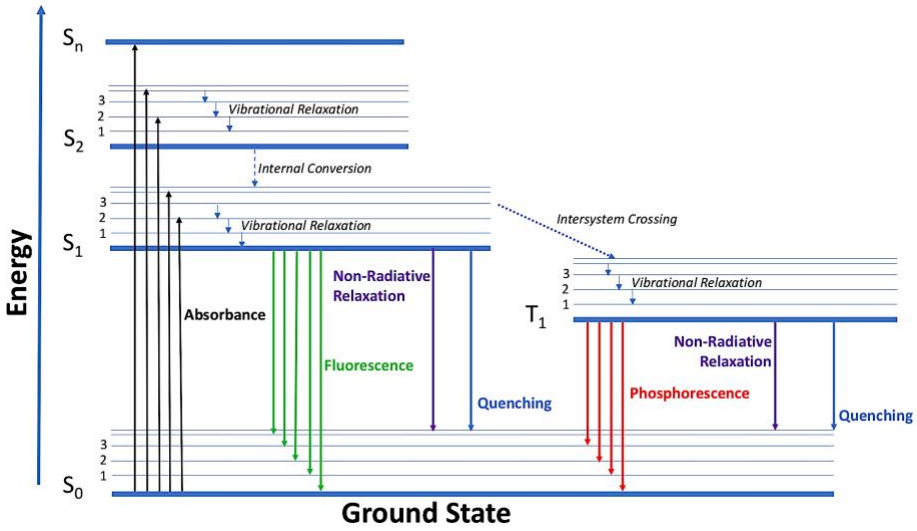

Figure 1.2. Standard Jablonski Diagram. A Jablonski diagram detailing the energetic promotion, and subsequent relaxation of molecules, releasing energy via either light or heat.

Radiative emission of energy includes vibrational relaxation, fluorescence, and phosphorescence. Vibrational relaxation describes the collisions of excited molecules. Upon collision, molecules release energy in the form of heat. Vibrational relaxation occurs at incredibly rapid pace, on the scale of 10^{-12} seconds[34]. Fluorescence and phosphorescence are the release of radiative energy by means of light. Phosphorescence occurs by energy transfer to

the ground state from molecules in excited triplet states, whereas fluorescence occurs by energy transfer from molecules in excited singlet states to the ground state[33,34].

Emission of energy includes vibrational relaxation, fluorescence, and phosphorescence. Vibrational relaxation describes the release of energy in the form of heat. Vibrational relaxation occurs at incredibly rapid pace, on the scale of 10^{-12} seconds[34]. Fluorescence and phosphorescence are the release of electromagnetic light energy. Phosphorescence occurs from the deactivation of excited triplet state molecules, while fluorescence occurs from the deactivation of singlet state molecules[33,34].

Quantum efficiency is defined as the ratio of molecules that luminesce compared to the total number of excited molecules. Molecules that are highly fluorescent have quantum efficiencies approaching 1, while non-fluorescent molecules have quantum efficiencies of 0. This can be extrapolated to mean that a higher quantum efficiency results in a higher degree of fluorescent intensity given excitation by the same amount of light[34]. Quantum efficiency is structure-specific, so changes in molecular structure affect fluorescence intensity.

There are a number of fluorescent molecules that interact with radicals, particularly hydroxyl radicals. Hydroxyl radicals are known to hydroxylate aromatic rings; hydroxylation can either reduce, or increase the intensity of fluorescence, as shown by the interaction of hydroxyl radicals and fluorescein in Figure 1.3. Intensity increase or decrease depends on the identity of the substrate interacting with the radical. Hydroxyl radical oxidation of benzene results in quenching of florescence, whereas benzoate, coumarin or phenoxazainone substrates will result in a highly fluorescent derivative[20]. Fluorescein, and derivatives 3'[p-aminophenyl] fluorescein (APF) and 2'7'-dichlorodihydrofluorescein diacetate are common indicators (the latter two being more specified for hydroxyl radical)[35], as well as amplex ultrared and

dichorofluorescein[36]. Other probes to measure hydroxyl radical include terephthalic acid[37,38], and dipyridamole and 2-(2-Pyridil)-benzothiazoline, which can be used to also measure superoxide[38]. Singlet oxygen can be measured using 9,10-dimethylanthracene (DMA), 9-[2-(3-carboxy-9,10-diphenyl)anthryl]-6-hydroxy-3H-xanthen-3-ones (DPAXs) and 9-[2-(3-carboxy-9,10-dimethyl)anthryl]-6-hydroxy-3H-xanthen-3-one[38]. Using these probes, it is possible to measure the generation of ROS from TiO_2 NPs.

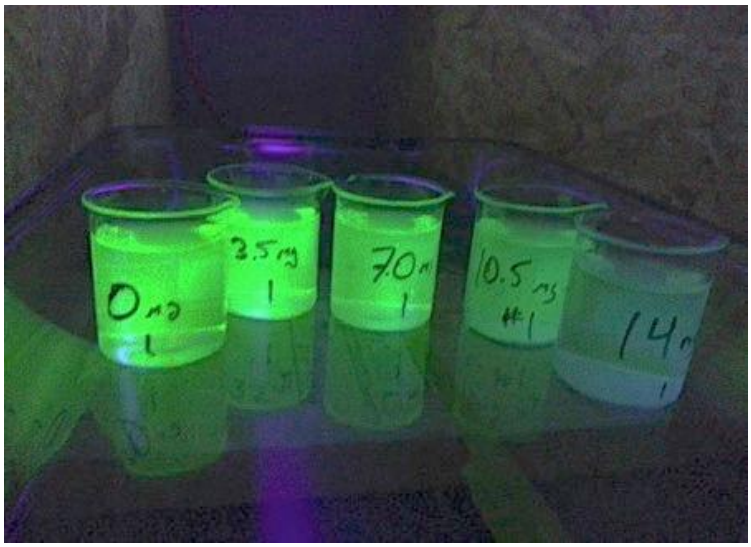

Figure 1.3: Fluorescein Dyed TiO_2 Suspensions under UV-A Blacklight. TiO_2 and fluorescein under UV-A irradiation generated by CLX Blacklight Blue fluorescent bulbs. Radical generation from TiO_2 NPs produce radicals, which will reduce the intensity of fluorescein via an oxidative reaction.

Uses of TiO_2 Nanoparticles

Radical generation from the irradiation of TiO_2 NMs has prompted industrial use in a plethora of applications. Surface coating applications is becoming increasingly prevalent as a means to control various fouling types. The photocatalytic properties allow for the decomposition of organic oils[13] and other organic pollutants such as benezene, toluene, or

xylene[8], while the superhydrophilic properties of TiO_2 allow for quick wicking of water, allowing rain to wash off dust and dirt. This is useful for tall buildings, or difficult to clean surfaces such as domes, or flexible canopies and tents[13]. Nanocoating can also reduce the amount of microalgal growth on bricks[6]. So-called 'self-cleaning tiles', resistant to soiling from roof-water runoff can also decompose air pollution such as nitrous oxides (NOx), and reduce amounts of cleaning detergents needed.

Applications for cleaner air and water are also possible. Air filters can also incorporate TiO_2 and UV light, allowing for reduction of NOx levels to below environmental standards in a fraction of the time a natural decrease, or using an air cleaner would require[8,13]. TiO_2 enabled applications have been shown to reduce the amount of natural organic matter (NOM) fouling on micro- and ultra-filtration systems, reducing costs of energy needed for increased pressure, and filter maintenance costs[7]. The potential of organic compounds such as benzene and chlorinated compounds to be oxidized using TiO_2 applications is advantageous for reducing contaminants from chlorine-based water treatments[39]. Oil degradation from the destruction of aromatics, approaching 90% removal has been shown[8]. Significant removal of microorganisms and pathogens is also well reported, with gram negative bacteria being more susceptible to attack[40].

TiO_2 Nanoparticles Flow to Environmental Compartments

The increased inclusion of TiO_2 NPs in materials has driven production of TiO_2 nanoparticles exponentially. Robichaud et al. (2009), estimates that by 2022, TiO_2 NP production will surpass bulk TiO_2 production. Following upper bound trends, by 2025 a complete conversion of the TiO_2 production industry to nano-sized is expected to occur, generating approximately 2.5 million metric tons of TiO_2 NPs per year[41]. From 2002 to 2025, Robichaud

estimates a cumulative 12 million metric tons of TiO_2 nanoparticles will be produced[41]. These estimates represent the maximum upper bounds of TiO_2 nanoparticle production, and the trends are shown in Figure 1.4. However, as production increases, so too does the flow of nanoparticles to environmental compartments.

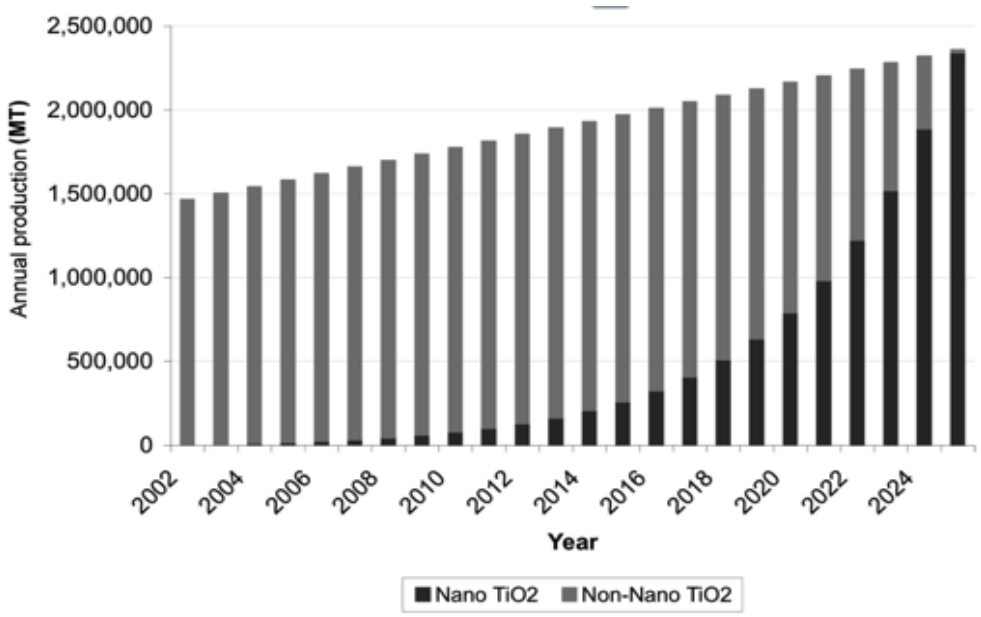

Figure 1.4. Estimated TiO_2 Production Trends from 2002 to 2026. Exponential rise in TiO_2 nanoparticle production, driven by increasing application use, will surpass bulk TiO_2 production by 2023, and almost completely convert to nano-sized production by 2026. Reprinted (adapted) with permission from [41]. Copyright 2009. American Chemical Society.

Lazevera (2014) and Keller (2013) have estimated that between 83,500 and 88,000 metric tonnes (MT) of TiO_2 nanoparticles enter North American environmental compartments per year (Figure 1.5)[42,43]. These calculations include NPs that pass through waste treatment plants (water, incineration, and landfill), thus resulting in numerous distinct breakdowns of TiO_2 waste compartmentalization. Keller (2013) estimates between 779 and 2769 MT/yr enter water systems (with only 60% of this amount passing through waste water treatment plants (WWTPs)[42], while Sun (2010) estimates that almost 1900 MT/yr enter water systems (1240 MT/yr directly

from non-treated wastewater)[44]. Gottshalk estimates that on average, 21 ng/L TiO_2 NPs exist in surface freshwaters[45].

Wastewater treatment plants in North America are extremely efficient at removing TiO_2 nanoparticles during treatment. Keller (2014) estimates 82% of TiO_2 nanoparticles passing through NA wastewater treatment plants are removed[46]. Gottschalk (2009) puts removal efficiency between 90.3%-99.5%[45], while Westerhoff found that approximately 96% of TiO_2 nanoparticles are removed from wastewater in North America WWTPs[47]. A numerical estimate is provided by Sun (2010), estimating that approximately 478 MT/yr of TiO_2 NPs pass through WWTPs[44]. Lazevera estimates 1.33-43.88 ug/L TiO_2 in WWTP effluent[43], Sun (2010) estimates 16 ug/L in effluent[44], Gottshalk estimates 1.37-6.70 ug/L TiO_2 NPs[45], Keller (2014) estimates 5 -15 ug/L TiO_2 in effluents[46]. These estimates were obtained from measurements using filters greater than 100 nm, so amounts of NPs of lower dimensional size may be higher. Westerhoff, however, asserts values of 25 ug/L and less, in the size range of 4 nm to 30 nm.

The majority of TiO_2 NPs aggregate and drop out into biosolids/sludge. Gottschalk estimates between 107 and 523 mg/kg of TiO2 NPs in sewage treatment plant sludge(STP)[45], and Sun (2010) agrees (150 to 540 mg/kg), while Lazevera estimates slightly higher, between 273-342 mg/kg TiO_2 NPs in STP sludge[43]. Alternatively, Keller (2013) found much lower numbers in North America, only 10-70 mg/kg[43]. Biosolids are used as fertilizer in many world regions. Gottshalk (2009) estimates 63% of biosolids are used for soil application[45]; Keller (2013) estimates 47% of biosolids are applied to land[46]. Should the sludge containing these NPs be used as a field applicant or fertilizer source, there is a high probability the NPs will reenter the water systems during irrigation or rain events.

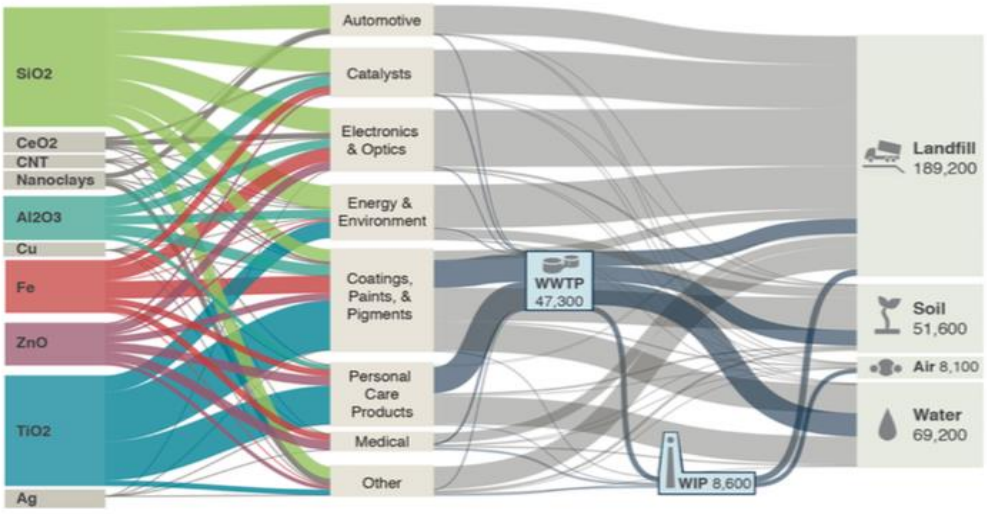

Figure 1.5 Fate Diagram of Nanoparticle Movement from Use to Environmental Compartment. Flow of nanoparticles through usage to environment. TiO_2 nanoparticles account for 80000 MT to all environmental compartments per year, with between 779 and 2769 MT entering water systems. Reprinted (adapted) with permission from [46]. Copyright 2014. American Chemical Society.

Once in freshwater systems, the majority of TiO_2 nanoparticles are expected to stay within the water column, as they are generally stable. In waters of low conductivity stability occurs at aggregate sizes of 300 nm and smaller, with low rates of sedimentation, with increasing aggregation occurring rapidly as ionic content increases [48,49]. This effect was found to not be concentration dependent at reasonable environmental values (up to 10 mg/L)[48,49]. Above these values, stability was inversely proportional to concentration[48].

Natural Organic Matter in Freshwater

The addition of natural organic matter (NOM) has been found to stabilize nanoparticles in waters[17,50]. Natural organic matter is loosely defined large, ubiquitous molecule composed of humic acids, fulvic acids, and hydrophobic compounds, consisting of a variety of aliphatic, aromatic, phenolic and quinone structures, lignins and proteins[51]. These structures vary in size

and properties, giving it a complex, heterogenic nature that is difficult to quantify. NOM plays a crucial environmental role, specifically in contaminant binding, making NOM very important in considerations of metal bioavailability and transport through soils and water[52]. NOM adsorbs to the surface of the nanoparticle, reducing the surface charge. This decrease in surface charge (and subsequently, zeta potential), allows the particles to remain in generally unaggregated states. Thus, nanoparticles are expected to remain in the water column for a significant amount of time in natural freshwaters[48,53].

TiO_2 Phototoxicity

TiO_2 NP photocatalysis is an important driver of toxicity. Most recent research on the ecotoxicological effects of TiO_2 nanoparticles has shown definitive link between UV-A irradiation of TiO_2 NPs and dramatic increases in toxicity, often by orders of magnitudes[14,15,17,35,54]. Ma et al. (2012) exposed *D. magna* and Japanese medaka to photocatalytic standard 25 nm size (P25) TiO_2 NPs and simulated solar spectrum (SSR) irradiation. Both organisms exhibited toxicity increases of 2-4 orders of magnitude under SSR compared to non-radiative lab lighting. *D. magna* 48-hr LC_{50} toxicity increased from over 500 mg/L TiO_2 to 29.8 ug/L TiO_2. Japanese medaka LC_{50} toxicity increased from 294 mg/L TiO_2 to 2.64 mg/L TiO_2 [17].

Ma et al. (2012) further elucidated the effects of wavelength on TiO_2 NP toxicity to *D. magna*. Using filters, the researchers were able to expose organisms to specific wavelengths (and intensities) of light, demonstrating significant toxicity as a result of radical generation occurred at UV-A and UV-B wavelengths. Removing the UVB range had no effect of the NP photocatalytic properties in regard to radical generation [35].

Using *D. magna,* Mansfield et al. (2015) investigated how the ingested TiO_2 body burden affected toxicity, while co-exposing to varying UV irradiation, and a range of TiO_2 concentrations. They further modified the experiment slightly to allow for only partial sunlight exposure, replicating the natural swimming patterns of *D. magna* during the day. These exposures were done under ambient natural sunlight. 1-hr body burdens were determined to not have an effect on toxicity at all; in fact, significantly higher toxicity was found in aqueous low body burden suspensions than in the 1-hr TiO_2 body burden exposures [15]. This study demonstrates the importance of the direct interaction of UV irradiation and the nanoparticle surface, and how formerly established phototoxic models do not similarly apply to TiO_2 phototoxicity.

As NOM is a major component of freshwater, the importance of understanding how NOM affects the behavior of TiO_2 NPs, and the toxicity to organisms is of significant interest. Wormington et al. (2017) investigated the effect of natural organic matter (NOM) on TiO_2 toxicity to *D. magna*. In suspensions of up to 1.5 mg/L TiO_2 NPs and 4 mg/L NOM, there was no significant change in hydrodynamic particle size or in zeta potential. However, they found that the addition of NOM reduced the toxicity of TiO_2 in a concentration dependent manner, finding a mean mortality of 93.3%, 76.7%, 23.3% and 3.3% in suspensions with 0, 1, 2, and 4 mg/L NOM [55]. These results demonstrate the necessity to include NOM as a dynamic component of TiO_2 toxicity studies.

Uncertainty in Describing Toxicity in Terms of TiO_2 Concentration

The toxicity of TiO_2 is a result of ROS generation [56,57], manifesting as oxidative damage[58,59]. The noticeable difference in TiO_2 toxicity across the field is driven by the amount of hydroxyl radicals produced in differing environments. Physical nanoparticle

factors[60,61] play a large role in radical generation, thus affecting toxicity. Significant evidence shows clear links between increases in nanoparticle concentration and toxicity[14,54,56,62,63], as well as positive correlation with ROS generation [54,63]. Decreasing particle size also increases toxicity[54,57,63], ROS/hydroxyl generation [57,63], and production of oxidative stress defenses[64]. The increase in hydroxyl generation as size decreases is a function of available surface area[56], and also occurs as a function of aggregate size [65]. Crystallinity also plays a role in toxicity[66], wherein mixtures of anatase and rutile, as well as anatase crystals are more toxic than rutile. Again, the anatase configuration's generation of hydroxyl/ROS species under UV-A light is the reason that TiO_2 nanoparticles are used so frequently.

Environmental factors also play an important role in the generation of hydroxyl radical[67], and need to be accounted for when describing toxicity. There are well established links between the intensity, and specific light wavelengths[15,62,68] and toxicity and ROS generation. Time of exposure also plays a significant role, positively correlated to toxicity and ROS generation [35,62]. An aspect that is just beginning to be incorporated in testing but of high importance is NOM concentration with respect to nanoparticles. Literature shows significant attenuation of toxicity, and radical generation as NOM concentration increases[55,69]. Increasing ionic strength of solution reduces the generation of hydroxyl radicals (and thus toxicity), a result of decreased particle stability[57]. Alkalinity and pH likewise affect the generation of hydroxyl radicals[70], and therefore could play a role in moderating TiO_2 nanoparticle toxicity.

CONCLUSIONS AND OVERVIEW:

Being able to adapt these factors into a harmonious measurement system will go far to resolving the differences in TiO_2 toxicity from lab to lab and to the environment. It is impossible

to test for an arguably infinite number of environmental conditions. It is well agreed that the generation of hydroxyl radicals is a root cause for TiO_2 toxicity. A means of describing how the generation of these radicals is affected by varying conditions will go far to aiding more resolved toxicity measurements. Models such as the Biotic Ligand Model allow for a large scale of input conditions to determine metal ion binding efficiency; a model estimating hydroxyl radical generation from irradiated TiO_2 would similarly aid toxicity studies, as well as regulatory decisions. This dissertation attempts to lay the groundwork for such a model. By developing a method to measure hydroxyl radical generation under varying conditions and creating a model to predict how conditions affect radical generation, some knowledge gaps concerning TiO_2 nanoparticle toxicity can be closed.

This dissertation will accomplish these goals in the following chapters. In Chapter Two, the production of radicals by irradiating TiO_2 nanoparticles with low intensity UV-A wavelengths, and characterization using EPR spectroscopy is detailed. Radical concentration will be measured using fluorescent spectroscopy across 48 hours to determine the rate of radical generation under environmentally relevant conditions. These conditions include UV-A intensities found in freshwater water columns, and equivalent DOC amounts found in numerous and rivers throughout the continental United States. The 48-hour acute toxicity of TiO_2 to *D. magna* is measured at three conditions (UV- DOC+, UV+ DOC-, UV+DOC+) and the TiO_2 concentration resulting in toxic effects is translated to hydroxyl radical concentration.

In Chapter Three and Chapter Four, the rates produced from the full factorial exposure design are used to build models to predict the rate of hydroxyl radical generation. Chapter Three predicts the rate of radical generation without the NOM component to try to better understand the reciprocal interplay between UV intensity and TiO_2 concentration. Chapter Four detailed the

effects the addition of NOM on rate production, in an effort to better understand why toxicity is attenuated in higher concentrations of NOM. The inclusion of NOM in Chapter Four generates a more reasonable prediction under environmental conditions. Both models are compared to hydroxyl radicals measured in literature sources under a range of conditions that are in between and exceed the bounds of the model to assess prediction limits and overall weaknesses.

In Chapter Five, the biological impact of conditional changes on TiO_2 exposure to *D. magna* is assessed. Using 10 conditions (UV intensity and DOC concentration) from rate measurements, freshwater cladocera were exposed to the same experimental TiO_2 gradient and mortality was assessed. Toxicity was redescribed as hydroxyl radicals, to determine how rate of radical generation affected injury as a result of TiO_2 exposure, implying that rate of radical generation, and an organism's ability to deal with burdens of oxidative stress is an integral part in understanding TiO_2 toxicity.

Finally, the Future Directions section focuses on the future of TiO_2 toxicity research. Through a better understanding of nanoparticle flow from production to pollution, usage, and the improvement of disposal systems, and remediation techniques, the hazard represented by the NP movement to aquatic compartments can be better described. Techniques and means of model improvements are discussed, such as the inclusion of particular terms, and the reevaluation of data via higher-order modeling techniques. Evaluation of the biological effects of hydroxyl radical and ROS produced by TiO_2 NP irradiation is also recommended, with a number of suggested focuses.

CHAPTER TWO

QUANTITATIVE MEASUREMENTS OF HYDROXYL RADICALS GENERATED BY IRRADIATED TITANIUM DIOXIDE NANOPARTICLE SUSPENSIONS USING SIMPLE FLUOROMETRIC METHODOLGY

INTRODUCTION:

Titanium dioxide is an active component in a multitude of industrial, personal, and everyday products. Uses include food additives, photocatalysts, paints, surface coatings, and personal care products such as cosmetics and sunscreens [1]. Recently, attention has turned to TiO_2 nanoparticles (TiO_2 NPs), due to the intrinsic abilities to generate excited electrons when exposed to ultraviolet (UV) radiation. The photo-induced mechanism of electron promotion generates free radicals, which can be used generate H_2 gas, decompose organic molecules and persistent chemicals, and help to kill microbes and bacteria [2,71].

TiO_2 Nanoparticle Production and Flow Trends

Growth in the use of TiO_2 NPs is such that Robichaud et al. estimates that upper bound production of TiO_2 NPs will surpass production of bulk TiO_2 by 2022. By 2025, worldwide production of TiO_2 NPs is expected to exceed 2 million metric tons per year [41]. Keller et al., predicts that approximately 88,000 tons of TiO_2 NPs per year will be released (either through natural processes, disposal, or accident) to global environmental compartments[43]. Of this, almost 50,000 metric tons are estimate to escape WWTPs in the effluent, although the efficacy of removal is often dependent on the WWTP global location. In WWTPs with the most modern treatment methods, close to 97% of TiO_2 NPs are expected to be sequestered in biosolids. However, these biosolids can be reutilized as fertilizer, possibly reintroducing the nanoparticles into freshwater systems[43]. Additional TiO_2 NPs loads to water systems may be contributed by surface coating/paint runoff, most likely more problematic in urban areas. As predictions of

exponential increases in NP manufacturing over the coming years, increasing amounts of nanoparticles can be expected to reach environmental compartments. Keller estimates TiO_2 NP release to soil and water at 39,760 metric tons per year[46].

Radical Generation from Irradiated TiO_2 Nanoparticles

The hazard of TiO_2 NPs to aquatic organisms lies within the total amounts released, but the risk can be understood when considering the photocatalytic effects of the nanoparticle. UV-A radiation at wavelengths of 382 nm has the equivalent energy of approximately 3.2 eV. This is equal to the bandgap energy of anatase TiO_2 NPs. Energy of this wavelength excites electrons in the valance band, promoting them to the conductance band, and leaving behind areas of positive charges referred to as 'holes'. To return back to electronic stability, the nanoparticle will abscond an electron from surrounding water molecules, generating hydroxyl radical ($OH^{\bullet}$), and initiating oxidative reactions. The promoted electron will induce reductive pathway reaction via transfer to oxygen molecules, generating superoxide anions ($^{\bullet}O_2^-$)[18]. It is this photocatalyzed radical generation that degrades chemicals and kills microbes which makes TiO_2 nanoparticles so attractive for biocides and surface treatments.

Fujishima (2008) details the following hydroxyl generation schemes from the oxidation of superoxide, resulting in both surface adsorbed, and free hydroxyl radical:

$$O_2 + 2e^- + 2H^+ \rightarrow H_2O_2$$

$$O_2^{\bullet-} + O_2^{\bullet-} + 2H^+ \rightarrow H_2O_2 + O_2$$

$$H_2O_2 + e^- \rightarrow OH^{\bullet} + OH^- \qquad \text{(surface adsorbed } OH^{\bullet}\text{)}$$

$$H_2O_2 + O_2^{\bullet-} \rightarrow OH^{\bullet} + OH^- + O_2 \qquad \text{(free and surface adsorbed } OH^{\bullet}\text{)}$$

$$H_2O_2 + h\nu \rightarrow OH^{\bullet} + OH^{\bullet} \qquad \text{(free and surface adsorbed } OH^{\bullet}\text{)}$$

Further evidence for describing radical generation solely as the hydroxyl radical is provided by observing organic intermediates in reactions photocatalyzed by TiO_2 and comparing these intermediates to those produced by reactions with known hydroxyl radical sources, which are consistent[72,73]. These radical intermediates include DMPO-OH adducts, of which there is significant evidence indicating majority hydroxyl radical generation [72,74-77]

Observations of photocatalytic reactions run in water-free, aerated organic solvent (D_2O) show significant decrease in oxidation rates of organic molecules compared to reactions run in water[72]. This was further characterized by $(CH_3)_2CHOH$ lack of complete degradation to CO_2, which occurs in water/TiO_2 reactions. Replacing H with D in the organic molecule, while retaining the aqueous solvent showed no rate reduction. This implies that the reaction is limited by the formation of active oxygen species. O-D bonds have lower ground state energies, that are not able to be overcome[72].

Toxicity from Irradiated TiO_2 Nanoparticles

Reactive oxygen species (ROS) are well known to cause a number of biological dysfunctions through oxidative damages. Hydroxyl radicals exhibit the highest reduction potential of all ROS. These radicals are responsible for initiating lipid peroxidation cycles resulting in membrane disruption, can generate DNA adducts causing sequence mutations, and will initiate radical cycling cascades within cells. Superoxide anions are likewise responsible for initiating cellular response cascades, often generating hydroxyl radical in the process[67]. Taking this into consideration, it should come as no surprise that TiO_2 nanoparticle toxicity drastically increases under UV irradiation[78].

Multiple researchers have investigated the toxicity of TiO_2 under UV irradiation[14,15,17,79,80]. Ma et al.(2012), conducted an excellent battery of tests showing that

the phototoxicity of TiO_2 nanoparticles to *D. magna* is partially dependent on the intensity and wavelength of UV light[35]. Li et al. (2015), has demonstrated the effect of exposure time on TiO_2 toxicity, as well as UV intensity on TiO_2 toxicity to *Hyalella azteca* [62]. Multiple studies indicate that the toxicity can vary by multiple orders of magnitude, where the extent of this enhancement is dependent on a number of physical particle factors, such as crystal configuration[81], size of nanoparticle[57], aggregation [61], and coatings [81,82]. TiO_2 nanoparticle toxicity has been shown to follow the Bunsen-Roscoe Law of Reciprocity, which describes the generation of photochemical products as being proportional to the product of light intensity and time[83]. This relationship is well demonstrated by PAHs, wherein low concentrations of chemicals and high doses of UV light produce equivalent impact as high concentrations of chemicals and low doses of UV light[84,85].

Attenuation Effects of Natural Organic Matter

Another important factor to consider is the effect of natural organic matter (NOM). NOM is a significant component of natural water systems, comprised of humic acids, fulvic acids, lignin, proteins, and many other organic compounds. It is ubiquitous in natural waters but the particular molecular configuration and relative concentration varies spatially and temporally[86]. Due to the persistence of NOM in water systems, it is important to determine its effects on TiO_2 toxicity. Although there are studies that investigate the interaction of TiO_2 NPs and NOM[81,87,88], there are few studies that investigate the effect of NOM on TiO_2 NP toxicity. Wormington et al. (2017), shows a decrease in toxicity to *D. magna* proportional to increases in NOM concentration. They link low mortality to decreased ROS concentration and contend that the less than 10% decrease in light transmission did not contribute to decreases in toxicity, based on the high intensities of light used in their experiment. This was [55]. Lin et al. (2015), also

showed TiO_2 phototoxicity in unicellular green algae was attenuated by addition of NOM. They propose this protective effect is due to NOM scavenging photocatalyzed ROS[69].

Purpose of Study

Comparing toxicity studies for TiO_2 nanoparticles is difficult due to variability in exposure conditions from laboratory to laboratory. These conditional variations can include light intensities, exposure wavelengths, exposure durations, water qualities. Variation of nanoparticles may also occur, such as size and crystallinity. Although this is inconvenient when attempting to discern a "true" LC_{50} value for TiO_2 nanoparticles, it is not necessarily detrimental. Lighting conditions, size, crystal configuration, and inclusion of NOM vary from study to study, but these variations in lighting, NOM type and content will vary spatially and temporally in nature. Further, toxicity is not a direct result of the nanoparticle itself, but by the reactive oxygen species produced[17,67].

Identifying the influences of changing environmental conditions on the TiO_2 nanoparticle would help to develop a better understanding of the link between ROS generation and TiO_2 toxicity. By understanding how hydroxyl radical generation changes under varying conditions, a more refined link to toxicity can be elucidated. By bounding experiments at reasonable environmental concentrations of TiO_2 and NOM, and light intensities, better predictions about the behavior of TiO_2 NPs outside of a laboratory setting can be made. Based on previous literature, variations in TiO_2 concentration will result in changes in hydroxyl radical generation; that variations in light intensity will alter hydroxyl radical generation; and that a change in NOM will result in changes in generation of hydroxyl radical is hypothesized.

MATERIALS AND METHODS:

Full Factorial Design:

A full factorial approach to exposures was used for this experiment. The TiO_2 NP concentrations tested were 0, 0.500, 1.00, 3.50, 5.00, 7.00, 10.5, and 14 mg/L. Dissolved organic carbon (DOC) concentrations were 0, 1.57, 2.95, 4.28, and 5.71 mg/L. UV intensities were measured as irradiant intensity per nm, averaged across 320-400 nm, and were 0, 2.671, 4.301, and 5.167 $\mu W/cm^2/nm$.

Titanium Dioxide Nanoparticle Suspensions

Anatase titanium dioxide nanoparticles (Aldrich, <25-nm, 99.7% metals basis) were suspended in 18 mega-Ohm water, at a concentration no greater than 100 mg/L. Upon the intial dispersion into stock suspensions, TiO_2 NPs were stirred for 10 minutes and sonicated for 2 hours (in 15 minutes on/5 minute off) intervals using an immersion-tip sonicator. Before use, stock suspension was sonicated for 15 minutes, and lightly stirred during dilutions to ensure complete suspension. All suspensions were diluted with EPA recipe Moderately Hard Water (96.0 mg/L $NaSO_4$, 60 mg/L $CaSO_4$-H_2O, 60 mg/L $MgSO_2$, 4.0 mg/L KCl; pH: 7.9-8.3, Hardness: 80-100, Alkalinity: 57-64) [89]. Nanoparticle size was measured using Hitachi H7600 TEM. Intensity weighted hydrodynamic particle size was determined by DLS using a Wyatt Dawn Heleos-II Dynamic, at ambient temperature. UV transmission was determined, using a Varian 50 Bio UV-Vis spectrophotometer, analyzed in dual beam mode from 300 to 700 nm at a scan rate of 100 nm/min, with 1-nm intervals. 0.5-mL aliquots were removed and analyzed using quartz 1-cm x 1-cm x 4.5-cm plastic cuvettes (Spectrasil), at room temperature. Zeta potential was determined using a Malvern Zetasizer ZS, at room temperature. DLS and UV transmission were run for the full factorial of TiO_2, DOC concentrations and UV intensities, measured at 0, 24

and 48 hours. Due to time constraints, zeta potential was only determined at initial time of preparation, for the full factorial of DOC and TiO_2.

Natural Organic Matter

Natural organic matter was obtained directly from the Suwannee River headwaters, at Suwannee River Visitors Center in Fargo, Georgia**.** Water was filtered through 0.45-micron filters to remove all non-dissolved components. Total organic carbon concentration was determined using a Shimadzu TOC-V Carbon Analyzer. Stock concentrations were directly diluted to achieve working concentrations.

Light System

UV irradiance was generated using CXL Topaz 40W Blacklight Blue T-12 Fluorescent lights. Standard Lab lighting was generated using Sylvania 40W Cool White T-12 Fluorescent lights. Lights were installed in a plywood light box, measuring 48" x 12" x 12/5", with an 8" distance from bulb to bench surface. Intensity and spectral output was measured using an OceanOptics JAZ Photospectrometer equipped with a cosine corrector. Spectroscopic data was analyzed using OceanView 1.5.2.

Electron Paramagnetic Resonance Spectroscopy

EPR spectroscopy was used to characterize radicals produced from the irradiation of TiO_2 NP suspension. EPR measurements at the X-band were acquired using a Bruker EMX spectrometer, with a quartz flat cell inserted directly into the microwave cavity, at ambient temperature. For all experiments, the following parameters apply: Modulation frequency and amplitude were 100 kHz and 0.5 G, microwave frequency was 9.759 GHz, microwave power was 1.00 mW. Time constant and conversion time equaled 81.92. Sweep width was 100 G centered at 3479 G. The g-factor of 2,2,-diphenyl-1-pierylhydrazyl (DPPH; g=2.0036) was used

as reference. Approximately 60-90 seconds elapsed between sample addition to flat cell and insertion. Spectra were analyzed using WIN EPR software.

5,5-Dimethyl-1-pyrroline-N-oxide (DMPO) was used as a spin trap for both standards and samples. Copper sulfate/ascorbic acid/hydrogen peroxide standards were used to verify the EPR hydroxyl radical signature. $CuSO_4$ (15 uL, 300 µM) ascorbic acid (9.38 uL, 375 µM), 3-morpholinopropane-sulfonic acid (MOPS) buffer (50 uL, 10 µM), H_2O_2 (11.25 uL, 22.5 µM), and ultra-pure deionized water (414.38 uL) were combined in a microcentrifuge tube and mixed. DMPO (25 uL, 25 mM) was immediately added, mixed, and the solution was transferred to the quartz flat cell and immediately inserted into the EPR microwave cavity.

TiO_2 suspensions were made in 50-mL volumetric flasks, and separated into triplicate scintillation vials of 15-mL per vial and covered with UV transparent Aclar® film. Samples were irradiated under CLX black lights for 48 hours, with analysis points at 0, 24, and 48-hr. At each time point, the DMPO was added to the samples, and the vials were removed from the UV box. Aliquots of 0.5 mL for each sample were taken, added to the quartz flat-cell and immediately inserted into the microwave cavity for analysis.

Fluorescence Spectroscopy

Fluorescein was prepared by dissolving 0.047 g HEPES buffer into 10 ml ultrapure DI water in a scintillation vial. 500 uL of 10M KOH was added and stirred. 0.0367 g of fluorescein, sodium salt was added and stirred until complete dissolution occurred. The solution was acidified with 130 µL HNO_3 and adjusted to pH 7.5. Final stock concentration was 100 mM. Working concentration did not exceed 7.5 µM. Sample dye concentrations were varied depending the ranging of hydroxyl radical generation.

Fluorescence analysis was performed on a Horiba Fluoromax-4 fluorescence spectrometer. Excitation wavelength was 467 nm and emission intensity was measured from from 400 to 700 nm. Excitation slit width was 1.0 nm; emission slit width was dependent on initial concentration of fluorophore.

Calibration curves were generated using horseradish peroxidase and hydrogen peroxide, as per the Hydroxyl Radical Antioxidant Capacity (HORAC) assay[90]. 5 mg of horseradish peroxidase (HRP) (Sigma, lyophilized powder, AU: 310 units/L) was dissolved in 5 mL of 18 mega-Ohm DI water to give solution of 310 AU/L. Hydrogen peroxide (BDH, 30%) concentrations (0 to 10 µM) were combined with 107.6-uL of HRP solution, 150 uL of 1M potassium phosphate buffer (BDH, 98%) and requisite amount of fluorescein. Solutions were then diluted to 3 mL. Separate calibrations curves were made for each dye concentration.

All sample solutions were made in 100 ml volumetric flasks. TiO_2 was diluted to testing volume (0, 0.500, 1.0, 3.5, 5.0, 7.0, 10.5. or 14 mg/L) along with DOC (0, 1.57, 2.95, 4.28, 5.71 mg/L) and fluorescein dye (1.5, 5, 7.5, 10 µM/L). 30 ml was dispensed into beakers, in triplicate. A 3 ml aliquot was removed from each for analysis, and these suspensions were immediately covered with Aclar ® Fluoropolymer film, a UV transparent film, and placed in the lightbox. 0 $\mu W/cm^2/nm$ samples were additionally covered with aluminum foil to ensure the complete blockage of UV irradiation. The samples were only removed to take 3 mL for analysis every 12 hours.

Hydroxyl radical generation was determined by measuring the difference in emission from time zero. All concentrations were run in triplicate, and each sample scan was the result of an averaged triplicate scan. All hydroxyl radical concentrations were subtracted from the radical concentration in the '0 mg TiO_2' samples, thus determining the total amount of radicals produced

by irradiated TiO_2 per time point. Rate was determined by the slope of the regression line plotted through each concentration across 48 hours.

Daphnia magna Bioassays

Daphnia magna 48-hour acute toxicity bioassays were performed, all conforming to EPA protocol and standards[91]. Less than 24-hour old neonates were randomly selected from a pool of 500 and transferred to freshly made TiO_2 nanoparticle suspensions. Suspension concentrations exposed to UV light ranged from 0 mg/L to 1.5 mg/L TiO_2 for suspensions without DOC and 0 mg/L to 14 mg/L TiO_2 for UV (4.301 $\mu W/cm^2/nm$) exposures with DOC. Suspensions exposed to fluorescent lab lighting (0.0423 $\mu W/cm^2/nm$) ranged from 0 mg/L to 1500 mg/L TiO_2. Each concentration was replicated 3 times, each exposure vessels containing 20 mL of suspension and 5 *D. magna*. Standard 16 h light/8 h dark cycles were used, and all exposure vessels were kept at 22.5°C ± 1°C for the entire duration of testing. Mortality was assessed at 0, 24, and 48 hours; water quality assessed at the beginning and end of the testing period.

Statistical Analysis

All statistical analysis was performed using JMP software (version 12.1.0). Residuals were analyzed using the Sharpiro-Wilk test for normativity and confirmed. Comparative analysis was performed on all rate data using a comparative analysis of means with a Sidak adjustment, and Tukey's HSD to determine significant differences between rates (α=0.05). Bioassay data is described as LC_{50} values. LC_{50} values for phototoxic dose were calculated using standard Spearman-Karber methodology[92].

RESULTS:

TiO_2 Suspension Characterization

Primary particle size was measured by TEM to be 21.3 ± 0.3(SE) nm (Figure 2.1). The intensity weighted hydrodynamic diameter of the aggregates was measured using dynamic light scattering. The full factorial experimental design was analyzed at 0, 24, and 48 hours (Table 2.2, Graphs in Appendix C). Aggregate size increased as the TiO_2 concentration gradient increased, at all concentrations of dissolved organic carbon (DOC), at 0 hrs. The amount of DOC at any one TiO_2 concentration did not appear to play a role in aggregate size at 0 hrs. At 24 hrs, aggregate size increased in higher concentrations of DOC, and at higher UV-A intensities. Increasing aggregate size was slightly correlated with increasing TiO_2 concentrations. For example, the 0.5 mg/L TiO_2 under 5.177 μW/cm^2/nm UV-A had an aggregate size of 81 nm at time zero, and 124 nm at 24 hours, while the 14 mg/L TiO_2 had an aggregate size of 237 nm at time zero, and 622 nm at 24 hours. A general decrease in aggregate sizes occurred from 24 to 48 hours, for example the 0.5 mg/L TiO_2 under 5.177 μW/cm^2/nm UV-A from 124 nm to 25 nm, while the 14 mg/L TiO_2 decreased from 622 nm to 203 nm.

Lower concentrations of nanoparticles remained relatively stable across the testing period, regardless of DOC concentration, and greater variation in size occurred at higher TiO_2 concentrations at all DOC concentrations. For example, under 4.301 μW/cm^2/nm UV-A 1.0 mg/L TiO_2 in 2.95 mg/L DOC had an initial size 94 nm, 102 nm at 24 hours and 90 nm at 48 hours, whereas under the same conditions 10.5 mg/L TiO_2 measured 208 nm, 314 nm, and 454.27 nm.

Light intensity appears to play the biggest role in the change in aggregate size. Comparing the size of aggregates at 48 hrs under 0 μW/cm^2/nm UV-A, and the size of

aggregates at 48 hours under 5.177 μW/cm^2/nm UV-A, a number of significantly different aggregate sizes were found. There are a number of different reasons for these changes under UV-A light. The polydispersity of a nanoparticle-NOM suspension generates a wide variety of possible configurations of particles and NOM molecules. As time passes, nanoparticles can become coated in NOM, resulting in changes in surface charge, leading to both attractive and repulsive effects, depending on the degree of surface charge change[50]. NOM molecules will also break down in the presence of TiO_2 and UV-A light, leading to modifications of the overall charge of molecules within[93]. However, surface charge was not measured at time points other than 0, so it is difficult to pinpoint the exact causes for these aggregate size changes.

Zeta potential was measured at 0 hours using a Malvern Zetasizer. These values are shown in Table 2.3, and graphically expressed in Figure 2.2. The zeta potential slightly decreased upon addition of DOC and TiO_2 nanoparticles. No trends were evident across the TiO_2 gradient at any DOC concentration, nor across the DOC gradient at any one TiO_2 concentration. Zeta potential ranged from ~11 mV to ~20 mV.

UV-Vis percent transmission spectra were examined, at 0-hr, 24-hr, and 48-hr to measure light impedance as a result of increasing DOC. This data is summarized in Table 2.4 and Figure 2.3. Percent transmission measurements were influenced by the scattering of light from the nanoparticles, with decreases in light transmission with increasing TiO_2 NP concentration, most noticeably at 0 hrs. Within the working range of the experiment (0 mg/L DOC to 5.71 mg/L DOC), the increases in DOC concentration result in a maximum of 10% transmission decreases.

Natural Organic Matter Characterization

Suwanee River water (SWR) was filtered through 0.45 micron filters. Filtered SWR was lyophilized to determine total amount of dissolved organic matter (DOM) per liter. Triplicate

measurement determined a concentration of 107.46 (±19.84) mg/L DOM in solution. Dissolved organic carbon was determined to be 61.34 (±0.43) mg/L by Total Organic Carbon analysis. HPLC-ICP determined metal content, shown in Table 2.1**.**

Lighting Characterization

The absolute irradiance of the light sources was measured periodically throughout testing to ensure no decrease in irradiant output occurred. Intensity was measured across the light spectrum**.** Dark conditions (no lights), exhibited no peaks within the UV spectra. UV irradiance was measured as average intensity across the UV-A spectrum (320 - 400 nm) Figure 2.4. The lowest UV intensity exposure measured an average irradiant intensity of 2.671 (±0.004) $\mu W/cm^2/nm$ with maximum intensity at 365 nm measured 6.263 (±0.012) $\mu W/cm^2/nm$. Midrange intensity generated average irradiant intensity of 4.301 (±0.017) $\mu W/cm^2/nm$, with a maximum peak of 9.578 (±0.034) $\mu W/cm^2/nm$ at 365 nm. The highest light intensity for exposures was measured at 5.188 (±0.032) $\mu W/cm^2/nm$ with a maximum intensity peak of 10.833 (±0.054) $\mu W/cm^2/nm$ at 365 nm. The light intensities were compared to peak intensity from the sun on a summer day in Pendleton, SC (34.6518 ° N, 82.7838°W). Average absolute irradiance was measured as 45.08 (±0.012) $\mu W/cm^2/nm$ and a maximum irradiance at 365 nm of 50.86 (±0.023) $\mu W/cm^2$. Output spectra are found in Figure 2.4, and listed in Table 2.5.

Identification of Hydroxyl Radical

EPR spectra indicated the formation of hydroxyl radical, superoxide anions and free electrons. Hydroxyl radical generation was confirmed via comparison of irradiated spectra to the standard spectra generated with copper sulfate/ascorbic acid/hydrogen peroxide (Figure 2.5A**)** with the irradiated samples (Figure 2.5B). The DMPO-$OH^{\bullet}$ adduct generates a clear 1:2:2:1 quartet indicative of this hydroxyl radical adduct, plainly recognizable in the standard, shown in

Figure 2.5A The spectrum from the irradiated TiO_2 suspensions confirms hydroxyl radical generation, as well as that of superoxide anions and free electrons. The non-specificity of the DMPO spin-trap allows these species to be identified simultaneously. The spectra generated are point-in-time; there is no internal standard, therefore, these spectra are used for species identification only.

Quantitation of Hydroxyl Radical

Calibration curves generated for each concentration using horseradish peroxidase and hydrogen peroxide to generate hydroxyl radicals. Figure 2.6 shows the linear response with R^2 greater than 0.98. To determine μM of hydroxyl radicals, the concentration of H_2O_2 is multiplied by two, as horseradish peroxidase generates hydroxyl radicals in stoichiometric proportions. New calibration curves were made for each fluorescein stock solution.

Hydroxyl radical generation over 48 hours were observed to be linear. Generation followed distinct trends, with total amounts of radicals increasing as TiO_2 concentration increased, as well as increasing with UV intensity. Addition of DOC decreased the total amount of radicals produced. Reciprocity was demonstrated where lower concentrations of TiO_2 and high intensities of UV light generated similar hydroxyl radical concentrations compared to high TiO_2 concentrations and low UV intensities. All samples exposed to 0 $\mu W/cm^2/nm$ generated zero, or extremely close to zero hydroxyl radicals. The calculated rates are expressed graphically in Figure 2.7.

0 mg TiO_2 concentrations were treated as a blank. 0 mg/L rates were subtracted from all rates to account for decreases in emmison not related to hydroxyl radical generation. The hydroxyl radical generation rates were determined from the slope of linear regression over the 48 hours for each concentration. These rates, and associated R^2 values are organized in Table 2.6.

Daphnia magna 48-hour Acute Bioassays

Figure 2.8 shows that *Daphnia magna* mortality was well correlated with increasing TiO_2 concentration and UV intensity. *D. magna* exposure to TiO_2 under fluorescent lighting (0.0432 $\mu W/cm^2/nm$ UV intensity) resulted in LC_{50} toxicity of 1090.0 (920, 1330.0) mg/L TiO_2. Exposure to UV light at a wavelength of 320-400 nm and an intensity of 4.301 $\mu W/cm^2/nm$ resulted in nearly four orders of magnitude increase in toxicity, with an LC_{50}, 0.220 (0.163, 0.252) mg/LTiO_2. Significant attenuation occurs with addition of 4.28 mg/L DOC to suspensions exposed to UV light resulting in *D. magna* LC_{50} toxicity of 8.55 (8.08, 9.05) mg/L TiO_2.

Figure 2.9 shows the toxicity with UV (4.301 $\mu W/cm^2/nm$) exposure as a function of generated hydroxyl radical. Exposures with 0 mg/L DOC experienced much lower hydroxyl radical LC_{50} toxicity (0.458 (0.415, 0.503) $\mu M\ OH^{\bullet}$) than in the presence of with 4.28 mg/L DOC (6.216 (5.771, 6.691) $\mu M\ OH^{\bullet}$) indicating decreased toxicity in the presence of DOC. No hydroxyl radicals were generated under lab light conditions; thus, the data is not included in the figure.

DISCUSSION:

Photocatalytic hydroxyl radical generation rate measurements showed significant differences for TiO_2 nanoparticle suspensions with dissolved organic carbon (DOC) concentrations up to ~6 mg/L under UV irradiation, as light intensity increased, as TiO_2 nanoparticle concentration increased and as DOC concentration increased. Rates exhibited expected photochemical reciprocity. A robust and effective fluorescent spectroscopy method was used to probe the hydroxyl radical generation rate and identify trends produced, under environmentally reasonable conditions in order to best describe the generation of hydroxyl radicals from TiO_2 nanoparticles undergoing complex interactions in surface freshwaters.

Using the fluorescent radical detection method, measurable radical generation in bioassays can be compared to toxicity in terms of the hydroxyl radical concentration. This is a more accurate description of toxicity than simply using TiO_2 nanoparticle concentration. TiO_2 alone is not toxic in the absence of UV-A light, exhibited by low mortality under no-UV or low UV conditions. Rather, the hydroxyl radical is the actual toxicant in this relationship, and irradiated TiO_2-mediated hydroxyl radical LC_{50} would be better described as such. NOM is demonstrated to provide protection from toxicity. Significantly more radicals are required to induce a similar mortality in suspensions with DOC, as compared to suspensions without DOC. Thus, longer exposure periods, and/or higher TiO_2 concentrations in the system would be required for comparable toxicity. This is a significant factor to consider with respect to regulatory decisions for TiO_2 nanoparticle usage and disposal.

Suspension Characterization

DLS measured aggregate size showed a concentration-dependency with higher TiO_2 concentrations. These aggregate sizes generally decreased past 24 hours. Settling was visually observed, and higher initial concentrations of nanoparticles resulted in a larger observable amount of settled particulate. It is possible that larger aggregations formed under higher TiO_2 concentrations settled, resulting in smaller aggregate sizes left in suspension, and has been observed in published literature[17].

The data, on whole, was varied, making distinguishable trends difficult to identify. Published data on behavior of TiO_2 nanoparticles in various media confirms that higher concentrations of nanoparticles will experience gravimetric settling, and the increases in NOM will stabilize suspensions. [17,55]. Loosli et al, saw nanoparticle aggregation is enhanced by humic acid, with maximum aggregate size occurring at between 2.0 to 3.0 mg/L of humic

acid[50]. A rapid decline in aggregate size occurs at concentrations above 3 mg/L, a trend that is generally exhibited by the data. Stabilization occurs from modifications of the nanoparticle surface charge; increased humic coating results in decreased zeta-potentials, resulting in increased nanoparticle stability[50]. Zeta potential trends indicate a slight decrease in overall zeta potential correlated with TiO_2 and DOC concentration increases, although based on the variation of the aggregation data, it is difficult to associate this decrease with a change in suspension stability.

Light Characterization

Light intensities generated by BLX black lights in the UV-A range (320-400 nm) measured between 2.671 $\mu W/cm^2/nm$ to 5.188 $\mu W/cm^2/nm$, with peak intensity occurring at 365 nm. These light intensities can be compared to the intensity of sunlight at noon in South Carolina, 45.08 $\mu W/cm^2/nm$. Although exposures were, at a maximum, 12.5% of natural sunlight irradiance, all intensities exhibit significant radical generation, and significant increases in toxicity in *D. magna* bioassays at exposed intensities. The implications of these results underline the substantial increase in risk of toxicity as a result of UV irradiation of nanoparticles.

Identification of Hydroxyl Radical

Electronic paramagnetic resonance spectroscopy indicated generation of hydroxyl radical in irradiated suspensions. DMPO-$OH^{\bullet}$ adduct was detected in both copper sulfate/ascorbic acid/hydrogen peroxide standards and in irradiated TiO_2 suspensions as a 1:2:2:1 peak signature. Spectra were comparable to published irradiated TiO_2 spectra by a number of researchers[30,94,95]. Although there are other species detected in or suspensions using the DMPO spin trap (superoxide and free electrons), the generation of ROS can be described entirely as hydroxyl radical for a number of reasons. These include concentration of radicals, empirical

chemistry concerning hydroxyl radicals produced by irradiated TiO_2 suspensions, and biological effects of hydroxyl radicals.

TiO_2 nanoparticle irradiation produces majority superoxide ($O_2^{\bullet-}$) and hydroxyl radicals ($OH^{\bullet}$). Although the superoxide radicals produced by the photocatalytic reaction have consistently higher quantum yields than hydroxyl radicals[19,96], multiple researchers show that superoxide more readily acts as an oxidizing agent for H_2O, and catalyze the formation of H_2O_2. H_2O_2 will then readily react with free electrons to generate $OH^{\bullet}$[18,74,76,96-99], with a cycling reaction possible.

Toxicity driven by TiO_2 photocatalysis generally indicates the importance of ROS species. Certainly, both radicals produced (superoxide, hydroxyl radicals) are capable of inducing cellular antioxidant effects, however, superoxide is biologically unstable and generally has poor biological reactivity[67,100]. Intracellular superoxide will be readily catalyzed by superoxide dismutase (SOD) to hydrogen peroxide, which is then reduced to water and oxygen radicals via catalase or glutathione peroxidase. [67] Regardless, the hydroxyl radical is much more biologically disruptive, reacting with every type of biomolecule and nucleic acids[67,100,101]. There are no known enzymatic reactions that can scavenge $OH^{\bullet}$, instead, antioxidants are the sole source of removal without reaction with a biomolecule [67,100]. Because the TiO_2 nanoparticle must be activated by light outside the cell, hydroxyl radical interactions with the outer cellular membrane resulting in lipid peroxidation are the most common cause of toxicity[102]. Singlet oxygen, catalyzed by reactions of superoxide with trapped holes has shown some influence on toxicity, based on increased production in lipids[13,102], but the $^1O_2$ short lifetime compared to the hydroxyl radical (2 μs and 10 μs, respectively) makes this possibility less reasonable[13]. Given the numerous mechanisms of

hydroxyl radical generation, the wealth of data implying that hydroxyl radicals are ultimately the most relevant radical produced, and the known biological implications, generalizing radical generation as hydroxyl radical is within the bounds of this study.

Hydroxyl Radical Generation Rates

Until recently, literature regarding toxicity of TiO_2 nanoparticles did not focus on the more complex interactions that nanoparticles undergo in surface freshwaters, and the resulting effect on toxicity. Studies were focused mainly on the effect of UV light and physical characteristics of the nanoparticle, such as size, crystalline configurations and coatings[80]. More recent work has demonstrated the necessity of incorporating NOM into studies, due to both the ubiquitous presence of NOM in all surface waters, and the inherent ability of the macromolecule to quench radicals[55,78]. By choosing a full factorial design incorporating reasonable TiO_2 concentrations, NOM (measured as dissolved organic carbon), and light intensity, the generation of hydroxyl radicals across a wide range of naturally relevant conditions is described.

The nanoparticle concentration ranged from 0.500 mg/L to 14 mg/L to encompass reasonable amounts of TiO_2 in surface freshwaters. The variability in this amount is debatable, although estimates the amounts released to US waters are between 800 and 2800 metric tons a year, with 9% to 37% passing through wastewater treatment plants into effluent. TiO_2 entrenching within biosolids (average 137 mg/kg, upper bounds >500 mg/kg) could be reintroduced to water systems after being spread on agriculture fields[46]. Additional uncertainty as a result of urban runoff must also be considered[19]. The TiO_2 range will encompass current measured TiO_2 NP amounts in effluents, while allowing for uncertainty in future concentrations, or point release events.

Generation rates showed significant increases correlated directly with increases in TiO_2 concentration. Radical generation across 48 hours under all conditions could be described as linear, and generation rate was determined from the slope of the linear regression across 48 hours. These rates and R^2 are listed in Table 2.6. Radical generation was the greatest with the highest TiO_2 concentrations (14 mg/L), particularly under higher UV-A light intensities. These exposures consistently generated such excess hydroxyl radicals that the fluorescent dye used to measure generation was routinely diminished around the 36-hour mark, such that increased concentrations of dye were required.

These results fall in line with expected dependence of radical rate on TiO_2 concentration. Increased concentrations allow for photon impingement on a greater surface area, generating more electron-hole pairs. This in turn generates more overall hydroxyl radicals per hour. These results are in agreement with multiple researchers[18,25], and correlate well with organismal toxicity, both presented later in this chapter, and from literature[25].

Rate generation increased significantly as light intensity was increased. This is in agreement with literature[35,62,103], and also well correlated to organism toxicity[20]. Reciprocity effects were apparent in samples; exposures with low concentrations of TiO_2 exposed to high UV intensities had similar rates of high concentrations of TiO_2 exposed to low intensities of light. UV-A is attenuated by DOC, with a hyperbolic inflection point occurring at 1-2 mg/L DOC[104]. In waters of less than 2 mg/L of DOC, UV-A has a 1% attenuation depth (that is, the depth at which 1% of surface irradiation will penetrate) of 2 to 12 meters[13]. The testing intensities mimic those found at depths of 0 to 10 meters in water columns of ranging DOC concentrations.

The testing intensities were lower than some reported in literature, but the significance of the radical generation at these low intensities should not be understated. The intensities studied generally occur lower in water columns, so increased rates of hydroxyl radical generation from TiO_2 irradiation occurring in upper levels of the water, with higher UV intensity is expected. TiO_2 NPs will aggregate, and settle over time, with higher concentrations settling more quickly. Keller et al. made settling measurements of multiple TiO_2 NP concentration and found that aggregates below 300 nm remain stable in suspension. Concentrations of 10 mg/L TiO_2 NPs have sedimentation rates that range from 10^{-7} to 10^{-4} per second, with faster sedimentation occurring in waters with higher ionic strengths[26]. Brunelli found low settling rates (10^{-6} to 10^{-5} per second) in freshwater at 1mg/L and lower concentrations of TiO_2 after 50-hrs. These results indicate that substantial amounts of TiO_2 will be suspended in freshwater water column and exposed to sunlight. The test intensities may therefore be reflective of the lower end of radical generation rates.

Rate generation significantly decreased on the addition of natural organic matter, at all concentrations and under all intensities. Although there is little published data on the effect of NOM on TiO_2 radical generation, these results are well correlated with toxicity data, showing that increased amounts of NOM provide a protective effect against toxicity to *D. magna* [27] and to *Chlorella* sp.[28] resulting from TiO_2 irradiation. Implications of the decreased radical generation rates associated with the toxicity data indicate that either less generation of hydroxyl radical is occurring due to decreased light penetration to samples, or a result of NOM quenching radicals as they are formed. Thus, the decrease in measured generation rate is a result of the immediate quenching of the radical by the many oxidizable functionalities of NOM. Correlations

to toxicity and hydroxyl radical concentration are made later in this chapter to provide additional evidence for this claim.

Our DOC concentration range, 0 mg/L (as negative controls) to 5.71 mg/L fall within the ranges for multiple locations within the United States (1.7 m/L to 8.7 mg/L)[27,28]. DOC concentration will vary substantially however, with concentrations ranging to much higher values[55] For example, undiluted Suwanee River water used in this experiment has 61.34 mg/L. TiO_2 photocatalysis is able to break down humic acids, removing up to 80% of DOC and 90% of UV_{254} absorbance[87,93,105] and has been used as a method to reduce filter biofouling[7]. Additionally, drought-induced acidification (from the reoxidation of sediment sulfur) of freshwater arboreal lakes results in DOC decreases sufficient enough to increase UV penetration depth by 3-fold. This is a relevant issue with significant relevance due to worldwide climate change events[106].

Acute Toxicity of TiO_2 Nanoparticles to D. magna

Daphnia magna mortality was dependent on the interplay between TiO_2 concentration, UV intensity, and DOC concentration (Figure 2.8). A 3 order of magnitude increase in toxicity occurred when *D. magna* were co-exposed to TiO_2 nanoparticles and UV-A radiation, a well-documented phenomenon[78]. The toxicity was significantly attenuated with DOC addition, but still generated a 138-fold more toxic response than in UV negative exposures. The UV exposed LC_{50} (0.220 mg/L) is comparable to multiple literature sources 0.030 μg/L[17], 1.2 mg/L[14], 0.85 mg/L[55], considering variation for light intensity. Natural organic matter attenuation is not well studied in literature, although NOM included toxicity results (LC_{50}: 8.55 mg/L) compare with Wormington, et al., where significant decreases in toxicity from UV-A irradiated TiO_2 NPs when exposing *D. magna* to 2 mg/L and 4 mg/L DOC were observed[55]. Lin et al. (2012) saw

toxicity attenuation in *Chlorella* sp. from 4.9 mg/L to 18 mg/L TiO_2 NP in 5 mg/L humic acid[69].

The variability in reported toxicities can be attributed to exposure conditions, as normalization regarding UV intensity, or DOC, in toxicity testing of TiO_2 NPs can be difficult to control. This is not a detriment, as precisely controlled conditions never exist outside the laboratory, so a wealth of data over a variety of conditions is rather helpful. In order to overcome this variability, determining toxicity with respect to hydroxyl radicals instead of TiO_2 nanoparticles may provide for greater consistency.

Acute Toxicity of Hydroxyl Radical to D. magna

Measuring hydroxyl radical generation under identical conditions to *D. magna* bioassays allowed us to correlate toxicity with hydroxyl radicals (Figure 2.9). Doing so will enable the quantification of the contributions of light intensity and DOC. Exposures without NOM had a rapid increase in toxicity per µM of hydroxyl radical, resulting in LC_{50} mortality at 0.451 µM $OH^{\bullet}$. Including DOC results in attenuation of toxicity to 6.5 µM $OH^{\bullet}$. At $LC_{50,}$ the rate of hydroxyl radical generation in the 4.28 mg/L DOC exposures is ~ 0.203 µM/h, while in the 0 mg/L DOC exposures, rate is ~ 0.0141 µM/h. The rate difference is a result of much more TiO_2 need to produce a toxic effect in suspensions with DOC.

The toxic effect therefore appears to be a result of the rate of radical generation overwhelming the organism. In exposures with DOC more radicals are required to cause induce equivalent toxic effects, a result that must be attributed to radical quenching by NOM.

Due to the short lifetime of hydroxyl radicals, the nanoparticle needs to be in extremely close proximity to the organism to cause effects. Increasing the amounts of TiO_2 would allow for more particles and hydroxyl generation to interact with the organism. If quenching was not a

factor, similar toxicity at equivalent amounts of TiO_2 would be expected, regardless of DOC concentration. In the presence of NOM, there is a competitive date for hydroxyl radical quenching between NOM and the organism. Increased concentrations of TiO_2 NPs resulting in increased radical generation of equivalent toxicity due to increased DOC concentrations must be attributed to a mechanism of attenuation. Although the implications of radical detoxification on organisms is important to understand, it is outside the scope of this study. This would be a worthwhile avenue of investigation for future studies.

CONCLUSION:

In an effort to harmonize TiO_2 toxicity measurements, radical generation rate was measured under a full factorial experiment incorporating environmentally realistic TiO_2 NP, and DOC concentrations, and UV-A intensities that would reasonably be found in multiple depths of the water column in surface freshwaters. The developed method is simple and robust. The range of rates measured help to explain how the radical generation from irradiated TiO_2 is affected by conditional changes, relevant spatially and temporally. Organism toxicity is correlated to hydroxyl radical generation, allowing the effects of UV light and DOC to be accounted for. Further, by describing mortality in terms of the hydroxyl radical, provides more insight on to NOM's contributions to radical quenching as a means to attenuate organismal toxicity. Moving forward, this rate data will be used to construct a model to predict radical generation rate, reducing the need for time-consuming benchtop chemistry.

Tables and Figures:

Table 2.1: Elemental Analysis of Suwanee River Water. Elemental analysis of filtered Suwannee River Water by ICP/MS. Content was consistent with elemental analysis of Suwannee River NOM certified by the Humic Substances Society.

Sample	P	K	Ca	Mg	Zn	Cu
	ppm	ppm	ppm	ppm	ppm	ppm
1	0.071	1.735	2.698	1.186	0.012	0.008
2	0.066	1.699	2.669	1.184	0.012	0.009
3	0.074	1.683	2.673	1.191	0.012	0.007
Ave	**0.070**	**1.706**	**2.680**	**1.187**	**0.012**	**0.008**
Std Dev	*0.003*	*0.022*	*0.013*	*0.003*	*0.0000*	*0.001*
Sample	Mn	Fe	S	Na	B	Al
	ppm	ppm	ppm	ppm	ppm	ppm
1	0.030	1.150	0.923	5.647	0.025	0.830
2	0.029	1.143	0.937	5.536	0.024	0.804
3	0.028	1.168	0.916	5.505	0.024	0.834
Ave	**0.029**	**1.154**	**0.925**	**5.563**	**0.024**	**0.823**
Std Dev	*0.001*	*0.011*	*0.009*	*0.061*	*0.001*	*0.013*

Hydrodynamic diameter at 0 hrs

Table 2.2A: Size of TiO_2 and NOM aggregates (nm) at 0 hrs. Aggregate size determined by DLS. UV light intensity measured as µW/cm^2/nm, NOM measured as mg/L DOC. Graphs of data can be found in Appendix C.

0.5 mg/L TiO2					
Light	**0 mg/L DOC**	**1.57 mg/L DOC**	**2.95 mg/L DOC**	**4.28 mg/L DOC**	**5.71 mg/L DOC**
0	125 ± 24	158 ± 30	132 ± 16	84 ± 12	186 ± 24
2.761	95 ± 28	183 ± 24	204 ± 20	104 ± 10	123 ± 26
4.301	61 ± 12	107 ± 33	70 ± 10	83 ± 18	88 ± 10
5.177	81 ± 24	81 ± 16	102 ± 14	134 ± 14	108 ± 20
1.0 mg/L TiO2					
Light	**0 mg/L DOC**	**1.57 mg/L DOC**	**2.95 mg/L DOC**	**4.28 mg/L DOC**	**5.71 mg/L DOC**
0	130 ± 48	60 ± 30	124 ± 32	147 ± 20	133 + 22
2.761	96 ± 20	117 ± 22	89 ± 20	120 ± 20	75 ± 12
4.301	119 ± 16	97 ± 22	94 ± 14	81 ± 22	75 ± 20
5.177	110 ± 14	131 ± 26	138 ± 26	139 ± 36	84 ± 30
3.5 mg/L TiO2					
Light	**0 mg/L DOC**	**1.57 mg/L DOC**	**2.95 mg/L DOC**	**4.28 mg/L DOC**	**5.71 mg/L DOC**
0	189 ± 48	157 ± 26	235 + 34	253 ± 48	237 ± 42
2.761	145 ± 22	164 ± 56	142 ± 40	115 ± 36	178 ± 34
4.301	156 ± 20	135 ± 24	111 ± 22	164 ± 22	135 ± 28
5.177	166 ± 14	143 ± 26	207 ± 48	163 ± 40	154 ± 30
5.0 mg/L TiO2					
Light	**0 mg/L DOC**	**1.57 mg/L DOC**	**2.95 mg/L DOC**	**4.28 mg/L DOC**	**5.71 mg/L DOC**
0	214 ± 46	146 ± 40	277 ± 74	210 ± 64	161 ± 26
2.761	105 ± 26	155 ± 58	239 ± 66	204 ± 50	229 ± 68
4.301	218 ± 42	155 ± 30	169 ± 38	x	132 ± 34
5.177	204 ± 92	186 ± 40	233 ± 40	202 ± 72	197 ± 28
7.0 mg TiO2/L					
Light	**0 mg/L DOC**	**1.57 mg/L DOC**	**2.95 mg/L DOC**	**4.28 mg/L DOC**	**5.71 mg/L DOC**
0	204 ± 32	277 ± 52	225 ± 24	206 ± 40	187 ± 72
2.761	258 ± 96	217 ± 46	220 ± 72	179 ± 44	165 ± 44
4.301	261 ± 50	184 ± 50	208 ± 64	168 ± 42	204 ± 50
5.177	249 ± 92	208 ± 82	205 ± 36	284 ± 72	192 ± 72
10.5 mg/L TiO2					
Light	**0 mg/L DOC**	**1.57 mg/L DOC**	**2.95 mg/L DOC**	**4.28 mg DOC**	**5.71 mg/L DOC**
0	251 ± 94	191 ± 166	224 ± 42	209 ± 52	245 ± 60
2.761	206 ± 44	222 ± 64	172 ± 102	199 ± 50	187 ± 36
4.301	279 ± 56	292 ± 112	208 ± 70	190 ± 62	194 42
5.177	266 ± 124	250 ± 80	225 ± 64	231 ± 52	308 ± 50
14 mg/L TiO2					
Light	**0 mg/L DOC**	**1.57 mg/L DOC**	**2.95 mg/L DOC**	**4.28 mg/L DOC**	**5.71 mg/L DOC**
0	357 ± 96	215 ± 206	245 ± 60	245 ± 102	242 ± 72
2.761	238 ± 52	295 ± 84	196 ± 62	184 ± 46	235 ± 56
4.301	470 ± 150	208 ± 70	208 ± 70	195 ± 32	212 ± 42
5.177	237 ± 60	219 ± 80	251 ± 30	224 ± 48	237 ± 52

Hydrodynamic diameter at 24 hrs

Table 2.2B: Size of TiO_2 + NOM aggregates (nm) at 24 hrs. Aggregate size determined by DLS. UV light intensity measured as µW/cm^2/nm, NOM measured as mg/L DOC. Graphs of data can be found in Appendix C.

0.5 mg TiO2					
Light	**0 mg/L DOC**	**1.57 mg/L DOC**	**2.95 mg/L DOC**	**4.28 mg/L DOC**	**5.71 mg/L DOC**
0	66 ± 12	201 ± 36	107 ± 8	99 ± 10	107 ± 34
2.761	85 ± 12	102 ± 20	126 24	76 ± 22	87 ± 18
4.301	95 ± 16	81 ± 14	108 ± 22	196 ± 32	95 ± 12
5.177	124 ± 16	214 ± 34	222 ± 40	91 ± 12	91 ± 16
1.0 mg TiO2					
Light	**0 mg/L DOC**	**1.57 mg/L DOC**	**2.95 mg/L DOC**	**4.28 mg/L DOC**	**5.71 mg/L DOC**
0	68 ± 10	112 ± 22	95 ± 8	134 ± 24	137 ± 24
2.761	176 22	390 ± 336	157 ± 28	105 ± 26	121 ± 22
4.301	101 ± 18	145 ± 14	103 ± 16	94 ± 16	136 ± 16
5.177	106 ± 18	106 ± 14	32 ± 2	89 ± 12	142 ± 20
3.5 mg TiO2					
Light	**0 mg DOC**	**1.57 mg DOC**	**2.95 mg DOC**	**4.28 mg DOC**	**5.71 mg DOC**
0	119 ± 28	132 ± 36	204 ± 28	181 ± 32	160 ± 28
2.761	148 ± 26	256 ± 34	204 66	125 ± 20	x
4.301	284 ± 70	87 ± 14	88 ± 12	260 ± 74	127 ± 24
5.177	79 ± 14	79 ± 48	121 ± 22	73 ± 18	111 ± 16
5.0 mg TiO2					
Light	**0 mg/L DOC**	**1.57 mg/L DOC**	**2.95 mg/L DOC**	**4.28 mg/L DOC**	**5.71 mg/L DOC**
0	150 ± 28	139 ± 32	133 ± 48	187 ± 48	183 ± 62
2.761	153 ± 28	150 ± 34	214 ± 40	180 ± 34	158 ± 20
4.301	231 ± 32	96 ± 12	127 ± 24	124 ± 16	380 ± 80
5.177	138 ± 14	138 ± 220	553 ± 130	101 ± 22	39 ± 8
7.0 mg TiO2					
Light	**0 mg DOC**	**1.57 mg DOC**	**2.95 mg DOC**	**4.28 mg DOC**	**5.71 mg DOC**
0	292 ± 214	202 ± 48	230 ± 28	175 ± 34	170 ± 34
2.761	47 ± 48	183 ± 34	216 ± 44	177 ± 56	187 ± 42
4.301	159 ± 26	121 ± 16	217 ± 40	225 ± 22	323 ± 56
5.177	227 ± 36	227 ± 40	116 ± 32	101 ± 20	162 ± 34
10.5 mg TiO2					
Light	**0 mg DOC**	**1.57 mg DOC**	**2.95 mg DOC**	**4.28 mg DOC**	**5.71 mg DOC**
0	258 ± 56	207 ± 36	198 ± 34	200 ± 34	192 ± 40
2.761	229 ± 66	224 ± 38	253 ± 63	177 ± 36	180 ± 54
4.301	260 ± 50	303 ± 32	315 ± 80	157 ± 26	350 ± 50
5.177	251 ± 84	284 ± 62	173 ± 40	28 ± 6	206 ± 64
14 mg TiO2					
Light	**0 mg/L DOC**	**1.57 mg/L DOC**	**2.95 mg/L DOC**	**4.28 mg/L DOC**	**5.71 mg/L DOC**
0	251 ± 84	247 ± 66	229 ± 42	239 ± 54	181 ± 48
2.761	296 ± 92	300 ± 90	321 ± 146	190 ± 44	191 ± 40
4.301	295 ± 56	385 ± 68	559 ± 252	256 ± 62	213 ± 50
5.177	623 ± 226	x	617 ± 144	370 ± 92	474 ± 64

Hydrodynamic diameter at 48 hrs

Table 2.2C: Size of TiO_2 + NOM aggregates (nm) at 48 hrs. Aggregate size determined by DLS. UV light intensity measured as µW/cm^2/nm, NOM measured as mg/L DOC. Graphs of data can be found in Appendix C.

0.5 mg TiO2					
Light	**0 mg/L DOC**	**1.57 mg/L DOC**	**2.95 mg/L DOC**	**4.28 mg/L DOC**	**5.71 mg/L DOC**
0	153 ± 26	143 ± 24	122 ± 30	138 ± 24	234 ± 42
2.761	135 ± 24	85 ± 18	88 ± 14	141 ± 14	76 ± 10
4.301	75 ± 14	88 ± 14	105 ± 24	98 ± 16	180 ± 72
5.177	25 ± 2	112 ± 2	8 ± 2	176 ± 16	99 ± 18
1.0 mg TiO2					
Light	**0 mg/L DOC**	**1.57 mg/L DOC**	**2.95 mg/L DOC**	**4.28 mg/L DOC**	**5.71 mg/L DOC**
0	168 ± 12	43 ± 22	154 ± 12	150 ± 32	134 ± 30
2.761	109 ± 12	88 ± 14	77 ± 22	110 ± 16	95 ± 14
4.301	112 ± 14	253 ± 34	90 ± 12	120 ± 18	134 ± 12
5.177	55 ± 10	5 ± 1	14 ± 2	78 ± 10	173 ± 40
3.5 mg TiO2					
Light	**0 mg/L DOC**	**1.57 mg/L DOC**	**2.95 mg/L DOC**	**4.28 mg/L DOC**	**5.71 mg/L DOC**
0	179 ± 56	150 ± 24	128 ± 36	144 ± 34	155 ± 28
2.761	103 ± 34	149 ± 28	96 ± 30	118 ± 32	126 ± 24
4.301	32 ± 2	49 ± 10	54 ± 12	96 ± 18	76 ± 12
5.177	52 ± 12	49 ± 6	62 ± 12	119 ± 16	304 ± 92
5.0 mg TiO2					
Light	**0 mg/L DOC**	**1.57 mg/L DOC**	**2.95 mg/L DOC**	**4.28 mg/L DOC**	**5.71 mg/L DOC**
0	129 ± 22	139 ± 32	189 ± 30	171 ± 14	80 ± 30
2.761	212 ± 46	116 ± 32	167 ± 46	179 ± 48	167 ± 62
4.301	188 ± 20	220 ± 32	149 ± 20	131 ± 14	38 ± 8
5.177	63 ± 12	117 ± 26	155 ± 30	25 ± 4	340 ± 42
7.0 mg TiO2					
Light	**0 mg/L DOC**	**1.57 mg/L DOC**	**2.95 mg/L DOC**	**4.28 mg/L DOC**	**5.71 mg/L DOC**
0	179 ± 34	195 ± 34	161 ± 28	140 ± 34	91 ± 38
2.761	186 ± 32	195 ± 50	235 ± 66	206 ± 54	171 ± 36
4.301	243 ± 34	118 ± 34	255 ± 44	211 ± 26	125 ± 34
5.177	139 ± 30	258 ± 44	222 ± 34	73 ± 10	266 ± 52
10.5 mg TiO2					
Light	**0 mg/L DOC**	**1.57 mg/L DOC**	**2.95 mg/L DOC**	**4.28 mg/L DOC**	**5.71 mg/L DOC**
0	160 ± 32	186 ± 52	189 ± 40	246 ± 62	118 ± 48
2.761	201 ± 46	174 ± 42	272 ± 86	205 ± 46	220 ± 42
4.301	380 ± 102	209 ± 52	454 ± 130	153 ± 26	208 ± 34
5.177	439 ± 168	363 ± 186	340 ± 84	244 ± 74	148 ± 36
14 mg TiO2					
Light	**0 mg/L DOC**	**1.57 mg/L DOC**	**2.95 mg/L DOC**	**4.28 mg/L DOC**	**5.71 mg/L DOC**
0	217 ± 58	238 ± 56	196 ± 44	199 ± 34	198 ± 208
2.761	212 ± 48	194 ± 48	196 ± 52	180 ± 56	212 ± 46
4.301	222 ± 74	260 ± 60	331 ± 102	383 ± 84	357 ± 72
5.177	203 ±40	243 ± 76	x	204 ± 70	339 ± 90

*Table 2.3: Zeta Potential of TiO_2/*Natural Organic Matter (NOM) Suspension. 0 hour *zeta potentials of suspensions of increasing TiO_2 concentrations and increasing DOC concentrations*

	0 mg/L DOC		**1.57 mg/L DOC**		**2.95 mg/L DOC**		**4.28 mg/L DOC**		**5.71 mg/L DOC**	
TiO_2 mg/L	mV	Std Dev	mV	Std Dev	mV	Std Dev	mV	Std Dev	mV	Std Dev
0	n.a.	n.a.	-11.43	0.21	-11.54	2.66	-14.07	2.12	-15.07	0.94
0.5	-13.97	0.58	-17.67	0.90	-15.63	0.35	-14.37	0.51	-16.93	1.58
1	-14.83	0.59	-16.03	0.32	-15.80	0.69	-12.83	0.65	-14.87	1.57
3.5	-14.03	0.12	-13.10	0.27	-15.67	1.05	-15.90	0.36	-16.27	1.01
5	-13.60	0.56	-17.20	0.58	-16.90	0.40	-20.37	0.38	-15.33	1.29
7	-14.33	0.55	-15.77	0.58	-16.90	0.61	-16.57	0.55	-16.50	0.53
10.5	-14.27	0.23	-15.57	0.51	-15.13	0.12	-14.93	0.31	-20.03	0.38
14	-14.37	0.38	-16.30	0.82	-12.10	0.36	-15.57	0.21	-15.97	0.25

Table 2.4. Decrease of UV-A Transmission through Moderately Hard Water with Increasing NOM Concentrations. Decrease in incident light intensity as DOC concentration is increased in MHW. Associated with Figure 2.3

% Transmission at 365 nm									
0 mg/L DOC	0.5 mg/L DOC	1.0 mg/L DOC	2.5 mg/L DOC	5.0 mg/L DOC	10 mg/L DOC	20 mg/L DOC	40 mg/L DOC	50 mg/L DOC	60 mg/L DOC
100.05	**99.72**	**98.53**	**95.97**	**90.85**	**84.40**	**68.09**	**54.08**	**46.01**	**40.85**

Table 2.5. Absolute Irradiance from CLX-Blacklight Blue Fluorescent Bulb Ultraviolet-A (UV-A) Light Exposure System. Absolute irradiance measurements associated with Figure 2.4.

Light	Maximum Abs Irradiance (365 nm)	Average Abs Irradiance (320 nm to 400 nm)
Dual Light	10.833 (±0.054)	5.188 (±0.032)
Single Light	9.578 (±0.034)	4.301 (±0.017)
Screened Light	6.263 (±0.012)	2.671 (±0.004
Sunlight	50.86 (±0.023)	45.08 (±0.012)

Table 2.6: Hydroxyl Generation Rate at Varying TiO_2, Dissolved Organic Carbon (DOC)Concentrations and UV-A Intensities. Rate Generation at Varying TiO_2, DOC, and UV intensity. TiO_2 concentration in mg/L, DOC in mg/L, and UV intensity in $\mu W/cm^2/s$. Non-similar letters indicate significant difference. This data is graphed in Figure 2.7.

TiO_2	UV	DOC	Rate	R^2	Std Dev
0.5	0	0	0.009	0.7128	0.0015
0.5	0	1.57	0	0.9513	0.0006
0.5	0	2.95	0	0.879	0.0333
0.5	0	4.28	0	0.525	0.0009
0.5	0	5.71	0.0004	0.4218	0.0009
1	0	0	0	0.711	0.0007
1	0	1.57	0	0.9564	0.0165
1	0	2.95	0	0.8861	0.0333
1	0	4.28	0	0.818	0.0016
1	0	5.71	0	0.333	0.0006
3.5	0	0	0.0006	0.7612	0.0020
3.5	0	1.57	0.0009	0.9891	0.0008
3.5	0	2.95	0	0.9023	0.0335
3.5	0	4.28	0	0.77	0.0004
3.5	0	5.71	0	0.367	0.0008
5	0	0	0	0.6721	0.0006
5	0	1.57	0.0003	0.9835	0.0005
5	0	2.95	0.0007	0.894	0.0331
5	0	4.28	0	0.793	0.0012
5	0	5.71	0	0.264	0.0011
7	0	0	0.0024	0.4651	0.0005
7	0	1.57	0.0012	0.9588	0.0012
7	0	2.95	0.0019	0.879	0.0336
7	0	4.28	0.001	0.919	0.0004
7	0	5.71	0.0004	0.4072	0.0012
10.5	0	0	0.0005	0.4665	0.0004
10.5	0	1.57	0.0021	0.9046	0.0006
10.5	0	2.95	0.004	0.875	0.0332
10.5	0	4.28	0.002	0.798	0.0005
10.5	0	5.71	0.0045	0.577	0.0095
14	0	0	0.0027	0.638	0.0016
14	0	1.57	0.0016	0.9114	0.0004
14	0	2.95	0.0026	0.942	0.0337
14	0	4.28	0	0.99	0.0010
14	0	5.71	0	0.097	0.0016

TiO_2	UV	DOC	Rate	R^2	Std Dev
0.5	2.671	0	0.0287	0.8145	0.0127
0.5	2.671	1.57	0.0071	0.8632	0.0096
0.5	2.671	2.95	0.0026	0.9000	0.0018
0.5	2.671	4.28	0.0034	0.5615	0.0015
0.5	2.671	5.71	0.0036	0.9243	0.0014
1	2.671	0	0.0679	0.9271	0.0158
1	2.671	1.57	0.0163	0.9856	0.0183
1	2.671	2.95	0.0077	0.9676	0.0010
1	2.671	4.28	0.0077	0.9296	0.0022
1	2.671	5.71	0.0060	0.8226	0.0001
3.5	2.671	0	0.1189	0.9569	0.0110
3.5	2.671	1.57	0.0966	0.8699	0.0019
3.5	2.671	2.95	0.0695	0.8863	0.0087
3.5	2.671	4.28	0.0278	0.9913	0.0030
3.5	2.671	5.71	0.0659	0.8852	0.0050
5	2.671	0	0.2063	0.9998	0.0052
5	2.671	1.57	0.1306	0.9925	0.0025
5	2.671	2.95	0.0625	0.9897	0.0039
5	2.671	4.28	0.0541	0.9963	0.0046
5	2.671	5.71	0.0345	0.9983	0.0031
7	2.671	0	0.2019	0.9973	0.0162
7	2.671	1.57	0.1866	0.9956	0.0225
7	2.671	2.95	0.1778	0.9680	0.0095
7	2.671	4.28	0.1109	0.9505	0.0258
7	2.671	5.71	0.0873	0.8860	0.0078
10.5	2.671	0	0.3240	0.9841	0.0165
10.5	2.671	1.57	0.3013	0.9966	0.0189
10.5	2.671	2.95	0.2651	0.9867	0.0198
10.5	2.671	4.28	0.2148	0.9998	0.0201
10.5	2.671	5.71	0.1482	0.9642	0.0274
14	2.671	0	0.4223	0.9906	0.0088
14	2.671	1.57	0.4011	0.9975	0.0085
14	2.671	2.95	0.3925	0.9869	0.0086
14	2.671	4.28	0.3156	0.9911	0.0373
14	2.671	5.71	0.2630	0.9884	0.0304

TiO_2	UV	DOC	Rate	R^2	Std Dev
0.5	4.301	0	0.0274	0.8783	0.0036
0.5	4.301	1.57	0.0078	0.9717	0.0006
0.5	4.301	2.95	0.0035	0.7139	0.0018
0.5	4.301	4.28	0.0027	0.7816	0.0009
0.5	4.301	5.71	0.0028	0.7892	0.0003
1	4.301	0	0.0594	0.9563	0.0050
1	4.301	1.57	0.0186	0.7378	0.0010
1	4.301	2.95	0.0143	0.9074	0.0010
1	4.301	4.28	0.0067	0.8690	0.0009
1	4.301	5.71	0.0053	0.9602	0.0020
3.5	4.301	0	0.1578	0.8277	0.0273
3.5	4.301	1.57	0.0982	0.9389	0.0312
3.5	4.301	2.95	-	-	-
3.5	4.301	4.28	0.0650	0.8680	0.0030
3.5	4.301	5.71	0.0374	0.9566	0.0020
5	4.301	0	-	-	-
5	4.301	1.57	0.1172	0.9860	0.0008
5	4.301	2.95	0.1277	0.9920	0.0039
5	4.301	4.28	0.0505	0.9857	0.0060
5	4.301	5.71	0.0355	0.9765	0.0020
7	4.301	0	0.3233	0.9726	0.0485
7	4.301	1.57	0.2759	0.9829	0.0357
7	4.301	2.95	0.1192	0.9088	0.0108
7	4.301	4.28	0.1342	0.9713	0.0258
7	4.301	5.71	0.0873	0.9818	0.0009
10.5	4.301	0	0.5869	0.9688	0.0718
10.5	4.301	1.57	0.4240	0.9840	0.0293
10.5	4.301	2.95	0.3723	0.9901	0.0798
10.5	4.301	4.28	0.3063	0.9942	0.0201
10.5	4.301	5.71	0.1460	0.9818	0.0128
14	4.301	0	0.7539	0.9840	0.0293
14	4.301	1.57	0.5854	0.9893	0.0644
14	4.301	2.95	0.5757	0.9720	0.0760
14	4.301	4.28	0.4163	0.9962	0.0373
14	4.301	5.71	0.2496	0.9798	0.0113

TiO_2	UV	DOC	Rate	R^2	Std Dev
0.5	5.188	0	0.0317	0.9878	0.0052
0.5	5.188	1.57	0.0179	0.9865	0.0016
0.5	5.188	2.95	0.0080	0.9768	0.0055
0.5	5.188	4.28	0.0089	0.9994	0.0032
0.5	5.188	5.71	0.0051	0.9622	0.0015
1	5.188	0	0.0693	0.9712	0.0041
1	5.188	1.57	0.0461	0.9889	0.0063
1	5.188	2.95	0.0191	0.9806	0.0015
1	5.188	4.28	0.0161	0.9593	0.0038
1	5.188	5.71	0.0112	0.9941	0.0020
3.5	5.188	0	0.5748	0.9999	0.0868
3.5	5.188	1.57	0.1891	0.9046	0.0411
3.5	5.188	2.95	0.1097	0.9288	0.0274
3.5	5.188	4.28	0.1976	0.9924	0.0051
3.5	5.188	5.71	0.0370	0.0954	0.0363
5	5.188	0	-	-	-
5	5.188	1.57	0.1876	0.9589	0.0101
5	5.188	2.95	0.1972	0.9598	0.0012
5	5.188	4.28	0.1257	0.9916	0.0060
5	5.188	5.71	0.0631	0.9600	0.0058
7	5.188	0	1.1375	0.9943	0.0296
7	5.188	1.57	0.5664	0.9825	0.0665
7	5.188	2.95	0.4543	0.9771	0.0379
7	5.188	4.28	0.3966	0.9793	0.0454
7	5.188	5.71	0.0797	0.8920	0.0472
10.5	5.188	0	1.4552	0.9992	0.0055
10.5	5.188	1.57	0.9077	0.9930	0.0493
10.5	5.188	2.95	0.7957	0.9852	0.0116
10.5	5.188	4.28	0.5239	0.9443	0.0471
10.5	5.188	5.71	0.5234	0.9683	0.0665
14	5.188	0	1.5701	0.9907	0.0440
14	5.188	1.57	1.0980	0.9714	0.0132
14	5.188	2.95	0.9872	0.9910	0.0374
14	5.188	4.28	0.8574	0.9537	0.0201
14	5.188	5.71	0.8186	0.9394	0.0058

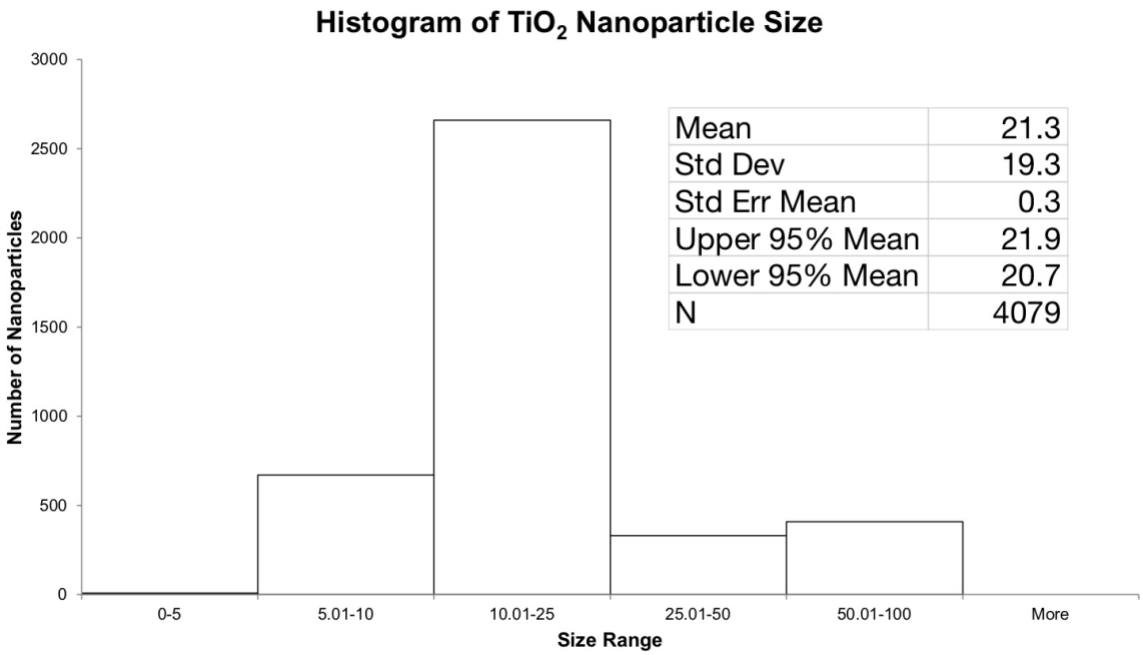

Figure 2.1 Size of TiO_2 Nanoparticle as Measured by Transmission Electron Microscope. Size of TiO_2 nanoparticles determined by TEM.

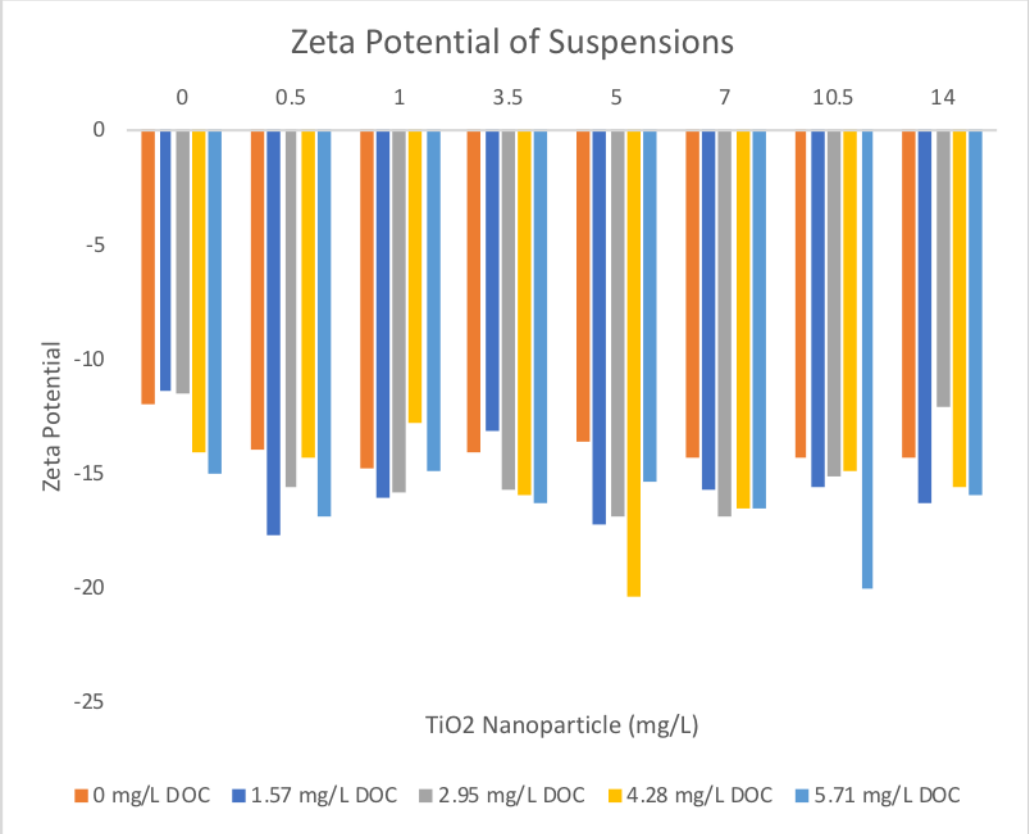

Figure 2.2 Change in Zeta Potential with Increasing TiO_2 and DOC Concentrations. Zeta potential of suspensions on increasing DOC and TiO_2 concentrations

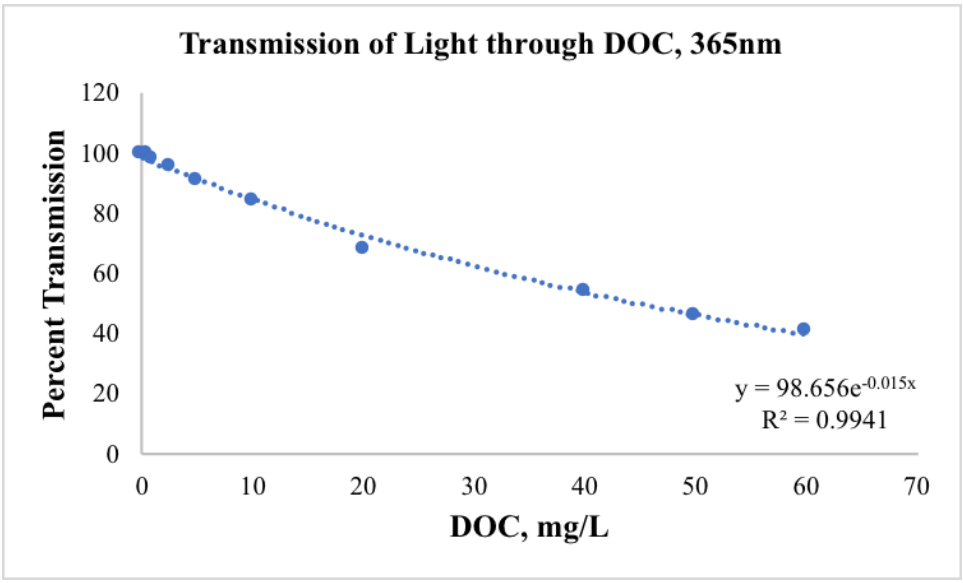

Figure 2.3 Decrease in Light Transmission through Water with Increasing Amounts of Natural Organic Matter. Increasing DOC concentration results in the exponential decrease of light transmission through MHW. Experimental working concentrations did not exceed 6mg/L, so it is the authors' opinion that screening effects were negligible.

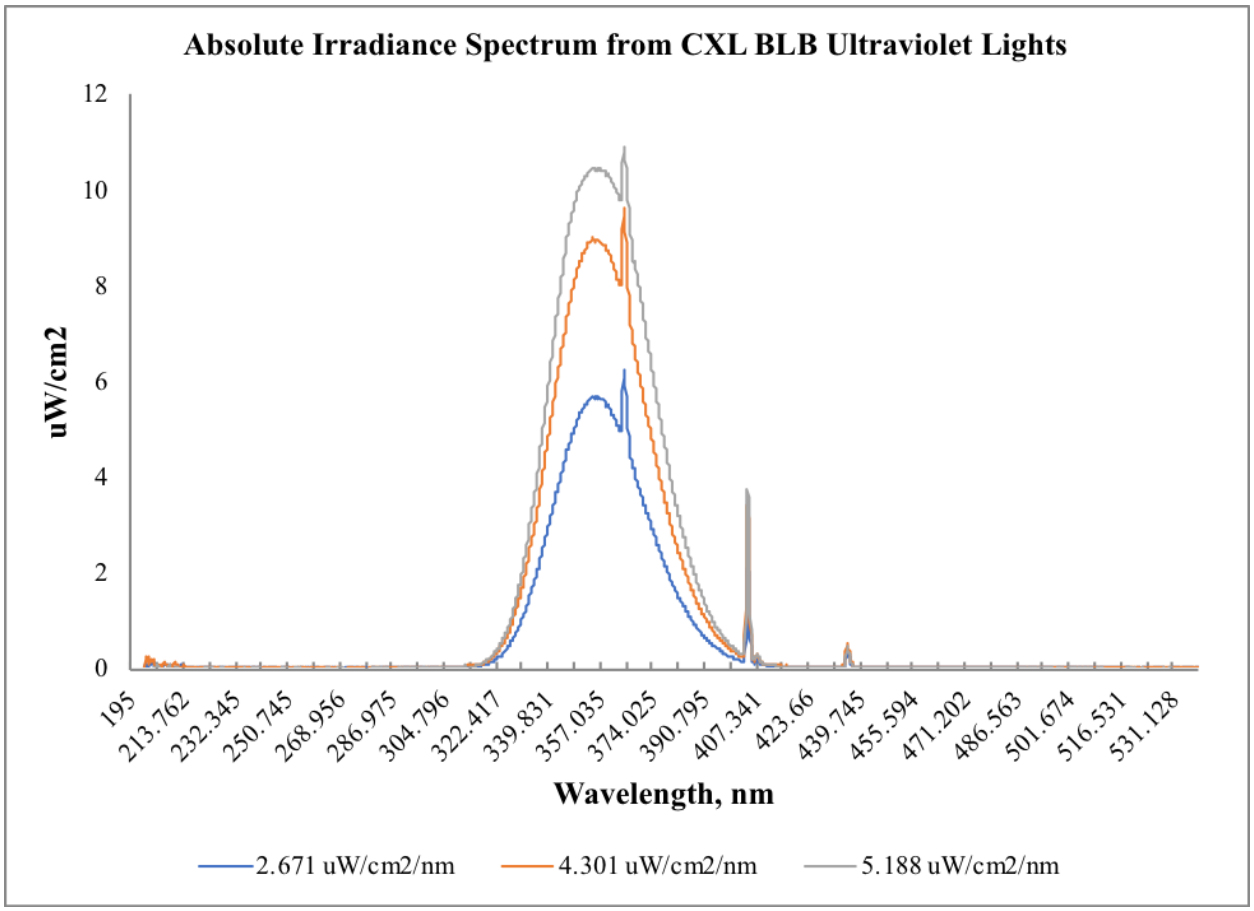

Figure 2.4 Absolute Irradiance Spectra of CLX-Blacklight Blue Fluorescent Bulbs. Absolute Irradiance Spectra from UV treatments. Peak wavelength is measured at 365 nm.

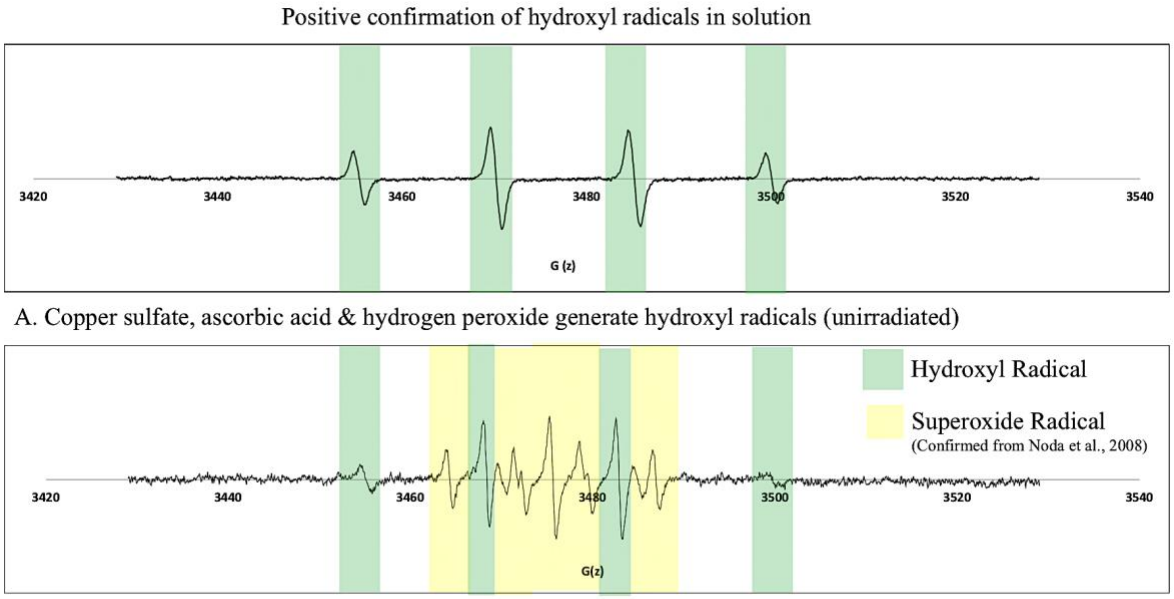

Figure 2.5 Spectra of ROS Characterized by Electron Paramagnetic Resonance Spectroscopy. EPR characterization of hydroxyl radical formation. Characterization of radicals formed in irradiated nano-TiO_2 suspensions. A) copper sulfate, ascorbic acid and hydrogen peroxide generate hydroxyl radical without irradiation. B) TiO_2 nanoparticles under ultraviolet irradiation generate a hydroxyl radical signature, along with signatures for superoxide. DMPO was used as a spin trap to generate both EPR spectra.

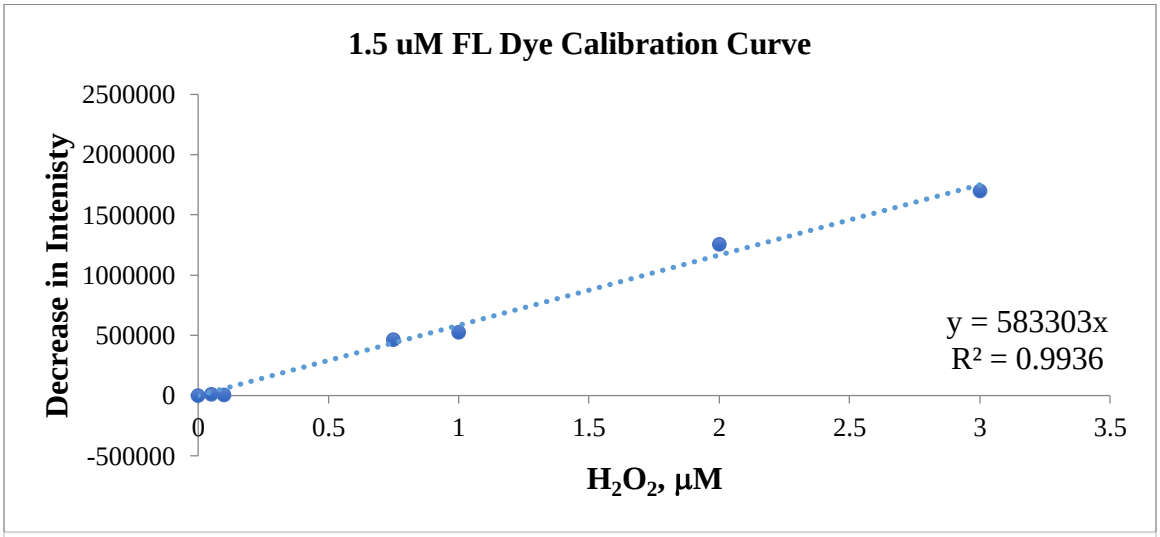
1.5 uM FL Dye Calibration Curve
Decrease in Intenisty
2500000
2000000
1500000
1000000
500000
0
-500000
0
0.5
1
1.5
2
2.5
3
3.5
y = 583303x
R² = 0.9936
H2O2, µM

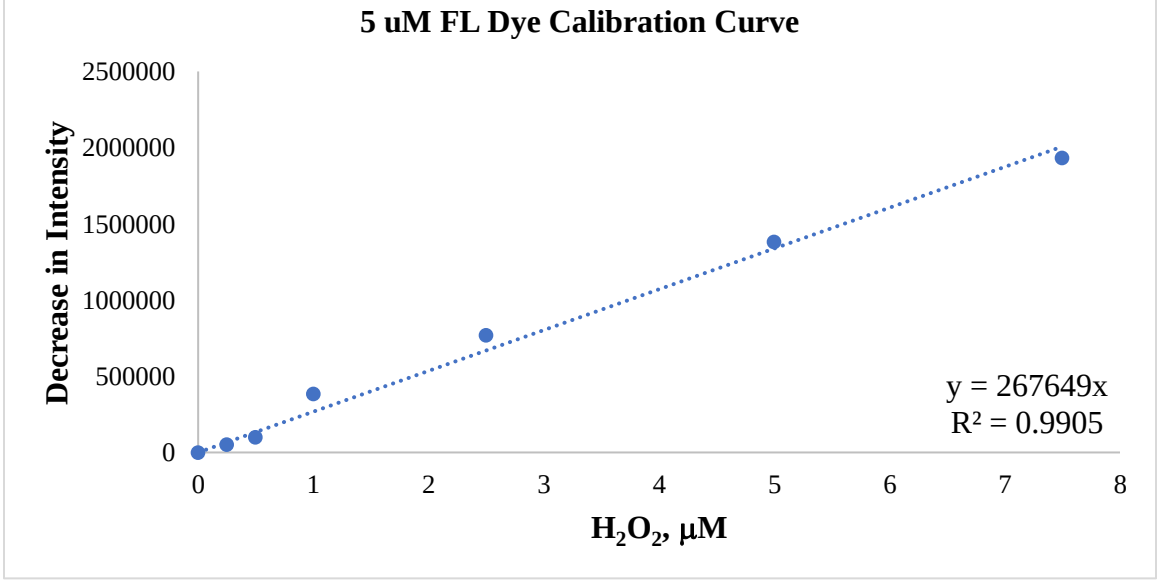
5 uM FL Dye Calibration Curve
Decrease in Intensity
2500000
2000000
1500000
1000000
500000
0
0
1
2
3
4
5
6
7
8
y = 267649x
R² = 0.9905
H2O2, µM

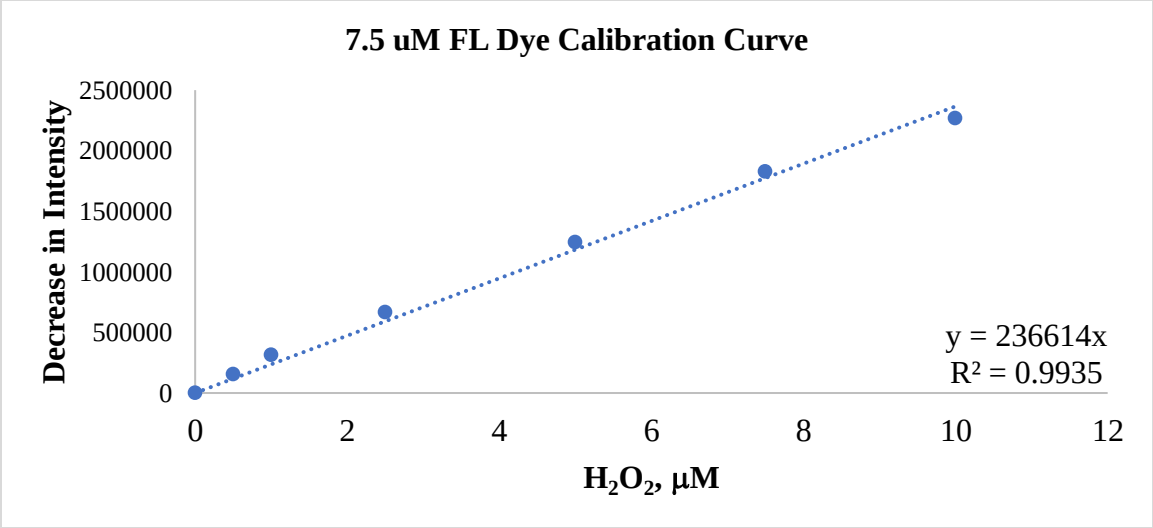

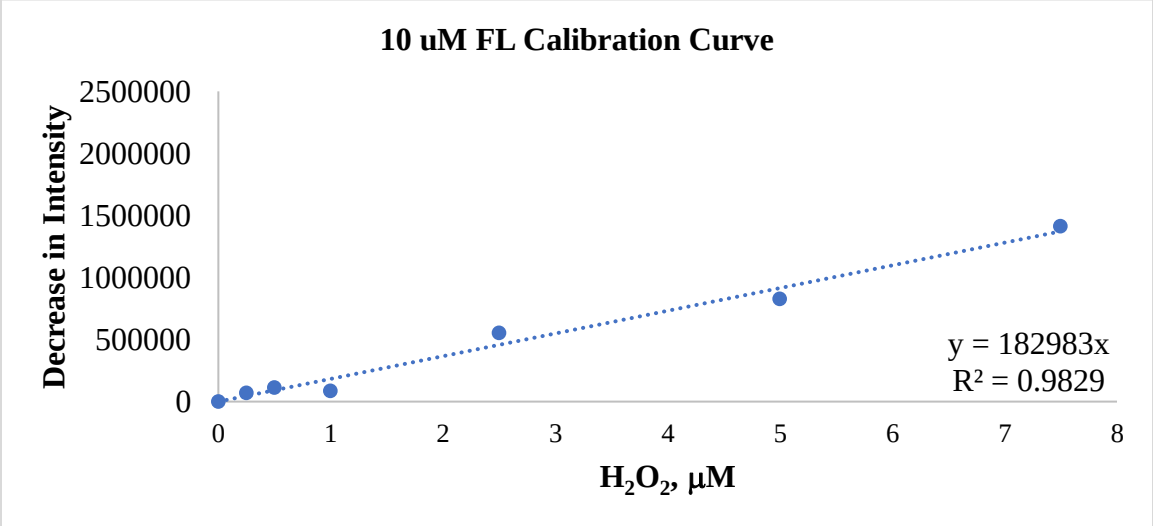

Figure 2.6 Hydroxyl Radical Concentration Calibration Curves as Measured by Fluorescence Spectroscopy. Calibration curves for varying dye concentrations. A: 1.5 µM fluorescein dye; B: 5.0 µM fluorescein dye; C: 7.5 µM fluorescein dye; D: 10.0 µM fluorescein dye.

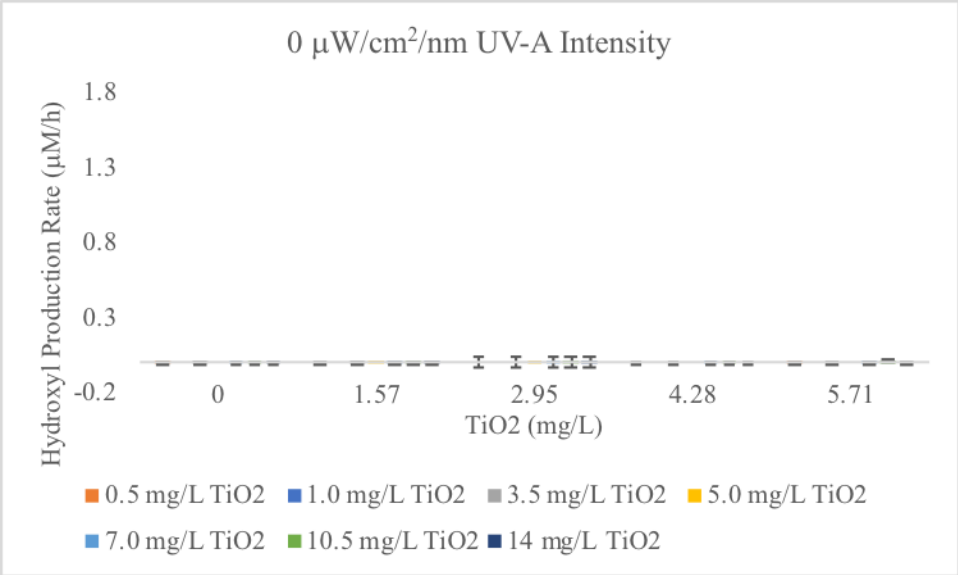
0 µW/cm²/nm UV-A Intensity
Hydroxyl Production Rate (µM/h)
1.8
1.3
0.8
0.3
-0.2
0
1.57
2.95
4.28
5.71
TiO2 (mg/L)
0.5 mg/L TiO2
1.0 mg/L TiO2
3.5 mg/L TiO2
5.0 mg/L TiO2
7.0 mg/L TiO2
10.5 mg/L TiO2
14 mg/L TiO2

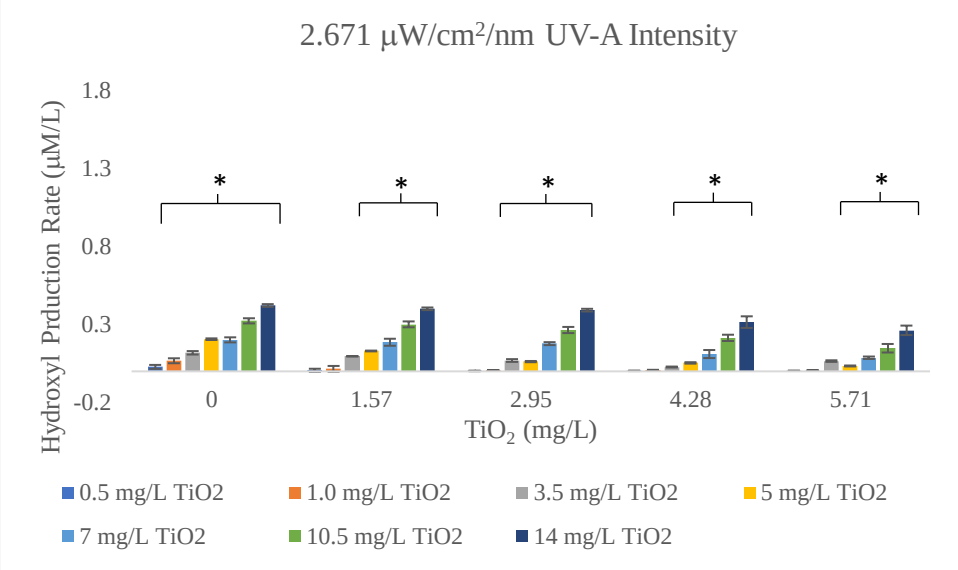
2.671 µW/cm²/nm UV-A Intensity
Hydroxyl Prduction Rate (µM/L)
1.8
1.3
0.8
0.3
-0.2
*
*
*
*
*
0
1.57
2.95
4.28
5.71
TiO2 (mg/L)
0.5 mg/L TiO2
1.0 mg/L TiO2
3.5 mg/L TiO2
5 mg/L TiO2
7 mg/L TiO2
10.5 mg/L TiO2
14 mg/L TiO2

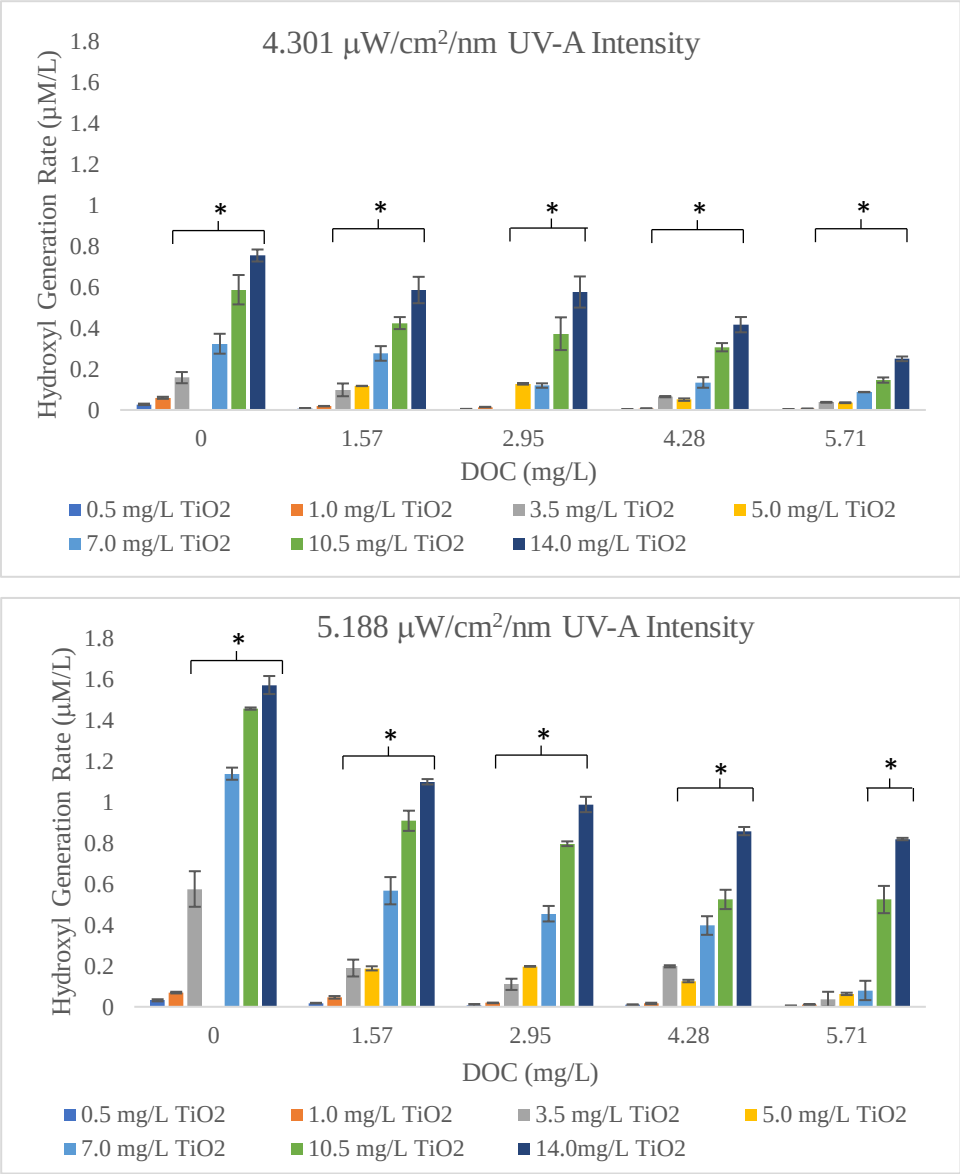

Figure 2.7 Hydroxyl Radical Generation Rates. Radical generation rate as measured by fluorescence spectroscopy. Radical generation rate increased as TiO_2 concentration increased and UV_i increased. Generation rate decreased as DOC concentrations increased. Starred rates are significantly different from the control.

48-hour Acute Bioassays for *D. magna* toxicity to TiO_2 Nanoparticles

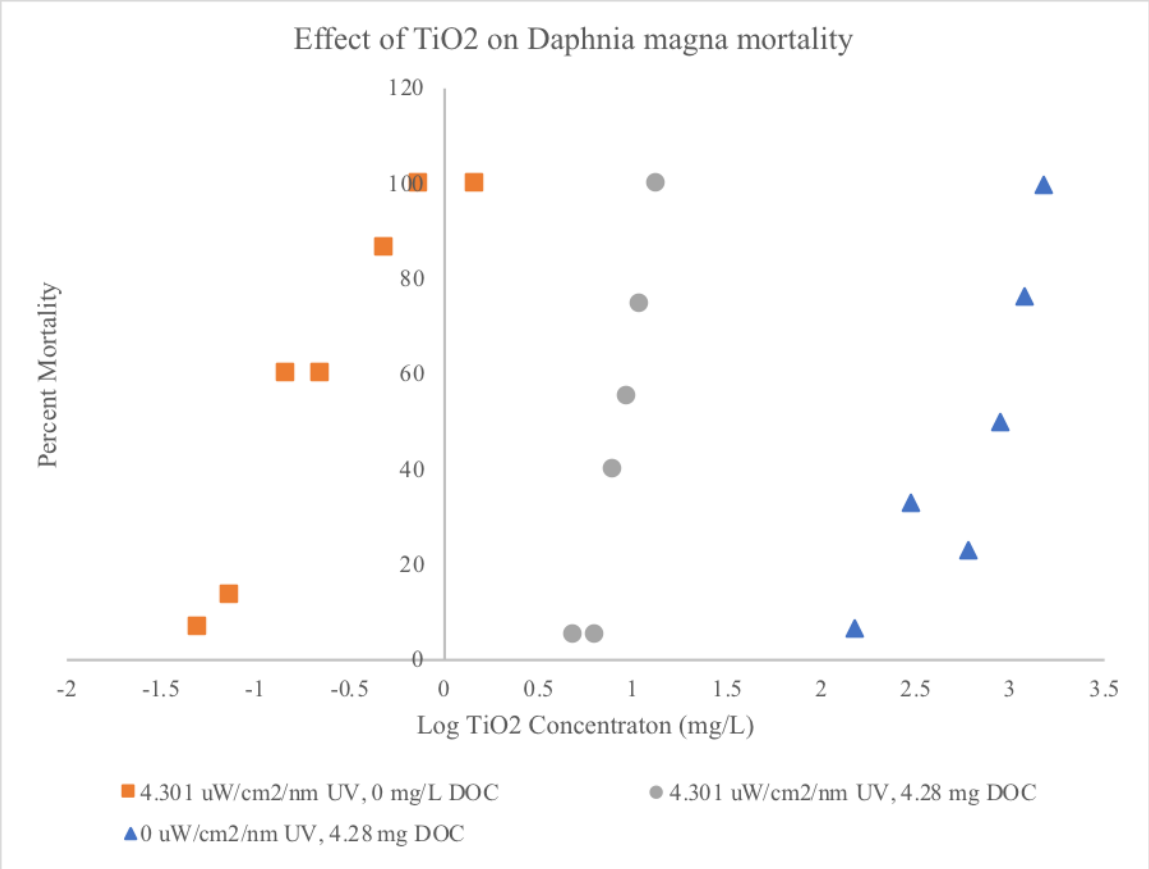

Figure 2.8 *Daphnia magna* LC_{50} toxicity to TiO_2 nanoparticles is dependent on the presence of UV light. *D manga* 48 hour acute LC_{50} toxicity exposed to 0 µW/cm^2/nm UV-A, 0 mg/L DOC: 1090.0 (920,1338.0) mg/L TiO_2 NPs; 4.301 µW/cm^2/nm UV-A, 0 mg/L DOC: 0.220 (0.163, 0.252) mg/L TiO_2 NPs; 4.301 µW/cm^2/nm UV-A, 4.28 mg DOC: 8.55 (8.08, 9.05) mg/L TiO_2 NPs.

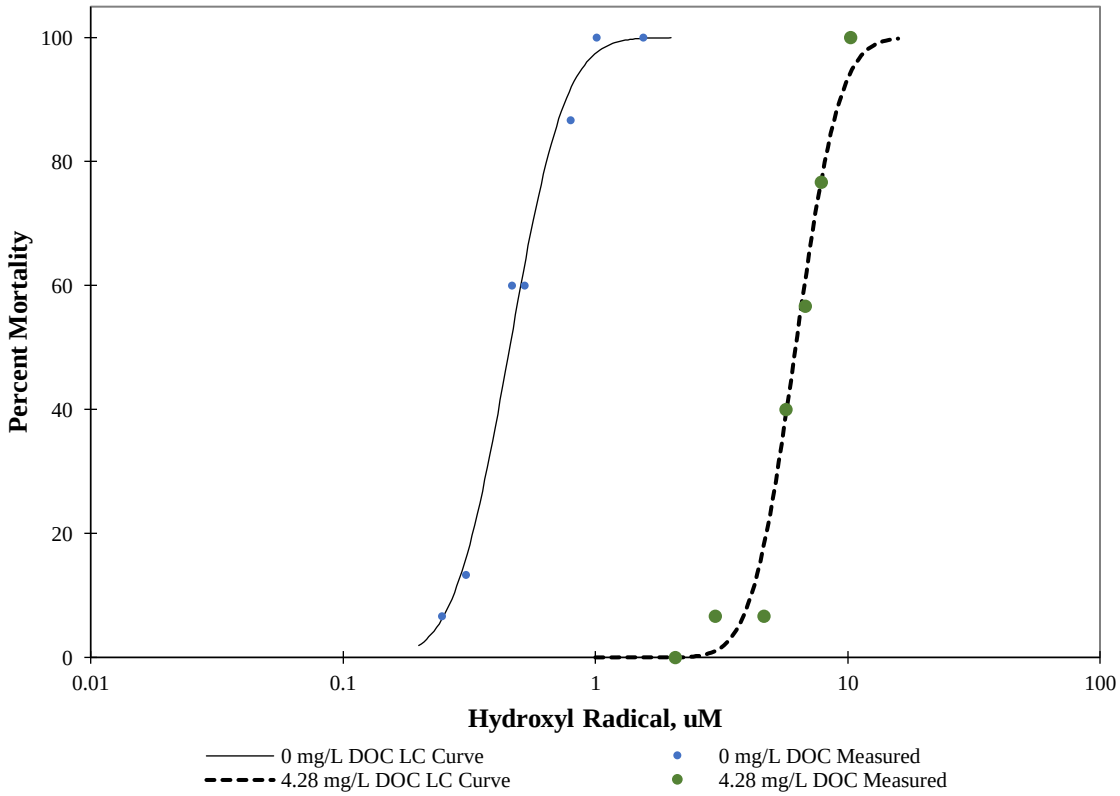

Figure 2.9 *D. magna* toxicity described in terms of hydroxyl radical. TiO_2 generates radicals at an environmentally dependent rate. This rate is dependent on the interplay of UV intensity, DOC concentration, and TiO_2 concentration. *D. magna* LC_{50} toxicity for hydroxyl radical at 4.301 µW/cm^2/nm, 0 mg DOC: 0.458 (0.415, 0.503) µM $OH^{\bullet}$; 4.301 µW/cm^2/nm, 4.28 mg DOC: 6.216 (5.771, 6.691) µM $OH^{\bullet}$.

CHAPTER THREE

PREDICITING HYDROXYL RADICAL GENERATION IN IRRADIATED TiO_2 NANOPARTICLE SUSPENISONS UNDER LOW INTENSITY UV-A LIGHTING

INTRODUCTION:

Photocatalyzed TiO_2 has been used recently as an effective means to break down organic contaminants, as well as an algaecide and bactericide, through the generation of reactive oxygen species (ROS) [6,78,107,108]. Through the UV-induced generation of free radicals, decomposition or complete mineralization of many contaminants can be achieved. Use of TiO_2/UV light as a detoxification system removes the need for harsh chemicals, and reduces the risk of dangerous chlorinated byproducts in drinking waters [107,108]. Thus, TiO_2 nanoparticles are quickly becoming an important component in a multitude of industrial processes and personal-use products[41].

Radical Generation through Photocatalysis

TiO_2 nanoparticles produce radicals under light irradiances corresponding to UV-range wavelengths. Electrons at the low energy valence band are excited to conductance band by photons with energies greater than 3.23 eV (corresponding to wavelengths less than 400 nm), generating a positively charged area in the valance band referred to as a 'hole'. Electrons are absconded from water molecules to fill these 'holes', generating hydroxyl radicals ($OH^{\bullet}$) [74,97,109]. Photodegradation of contaminants occurs directly at these hole sites, or with the produced hydroxyl radical[107,110]. Promoted electrons in the valence band that do not recombine with holes are transferred to oxygen molecules, generating superoxide anions ($^{\bullet}O_2^-$) [74,97,109].

In aquatic settings, the majority of produced ROS are in the form of hydroxyl radicals due to a number of reasons detailed by Turchi and Ollis, and Shibata. Degradation products in TiO_2 nanoparticle systems are consistent with hydroxylated intermediates from reactions with known hydroxyl radical sources. Furthermore, a wealth of evidence produced by EPR spectroscopy studies exists to support the claim that the majority produced species in TiO_2/UV/water systems is the hydroxyl radical[72,109].

Identification of Hydroxyl Radical

Due to extremely short half-lives, radical detection can difficult. Electron Paramagnetic Resonance is a common tool used to investigate irradiated TiO_2 particulate systems[30,94]. Radicals are bound using spin-traps to create adducts, the actual detected species. EPR detects the unpaired electrons by measuring change in electron energy state, through monitoring the amount of absorbed energy. This energy absorption is monitored and changes as the electron moves between energy states. Using a spin trap to increase radical lifetime, the first derivative of the absorbance curve can be characterized as specific ROS. Hydroxyl radical can be detected using 5,5-dimethyl-1-pyrroline-*N*-oxide (DMPO), 3-carboxy-2,2,5,5-tetramethyl-1-pyrrolidine-1-oxyl (CTPO), 3-carboxy-2,2,5,5-tetramethylpiperdine-1-pyrrolidine-1-oxyl (CTMPO), 4-hydroxy-2,2,6,6-tetramethylpiperdine-1-oxyl (TEMPOL), and 3-carboxyproxyl. DMPO is an efficient diamagnetic radical scavenger is known to trap both superoxide and hydroxide radicals, the two main radical species formed by TiO_2 irradiation, producing a nitroxide EPR signal from addition reactions[13,21,31,32]. There is some conjecture on whether the trap only detects free hydroxyl radicals, or is also being oxidized on holes [13,21]. Brezova *et*

al. has produced evidence that negligible amounts of spin trap molecules are absorbed onto TiO_2 surfaces, and thus oxidized by the holes can be considered negligible[111].

EPR is effective at detecting the presence of free radicals, but quantitative limitations exist. Short term (less than an hour) quantitative measurements are feasible, as well as 'snap-shots' of radicals at any given time. The short half-lives of spin trap adducts (ca. ~1 hour or less) make extended temporal measurements difficult[112]. Therefore, for quantitative measurements that extend across longer time periods, a different technique must be used.

Quantitation of Hydroxyl Radical

Measuring the increase or decrease of fluorescence emission as an indicator of hydroxyl radical generation allows for quantitation across larger time periods. Through this, the total amounts of radicals be measured, as well as the rates of radical generation. A number of different probes are utilized to detect hydroxyl radicals: *p*-benzoquinone[113], terephthalic acid[97,114,115], coumarin[20,96], and fluorescein[55,90].

Regardless of the method of detection, significant and tedious wet chemical bench work and highly sensitive instrumentation is required. A model that can predict radical generation in systems that are known to produce hydroxyl radical (such as an irradiated TiO_2 nanoparticle system) would be very valuable for determining possible downstream environmental effects that result from hydroxyl radical generation from nanoparticles that have been released into the environment. Models predicting hydroxyl radical generation at environmentally relevant conditions are currently few and far between, and often

encompass far greater concentrations of TiO_2 and far greater intensities of UV irradiance than are found in environmental settings. To better understand and more accurately assess potential impacts, it is important to well define and utilize standardized environmental parameters, and ensure tested organisms are relevant to the studied toxicant[78,116,117]. The aim of this work was to produce this time-saving modeling tool using hydroxyl radical generation rate data at environmentally relevant concentrations and conditions.

Model Selection Criteria

Successful parsimonious models generally explain data or predict effects with as few variables included as possible[118]. Linear regression modeling can be scored using Akaike Information Criterion (AIC), or Bayesian Information Criterion (BIC). AIC modeling is derived by assuming an infinite number of parameters to account for in the 'true model'. AIC modeling allows for the continued expansion of parameters, while making predictions using values that may lie outside the original dataset. To that end, BICc often runs the risk of under fitting data, while AIC is rather efficient when attempting to maximize predictive discrimination[119,120].

Larger datasets are generally better fit by AIC modeling, as AIC penalizes for additional parameters, removing smaller (and thus somewhat non-essential) parameters while still allowing for a higher degree of precision, which can be lost when including too many variables. [119,121]. Attempting to find the model that is most simplistic, while also being the most parsimonious, is of course, the innate goal of this work. Furthermore, BIC penalizes free parameters (predicted parameters) heavier with more observations, where AIC does not[118]. Considering environmental regulations, a more cautious

approach to risk assessment overestimates the effects of exposure to TiO_2 nanoparticles compared to underestimating the risk of exposure.

In the previous chapter, rates of hydroxyl radical generation in varying amounts of TiO_2 nanoparticles, under varying UV irradiance intensities were measured. Hydroxyl radical generation was determined by measuring the decrease in fluorescence emission at 513 nm, using methodology similar to Wormington *et al.*[55]. Hydroxyl radicals were positively identified using EPR spectroscopy, and a calibration curve to quantify generation over time was generated with horseradish peroxidase and H_2O_2[90]. These rates were input into a stepwise AICc linear regression to predict the generation rate of hydroxyl radicals (µM/h) under similar conditions. The model was validated by comparing predicted hydroxyl radical generation rates to literature rates of hydroxyl radical generation.

MATERIALS AND METHODS:

System Characterization:

The factorial design, and system characterization was performed in Chapter 2. Briefly, TiO_2 nanoparticle suspensions of 0, 0.500, 1.00, 3.50, 5.00, 7.50, 10.5 and 14.0 mg/L were irradiated under 0, 2.671, 4.301, and 5.188 µW/cm^2/nm UV-A lights (320 nm to 400 nm). Primary particle size was determined using a TEM, UV transmission was determined using a Varian 50 Bio UV-Vis spectrophotometer, nanoparticle aggregate size was measured by dynamic light scattering (DLS) with a Wyatt Dawn Helios-II Dynamic, and zeta potential determined using a Malvern Zetasizer ZS.

Electron Paramagnetic Resonance spectroscopy was used to characterize radical generation. Resonance spectra of irradiated TiO_2 suspensions were compared to copper sulfate/ascorbic acid/hydrogen peroxide standard spectra, using 5,5-dimethyl-1-pyrroline-N-oxide (DMPO) as a spin trap. Fluorescent spectroscopy was utilized to quantify radicals over time[36,122]. Using fluorescein dye as a probe, radical generation was measured over 48 hours, with time points every 12 hours. A linear regression of radical concentration as a function of time was performed in Excel to determine a rate constant for each TiO_2 NP concentration of under four distinct UV-A light intensities.

AICc Linear Regression Model

Using JMP software (version 13.2.0) was used to apply a stepwise Akaike information criterion (AICc) method to the rate data. Rate data was checked for normativity with a Sharpiro-Wilks test for normativity on the residuals. Multiple criteria were used to select the most reasonable model produced by the AICc regression. A number of selection criteria are listed in Table 3.4. The most likely model was selected by having the minimum number of parameters while exhibiting the lowest AICc value, highest log (-likelikhood), the difference in AICc values (ΔAICc), Akaike weight ratios, and the overall evidence ratio. Likelihood is a measurement of plausibility, in you're the model has the highest plausibility of describing data well. ΔAICc is a relative measure of each model AICc to the 'top' model's AICc. Models with $\Delta AICc < 2$ indicate there is substantial evidence the compared model preforms similar to the top model, $3 < \Delta AICc < 7$ indicates a less likely model, while $\Delta AICc > 10$ demonstrates that the compared model is very unlikely to adequately predict the data [119,121].

Akaike weights were calculated to define the probability of being a better model compared to the 'top' model. The Akaike weight can be considered a probability of being the best compared to all the candidate models[119-121]. Each model's reasonability was also compared to the top model as an evidence ratio, based on the ratio of Akaike weights. A model that is more than 2.0 likely to express the data correctly can be considered the most reasonable working model. Models with evidence ratios between 1 and 2.0 are considered as likely top model candidates[119,121], and may be subject to multi-model averaging. The entirety of models generated were compared to determine if the top model alone should be used, or if it was necessary to average a number of the more robust models, to assure that closely competing models are not discounted. Multi-model averaging produces weighted parameters and error averaged estimates across multiple reasonable models. Models with evidence ratios within 2 of the top model are considered within this range. Based on the calculated Akaike statistical and model selection criterion, there was no need to average these models.

Statistical Analysis

Comparative statistical analysis was performed using JMP software (version 13.2.0). Sharpiro-Wilk normativity test on residuals confirmed normal distribution of data. Comparisons for determining significant differences in rates was performed using comparative analysis of means with a Sidak adjustment and Tukey's HSD (α=0.05).

RESULTS:

Hydroxyl radical generation rate was successfully measured at all conditions using a simple fluorescence spectroscopy method. The rate was calculated by the linear

regression of total generation measured across 48 hours, at 12-hour time points. Radical generation rates and the associated experimental conditions are detailed in Table 3.1. Rate generation was well correlated to increases in TiO_2 concentration and increases in light exposure intensity. Rate generation was lowest under conditions with small concentrations of TiO_2 NPs and UV light intensities, and highest at large concentrations of TiO_2 NPs and high UV light intensity. The effect of reciprocity was well established: hydroxyl generation rate at low concentrations of TiO_2 and high UV light intensities resulted in similar rates to those produced by high concentrations of TiO_2 and low intensities of UV light.

Hydroxyl Radical Rate Prediction Mode

Hydroxyl radical generation rate, in µM/hour can be predicted by the following equation, produced from experimentally hydroxyl radical generation rates organized into an AICc stepwise linear regression model:

$$OH^{\bullet} = (TiO_2 * UV_i * 0.072187) + (TiO_2 * UV_i^2 * -0.037001) + (TiO_2 * UV_i^3 * 0.0053670)$$

The parameters considered during the model build were TiO_2 concentration (mg/L), UV intensity ($\mu W/cm^2/nm$), and the squared term of UV light intensity, and the full factorial of these individuals' interactions. UV_i is the average irradiance across the UV-A spectrum, 320 to 400 nm. The inclusion of parameter 'UV_i^2' was necessary when examining the effects of radical generation against each term. Radical generation plotted against light intensity exhibited a quadratic relationship, which necessitates inclusion of the squared UV_i term, shown in Figure 3.2.

The output value is the rate of hydroxyl radical generation per hour. R^2_{adj} (agreement between the actual and predicted data) was 0.9730, indicating a very good fit. The plot comparing predicted values to experimental values, Figure 3.1, exhibits increasing heteroscedasticity on the upper bounds of predictions, in congruence with increasing variance, likely as a result of reaching the maximum capacity of the dye concentration.

The summary of analysis of variance for the model terms is found in Table 3.3, which details the contribution of each factor to the hydroxyl radical generation rate. Factors with *p-values* less than 0.05 influence the generation with a 0.95 confidence level. Multiple models were considered during the selection process. Two sets of models were developed, one set that were not forced through zero, allowing the data to naturally be fit, and another set where the models were forced through zero to account for no radicals being produced when all variables are zero. The most reasonable model was selected from this second group and based on Akaike modeling criterion such as the highest log(-likelihood), lowest AICc value, and comparisons using Akaike weights and evidence ratios. A listing of models, the model selection criteria is found in Table 3.4, with detailed model statistics found in Appendix A.

Model A was selected as the most reasonable model, based on the selection criteria in comparison to the other model iterations. Model A has three parameters, an AICc of -64.37, a log(-likelihood) of 32.45, a relative probability of 59.3% as the best model to describe the data. The next most likely model, Model B, has 4 parameters, an AICc of -67.44, a relative probability of being the best model of only 23%, and an

evidence ration of 2.62, meaning Model A is 2.62 times more likely to accurately describe the data than that next most probable model. Based on the calculated Akaike statistical and model selection criterion, there was no need to average these models.

Model Reliance on UV Intensity

Multiple UV_i terms within the prediction equation was a result of heavy emphasis being placed on the importance of UV as a predictor to the system. Comparisons of parameter changes shown in Table 3.5 demonstrates this. Increases in UV_i resulted in a higher increase in rate predictions when compared to similar increases in TiO_2. For example, a 10x increase in UV_i compared to a 10x increase in TiO_2 concentration resulted in a 5.8 times greater rate prediction. This trend increased as the magnitude of change increased, a 2x increase of parameters resulted in a 1.7x difference, compared to a 10x increase change in parameters resulted in the 5.8x difference between UV_i and TiO_2. Increases within a single parameter were also more substantial for UV_i. Increasing UV_i by 10x compared to 2x resulted in an 18-fold increase in predicted rate. Increasing TiO_2 by 10x compared to 2x resulted in only a 5-fold increase in predicted rate.

Model Validation through Literature Comparisons

To validate the model, predictions of hydroxyl radical concentration were compared to 11 literature sources, shown in Appendix B1, Generation Rates from Literature Compared to Predicted Generation Rates, with TiO_2 and UV_i. Conditions for predictions were bounded by similar TiO_2 concentrations, irradiance intensities, sizes, and crystalline structure of TiO_2 nanoparticles. A subset of the 11 comparisons are detailed in Table 3.6. Rates from literature with conditions falling within the model bounds

compared reasonably to rates predicted from the model equation. As parameters deviated beyond the bounds of experimental observations used to build the model, predictions began to deviate from measured literature predictions; the farther the parameter difference from bounds, the greater the deviations became, especially with respect to irradiant intensity.

Hu et al. (2007) observed the rate of hydroxyl radical generation as the oxidation of sulfamethoxazole. This study used 100 mg/L TiO_2 concentrations, which are an order of magnitude higher than those used in the model development. UV-A intensities of 0.43 $\mu W/cm^2/nm$ were an order of magnitude lower. The literature observed hydroxyl generation rate of 3.64 µM/h, whereas predicted rate was 0.663 µM/h. Comparison with the results from Ba-Abbad et al. (2012), suggests that the influence of light intensity is a significant driver of the over predictions. Although the literature concentration (200 mg/L) was higher than this study's testing concentrations, the UV intensity (1.638 $\mu W/cm^2/nm$) was within bounds. Although predictions (85.11 µM/h) were about 5 times the literature observed rate (17.22 µM/h). Zhang et al. (2007) used coumarin as a probe with TiO_2 concentration (4286 mg/L) and UV intensity (640 $\mu W/cm^2/nm$) multiple orders of magnitude above experimental conditions used for model development. As such, the predicted rate of generation (5.40E6 µM/h) were far above the measured rate of radical generation (115.9 µM/h). Ma et al. (2012) was the most comparable to ours, with no predictions exceeding more than around 3 times that of the observed rates. Under the highest intensity (19.8 $\mu W/cm^2/nm$) in 0.1,0.5 and 1 mg/L TiO_2, the author observed

radical production of 1, 4, and 12 µM/h, whereas the model predicted 3, 14 and 28 µM/h respectively.

DISCUSSION:

The hydroxyl radical generation rates predicted by the model are well fit to experimentally measured observed hydroxyl radical generation rates (0.9730). This qualifies the model as a feasible alternative to experimental determination of hydroxyl radical generation rate. The time-consuming nature of extensive experimental rate determination under multiple conditions is evidenced by the magnitude of data used to produce this model; nearly 3500 samples were analyzed to generate the model. Using this model to approximate hydroxyl radical generation saves time, and resources. Based on literature review, it is the first model that directly approximates radicals under environmentally relevant conditions (low concentrations of TiO_2 NPs and low intensities of UV light).

Model Inclusion Parameters

When considering potential models, the inclusion parameters should be representative of both theoretical interactions of conditions and of experimentally observed interactions. For example, TiO_2 concentration, and UV_i (and by extension, UV_i^2), are not individual drivers of radical generation. This is demonstrated by the UV_i and TiO_2 negative controls; no radical generation was demonstrated in the absence of either. These parameters should therefore not be included as individuals. A wealth of literature the photocatalytic nature of TiO_2, wherein the photon absorption results in the

oxidative production of hydroxyl radicals; thus inclusion of the interaction terms is expected.

Validation of Model Using Literature Comparisons

The broad applicability of the model's ability to estimate hydroxyl radical generation from conditions not used to build the model was tested as a means of model validation. Literature measured hydroxyl generation rates were estimated using the model, a subset of 4 sources shown in Table 3.6, and a total of 11 sources shown in Appendix B, Table B1.1. There were a number of challenges associated with validating the model using literature values. There are few studies that measure hydroxyl radical generation under environmentally relevant conditions. Many of the compared TiO_2 nanoparticle studies measuring rate constants were interested in measuring quantum efficiencies[73,96,97,109,113,114], or looking at degradation rates of dyes[110,123] and persistent chemicals[124]. These studies used TiO_2 concentrations and UV-A intensities that were well outside the bounds of the experimental data used to produce the model. Many of the available studies under environmentally relevant conditions evaluate mortality directly and do not consider hydroxyl concentration as the primary toxicant. These studies are outside the scope of this study.

The result of predicting hydroxyl radical rates under similar conditions that the model was constructed resulted in comparable results, justified by the residual plot of shown in Figure 3.3. The residuals exhibit slight heteroscedasticity, most likely relating to the small sample size of available studies. Although sources with intensities above model bounds did not result in entirely the comparable rates, the predictions are reliable

enough to be of cursory worth. Some assumptions on literature data had to be made, particularly with Ma et at., particularly concerning intensity measurements, possibly leading to slightly inaccurate predictions. The least comparable predictions are those made using wavelength cutoff conditions. The removal of the lower wavelengths underlines a mechanistic importance of irradiant wavelengths in the lower UV-A range. The accuracy of the equation is somewhat bound reliant; this becomes more apparent the further the conditions are removed from the model bounds. Therefore, the extreme outliers produced from literature with bounds far outside the model (i.e. Zhang et al.), were not included in the residual plot.

In the majority of papers analyzed, TiO_2 loading was extremely high (orders of magnitude above the current study and environmentally relevant concentrations), UV intensities far exceeded that found in natural conditions, or a combination of both. The bulk of these studies were investigating process effects to mineralize pollutants. To accomplish this in wastewater process plants, both the photocatalyst and the UV intensity must be in large quantities[96,97,113]. However, the amounts from the many of the studies are well outside the concentrations of TiO_2 found within environmental aquatic compartments [41,45,46,78], and the UV irradiation intensity far exceeds that impinging on surface waters [125,126].

Low intensities, such as Hu et al. resulted in much lower predictions than those observed. The model underestimated the rates observed by Hu et al. substantially, possibly indicating the influence of UVi intensity on the equation. A high TiO_2 concentration and a low UV_i would have theoretically resulted in more equivalent results

to experimental results based on reciprocity. The reciprocal effect at such a low intensity did not occur. Predictions by Ba-Abbad et al. better demonstrated reciprocity, with a UV_i within model bounds. However, TiO_2 concentrations above model bounds contributed to over estimation of total literature observed radicals, by about 5-fold. The exposure conditions used by Zhang et al. far exceeded model bounds, and the comparative results underline the limitations of the model. Intensities used by Ma et al. were all comparable to experimental intensities, the highest being approximately 4 times that of experimental exposures. TiO_2 concentrations (0.1 mg/L to 1 mg/L) were comparable as well. Assumptions regarding the wavelengths and irradiant intensities were made for studies of conditions were not explicitly defined. These assumptions are noted in Appendix B.

These results emphasize the weight the model puts on higher UV intensities as a determining factor when predicting hydroxyl generation rate. Lower UV intensities will result in a greater model dependency on TiO_2. All of the model parameters include the UV_i, shown in Table 3.2. UV_i is an important driver of the prediction equation, exhibited in Table 3.5. Increases in light intensity result in higher predicted rates when compared to similar increases in TiO_2. These trends were conserved both within the model bounds and outside the model bounds, with greater increases of UV_i resulting in greater predicted rates, compared to increases of TiO_2. The contribution of higher intensities of UV_i holds considerable weight based on the squared and cubed functions of the second and third parameter UV_i terms. This quadratic functionality is a result of the model describing the data from which the model was built (as shown in Figure 3.2**),** underlining the importance

of the UV term. To this end, the model is limited by the small range of UV intensities, and could be improved with expansion of these experimental data parameter.

CONCLUSION:

This research has produced a model that predicts the rate of hydroxyl radical generation using TiO_2 nanoparticle concentration and UV light intensity, averaged across the UV-A spectrum. The model is well-fit (R^2_{adj}=0.9640), and parameters are minimized, providing a simplistic and parsimonious prediction equation, and is to the author's knowledge the first model directly predicts hydroxyl radical generation at environmentally realistic conditions.

The rates were calculated using environmentally relevant concentrations of TiO_2 nanoparticles and UV intensities. The model allows for a workable range of titanium dioxide nanoparticle concentrations encompassing post-effluent concentrations, downstream concentrations, and runoff concentrations. Lower light intensity allows for estimations within the water column, as TiO_2 nanoparticles will not generally be suspended at the water surface. The model was validated by comparing model predictions to literature. The model behaves well when the parameters are within the model's experimentally developed bounds but deviates outside of these bounds, exhibited by the lack of reciprocity at high UV_i intensities, and excessive overestimation of radical generation at high UV_i intensities. The model placed heavy influence on the UV_i terms, exhibited by the quadratic inclusion of the UV_i term, as this best described the data used to build the model. Further expansion of the UV_i data encompassing a wider range of light conditions would be advantageous.

Future improvement of the model should focus on other parameters that will affect hydroxyl radical generation, such as primary nanoparticle size[65], crystallinity[102], pH[50], UV wavelength[35]. Significant improvement can be made by including the effects of natural organic matter in the model. The ubiquitous nature of NOM in surface waters leads to its inclusion being a necessity in a working rate prediction model.

This model has potential to be a worthwhile tool for better understanding the implications of TiO_2 nanoparticle fate and determining risk assessment parameters for regulatory purposes. Similar models predict plant extract radical scavenging ability[127], and predict *D.* magna mortality[62]. Tools such as these are worthwhile additions to understanding interactions of TiO_2 nanoparticles with a complex environment. More experimental evidence to encompass other variables that affect radical generation rate would help to improve the accuracy and robustness of this model. In time, given the data, this model could be improved to function similarly to the Biotic Ligand Model.

Table 3.1: Hydroxyl Generation Rates and Associated TiO_2 and UV-A Intensities. Detail of exposure conditions generating specific hydroxyl radical generation rates, and associated R^2 values.

TiO_2 mg/L	Light µW/cm²/nm	Rate µM/h	R^2	Standard Deviation
0	0	0	NA	NA
0.5	0	0.0009	0.7128	0.0015
1	0	0	0.7110	0.0007
3.5	0	0.0006	0.7612	0.0020
5	0	0	0.6721	0.0006
7	0	0.0024	0.4651	0.0005
10.5	0	0.0005	0.4665	0.0004
14	0	0.0027	0.6380	0.0016
0	2.671	0	NA	NA
0.5	2.671	0.0287	0.8145	0.0158
1	2.671	0.0679	0.9271	0.0110
3.5	2.671	0.1189	0.9569	0.0052
5	2.671	0.2063	0.9998	0.0162
7	2.671	0.2019	0.9973	0.0165
10.5	2.671	0.324	0.9841	0.0088
14	2.671	0.4223	0.9906	0.0127
0	4.301	0	NA	NA
0.5	4.301	0.0274	0.8783	0.0050
1	4.301	0.0594	0.9563	0.0273
3.5	4.301	0.1578	0.8277	0.0485
5	4.301	n.d.	n.d.	n.d.
7	4.301	0.3233	0.9726	0.0718
10.5	4.301	0.5869	0.9688	0.0293
14	4.301	0.7539	0.9840	0.0036
0	5.188	0	NA	NA
0.5	5.188	0.0317	0.9878	0.0041
1	5.188	0.0693	0.9712	0.0868
3.5	5.188	0.5748	0.9999	0.296
5	5.188	n.d.	n.d.	n.d.
7	5.188	1.1375	0.9943	0.0055
10.5	5.188	1.4552	0.9992	0.0440
14	5.188	1.5701	0.9907	0.0052

Table 3.2 Parameter Estimates and Standard Error for Akaike Information Criteria corrected (AICc) Regression. Parameters, coefficients, and standard error generated by AICc regression. R^2=0.9730; adjusted R^2=0.964

Parameter	**Estimate**	**Standard Error**	**SS**
TiO_2	0	0	9.89E-06
Light	0	0	0.004249
TiO_2*Light	0.07218667	0.01214	0.195427
$Light^2$	0	0	0.004492
TiO_2*$Light^2$	-0.0370059	0.006317	0.189715
$Light^3$	0	0	0.004755
TiO_2*$Light^3$	0.00536999	0.000785	0.258641

Table 3.3 ANOVA data for AICc Regression. Analysis of Variance; Model Factors, term-wise contribution to model, p > F details the significance to model at a 0.95 confidence interval.

Parameter	**nDF**	**F Ratio**	***p* > F**
TiO_2	1	0.002	0.9672100
Light	1	0.762	0.3907100
TiO_2*Light	1	35.355	0.0000024
$Light^2$	1	0.807	0.3773100
TiO_2*$Light^2$	1	34.321	0.0000031
$Light^3$	1	0.856	0.3635000
TiO_2*$Light^3$	1	46.791	0.0000002

Table 3.4 Hydroxyl Radical Rate Prediction Model Selection Criteria and Alternative Models. Statistical, evidence to select the most reasonable model for hydroxyl radical rate prediction. Model ID 2 exhibited the most desirable selection criterion. Models 1 through 4 were forced through 0, while Models 5 to 7 were not.

Model	**Model ID**	**Log-likelihood**	**Parameters (K)**	**AICc**	**Δ AICc**	**exp(-Δ AIC/2)**	**Akaike weight**	**Evidence ratio**
Best Backward	***A***	***32.45***	***3***	***-64.37***	***0***	***1***	***0.5931***	***1***
Best Forward	B	31.66	4	-62.44	1.93	0.3810	0.2260	2.6243
All Parameters	C	27.80	7	-52.96	11.41	0.0033	0.0020	3.00E2
Nonlinear	D	22.15	4	-43.41	20.96	2.82E-05	1.61E-05	3.55E4
Models not forced through 0								
Best Model	E	31.24	3	-61.95	2.42	0.2975	0.1765	3.3613
All Parameters	F	27.81	7	-52.99	11.38	0.0034	0.0020	2.96E2
Nonlinear	G	25.58	5	-49.82	14.55	0.0007	0.0004	1.44E3

Table 3.5 Model Reliance on UV_i Intensity. Comparison of conditions to show the UV intensity is driving the predictions. Greater increases in light result in greater increases in predicted rate compared to a similar increase in TiO_2. Reciprocity is not demonstrated.

All Outside Bounds		
Light Intensity	TiO_2 Concentration	Predicted Rate
1	200	8.1106
10	200	477.754
1	20	0.81106
10	20	47.7754
	Comparison of High	Comparison of Low
Increase in Light	58.9048899	58.9048899
Increase in TiO2	10	10
All Inside Bounds		
Light Intensity	TiO_2 Concentration	Predicted Rate
2.5	14	0.46298875
5	14	1.49499
2.5	7	0.231494375
5	7	0.747495
	Comparison of High	Comparison of Low
Increase in Light	3.228998545	3.228998545
Increase in TiO2	2	2
Light Outside Bounds		
Light Intensity	TiO_2 Concentration	Predicted Rate
1	5	0.202765
10	5	11.94385
1	0.5	0.0202765
10	0.5	1.194385
	Comparison of High	Comparison of Low
Increase in Light	58.9048899	58.9048899
Increase in TiO2	10	10
TiO_2 Outside Bounds		
Light Intensity	TiO_2 Concentration	Predicted Rate
2.5	50	1.65353125
5	50	5.33925
2.5	25	0.826765625
5	25	2.669625
	Comparison of High	Comparison of Low
Increase in Light	3.228998545	3.228998545
Increase in TiO2	2	2

Table 3.6: Model Rate to Literature Rate Comparison. Comparison of measured concentrations of hydroxyl radicals from literature to model predicted concentrations of hydroxyl radicals. Model behaves well within experimental bounds but deviates as bounds are exceeded.

Author	Probe	TiO_2 (mg/L)	UV $\mu W/cm^2/nm$	Measured $OH^\bullet$ Generation ($\mu M/h$)	Predicted $OH^\bullet$ Generation ($\mu M/h$)
Ma, 2012	3'[p-amino	0.1	No Filter	~1	2.858418842
	phenyl]-	0.5	19.8	~4	14.29209421
	fluorescein	1		~12	28.58418842
		0.1	Silica Window	<1	0.334117013
		0.5	10.9	~3.5	1.670585067
		1		12	3.341170133
		0.1	Petri Dish Glass	< 1	0.893144046
		0.5	14.2	~4	4.465720228
		1		12	8.931440456
		0.1	Microscope Glass	< 1	1.061475657
		0.5	14.9	~4	5.307378287
		1		12	10.61475657
		0.1	Acrylic Glass	<1	0.012348725
		0.5	5.15	< 1	0.061743627
		1		< 1	0.123487254
			345 nm cutoff		
		0.1	11.6	< 1	0.423584347
		0.5		3.5	2.117921736
		1		~11.5	4.235843472
		0.1	360 nm cutoff	< 1	0.113603621
		0.5	8.33	2	0.568018103
		1		8	1.136036206
		0.1	400 nm cutoff	<1	0
		0.5	0	<1	0
		1		< 1	0
Hu, 2007	Antimicrobial	0		12.0	0
	agents	100	0.43	3.84	0.66284
Zhang, 2013	Coumarin	4285.71	640	116.85	5.399E6
Ba-Abbad, 2012	Chlorophenol	2000	1.638	17.22	85.1081

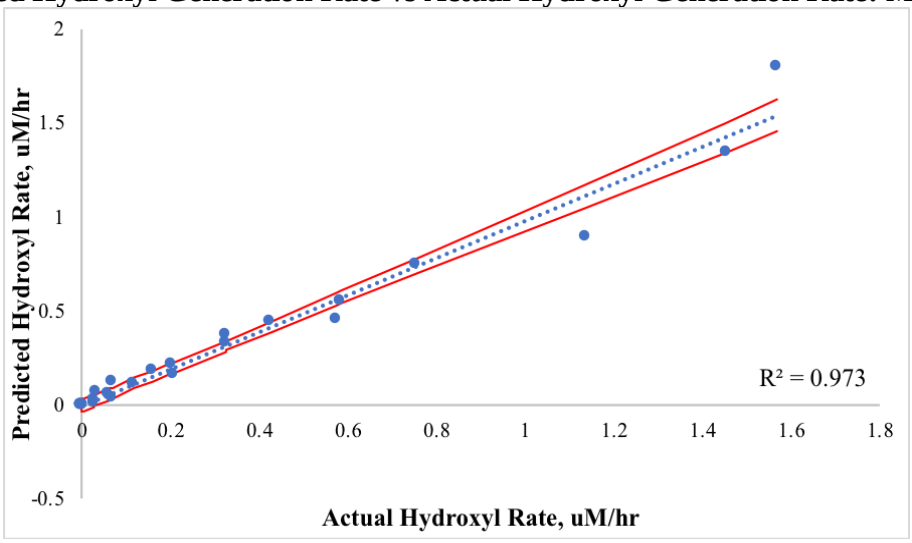

Figure 3.1 Model fitting shows very good fit between actual and predicted hydroxyl radical generation. R^2: 0.9730; R^2_{adj}: 0.9640. Each point represents a predicted vs measured rate. Red lines represent 95% confidence intervals. Heteroscedasticity increases at upper bounds due to increased variance of higher generation rates, mostly likely a result of approaching maximum fluorescein detections limit.

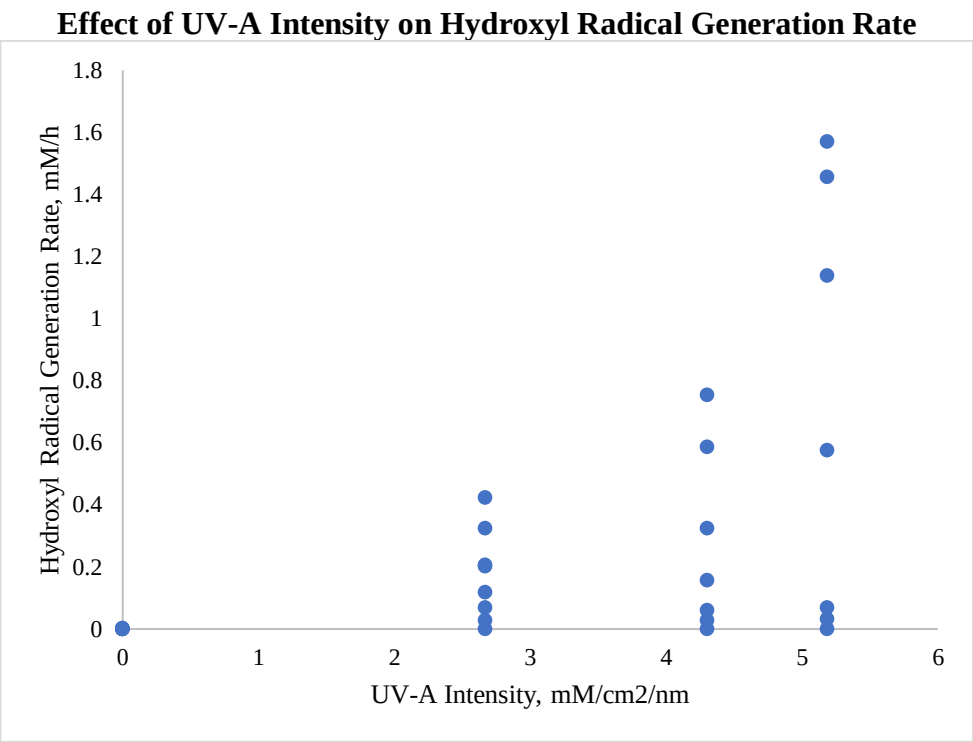

Figure 3.2 The effect of UV-A intensity of hydroxyl radical generation rate is quadratic, ultimately exhibited in the radical generation model, which uses squared UV_i and cubed UV_i terms to describe the data from which it was built.

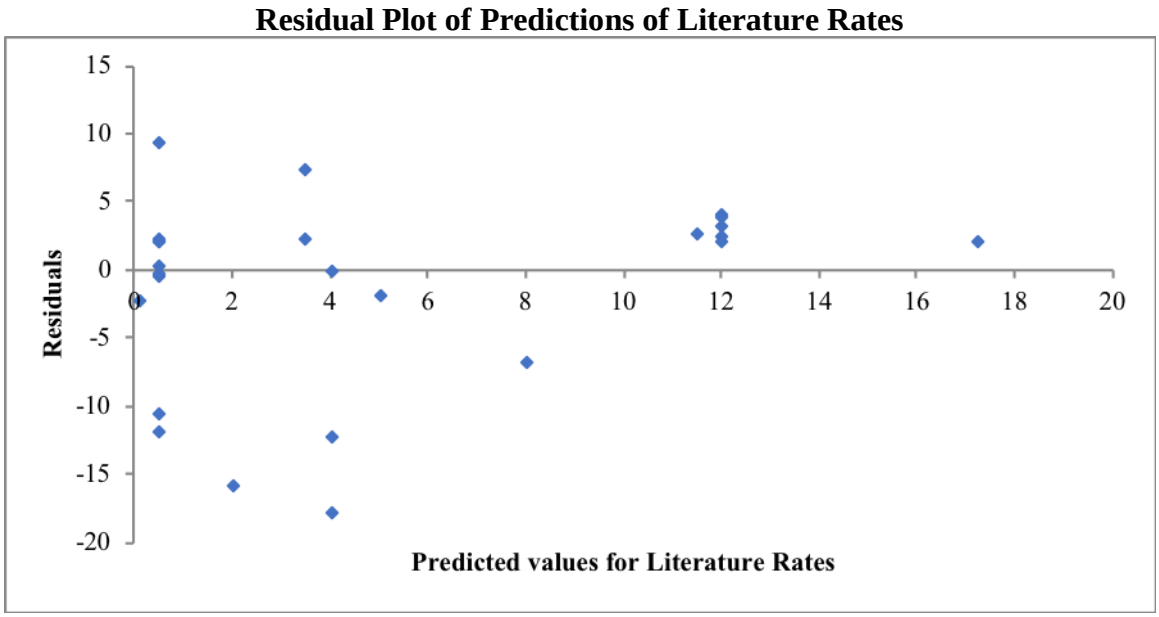

Figure 3.3 Residual plot of the predictions of literature, exhibiting heteroscedasticity, most likely as a result of a low sample size, or the need for more variables to increase the robustness of the model.

CHAPTER FOUR

PREDICTING THE EFFECT OF NATURAL ORGANIC MATTER ON THE GENERATION OF HYDROXYL RADICAL

INTRODUCTION

Recent research has underlined the importance of simulating realistic environmental conditions when determining the toxicity of nanoparticles. Historically, these nanoparticles were deemed relatively non-toxic to aquatic organisms, a result of not simulating important environmental conditions[1,128,129]. Ultraviolet wavelengths (specifically within the UV-A range) and natural organic matter (NOM) play a significant role in enhancing or modulating the toxicity of anatase TiO_2 nanoparticles[78]. Inclusion of these parameters is necessary to correctly assess the risk of the nanoparticles to aquatic organisms and ecosystems.

Radical Generation by TiO_2 Nanoparticles: Mechanisms and Factors

Toxicity attributed to TiO_2 nanoparticles is a result of the generation of ROS through the photocatalytic promotion of electrons, occurring when the TiO_2 nanoparticle is irradiated by UV-A wavelengths. TiO_2 bandgap energy is estimated to range from 3.2 eV to 3.0 eV, corresponding to wavelengths less than 414nm [35]. Ultraviolet radiation in this wavelengths range has enough energy to excite ground level electrons within the valance band to the conduction band. The promotion generates a high energy electron, and a positively charged hole on the surface of the nanoparticle. These photogenerated species will react with oxygen and water to generate superoxide and hydroxyl radicals, respectively[18]. These radicals react with water, free electrons and other ROS species to

generate more hydroxyl radicals[13,32]. These produced free radicals damage organisms' lipid membranes and generate free radical cascades which lead to a toxic response[64].

The generation of radicals is dependent on a number of factors: particle characteristics such as size[65] and crystallinity[102], light conditions such as intensity[62] and wavelength[35], water chemistry components[50,130], and the amount of natural organic matter in solution[55]. Small variations in conditions can have large impacts on radical production and organism toxicity. One of the largest gaps in TiO_2 toxicity is indeed the variations of experimental conditions from lab to lab, which result in varying toxic responses to TiO_2. These variations can be attributed spatial and temporal differences. One experimental condition that is not often not accounted for is the inclusion of natural organic matter in exposure suspensions.

Natural Organic Matter: Interactions with TiO_2

Natural organic matter (NOM) is a ubiquitous conglomeration of humic acids, fulvic acids, lignins, tannins, and other organics. NOM exists in all surface waters, increasing temporally and spatially, as the seasons and water flow rate change[52]. NOM (categorically measured as mg/L of dissolved organic carbon) can affect the generation of radicals from irradiated TiO_2 in a number of ways, either by decreasing light penetration depth, coating the nanoparticle to reduce available surface area for photon impingement, or causing aggregation of nanoparticles. The relationship between 1% UV attenuation (the depth to which 1% of surface UV-A radiation penetrates) and DOC concentration is inversely exponential. 1% UV penetration depth can vary between 0.5-m to 4-m, depending on amount of DOC in the water source. Increased DOC concentrations will

result in shallower attenuation depths[104]. Therefore, in waters with greater concentrations of DOC, UV-A intensities in the water column are expected to be low.

NOM can also adsorb to the surface of nanoparticles reducing the available surface area for photon/surface interaction. This coating has been shown to directly affect the toxicity of TiO_2 nanoparticles, as a result of reduction of overall ROS produced[69], as well as shifting the isoelectric point towards basic pH, although this occurs at high dissolved organic carbon (DOC) concentrations[131]. Along with coating to reduce the generation of radicals, the varying oxidizable substrates that exist within NOM provides act to effectively quench radicals before interaction with organisms can occur[55]. This mechanism has been shown to degrade NOM as well[132]. Interactions of TiO_2 nanoparticles and low concentrations of DOC has been shown to make zeta potentials more negative, resulting in increased nanoparticle suspension time within the water column[55]. Increased suspension time with less aggregation will therefore result in increased radical generation[65]. Research previously evaluated the effect of single NOM components, such as humic acid[50,131,133,134], but few papers exist that look at the effect of whole NOM[7,55,93]. In this study the influence of the NOM as a function of concentrations, multiple TiO_2 ratios, and multiple UV-A intensities.

Modeling Techniques to Predict Hydroxyl Radical Generation Rate

Using this full factorial design, changes in amount of NOM were correlated to hydroxyl radical rate production in the presence of other cofactors. The experimentally determined generation rates were organized into a number AICc regression models. Models were built using both no rules modeling and combined rules parameters. The

former allows for removal of individual terms in the model to best fit the input data. The latter disallows higher ordered terms when included lower-ordered terms are removed (if parameter [TiO_2] is rejected, all terms with [TiO_2] will likewise be removed). Forward step inserts parameters to the model one at a time, removing them if deemed statistically non-contributory, whereas backward step begins with all parameters included and removes the least significant contributors one by one until all parameters have a statistically significant contribution to the model[135,136].

These iterations were compared using a number of selection criteria (log(-likelihood), Akaike Information Criterion (AICc), Akaike weight ratios, and overall evidence ratios) to select the model that best predicted hydroxyl generation rate. The model with the lowest AICc is most likely the best candidate, the 'top model', but the supporting criterion ensures that there are no competing models that can also describe the data well[118,135,136].

Likelihood is a measurement of a model's plausibility to best describe the data. High values for log(-likelihood) can be interpreted as high plausibility the model is adequate[135,136]. ΔAICc is a comparison between two models based on AICc values. Models with $\Delta AICc < 2$ compared to the top model indicate similar model performance. $3< \Delta AICc < 7$ demonstrates performance less likely to be equivalent to the top model, and $\Delta AICc > 10$ generally indicates the compared model is an insufficient model relative to the top model[135,136]. Akaike weights calculate the probability of the a model being the top model compared to all models analyzed[118,135]. Model comparative reasonability can be compared using evidence ratios to ensure that models exhibiting

similar worth are not neglected. A model with an evidence ratio < 2 compared to the top model can be considered equally worthwhile and may be subject to multi-mode averaging. Multi-model averaging is a technique that produces a single model combined from similar models, using weighted averaged parameter and error averaged estimates[118,135].

Multimodel averaging is usually accomplished either through full average modeling, or natural average modeling. Natural average includes parameters that are only within the best AIC model, all other parameters from other models are not included. This option is best used when strong, but not unequivocal evidence exists (top model is strongly weighted but evidence exists to question worth of other models). Full-model averaging is used when there is no clear top model (particularly if the top AIC model is not strongly weighted. In this case, all models in question are averaged based on weight; models with low weights simply contribute nothing towards the calculation of the average. The non-essential models therefore have little influence on predictions[135].

Utilization of a model such as this reduces the need for resource intensive wet bench chemistry to determine hydroxyl generation from irradiated TiO_2 nanoparticle suspensions. This model has potential as a tool to aid regulatory work, and nanoparticle risk assessment. This study will contribute overall to understanding the conditional interactions affecting hydroxyl radical generation rate from irradiated TiO_2 nanoparticles.

MATERIALS AND METHODS:

Chapters 2 and 3 detailed an in-depth explanation and methodology to characterize the full factorial for developing a statistical model for the photocatalytic

generation of hydroxyl radicals by TiO_2 NPs. In this chapter, analogous methods were extended to incorporate NOM. Briefly, TiO_2 nanoparticle suspensions (0, 0.500, 1.00, 3.50, 5.00, 7.50, 10.5 and 14.0 mg/L), and NOM (0, 1.57, 2.95, 4.28 and 5.71 mg/L DOC) were suspended in EPA recipe Moderately Hard Water (MHW). Suspensions were exposed to 0, 2.671, 4.301, and 5.188 $\mu W/cm^2/nm$ UV-A intensity, using CXL Topaz Blacklight Blue T12 Fluorescent lights, for 48 hours. TiO_2 primary particle size was determined using Transmission Electron Microscopy (Hitachi H7600). NOM was filtered through 0.45-micron nylon filters from water obtained directly from the Suwanee River (Headwaters, Suwanee River Visitor Center, Fargo, Georgia). DOC content was analyzed using a Shimadzu TOC-V Carbon Analyzer. Size of TiO_2/NOM aggregates was measured by dynamic light scattering using a Wyatt Dawn Helios-II DLS, and zeta potential of suspensions was measured using Malvern Zetasizer ZS. UV transmission and UV intensity were measured using a Varian 50 Bio UV-Vis Photospectrometer and an OceanOptics JAZ Photospectrometer, respectively. Spectroscopic data acquired by the OceanOptics JAZ was analyzed using OceanView 1.5.2.

Hydroxyl Radical Characterization and Quantitation

Characterization of hydroxyl radical was accomplished using Electron Paramagnetic Spectroscopy. Using 5,5-dimethyl-1-pyrroline-N-oxide (DMPO) as a radical spin trap, resonance spectra of copper sulfate/ascorbic acid/hydrogen peroxide standards were compared to irradiated TiO_2 suspensions. Radical concentrations were quantified using fluorescence spectroscopy with fluorescein (FL) dye as the fluorophore probe; measured on a Horiba Fluoromax-4 fluorescent spectrophotometer. Using

fluorescein dye as a radical probe, radical generation under the full factorial design was measured across 48 hours, with time points analyzed every 12 hours. Fluorescein dye concentration was dependent on UV intensity and TiO_2 concentrations. All measurements were made in triplicate, with each spectrum the average of a triplicate scan. TiO_2 negative samples (0 mg TiO_2) were treated as blanks, to account for non-hydroxyl mediated decreases in fluorescent emission. These emissions were set to calibration curves as described in Chapter 2 to calculate the concentration of radicals generated at each time point. Using Microsoft Excel, rates of generation for each condition were obtained from the slopes from the linear regression of radical concentration as a function of time.

AIC Modeling of Hydroxyl Generation Rates

All hydroxyl radical rates were organized and input into a stepwise linear regression analysis. Using JMP software (v.13.2.0), multiple models were produced to predict the generation of hydroxyl radicals under varying conditions. All residuals were analyzed using the Sharpiro-Wilkes test for normativity; stepwise models were run both forwards and backwards, using combine restriction rules, and no rules, in order to determine the top model. Model selection criteria evaluated to determine the most likely model from the calculated iteration included number of parameters, AICc value, log(-likelihood), change in AICc (ΔAICc), Akaike weight ratio, and overall model comparison ratio. 12 models were generated and evaluated using these criteria.

Model averaging of the two top models were also completed by full average modeling and natural average modeling techniques, to ensure that the most probable model was selected. Neither of these models were deemed as appropriate predictor

models. The top model produced from the data set to predict the generation of hydroxyl radicals was selected from the initial set of 12, based on superior AICc information, model weight, evidence ratios and log(–likelihood) criterion.

Hydroxyl Radical Generation Rate Predictions and Comparison to Literature Rate Measurements

An in-depth literature search was conducted to find studies that had also measured or estimated the concentration of ROS/hydroxyls produced in TiO_2 suspensions. Specific focus was placed on studies that incorporated NOM, or NOM constituents (humic acid, fulvic acid, etc.). The linear regression equation determined from AICc criterion was applied, inserting the parameters from each source, to estimate radical generation per experiment. Occasionally conversion was required to adhere to parameter units. If simulated solar wavelengths were not directly specified to be UV-A, the total intensity was multiplied by 6% to approximate UV-A percentage of natural sunlight[17]. Original conditions from each experiment are included in the comparison table, along with the transformed condition used within the prediction equation.

RESULTS:

Hydroxyl Radical Generation Rate Prediction Equation

A stepwise linear regression equation chosen based on AICc criteria was produced from hydroxyl radical generation rate measurements and used to predict hydroxyl radical generation in a reasonable range of environmental conditions in simulated freshwater based on rate data, found in Table 4.1.

$[OH^{\bullet}] = (TiO_2*UV_i* 0.04766) + (TiO_2*UV_i^2 *-0.02300) + (TiO_2*UVi^3 *0.00346) + (DOC*UVi^3 *-0.00013) + (TiO_2*DOC*UVi^3 *-0.000007)$. This model, Model A, has an R^2_{adj} fit (predicted vs actual) of 0.946, resulting in predictions describing close to 95% of effects seen in experimental measurements. The predicted versus actual hydroxyl radical generation rate plot, shown in Figure 4.2, exhibits increasing heteroscedasticity with increasing concentrations. The increased uncertainty in these predictions is directly correlated to the increase in variance at the upper bounds of the measurements. Additionally, the linear regression was forced through 0 in the absence of each parameters as generation of radicals should be 0 µM/h.

This equation is comprised of parameters influencing the hydroxyl generation rate with $p \leq 0.05$ (95% confidence level). The parameters descriptors are as follows: $[TiO_2]$: mg/L; [DOC]: mg/L; UV_i: $\mu W/cm^2/nm$. UV intensity is described as UV-A, with measured wavelengths from 320 nm to 400 nm. The output value, $[OH^{\bullet}]$, µM/h can be multiplied by time to give time-based concentrations. Parameter statistics, parameter estimates, analysis of variance, and effect tests can be found in Table 4.3. The effect from the interaction of parameters (i.e. TiO_2*UV_i, TiO_2 *$DOC*UV_i^3$, etc) statistically influence the generation rate (*p-value* < 0.05 with 0.95 confidence). Individual parameters did not show statistically significant influence (*p-value* > 0.05 at a 0.95 confidence level).

Twelve models were evaluated to describe the generation of hydroxyl radical under experimental conditions. Models were split into two groups, those forced through 0 to account for no radicals being produced when all variables are 0, and models not forced

through zero which allowed the data to be naturally fit. Model A, a no-rules, backwards stepping model forced through zero, exhibited the highest probability as the most accurate. Model A was selected based on a number of model selection criteria such as lowest AICc (-396.25), Akaike weight (0.44), evidence ratio (1), and log(–likelihood) (198.23) and the least number of parameters (5). The next most reasonable model was a no rules, forward-stepping model forced through zero. It's selection criterion was AICc (-395.55), Akaike weight (0.31), evidence ratio (1.4), log(–likelihood) of (197.97)) and the seven parameters.

Due to the comparable evidence ratios and Akaike weights, models were averaged using both full and natural model averaging techniques. The resultant models did not indicate good predictions, as a result of the large differences between the parameters of the two top models. Calculated model criteria demonstrates both averaged models as poor predictors. These models were rejected, and Model A was selected as the most reasonable prediction equation. These criteria in comparison with those calculated from the other models can be found in Table 4.2. Further information about the other models, such as comparison statistics, as well as parameter information for each model can be found in Appendix A2, Models with DOC.

Model Parameter Interactions

Table 4.4 shows the correlations between model parameters. These correlations demonstrate the interactions of terms that result in hydroxyl radical rate prediction. Stronger correlations are represented by more intense colors, with blues representing

positive correlations and reds representing negative correlations. 1 represents complete positive correlation and negative 1 represents complete negative correlation.

Model Validation through Literature Rate Comparisons

The model was validated through a broad comparison of radical production rates obtained from 11 literature sources, and predicted rates based on the literature conditions. These literature rates are in shown in Appendix B, Table B1.2. A subset of these studies is shown in Table 4.5. These sources were bound by similar conditions with attempts made to only compare studies with similar concentrations of TiO_2, DOC, and light intensity.

The most comparable predictions were made to the Ma et al. (2012) study. Ma et al. used similar TiO_2 concentrations and similar light intensities, although the highest light intensities were about 3-4 times the highest intensity from which the model was built. Literature rates under the highest intensity (19.8) were 1, 4, and 12 µM/h compared to predicted rates of 1.9, 9, and 18.8 µM/h in 0.1, 0.5 and 1 mg/L TiO_2 respectively. Intensities within model bounds (acrylic glass) were most comparable, with rates of <1 µM/h compared to predicted rates < 1µM/h.

A number of studies outside of experimentally determined bounds were included to test the limitations of the model. Generally, literature conditions that fell outside of the model's experimentally determined bounds predictions that were orders of magnitude different from observed concentrations. This is especially evident when reviewing observations by Wormington et al. in comparison to model predictions. Wormington's intensity was one order of magnitude above model bounded experimental intensities.

Where Wormington saw a maximum of 4 µM/h of radicals under conditions with no DOC, the model predicted 1920 µM/h. The model's radical predictions followed Wormington's decreasing trends as DOC was increased, but all predictions were orders of magnitude below the observed radical production. In conditions with 0 mg/L TiO_2, the model predicts a negative hydroxyl radical generation rate, a result of the fourth term ($DOC*UV_i^3*-0.00013$).

A residuals plot, shown in Figure 4.3 was generated to determine how well the model predicted the observed literature data. Extreme outliers observed in Table 4.5, such as the predictions for Wormington et al.'s data set were removed following a residual plot analysis showing that these data points were unacceptable. An updated residual plot analysis with outliers removed demonstrated no trends, indicating acceptable predictive behavior.

DISCUSSION:

When considering the ultimate fate of TiO_2 nanoparticles in the environment, the influence of environmental conditions is an important aspect. The quantitative model generated from 155 rates produced from over 3500 data points predicts hydroxyl generation under varying conditions with good accuracy. The interactive nature of conditions, as demonstrated by the rate measurements and correlations shows the complexity of exposure environments. This model addresses some of these complexities by addressing the reciprocal effects of nanoparticle concentration and ultraviolet intensity, while including the attenuative effects from natural organic matter. Environmental conditions can vary spatially and temporally over relatively short

distances and timescales. Weather conditions not only affect the intensity of UV-A irradiation but can also affect the turbidity of water. Consistent experimental measurement of rate production under each is impossible. This model can account for variation in some of these conditions. Changes to conditions across time periods can be made as well, resulting in hydroxyl radical rate predictions without the need for wet bench chemistry.

Hydroxyl Radical Generation Rate Model Criteria

Production of a similar model was discussed in the previous chapter. A similar protocol was followed for the production of this model as well, looking for the simplest and most parsimonious model based on the large data set acquired from monitoring the hydroxyl generation rate. AICc linear regression assumes an infinite number of parameters to account for, works well with large data sets, penalizes for excessive 'non-essential' parameters, and will place heavier emphasis on measured parameters[118,135,136].

Based on the lowest AIC calculation, the Akaike weights and evidence ratio indicated two reasonable models, Model A and Model B. These models were averaged using both full modeling and natural modeling techniques. The results of the individual averaged models (Model K and Model L) were excessively unsatisfactory, established by model selection criteria, as result of the degree of difference between the two top models' individual parameters. This information is shown in Appendix A2. These averaged models were summarily rejected, and the most reasonable top model, Model A was selected as the prediction equation. The selected model accounts for the interacting

effects of TiO_2 concentration, DOC concentration, and UV intensity, to generate predictions of hydroxyl radical generation rates.

Inclusion Parameters

The model produced from the data describes radical generation as a result of multiple interactions. The statistically contributing parameters (TiO_2*UV_i, TiO_2*UV_i^2, TiO_2*UV_i^3, DOC*UV_i^3, TiO_2*DOC*UV_i^3) account for the generation of hydroxyl radicals from the irradiation of TiO_2 by UV-A light, with NOM in suspension. Chapter 2 explicitly defined the influence of each parameter on rate production. These effects on generation rate are conserved through the model.

Interactions between TiO_2 and UV_i are important as this is the driver of radical generation. It was noted that increases in both TiO_2 and in UV_i are correlated to increases in radical rate. The three terms (TiO_2*UV_i, -TiO_2*UV_i^2, TiO_2*UV_i^3) may account for this effect, and also describe the exponential and quadratic shape of generation due to the influence of other parameters, specifically at high concentrations of TiO_2 and DOC, as shown in Figure 4.2. The interaction between DOC and UV_i is important to the prediction equation as increases in DOC concentration (and therefore overall amount of NOM) will result in a decrease in light transmission (noted in Chapter 2). This dependence if described through the DOC*UV_i term. The full interaction of all three parameters is the final inclusion term (TiO_2*DOC*UV_i^3). This term contributed minimally to the equation but was still deemed a statistically significant component to predict radical generation.

Model Validation by Comparison to Literature Rates

To adequately assess the use of the model, a comparison of measured radical generation to predicted radical generation was necessary. The predictions of experiential measurements were sound (R^2= 0.946), but it is important to determine robustness when handling data that was not used to generate the model. Eleven literature measured radical generation rates and concentrations were estimated using the model. A subset of 4 of these shown in Table 4.5 contains sources with all conditions close to model bounds, conditions with TiO_2 and DOC within bounds but with UV_i outside bounds, and with UV_i inside bounds but DOC and TiO_2 exceeding bounds. This comparison resulted in mostly comparable predictions, exhibited by a plot of the residuals shown in Figure 4.4. To construct this residual plot, extreme predictions that deviated from observed radical rates were treated as outliers and removed. These values, such as predictions for Wormington et al.'s data demonstrate the importance of adhering to model bounds. The intensity for this study was an order of magnitude above the model training data.

Deviations from observed rates were generally observed when parameters exceeded bounds. High concentrations of TiO_2 in low UV intensities drove predictions to exceed observed radical concentrations, such as those in Huang et al.'s study. Considering the high radical predictions for Wormington under low TiO_2 and high UV_i conditions, it appears as though reciprocity is conserved. The model exhibited the best predictions under conditions that were closest to being within bounds. Ma et al. used comparable intensities of UV_i, exceeding model bounds by no more than 4-fold, a comparatively low amount. TiO_2 and DOC were within bounds, and the resultant

predictions showed good agreement, particularly those under acrylic glass and microscope glass.

There were comparatively few studies measuring radical concentration or radical generation within the bounds of the research. One of the gaps concerning TiO_2 nanoparticle behavior in aqueous systems is the lack of work under interacting environmental conditions[78]. Sources looking at the toxicological implications of TiO_2 have not focused on radical production in freshwater aquatic environments. Sources that do investigate the generation of radicals are interested in the rate of chemical decomposition[87,124,137] or looking at removal of NOM in a wastewater treatment plants(WWTP) [7,93]. As such, the exposure conditions of literature values are often in excess compared to this work. Titanium dioxide concentrations orders of magnitudes higher, DOC concentrations at WWTP conditions, and light intensities either at surface sunlight intensity or well above natural conditions are common. These parameters are noted in Appendix B2. The model did not account for differences in size as exhibited by the model predictions using conditions from Yin et al., and Wywroll et al.. In these cases, an increase in rate inversely correlated to nanoparticle size was expected[56,57,102]. The model also did not account for changes in crystallinity[63].

Future Suggestions for Model Improvement

There are a number of aspects that the model does not account for. Nanoparticle size[63,131,138] and crystallinity[57,63,102] are important to consider. Available surface area may be a better assessment parameter than size of nanoparticle, although it would be exceedingly difficult to truly account for. Intensity was measured as an average across the

UV-A spectrum however recent evidence suggests that nanoparticles coated by NOM may be generate radicals via photons within the visible spectrum. Further, there is evidence that NOM coated rutile nanoparticles may generate more radicals that anatase, as a result of apparent band gap changes[131]. Significant deviations of measured values as model bounds are exceeded were observed.

Additional data, specifically at higher UV intensities found within the water column would aid in predictions in clearer waters, and closer to shorelines, where waters are shallower resulting in higher penetrating UV-A intensities. Literature also indicates significant aggregation effects based on solution chemistry such as ionic strength, and pH[61,139,140], aspects the model does not address.

Further, including the mechanistic interactions between nanoparticles and NOM may also provide more insight on important absorption processes that will direct affect nanoparticle ability to absorb photons leading to radical generation. The model was trained using only data from Suwanee River NOM. There are many different variations of NOM worldwide, and the behavior of NPs in Suwanee River NOM is by no means how they will behave in different NOM. More accurate rate generation measurements may be achieved by accounting for the aliphatic/aromatic ratios of NOM[141] (measured by specific UV absorbance, SUVA), in addition to DOC.

CONCLUSION:

Despite the significant amount of research accomplished to understand the effects of TiO_2 NPs on aquatic environments, studies are only recently becoming multidimensional. Many studies focus on the interacting effects of TiO_2 and irradiated

light on organisms, but neglect to include NOM. These studies are helpful to understand the processes by which organisms are affected by the nanoparticle but are not completely indicative of interactions in natural waters. Waste treatment and process studies that investigate the breakdown of NOM through use of TiO_2 NPs and irradiant light generally use concentrations of TiO_2 and irradiant light that far exceed conditions found anywhere outside laboratories and waste reactors.

The research presented here is both a method of estimating the amount of hydroxyl radical produced and a means to assess the risk of these nanoparticles to organisms. This method of measurement allows estimations of generation trends to investigate the interactions TiO_2 has with an aquatic system in a broad scale. Hydroxyl radical generation data has been transformed it into a working model to estimate hydroxyl radical generation, under environmentally TiO_2, DOC, and UV_i conditions. Predicted rates achieved without any wet lab work, saving significant time and resources. Model demonstrated valid predictions within and close to bounds but deviates as bounds are exceeded. However, there are currently few studies evaluating the interaction of conditions affecting TiO_2 toxicity, and even fewer assessing radical production under environmentally relevant conditions, so the model was only validated on a small number of sources.

This model predicts hydroxyl radical produced by TiO_2 NPs, and has the potential to aid regulatory decisions on nanoparticle disposal, assess risk of exposure to hydroxyl radicals. Assessment on the effects of breakdown of TiO_2 incorporated material can use this model during product design. This model works as helpful tool to further develop

understanding of how environmental conditions affect the inherent risk of TiO_2 nanoparticles to aquatic environments, and the inherent hazard of introducing large amounts of anthropogenic contaminants into a natural system. As the model framework works to predict the overall effects of conditions on hydroxyl radical generation, it can be helpful in further assessment of phototoxic nanoparticle interactions, such as acute or chronic toxicity to aquatic species.

Tables and Figures

Table 4.1: Hydroxyl Radical Generation Rates and Associated TiO_2 and DOC Concentrations and UV-A Light. Rate tables detailing the measured rate of hydroxyl radical generation under various environmental conditions, and the predicted rate of hydroxyl radical generation calculated from the hydroxyl radical generation rate model.

TiO_2 (mg/L)	UV_i ($\mu W/cm^2/nm$)	DOC (mg/L)	Rate (µM/h)	R^2	Standard Deviation	Predicted Rate (µM/h)
0	0	0	0	NA	0.0015	0
0	0	1.57	0	NA	0.0006	0
0	0	2.95	0	NA	0.0333	0
0	0	4.28	0	NA	0.0009	0
0	0	5.71	0	NA	0.0009	0
0.5	0	0	0.0009	0.7128	0.0007	0
0.5	0	1.57	0	0.9513	0.0165	0
0.5	0	2.95	0	0.879	0.0333	0
0.5	0	4.28	0	0.525	0.0016	0
0.5	0	5.71	0.0004	0.4218	0.0006	0
1	0	0	0	0.711	0.0020	0
1	0	1.57	0	0.9564	0.0008	0
1	0	2.95	0	0.8861	0.0335	0
1	0	4.28	0	0.818	0.0004	0
1	0	5.71	0	0.333	0.0008	0
3.5	0	0	0.0006	0.7612	0.0006	0
3.5	0	1.57	0.0009	0.9891	0.0005	0
3.5	0	2.95	0	0.9023	0.0331	0
3.5	0	4.28	0	0.77	0.0012	0
3.5	0	5.71	0	0.367	0.0011	0
5	0	0	0	0.6721	0.0005	0
5	0	1.57	0.0003	0.9835	0.0012	0
5	0	2.95	0.0007	0.894	0.0336	0
5	0	4.28	0	0.793	0.0004	0
5	0	5.71	0	0.264	0.0012	0
7	0	0	0.0024	0.4651	0.0004	0
7	0	1.57	0.0012	0.9588	0.0006	0
7	0	2.95	0.0019	0.879	0.0332	0
7	0	4.28	0.001	0.919	0.0005	0
7	0	5.71	0.0004	0.4072	0.0095	0
10.5	0	0	0.0005	0.4665	0.0016	0
10.5	0	1.57	0.0021	0.9046	0.0004	0
10.5	0	2.95	0.004	0.875	0.0337	0
10.5	0	4.28	0.002	0.798	0.0010	0
10.5	0	5.71	0.0045	0.577	0.0016	0
14	0	0	0.0027	0.638	0.0015	0
14	0	1.57	0.0016	0.9114	0.0006	0
14	0	2.95	0.0026	0.942	0.0333	0
14	0	4.28	0	0.99	0.0009	0
14	0	5.71	0	0.097	0.0009	0

TiO_2 (mg/L)	UV_i ($\mu W/cm^2/nm$)	DOC (mg/L)	Rate ($\mu M/h$)	R^2	Standard Deviation	Predicted Rate ($\mu M/h$)
0	2.671	0	0	NA	0.0127	**0**
0	2.671	1.57	0	NA	0.0096	-0.0039
0	2.671	2.95	0	NA	0.0018	-0.0073
0	2.671	4.28	0	NA	0.0015	-0.0106
0	2.671	5.71	0	NA	0.0014	-0.0142
0.5	2.671	0	0.0287	0.81449	0.0158	0.0146
0.5	2.671	1.57	0.0071	0.86321	0.0183	0.0095
0.5	2.671	2.95	0.0026	0.90001	0.0010	0.0051
0.5	2.671	4.28	0.0034	0.56153	0.0022	0.0008
0.5	2.671	5.71	0.0036	0.92433	0.0001	-0.0038
1	2.671	0	0.0679	0.92712	0.0110	0.0292
1	2.671	1.57	0.0163	0.98564	0.0019	0.0230
1	2.671	2.95	0.0077	0.9676	0.0087	0.0175
1	2.671	4.28	0.0077	0.92955	0.0030	0.0122
1	2.671	5.71	0.006	0.82255	0.0050	0.0065
3.5	2.671	0	0.1189	0.95688	0.0052	0.1023
3.5	2.671	1.57	0.0966	0.86991	0.0025	0.0902
3.5	2.671	2.95	0.0695	0.88634	0.0039	0.0796
3.5	2.671	4.28	0.0278	0.9913	0.0046	0.0693
3.5	2.671	5.71	0.0659	0.8852	0.0031	0.0583
5	2.671	0	0.2063	0.99975	0.0162	0.1462
5	2.671	1.57	0.1306	0.99252	0.0225	0.1305
5	2.671	2.95	0.0625	0.98967	0.0095	0.1168
5	2.671	4.28	0.0541	0.99632	0.0258	0.1036
5	2.671	5.71	0.0345	0.99825	0.0078	0.0894
7	2.671	0	0.2019	0.99733	0.0165	0.2046
7	2.671	1.57	0.1866	0.99557	0.0189	0.1843
7	2.671	2.95	0.1778	0.96795	0.0198	0.1665
7	2.671	4.28	0.1109	0.9505	0.0201	0.1493
7	2.671	5.71	0.0873	0.88602	0.0274	0.1308
10.5	2.671	0	0.324	0.98405	0.0088	0.3069
10.5	2.671	1.57	0.3013	0.99659	0.0085	0.2784
10.5	2.671	2.95	0.2651	0.98674	0.0086	0.2534
10.5	2.671	4.28	0.2148	0.99975	0.0373	0.2292
10.5	2.671	5.71	0.1482	0.96427	0.0304	0.2033
14	2.671	0	0.4223	0.99057	0.0127	0.4093
14	2.671	1.57	0.4011	0.9975	0.0096	0.3725
14	2.671	2.95	0.3925	0.98688	0.0018	0.3403
14	2.671	4.28	0.3156	0.99109	0.0015	0.3092
14	2.671	5.71	0.263	0.98841	0.0014	0.2758

TiO_2 (mg/L)	UV_i ($\mu W/cm^2/nm$)	DOC (mg/L)	Rate ($\mu M/h$)	R^2	Standard Deviation	Predicted Rate ($\mu M/h$)
0	4.301	0	0	NA	0.0036	0
0	4.301	1.57	0	NA	0.0006	-0.0163
0	4.301	2.95	0	NA	0.0018	-0.0306
0	4.301	4.28	0	NA	0.0009	-0.0444
0	4.301	5.71	0	NA	0.0003	-0.0758
0.5	4.301	0	0.0274	0.87833	0.0050	0.0276
0.5	4.301	1.57	0.0078	0.97167	0.0010	0.0064
0.5	4.301	2.95	0.0035	0.7139	0.0010	-0.0122
0.5	4.301	4.28	0.0027	0.78163	0.0009	-0.0301
0.5	4.301	5.71	0.0028	0.7892	0.0020	-0.0494
1	4.301	0	0.0594	0.95625	0.0273	0.0552
1	4.301	1.57	0.0186	0.73779	0.0312	0.0291
1	4.301	2.95	0.0143	0.90744	-	0.0062
1	4.301	4.28	0.0067	0.86904	0.0030	-0.0159
1	4.301	5.71	0.0053	0.96017	0.0020	-0.0396
3.5	4.301	0	0.1578	0.82771	0.0485	0.1930
3.5	4.301	1.57	0.0982	0.93886	0.0008	0.1425
3.5	4.301	2.95	n.d.	n.d.	n.d.	0.0981
3.5	4.301	4.28	0.065	0.86799	0.0060	0.0553
3.5	4.301	5.71	0.0374	0.95663	0.0020	0.0093
5	4.301	0	n.d.	n.d.	n.d.	0.2758
5	4.301	1.57	0.1172	0.986	0.0357	0.2106
5	4.301	2.95	0.1277	0.99202	0.0108	0.1533
5	4.301	4.28	0.0505	0.98569	0.0258	0.0981
5	4.301	5.71	0.0355	0.97651	0.0009	0.0387
7	4.301	0	0.3233	0.9726	0.0718	0.3861
7	4.301	1.57	0.2759	0.9829	0.0293	0.3013
7	4.301	2.95	0.1192	0.90881	0.0798	0.2268
7	4.301	4.28	0.1342	0.97126	0.0201	0.1550
7	4.301	5.71	0.0873	0.98182	0.0128	0.0778
10.5	4.301	0	0.5869	0.96881	0.0293	0.5791
10.5	4.301	1.57	0.424	0.98401	0.0644	0.4601
10.5	4.301	2.95	0.3723	0.99005	0.0760	0.3555
10.5	4.301	4.28	0.3063	0.99418	0.0373	0.2547
10.5	4.301	5.71	0.146	0.98182	0.0113	0.1463
14	4.301	0	0.7539	0.98401	0.0036	0.7721
14	4.301	1.57	0.5854	0.98928	0.0006	0.6189
14	4.301	2.95	0.5757	0.97202	0.0018	0.4842
14	4.301	4.28	0.4163	0.99616	0.0009	0.3544
14	4.301	5.71	0.2496	0.97975	0.0003	0.2148

TiO_2 (mg/L)	UV_i ($\mu W/cm^2/nm$)	DOC (mg/L)	Rate ($\mu M/h$)	R^2	Standard Deviation	Predicted Rate ($\mu M/h$)
0	5.188	0	0	NA	0.0052	0
0	5.188	1.57	0	NA	0.0016	-0.0286
0	5.188	2.95	0	NA	0.0055	-0.0537
0	5.188	4.28	0	NA	0.0032	-0.0779
0	5.188	5.71	0	NA	0.0015	-0.1039
0.5	5.188	0	0.0317	0.98781	0.0041	0.0560
0.5	5.188	1.57	0.0179	0.98647	0.0063	0.0188
0.5	5.188	2.95	0.008	0.97676	0.0015	-0.0138
0.5	5.188	4.28	0.0089	0.99937	0.0038	-0.0453
0.5	5.188	5.71	0.0051	0.96221	0.0020	-0.0791
1	5.188	0	0.0693	0.97122	0.0868	0.1120
1	5.188	1.57	0.0461	0.98885	0.0411	0.0662
1	5.188	2.95	0.0191	0.98062	0.0274	0.0260
1	5.188	4.28	0.0161	0.95926	0.0051	-0.0127
1	5.188	5.71	0.0112	0.99409	0.0363	-0.0544
3.5	5.188	0	0.5748	0.99988	0.0296	0.3919
3.5	5.188	1.57	0.1891	0.90459	0.0101	0.3032
3.5	5.188	2.95	0.1097	0.92875	0.0012	0.2253
3.5	5.188	4.28	0.1976	0.99244	0.0060	0.1502
3.5	5.188	5.71	0.037	0.09537	0.0058	0.0694
5	5.188	0	n.d.	n.d.	n.d.	0.5598
5	5.188	1.57	0.1876	0.95891	0.0665	0.4454
5	5.188	2.95	0.1972	0.95984	0.0379	0.3448
5	5.188	4.28	0.1257	0.99157	0.0454	0.2479
5	5.188	5.71	0.0631	0.96004	0.0472	0.1437
7	5.188	0	1.1375	0.99434	0.0055	0.7837
7	5.188	1.57	0.5664	0.98247	0.0493	0.6350
7	5.188	2.95	0.4543	0.97716	0.0116	0.5042
7	5.188	4.28	0.3966	0.9793	0.0471	0.3782
7	5.188	5.71	0.0797	0.892	0.0665	0.2427
10.5	5.188	0	1.4552	0.99915	0.0440	1.1756
10.5	5.188	1.57	0.9077	0.993	0.0132	0.9667
10.5	5.188	2.95	0.7957	0.9852	0.0374	0.7831
10.5	5.188	4.28	0.5239	0.94429	0.0201	0.6062
10.5	5.188	5.71	0.5234	0.9683	0.0058	0.4160
14	5.188	0	1.5701	0.99071	0.0052	1.5675
14	5.188	1.57	1.098	0.97143	0.0016	1.2985
14	5.188	2.95	0.9872	0.991	0.0055	1.0621
14	5.188	4.28	0.8574	0.95368	0.0032	0.8343
14	5.188	5.71	0.8186	0.93944	0.0015	0.5893

Table 4.2: Hydroxyl Radical Generation Rate Model Selection Criteria. Models generated in JMP using AICc stepwise regressions, to determine the most reasonable model to predict hydroxyl radical generation rates. Models through 0 account for no generation under null conditions, models not forced through 0 are as-is models derived directly from data. The most reasonable model has the lowest AICc, the highest log(-likelihood), and the highest Akaike weight, indicated probability it is the best descriptor, as a percentage of combined sum of exp(-ΔAICc/2)

Model	Model ID	Log (-likelihood)	# of parameters (K)	AICc	ΔAICc	exp(-ΔAICc/2)	Akaike weight	Evidence Ratio
Models Through 0								
No Rules Backward	A	198.234	5	-396.25	0.00	1	0.44033	1
No Rules Forwards	B	197.972	7	-395.55	0.70	0.7036	0.3098	1.4212
No Rules All Parameters	C	190.131	15	-378.52	17.73	0.0001	0.0001	7090.4210
Combined Rules Best	D	191.669	13	-382.03	14.22	0.0008	0.0004	1224.1475
Nonlinear Bounded	E	95.433	12	-189.75	206.50	1.44E-45	6.35E-46	6.9321E+44
Models Not Through 0								
No Rules Backwards	F	197.137	5	-394.06	2.19	0.3340	0.1471	2.9937
No Rules Forwards	G	196.863	7	-393.33	2.92	0.2321	0.1022	4.3081
No Rules All Parameters	H	190.482	13	-379.66	16.59	0.0002	0.0001	4009.8135
Best Combined	I	188.868	15	-376.00	20.26	3.9905E-05	1.7571E-05	2.5059E+04
Nonlinear Bounded	J	91.901	12	-182.69	213.56	4.2207E-47	1.8585E-47	2.3693E+46
Averaged Models								
Full Average	K	-61.461	7	123.32	519.57	1.5034E-113	6.6199E-114	6.6516E+112
Natural Average	L	-43.950	5	88.11	88.11	7.3464E-20	3.2348E-20	1.3612E+19

Table 4.3: Statistical Summary of the AICc Linear Regression, Top Model. Model generated using No Rules, Backwards step. Model was forced through zero to account for zero µM/h radical generation under null conditions.

Summary of Fit

R^2	0.9476
R^2_{Adj}	0.9458
RMSE	0.0658
Mean of Response	0.1622
Observations	155

AICc	**BICc**
-396.253	-378.56

Analysis of Variance

Source	DF	Sum of Squares	Mean Square	F Ratio
Model	5	15.8168	3.1634	730.9005
Error	150	0.6492	0.0043	**Prob > F**
C. Total	155	16.4660		<.0001*
Tested against reduced model: Y=0				

Parameter Estimates

Term	Estimate	Std Error	t Ratio	Prob>|t|	Lower 95%	Upper 95%	Variance
TiO_2*UV_i	0.0477	0.0047	10.06	<.0001*	0.038	0.057	2.24E-05
TiO_2*UV_i^2	-0.0230	0.0025	-9.36	<.0001*	-0.028	-0.018	6.03E-06
TiO_2*UV_i^3	0.0035	0.0003	11.36	<.0001*	0.003	0.004	9.30E-08
DOC*UV_i^3	-0.0001	2.93E-05	-4.44	<.0001*	-0.0002	-7.23e-5	8.58E-10
TiO_2*DOC*UV_i^3	-7.832e-5	5.58E-06	-14.04	<.0001*	-8.93e-5	-6.73e-5	3.11E-11

Effect Tests

Source	Nparm	DF	Sum of Squares	F Ratio	Prob > F
TiO_2*UV_i	1	1	0.4383	101.266	<.0001*
TiO_2*UV_i^2	1	1	0.3794	87.665	<.0001*
TiO_2*UV_i^3	1	1	0.5583	129.003	<.0001*
DOC*UV_i^3	1	1	0.0854	19.742	<.0001*
TiO_2*DOC*UV_i^3	1	1	0.8528	197.038	<.0001*

Table 4.4 Correlation of Parameters for Model A. Color intensity indicates strength of correlation, where blue is positively correlated and red is negatively correlated. This demonstrates parameter interaction when predicting radical generation rate.

Term	TiO_2*UV_i	$TiO_2*UV_i^2$	$TiO_2*UV_i^3$	$DOC*UV_i^3$	$TiO_2*DOC*UV_i^3$
TiO_2*UV_i	1	-0.9898	0.9705	-0.0037	0.0032
$TiO_2*UV_i^2$	-0.9898	1	-0.9941	0.004	-0.0032
$TiO_2*UV_i^3$	0.9705	-0.9941	1	-0.0042	-0.0342
$DOC*UV_i^3$	-0.0037	0.004	-0.0042	1	-0.5539
$TiO_2*DOC*UV_i^3$	0.0032	-0.0032	-0.0342	-0.5539	1

Table 4.5 Abridged Model Validation via Literature Comparison of Literature Observed Radical Generation Rates and Model Predicted Radical Generation Rates

Author	Probe	TiO_2 (mg/L)	UV $\mu W/cm^2/nm$	DOC mg/L	Measured $OH^{\bullet}$ Generation (µM/h)	Predicted $OH^{\bullet}$ Generation (µM/h)
Ma, 2012	3'[p-amino	0.1	No Filter	0	~1	1.88180139
	phenyl]-	0.5	19.8	0	~4	9.40900695
	fluorescein	1		0	~12	18.8180139
		0.1	Silica Window	0	<1	0.227325193
		0.5	10.9	0	~3.5	1.136625963
		1		0	12	2.273251925
		0.1	Petri Dish Glass	0	< 1	0.595836042
		0.5	14.2	0	~4	2.979180212
		1		0	12	5.958360424
		0.1	Microscope Glass	0	< 1	0.706365121
		0.5	14.9	0	~4	3.531825606
		1		0	12	7.063651212
		0.1	Acrylic Glass	0	<1	0.010863403
		0.5	5.15	0	< 1	0.054317017
		1		0	< 1	0.108634034
			345 nm cutoff			
		0.1	11.6	0	<1	0.286540744
		0.5		0	3.5	1.432703722
		1		0	~11.5	2.865407444
		0.1	360 nm cutoff	0	< 1	0.113603621
		0.5	8.33	0	2	0.568018103
		1		0	8	1.136036206
		0.1	400 nm cutoff	0	<1	0
		0.5	0	0	<1	0
		1		0	< 1	0
Hu, 2007	Antimicrobial	0			12	0
	agents	100	0.43	0	252	1.652
		100	0.43	2	45.6	1.650
		100	0.43	10	32.4	1.645
		100	0.43	20	32.4	1.639
Huang et al., 2008	DOC	100	2.5	10	0.324	1.709380256
		300	2.5	10	0.924	5.168859206
		500	2.5	10	0.936	8.628338156
		1000	2.5	10	0.978	17.27703553
Wormington, 2017		0	0	0	0	0
		0		3	0	0
		0		6	0	0
		0		12	0	0
		0	52	0	~1.5	0
		0		3	~2	-54.96324538
		0		6	~1.5	-109.9264908
		0		12	~1.5	-219.8529815
		4.5	0	0	0	0
		4.5		3	0	0
		4.5		6	0	0
		4.5		12	0	0
		4.5	52	0	~4	1920.555
		4.5		3	~3.5	1732.84332
		4.5		6	~3.0	1545.13164
		4.5		12	~2.5	1169.70828

Predicted Hydroxyl Radical Generation Rate Versus Actual Hydroxyl Radical Generation Rate: Model Validation

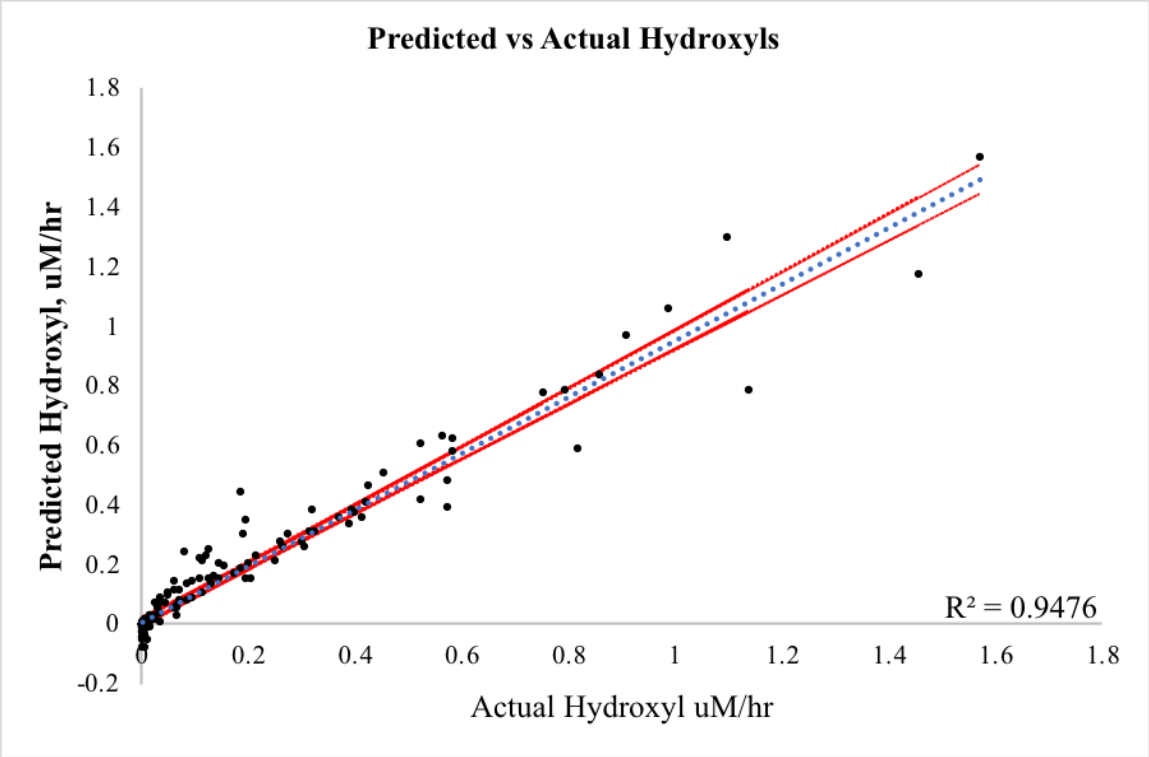

Figure 4.1. Fit plot of the predicted rate of hydroxyl radical generation verus the actual rate of hydroxyl radical generation. Each dot represents a measured hydroxyl generationn rate versus a model predicted hydroxyl generation rate, the red lines indicate the 95% confidence interaval of the model, while the dotted blue line indicates the fit curve for the data, demonstrating an R^2=0.948 demonstrating the predictions account for almost 95% of the effects shown by the data,

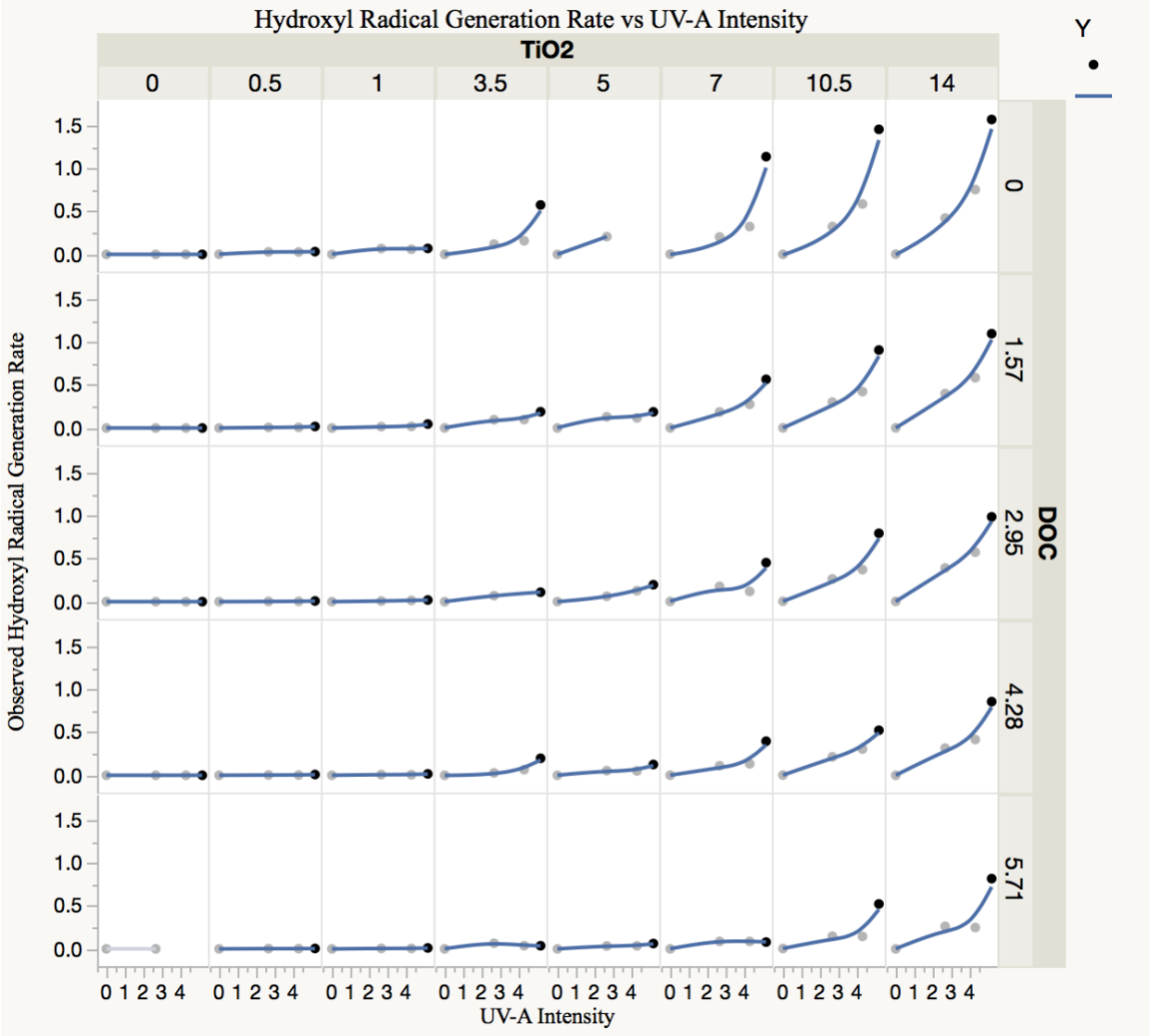

Figure 4.2 The effect of UV-A intensity on radical generation rate, organized by DOC and TiO_2 concentrations. The quadratic increase in rate as UV_i necessitated inclusion of a UV_i^2 term to better describe the data.

Residual Versus Literature Measurements: Model Validation

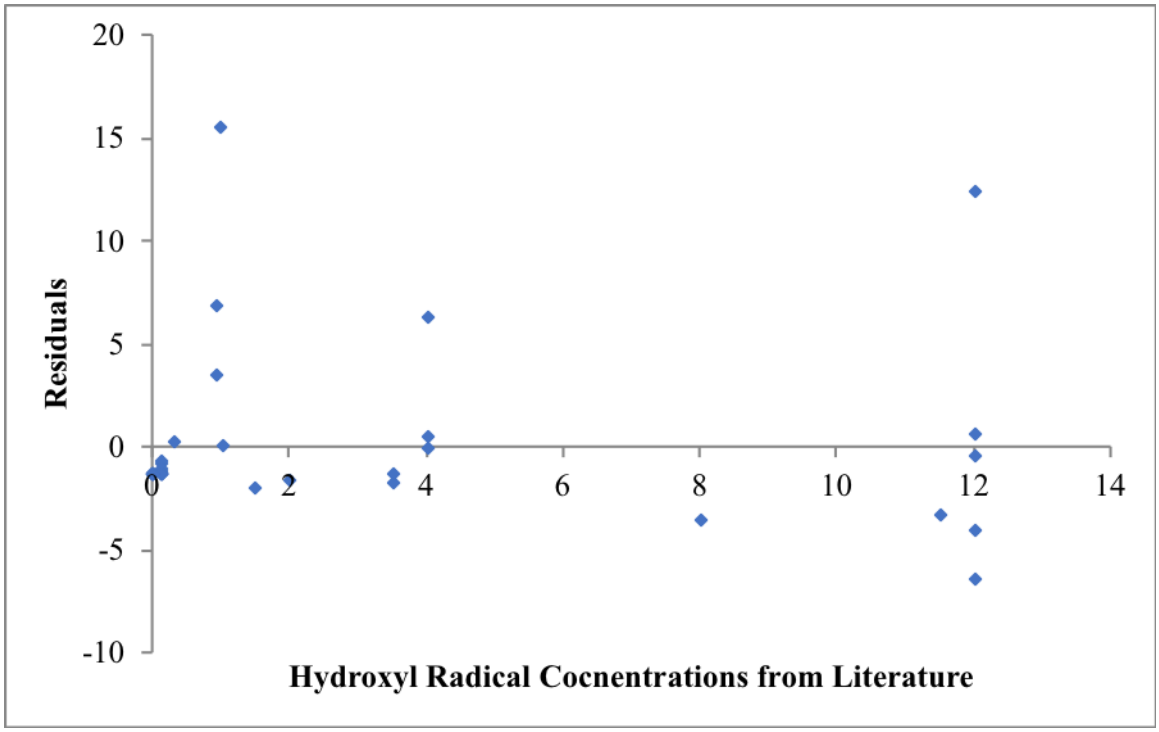

Figure 4.3 Residual plot of generated from the comparison of Literature Observed radical generation rates and radical generation rates predicted by Model A. 13 extreme outliers were removed to generate this residual plot of 30 observed hydroxyl radical concentrations from literature, underlining the importance of using the model within experimentally determined bounds.

CHAPTER FIVE

CORRELATING HYDROXYL RADICAL CONCENTRATION WITH *Daphnia magna* TOXICITY FROM IRRADIATED TiO_2 NANOPARTICLES AND EXPOSURE CONDITIONS

INTRODUCTION:

Assessing the phototoxicity of titanium dioxide nanoparticles (TiO_2 NPs) is a relatively novel line of research but has gained significant importance as use of TiO_2 NPs increases. Inclusion in a large variety of industrial and person use applications has driven the production of TiO_2 NPs exponentially across the last decade. Future production estimates place manufactured amounts above 2,000,000 metric tons per year by 2025[41]. TiO_2 NPs in applications such as food and cosmetics, paints, concretes and surface coatings, and as a source of microbial/wastewater treatment[142-145] are subject to natural movement to environmental compartments throughout the product lifecycle[42,146-148].

Current TiO_2 Toxicity Measurements and Estimates

The movement of TiO_2 NP to aquatic compartments represents a significant increase in hazard to aquatic species. TiO_2 NPs in water are relatively nontoxic (upwards of grams/L) until exposed to ultraviolet light. Exposure to natural sunlight dramatically increases the risk of toxicity to organisms within the water column. UV-A photoexposure results in multiple magnitude increases in toxicity measurements for multiple indicator species[78]. However, toxicity measurements vary substantially from lab to lab, and setting to setting. For example, Ma et al. (2012) found a 48-hr LC_{50} of 29.8 µg/L in *D. magna*[17]. Mansfield et al. (2016) found an 8-hr LC_{50} of 139 µg/L in *D. magna*[15].

Amiano et al. (2012) found a 48-hr LC_{50} between 1.2 to 3.4 mg/L in *D. manga*[14]. The differences in these toxicities can be directly correlated to the UV-A intensity exposure intensity. Clemente et al. (2014) note differing effects in *D. renio* embryos such as mortality, hatching times, physical deformations and increased activity directly correlated with UV-A intensity and crystallinity ratios of TiO_2 NPs[66].

Li et al. (2015) has produced a mathematical model to estimate phototoxicity of TiO_2 NPs to *H. azteca* considering the importance of nanoparticle concentration, light intensity, and time of exposure. This dosimetric model adequately addresses the Bunsen-Roscoe reciprocity relationship seen in the majority of photoactivated chemicals and materials[62]. However, the model, and previous TiO_2 toxicity assessments leave out an important component of natural waters, natural organic matter (NOM). Wormington et al. (2017) include 4 mg/L NOM (relative measurement) in toxicity assays and almost 100% reduction in mortality, with reduction in mortality well correlated with increasing NOM concentrations[55]. Lin et al. (2012) note a decrease in IC_{50} from 4.9mg/L to 18 mg/L in *Chlorella* sp. on the addition of 5 mg/L of dissolved humic acid (a main component of NOM)[69]. The ubiquitous nature of NOM in surface waters necessitates the addition to all toxicity testing.

These aforementioned toxicity results are a few of many examples of toxicity modulations given changing environmental and physiochemical conditions of TiO_2 exposure. To understand how such conditional changes have a direct effect on toxicity, the mechanism to generate toxicity must be examined. Photons with energy greater than 3.2 eV (corresponding to between 400 to 380 nm and less) are absorbed by the surface of

TiO_2 NPs, exciting electrons from the valance band to the conductance band. This photoexcitation process generates a high energy electron and a positively charged area on or within the TiO_2 lattice, commonly referred to as a 'hole'. The excited electron will reduce with oxygen to superoxide, while the hole will abscond and electron from a surrounding water molecule, generating hydroxyl radicals[13,18]. The rate of hydroxyl radical generation is a conditional function relying implicitly on environmental parameters, as shown in previous chapters, and physiochemical parameters of matrices and particles[39,131,149,150].

Physical Parameters Affecting Radical Production

Toxicity heavily depends on the nanoparticle characteristics. Increases in nanoparticle concentration result in greater mortality. Size also plays a significant effect on nanoparticle toxicity. Smaller TiO_2 nanoparticles produce greater toxic effects than larger[56,57,158]. These effects are linked to surface area: Lee et al. (2009) demonstrated, using the Brunauer-Emmett-Teller (BET) method, that smaller TiO_2 nanoparticles had a larger surface area[166] and Lin (2014) demonstrated that smaller TiO_2 nanoparticles with larger available surface areas were the most toxic to *E. coli*[158]. Lin et al. (2006) demonstrated exponential decreases in photocatalytic rate constants with increases in primary particle size Lin:2006ca}. These results demonstrate that increases in hydroxyl generation rate as a result of increasing are ultimately responsible for increased radical concentrations resulting in toxicity. Significant differences in toxicity are also seen in the specific morphology of TiO_2, comparing nanotubes, nanorods, nanosheets, and nanospheres to P25 nanoparticles[167,168]. This

can be further expanded to include modulations such as functionalized TiO_2 or other nanoTiO_2; increases in toxicity are seen in graphene-TiO_2[169] compared to simple anatase.

A significant driver of hydroxyl radial generation, and thus toxicity, is TiO_2 nanoparticle crystal phase. Anatase nanoparticles show significantly more radical generation, and greater phototoxic effects than rutile or amorphous counterparts under UV-A light[103,158]. Interestingly, He et al., (2016), has demonstrated increased toxicity of anatase nanoparticles when coated with humic acid. This increased toxicity was thought to be due to the alteration of bandgap properties, a result of the photosensitization of humic acid. The ability of HA to interact with photo-produced holes on the crystal's lattice results in a slight but significant increase in measured superoxide[131]. There are a number of pathways that superoxide can generate hydroxyl radicals during the irradiation of TiO_2[13], which has been discussed in depth in previous chapters.

Along with natural weathering and coating of TiO_2 nanoparticles, surface modified particles adapted for a variety of uses are apt to entire aquatic compartments. Surface functionalities to enhance and aid photocatalysis are becoming increasingly common. These functionalities can be carbon modified to enhance hydroxyl generation as a means of pollution elimination[170], but are more commonly used in sunscreen with a $Al(OH)_3$ coating, which captures photoactivated electrons in an effort to reduce generation of ROS[82]. These nanoparticles are washed directly into surface waters during recreation, where the surface coatings break down over time, exposing the TiO_2 core. Al-Abed et al. (2016) demonstrate a small but measurable increase in photocatalytic

behavior following a 14-day aging of $Al(OH)_3$ coated TiO_2 nanoparticles resulting in increased cellular toxicity compared to unaged equivalents[82]. Aged particles in sediment were measured to produce significant amounts of hydroxyl radical, and were shown to negatively impact growth rates of *Hyalella azteca*[171].

This multiplicity of factors including, but not limited to, coatings, size, and crystal phase of the TiO_2 has a significant effect on the generation. It would be an inaccurate measure to describe toxicity, on a whole, in terms of TiO_2 nanoparticle concentration, because the specific nature of the particle is difficult to define, especially in a post-life aquatic environment. Certainly, these weathered nanoparticles can be isolated and characterized, although the time and effort required cannot be overstated. Describing toxicity as hydroxyl radical generation inherently includes environmental conditions and particle characteristics.

Implications of Hydroxyl Radicals on Organism Toxicity

Hydroxyl radicals are known to be cellular oxidizers, initiating radical cycling, lipid peroxidation, generating DNA adducts, and cytotoxicity[151-154]. Indeed, the ability of TiO_2 NPs to generate these species for antiseptic and antimicrobial purposes is a substantial reasoning for inclusion in surface coating and wastewater treatment methodology. The direct effects of environmental conditions on radical generation rate have been previously correlated in Chapter 2. Herein, radical generation rate to is correlated to organism toxicity. Variations in toxicity can be directly linked to chances in environmental conditions, which have a direct impact on hydroxyl generation rate. Describing TiO_2 NP toxicity as concentration of the nanoparticle alone is unintentionally

misleading and does not account for important physical and chemical interactions that will directly impact the overall the phototoxicity of these nanoparticles to organisms. A correlation of to hydroxyl radical concentration will inherently include both environmental effects and physiochemical effects, leading to a more resolved description of risk to aquatic organisms.

MATERIALS AND METHODS:

System Characterization

Stock suspensions of titanium dioxide nanoparticles (Aldrich, Anatase nanopowder, <25nm, 99.7% metals basis) were distributed in 18-mega Ohm distilled water with 15 minutes stirring followed by 2 hours of 10 min on/5 min off sonication using immersion tip. Stock suspensions were volumetrically diluted to working suspensions in EPA recipe Moderately Hard water. Working suspension nanoparticle concentrations ranged from 0 mg/L to 14.0 mg/L. Size of nanoparticles in stock solution measured using a Hitachi H7600T TEM and Wyatt Dawn Helios-II Dynamic Light Scattering.

Suspensions also contained a varying concentration of natural organic matter (NOM), measured quantitatively as dissolved organic carbon (DOC). NOM was obtained directly from the headwaters of the Suwanee River, collected at Suwanee River Visitor Center, Fargo, Georgia. All water was filtered through 0.45 mm Nylon filters to remove non-dissolved particulate. Filtered water was lyophilized to determine amount of dissolved organic particulate; dissolved organic carbon measured in triplicate by TOC using a Shimadzu TOC-V Carbon Analyzer. Elemental analysis of NOM completed

using Thermo X series ICP-MS. DOC (0 mg/L to 5.71 mg/L) was volumetrically added to the above described nanoparticle suspension.

Initial zeta potential of suspensions, and aggregate size across 48 hours was measured as well, and reported in previous chapters. Zeta potential was measured across all 0-hr concentrations of TiO_2 and DOC using a Malvern Zetasizer Dynamic Light Scattering and Zeta Potential instrument. Aggregate size was measured across all TiO_2 and DOC concentrations, and under all intensities of UV light, at 0, 24 and 48 hours, using a Wyatt Dawn Helios-II Dynamic Light Scattering. All samples were measured under ambient room temperature.

Specific UV irradiance and spectral output was measured across the UV-A spectrum, 400-nm to 320-nm under CLX Topaz 40W Blacklight Blue (BLB) T12 fluorescent bulbs, using an OceanOptics JAZ photospectrometer with a cosign corrector. Bulbs were installed in a standard ballast seated within a plywood box measuring 48" long, by 12" wide, by 12.5" across, with a bulb to surface distance of 8". Spectroscopic data was analyzed using OceanView 1.5.2.

Radical Measurement Using Fluorescence Spectroscopy

Ten conditional schemes were chosen from the full factorial design of five DOC concentrations, and four UV-A light intensities. The hydroxyl rates produced by these conditions were measured in a previous chapter. Briefly, the specific TiO_2 and DOC concentrations, along with fluorescein dye (concentration dependent on TiO_2 concentration) were combined in a 100 mL volumetric flask. This flask was well mixed, and three 30 mL aliquots were distributed in 50 mL beakers. These beakers were covered

with UV-transparent Alcar® Fluoropolymer film, and then exposed to UV-A light for 48 hours. At 12-hour time points, a 3 mL aliquot was removed and the decrease in light emission at 513 nm was measured using a Horiba Fluoromax-4 fluorescent photospectrometer. The emissions differences between time point X and the 0 hour time point were set to a calibration curve, generated using horseradish peroxidase and hydrogen peroxide, a hydroxyl radical generation method utilized in the HORAC assay. Instrumental conditions are as follows: Excitement wavelength was 467 nm, slit-width 1nm, emission measured from 400 to 700 nm, with specifically measured emission peak at 513 nm, slit-width dependent on dye concentration. Both slit-width and dye concentration were modulated to not exceed the upper bounds of the instrument's limit of detection. Each sample was analyzed in triplicate, with the average emissions per wavelength resulting in a single value per wavelength. Finally, the 0 mg TiO_2 concentration radical generation were subtracted from all hydroxyl generation to account for dye bleaching effects and radicals not produced by TiO_2 irradiation.

Organisms and Bioassays

Daphnia magna were cultured at Clemson University using protocol provided by the Clemson University Institute of Environmental Toxicology. Organisms were reared in United States Environmental Protection Agency recipe moderately hard water. Temperature of incubator was maintained at 25±1 °C with a light intensity between 10 $\mu E/m^2/s$ to 20 $\mu E/m^2/s$ and a photoperiod of 16 hour light to 8 hour dark. Routine toxicity references testing using sodium chloride to ensure culture sensitivity were preformed

frequently. Results are available from the Clemson Institute of Environmental Toxicology.

All *D. magna* bioassays conformed to standard EPA *Daphnia magna* 48-hour Acute Bioassay protocols. Less than 24-hour-old neonates were randomly selected from a pool of organisms and exposed to TiO_2 nanoparticle suspensions, with varying amounts of DOC, irradiated by varying intensities of UV light. These experimental conditions were identical to the conditions used in the fluorescent spectroscopy experiments to determine radical generation. Fluorescein dye was not included in the bioassays. All concentrations were replicated four times, five *D. magna* per exposure chamber, with each exposure chambers holding 30 mL test solution. Mortality was assessed at 0, 24, and 48 hours; pH and temperature recorded at each time point, and water quality preformed and the onset of each test.

Following mortality assessment, mortality percentage was calculated. The mortality observed per TiO_2 concentration in specific DOC concentrations under specific irradiant light was linked to hydroxyl radical generation under the same conditions, as measured from fluorescence spectroscopy. Multiplying the rate of hydroxyl radical generation in µM/h by the amount of time irradiant intensity entered the exposure flasks, a total amount of generated hydroxyl radical was calculated. In this manner, toxicity was described as hydroxyl radical concentration. Bioassay data is described as LC_{50} values. LC_{50} values for phototoxic dose were calculated using standard Spearman-Karber methodology. LC_{50} values were determined using XLSTAT 2018.2.50628, and the Dose-Effect Anaylis Tool.

RESULTS:

Hydroxyl radical concentrations were measured by fluorescent spectroscopy in TiO_2 suspensions under varying simulated environmental conditions. Following *Daphnia magna* 48-hour acute bioassays, and combining mortality results with hydroxyl radical generation, *D. magna* LC_{50} mortality was correlated to hydroxyl radicals concentration(Table 5.1). Further, using the hydroxyl radical generation rate model developed in Chapter 4, these conditionally based LC_{50}s can be predicted to less than a μM of hydroxyl radicals. Conditional dependence of LC_{50} values is demonstrated, and NOM was determined to play a protective role to organisms through competitive radical quenching interactions.

Experimental Conditions

Experimental conditions have been characterized in previous chapters. Briefly, TiO_2 nanoparticles were measured as 21.3 nm ± 0.3(SE) nm, using TEM and DLS techniques. Zeta potential was negatively correlated with increases in TiO_2 concentration. Aggregate size was also measured using DLS techniques, with TiO_2 and DOC concentrations positively correlating to aggregate size. As time in suspension increased, aggregate size decreased, as gravitational settling pulled larger sized aggregates to the bottom of the flask, leaving aggregates between 200-400 nm in suspension.

Dissolved organic carbon was used as the measurement of natural organic matter in the system. DOC stock concentration, directly filtered from Suwanee River Water (SRW) was measured to be 61.34 mg/L (± 0.43 mg/L). Both DOC concentration and

elemental analysis were equivalent to SRW NOM characterized by the International Humic Substances Society. Similar to the TiO_2 trend, addition of DOC had negative correlation to zeta potential.

Absolute irradiance was averaged per nm across the UV-A spectra. Highest lighting output (2 BLB blubs) measured at 5.188 (±0.032) $\mu W/cm^2/nm$, with a maximum peak (365 nm) of 10.833 (±0.054) $\mu W/cm^2$. The midrange light intensity (1 BLB bulb) had an average absolute irradiance of 4.301 (±0.017) $\mu W/cm^2/nm$, with a maximum peak (365 nm) of 9.578 (±0.034) $\mu W/cm^2$. The lowest UV intensity level (1 BLB bulb, screened) average absolute irradiance (320-400 nm) was 2.671 (±0.004) $\mu W/cm^2/nm$, with a maximum peak (365nm) of 6.263 (±0.012) $\mu W/cm^2$. These intensities range from 6% to 12% of natural sunlight irradiance, 45.08 (±0.012) $\mu W/cm^2/nm$ and a maximum irradiance at 365 nm of 50.86 (±0.023) $\mu W/cm^2$, in Pendleton, SC (34.6518° N, 82.7838° W) on a summer day.

Radical generation by irradiation of TiO_2 nanoparticle suspensions has, in previous chapters, been characterized as hydroxyl radical. The rate of radical generation is affected by the exposure conditions, readily observable by the difference in generation rates. Hydroxyl radical generation was positively correlated with TiO_2 concentration increases, and with UV-A intensity increases. Rate was negatively correlated with increases in DOC concentration.

Daphnia magna Bioassays

Standard EPA 48-hour acute toxicity bioassays exposed *D. magna* to TiO_2 suspensions, with varying concentrations of DOC to UV-A intensities. For comparative

purposes shown in Figure 1, an initial set of experiments exposed *D. magna* to TiO_2 suspensions irradiated by extremely low UV-A light co-exposed with 4.28mg/L DOC (LC_{50}: 1109.0 (920.0, 1338.0) mg/L TiO_2), ~10% natural UV-A intensity with no DOC co-exposed in suspension (LC_{50}: 0.220 (0.163, 0.252) mg/L TiO_2 NPs), and ~10% natural UV-A intensity with 4.28 mg/L DOC co-exposed in suspension (8.55 (8.08, 9.05) mg/L TiO_2 NPs).

The exact conditions to generate these results were replicated and the hydroxyl radicals produced were measured using fluorescent spectroscopy. In this matter, TiO_2 toxicity could be translated into hydroxyl radical concentration as shown in Figure 5.2. Extremely low UV-A light co-exposed with 4.28 mg/L DOC was not measured. ~10% natural UV-A intensity with 0 mg/L DOC co-exposed in suspension: LC_{50}: 0.458 (0.415, 0.503) µM $OH^{\bullet}$, and ~10% natural UV-A intensity with 4.28 mg/L DOC co-exposed in suspension of 6.490 (5.990, 7.024) µM $OH^{\bullet}$.

Table 5.1 details the correlations of hydroxyl radical concentration to differing environmental conditions. Increasing amounts of DOC results in attenuation of hydroxyl radical LC_{50}. Toxicity increases further positively correlated with increasing light intensity. In conditions with no DOC, changes in light intensity result in no significant difference in hydroxyl radical LC_{50} 4.301: 1.353 (0.984, 1.892) µM $OH^{\bullet}$, LC_{50} 5.188: 1.222 (0.983, 1.478) µM $OH^{\bullet}$. Interestingly, at the high intensities of light (5.188 µW/cm_2/nm), toxicity is maximized, despite the influence of DOC (LC_{50}: 0.364 µM $OH^{\bullet}$ in 4.28 mg/L DOC compared to 1.222 µM $OH^{\bullet}$ in 0 mg/L DOC). These bioassay correlations are detailed in Figure 5.3.

DISCUSSION:

The successful characterization of *D. magna* mortality described as a function of hydroxyl radicals instead of the TiO_2 nanoparticle accomplishes a number of objectives. First, TiO_2 LC_{50}s can be directly correlated with hydroxyl radical LC_{50}, which inherently accounts for environmental based conditional effects; previous TiO_2 descriptions exhibit discrepancies in toxicity calculations from lab to lab. The hydroxyl radical LC_{50} can be predicted to good agreement to measured LC_{50}s using the hydroxyl radical generation model developed in the previous chapter. Moreover, toxicity is largely impacted by the rate of radical generation. Second, hydroxyl LC_{50} is affected by the conditions, as result of radical generation. Third, DOC attenuates hydroxyl toxicity through quenching, or binding of radicals, before interaction with organisms can occur. These objectives culminate in increasing the understanding of how environmental conditions affect the damages caused by organism interaction with hydroxyl radicals produced by the TiO_2 nanoparticle.

Correlating Toxicity to Hydroxyl Radical Concentration and Conditions

Translating titanium dioxide nanoparticle toxicity into hydroxyl radical toxicity implicitly describes the effects of the TiO_2 in a more accurate manner. Observing the TiO_2-measured LC_{50}s under a variety of conditions in Table 5.1, a number of associated trends are evident. Increases in DOC concentration result in a comparatively larger LC_{50}; conversely, increases in light intensity result in LC_{50} values that are continuously lower. These conditional effects underline the argument that toxicity cannot be describe as only

the concentration of nanoparticles. By correlating bioassay toxicity measured as TiO_2 concentrations to toxicity measured as hydroxyl radical concentration, a better understanding the role environmental conditions have in generating a toxic effect can be achieved.

Conditional Effects on Toxicity Measurements

By measuring the generation of hydroxyl radicals (using fluorescent spectroscopy) under the same conditions as *D. magna* bioassays, mortality can be directly correlated to hydroxyl radical concentration. Calculating LC_{50} toxicity to hydroxyl radicals using Spearman-Karber methodology results in resolved values with conditional correlations. Hydroxyl LC_{50} values still demonstrate conditional dependence. Observable trends show an increasing LC_{50} correlated with increases in DOC concentration. However, unlike TiO_2 LC_{50}s, the hydroxyl LC_{50}s do not show a decreasing correlation with increases in UV-A light intensity at a given DOC concentration. In fact, there is no difference between hydroxyl LC_{50}s under the 3 different intensities of light in 0 mg/L DOC.

Further, as light intensity increases, increases in DOC do not correlated to decreasing hydroxyl radial LC_{50}. As light intensity increases, TiO_2 concentrations to cause LC_{50} toxicity decreases, but as DOC increases, TiO_2 concentrations required to cause LC_{50} increases. This interplay ultimate affects the total hydroxyl radical concentration causing toxicity. By observing the rate of hydroxyl radical generation, the ultimate driver of toxicity becomes more evident. Higher amounts of TiO_2 result in higher rates of TiO_2 generation, which in turn result in higher LC50 measurements. This

implicitly implies that toxicity is a function of the measurable rate of hydroxyl radical generation. Speaking biologically, the rate at which radicals oxidize an organism's tissues will directly drive toxicity.

As DOC is added to the system, TiO_2 measured LC_{50} concentrations increase. By translating this to hydroxyl radicals, an increase in hydroxyl radical LC_{50} values occurs as well. This demonstrates that more hydroxyl radicals are necessary to cause mortality in conditions with higher amounts of NOM in solution. By matching the generation rate at the TiO_2 LC_{50} concentrations, increased rates of generation occur from low DOC to high DOC conditions. These increased rates result in the fact that more TiO_2 is needed to cause mortality under increasing DOC conditions.

Increasing TiO_2 increases measurable radical generation, and more radicals cause increased mortality under conditions without DOC. However, the increase in radical generation must be offset by NOM's ability to quench radicals as they are produced; a significantly large concentration of oxidizable functionalities exist within the molecular groups constituting NOM, available for radical reaction. These functionalities provide more accessible targets for hydroxyl radical oxidation compared to organism cellular membranes, effectively attenuating toxicity to the organism.

A wealth of sub-molecules composing the overall categorical description of NOM. These molecules include humic acids, fulvic acids, tannins, lignins, cellulose, and decaying plant and animal matter. These molecules, are in turn, composed of numerous aromatics, double bonded side groups, carboxylic acids, and long carbon chains, amines, and more, all are ready reactants for the oxidative power of the hydroxyl radical. The

breakdown of NOM by TiO_2 is moderately well described[132,155,156]. Measured breakdown of differing types of NOM, with varying concentrations of DOC, specific UV absorbance characteristics and UV_{254} values all showed similar degradation patterns and product distributions[93,155]. These results indicate a common pathway for oxidative breakdown. Resultant degradants resulted in a wide array of molecules indicating a nonspecific oxidative molecule, indicating a nonspecific oxidative species, the hydroxyl radical. These chemical results align well with the quenching hypothesis, and would result in less hydroxyl impact on organisms.

Aggregation will cause nanoparticles to drop out of suspension via gravitational settling. Brunelli et al. (2013), notes that significant settling in freshwater TiO_2 suspensions occurs in concentrations of 10 mg/L past 10 hours[157], although Keller et al. (2010), shows minimal settling even at 200 mg/L TiO_2[48], although these samples did have very high TOC levels. Samples were resuspended every 12 hours, keeping a relatively constant concentration in suspension. Loosli et al. (2013) notes moderate stability in TiO_2 suspensions with similar amounts of DOC[50]. Slight sedimentation at testing times was noticed, but samples were completely resuspended before aliquots were removed to ensure concentrations of TiO_2 were not impacted.

A portion of nanoparticles remaining in suspension may be coated by NOM over time, reducing the available surface area, but this coating would most likely not occur over the 48 hours, especially without consistent agitation. Further, removing the DOC component, with the same TiO_2 concentration would cause significantly more mortality, shown in the comparative bioassays in Figure 1**.** Bioassays with no DOC resulted in

complete mortality at 1 mg/L TiO_2, whereas the bioassay run with 4.28 mg/L DOC did not begin to exhibit mortal toxicity until 3 mg/L. Therefore, the radicals being produced by irradiated TiO_2 must be quenched by the available functionalities within the molecules of NOM components.

Organism Defense of ROS Damage

At low enough levels, an organism is able to detoxify and repair oxidative damage given sufficient time and energy. This indicates there is a specific rate of radical generation that *D. magna* can tolerate, until their oxidative defenses are overwhelmed. There is a wealth of research that shows the changes in of anti-oxidative and repair enzymes [66], such as catalase (CAT) and glutathione peroxidase (GPx), in organisms co-exposed to TiO_2 nanoparticles and UV-A irradiation, as well as enzymes associated with lipid peroxidation[102,158,159] and oxidative DNA damage[159]. Kim et al. 2010, demonstrate upregulation of CAT, GPx and glutathione-S-transferase in *D. magna* as a result of TiO_2 ingestion, only compounding the body burden of oxidative stress following[64]. The particulars of the exact mechanism of toxicity is outside the scope of this research, but toxicity is most likely a result of membrane disruption on the gill epithelia[35], evident through increased oxidative damages[64] such as lipid peroxidation and other stress markers in the gills[160,161]. Injuries as a result of photoactive TiO_2 nanoparticles were morphologically evident from disrupted membrane structures of the gills of rainbow trout at concentrations as low as 0.100 mg/L{Federici:2007he}. Such damage resulted in reduced ability for the gills to preform ion and gas exchange actions[161]. Degrees of success in dealing with and repairing the effects of oxidative

damage likely varies from species to species and will additionally be dependent on age[162].

Organism antioxidant defenses show changes in activity as ROS oxidative cycling occurs and attempts at repair are made. If the rate of radical generation exceeds a threshold level, the antioxidant defenses are overwhelmed resulting in organism mortality. Organisms also engage in physical behavior that effectively reduces potential damage caused by TiO_2. Zooplankton are known to migrate vertically through the water column throughout the day as a means of predator avoidance, ultimately affecting the dose of UV-radiation they receive throughout the day[163-165]. Considering these movements, there is a probable chance that an organism will not remain within a plume of nanoparticles for an equivalent time to test exposures (16-hr photoperiod). *D. magna* are also able to shed exoskeletons through molting. Excess TiO_2 buildup on *D. magna* exoskeletons may be removed through the molting process. In contrast, experimental exposures to TiO_2 nanoparticles were run in 30 mL beakers with constant irradiation.

The large range of TiO_2 LC_{50} values based on conditional effects underlines the argument that it is inaccurate to describe TiO_2 toxicity solely as the nanoparticle concentration. A wealth of experimental evidence shows that un-irradiated TiO_2 nanoparticles are non-toxic unless in large quantities. However, the toxicity rapidly elevates as UV-A intensity increases, a result of the hydroxyl radical produced by the TiO_2 nanoparticles. This hydroxyl radical will then react with the organism, at the cellular or molecular level, resulting in different types of damage, or death. Thus, it is the

hydroxyl radical that is the toxicant, and the nanoparticle that is merely the vector; toxicity descriptions solely as nanoparticles are inaccurate.

CONCLUSION:

Daphnia magna toxicity was correlated to hydroxyl radical concentration and shown to be dependent on both environmental conditions and TiO_2 concentration. Increases in DOC concentration requires more hydroxyl radicals to cause similar toxic effects as suspensions with lower amounts of DOC. Higher concentrations of TiO_2 are therefore required. Simultaneously, increases in light intensity will result in more radicals generated at a faster rate. This increase in radical generation rate results in a quicker onset of mortality, as radical concentrations reach higher amounts in a quicker time period. These results cannot be explained by TiO_2 concentration alone and must be correlated to associated environmental conditions. The influence of environmental conditions on toxicity can explain the differences in toxicity measurements between literature sources.

Ultimately, correlating organism toxicity to hydroxyl radical concentration (as opposed to TiO_2 NP concentration) as a more accurate means of describing TiO_2 nanoparticle toxicity. In this manner, damage is more elegantly described as a result of the toxicant hydroxyl radical, not the vector TiO_2 nanoparticle. The rate of hydroxyl radical generation is shown to play a significant role in assessing the toxicity imparted by TiO_2 nanoparticles, as organism antioxidant defenses will be overwhelmed given long enough exposure, or in the face of a rapid onslaught of radical generation. NOM plays a significant role in toxicity attenuation by quenching radicals as they are produced, giving

organisms more time to undergo cellular repairs. However, given large enough concentrations of TiO_2, radical interactions will still supersede antioxidant defenses.

Table 5.1: Environmental conditions for D. magna acute bioassays, and associated hydroxyl radical measurements. The hydroxyl LC_{50} measurements are driven by the rate of hydroxyl production, similar production rates result in similar hydroxyl LC_{50}s. These results indicate that an organism's ability to protect itself from oxidative stress is dependent on rate of radical production.

UV-A Intensity; µW/cm2/nm	DOC; mg/L	TiO_2 NPs LC50 (LB, UB); mg/L	Hydroxyl LC_{50} Measured (LB, UB); µM	Hydroxyl LC50 Predicted (LB, UB); µM	$OH^{\bullet}$ Generation Rate; µM/hr
0	0	NA	NA	NA	0
0	4.28	NA	NA	NA	0
2.671	0	0.632 (0.540, 0.747)	0.412 (0.237, 0.707)	0.591 (0.505, 0.699)	0.0287
2.671	1.57	2.996 (2.101, 3.993)	2.119 (1.347, 3.029)	2.705 (1.866, 3.639)	0.0966
2.671	4.28	11.203 (8.161, 18.230)	5.901 (4.009, 8.534)	9.637 (6.812, 16.725)	0.2652
4.301	0	0.738 (0.550, 1.021)	1.353 (0.984, 1.892)	1.302 (0.970, 1.802)	0.0434
4.301	2.95	6.396 (5.905, 8.233	6.588 (5.396, 8.050)	6.460 (5.380, 7.774)	0.1192
4.301	5.71	6.751 (4.754, 8.741)	2.207 (1.398, 3.390)	1.934 (0.636, 3.216)	0.0873
5.188	0	0.591 (0.488, 0.703)	1.222 (0.983, 1.478)	2.188 (1.750, 2.518)	0.0317
5.188	4.28	0.670 (0.428, 0.929)	0.364 (0.199, 0.544)	Unable to Predict	0.0125

48-hour Acute Bioassays for *D. magna* Toxicity to TiO_2 Nanoparticles

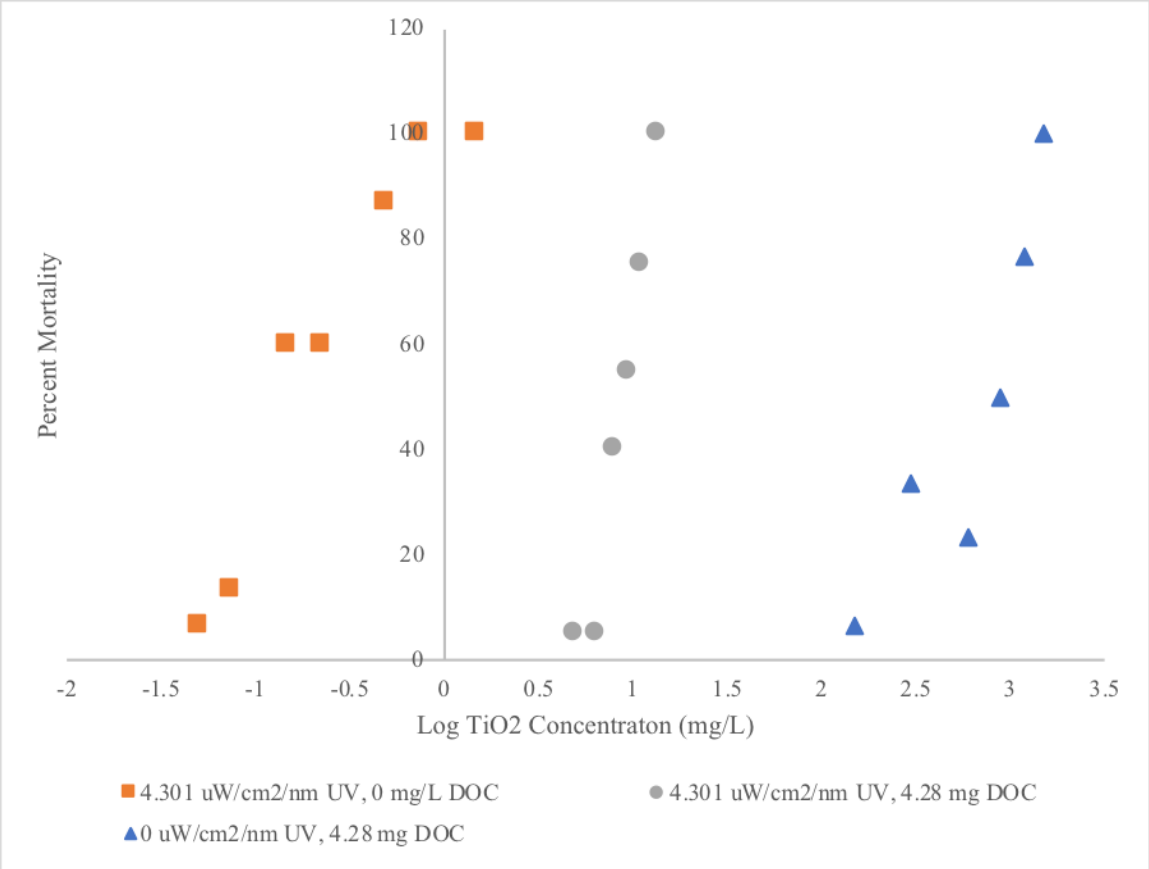

Figure 5.1 *Daphnia magna* LC_{50} toxicity to TiO_2 nanoparticles is dependent on the presence of UV light. *D manga* 48-hour acute LC_{50} toxicity exposed to 0 µW/cm^2/nm UV-A, 0 mg/L DOC: 1090.0 (920,1338.0) mg/L TiO_2 NPs; 4.301 µW/cm^2/nm UV-A, 0 mg/L DOC: 0.220 (0.163, 0.252) mg/L TiO_2 NPs; 4.301 µW/cm^2/nm UV-A, 4.28 mg DOC: 8.55 (8.08, 9.05) mg/L TiO_2 NPs.

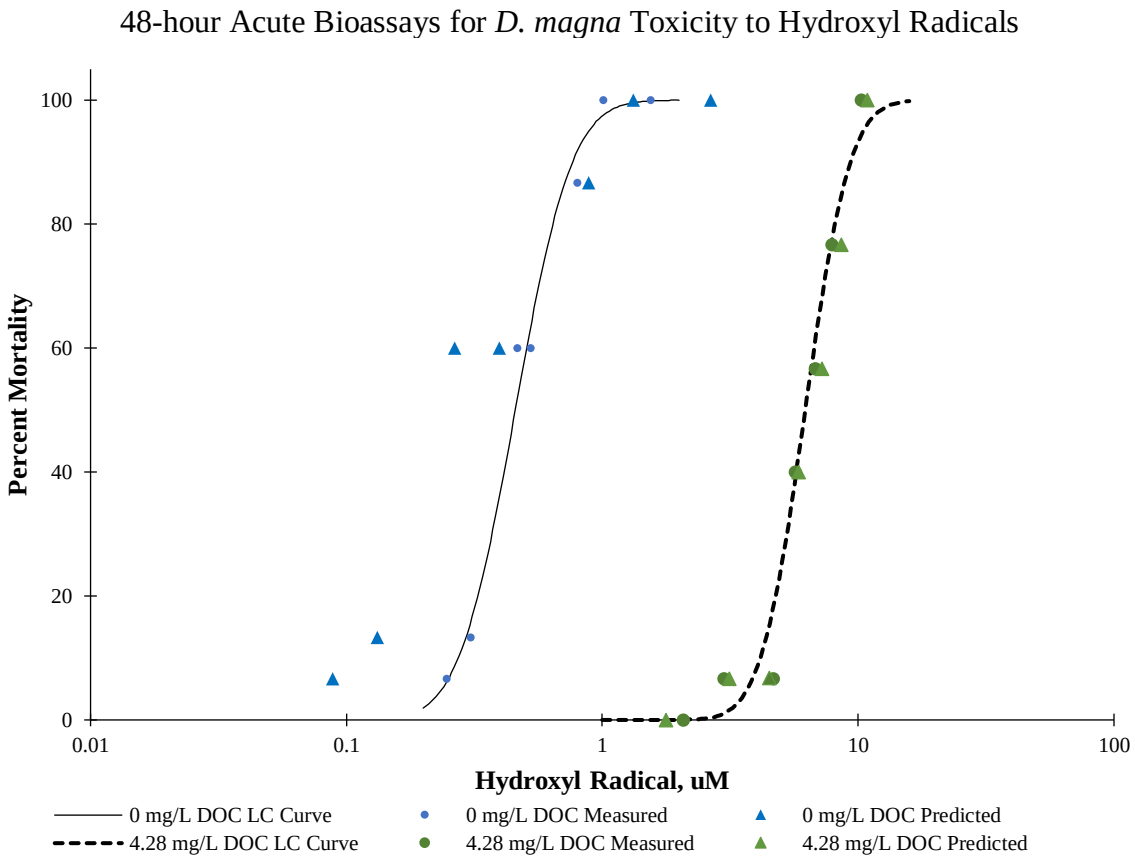

Figure 5.2: *Daphnia magna* acute bioassays described as hydroxyl radicals. (LC_{50}: 4.28 mg/L DOC Predicted: 6.490 (5.990, 7.024) µM; 4.28 mg/L DOC Measured: 6.216 (5.771, 6.691) µM; 0 mg/L DOC Predicted: 0.284 (0.235, 0.343) µM; 0 mg/L DOC Actual: 0.458 (0.415, 0.503) µM

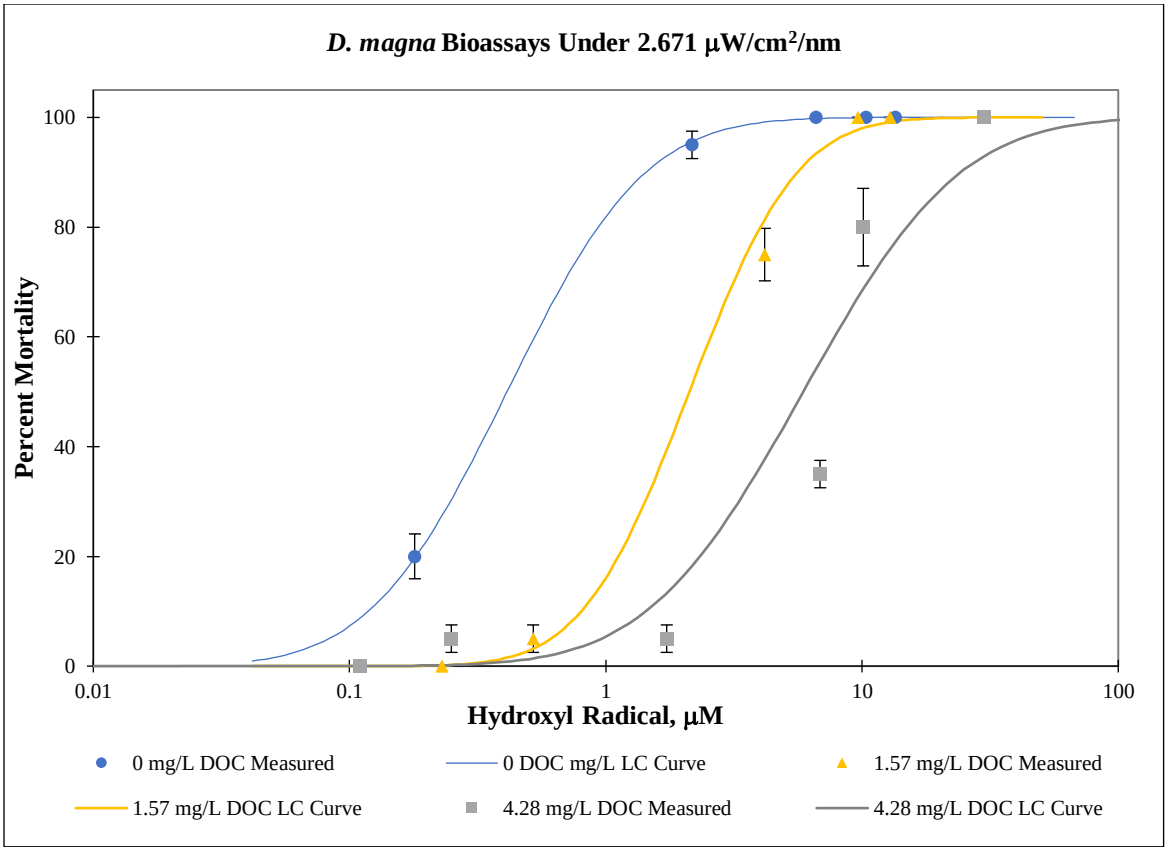

Figure 5.3 *Daphnia magna* bioassays under 2.1667 µW/cm^2/nm. Hydroxyl radical toxicity is well correlated to increasing amounts of DOC at low light intensities.

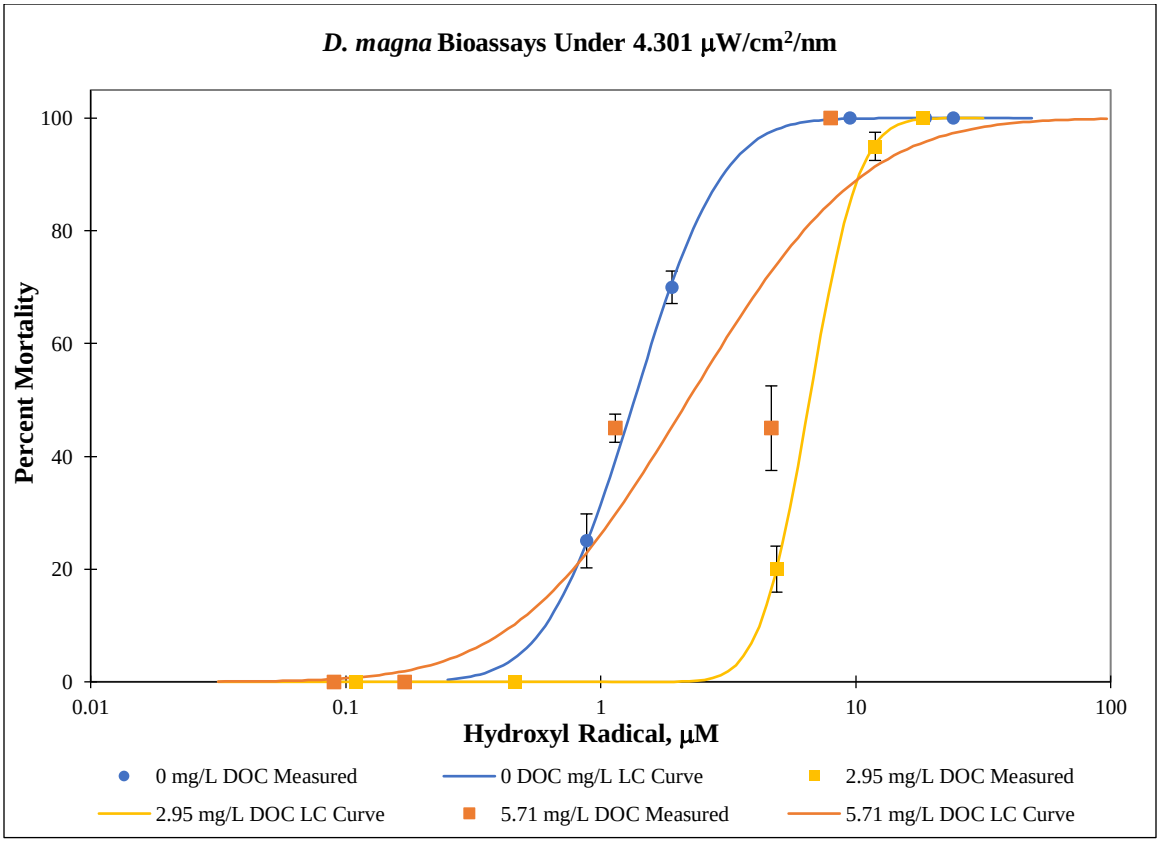

Figure 5.4 *Daphnia magna* bioassays under 4.301 µW/cm^2/nm. Hydroxyl radical toxicity is correlated to organism toxicity. Under conditions with high DOC, complete toxicity is delayed. A wider gradient concentration gradient causing mortality is also associated with higher DOC concentrations.

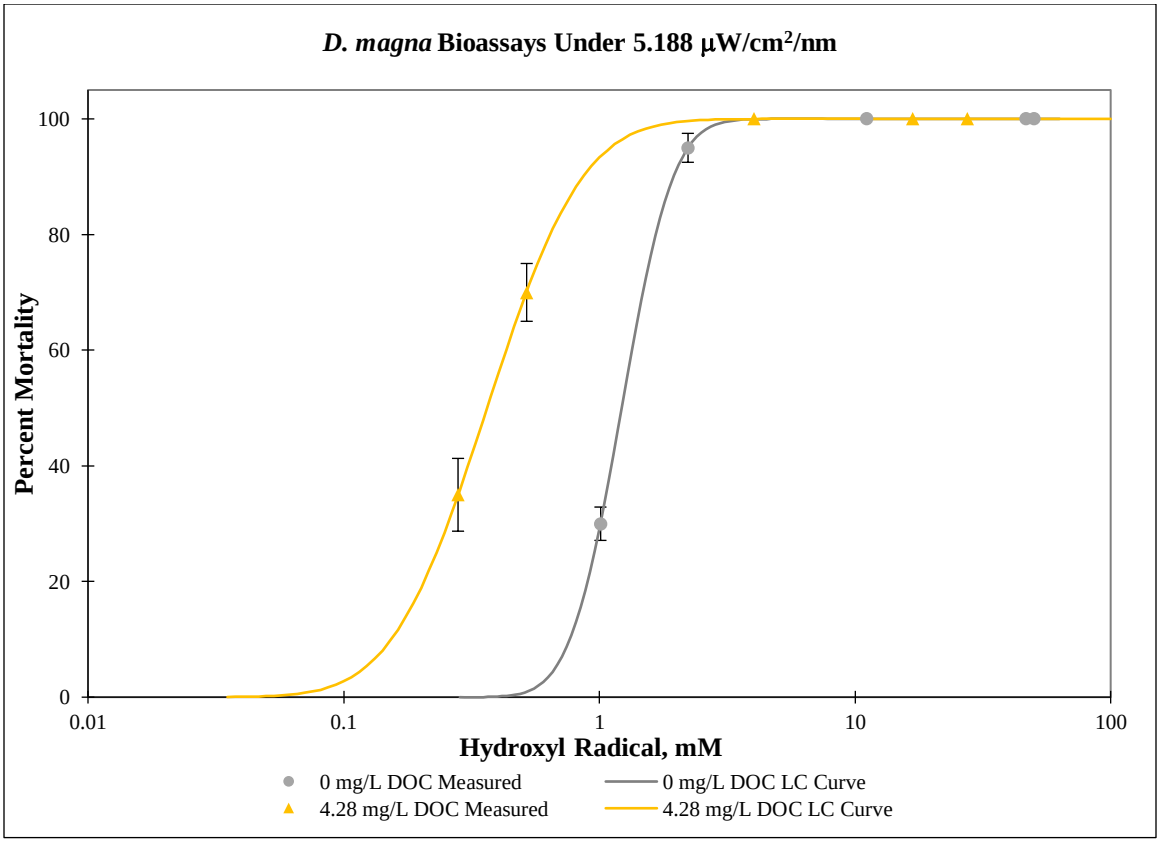

Figure 5.5 *Daphnia magna* bioassays under 5.188 µW/cm^2/nm. Hydroxyl radical toxicity is correlated to organism toxicity. Under conditions with high DOC, complete toxicity is delayed. A wider gradient concentration gradient causing mortality is also associated with higher DOC concentrations. These results demonstrate a higher toxicity in conditions with 4.28 mg/L DOC.

CONCLUSIONS

The increasing interest in including TiO_2 nanoparticles in optimized products for industrial and personal applications is ultimately driving production to exponential levels. Through usage, weathering, product breakdown, and disposal, these nanoparticles will eventually find their way to various environmental compartments. The ability of a specific area to properly dispose of these products will play a significant role in how, and how much of these nanoparticles transition to aquatic compartments. Once in the aquatic environment, these nanoparticles are subject to an array of interactions that heavily influence the particle's proclivity to generate reactive oxygen species.

Ultimately, the generation of reactive oxygen species is the driver of organism toxicity to titanium dioxide nanoparticles. Many of these interactions have previously been overlooked in toxicity studies, resulting in both under- and over-estimations of toxic amounts of nanoparticles. This dissertation has attempted to fill in some knowledge gaps surrounding TiO_2 toxicity by answering the overarching research question of how changes in environmental conditions modulate the generation of hydroxyl radical produced by irradiation of titanium dioxide nanoparticles. By understanding how the generation of radicals is affected by physicochemical interactions of both particle and environment, more accurate hypotheses regarding TiO_2 nanoparticle toxicity to any number of organisms can be made.

These goals were accomplished to a certain extent; there are many facets to the phrase 'environmental conditions' and addresses a number of important components. Focus was placed on the interactions of TiO_2 concentration, UV-A intensity, and amount

of NOM in a system, at environmentally relevant levels. Literature had presented few sources using NOM as a whole but had instead broken the conglomerate into a handful of its components, usually humic acid or fulvic acid. Although it is certainly important to understand how each part of NOM affects the particle, I ultimately see this as 'chasing a dragon'. NOM is far too complex, and too varied temporally and spatially to be able to adequately account for each part, every time. A singular component approach will ultimately fail to account for the complex interactions of the whole of NOM, which is vastly more important: the ubiquitous and pervasive nature of the molecule grouping in freshwater forces this to be true. Further, variation of NOM worldwide means that this model built from only one type of NOM (Suwanee River). Due to aforementioned variation, care must be taken when applying this model in situations using NOM that varies significantly from Suwanee River NOM. A more accurate approach would account for aromatic versus aliphatic ratios, in addition to overall DOC content.

Although there are many parameters that will affect radical generation and toxicity, the parameters were selected based on relevance to the overall paradigm. We are concerned with how changes in TiO_2 concentration is affected by changes in environmental conditions. Anatase crystallinity TiO_2 will absorb photons within the UV-A spectrum, but rutile will not. As absorption of photons within UV-A wavelengths within the water column is necessary to generate hydroxyl radicals, and these intensities will vary with water column depth, UV-A intensity was necessary to include. NOM will exist in all surface waters, and has been shown to attenuate TiO_2 toxicity, and was thus a necessary component. Heavy influence was placed on the environmental relevance of

testing conditions. TiO_2 concentrations are equivalent to environmental measurements. UV-A irradiance similar to that found within the water column, or shady banks. NOM concentrations are likewise close to average of many lakes found within the continental United States. The importance of using conditions of environmental relevance fulfils a classic environmental toxicology paradigm, simulating conditions found outside labs.

The effects these conditions have on the rate of photocatalytic generation of hydroxyl radicals from TiO_2 were determined based on 155 conditionally developed rate measurements. Introducing UV-A light, even at low intensities to TiO_2 nanoparticle suspensions will result in hydroxyl radical generation. Increasing the amount of TiO_2 under any amount of DOC, or light intensity will result in an increase in generation rates. Likewise, increases of light intensity result in increases of radical generation rate. Additions of NOM attenuate the generation of radicals, and as increasing amounts of NOM are included, rates decrease substantially. The interplay of these conditions shows the complex reciprocal effects influencing the radical, and also highlights areas information worthwhile to regulatory decision makers. Areas with high amounts of DOC or low amounts of light will be less sensitive to higher concentrations of TiO_2.

The time and effort to determine these rates was a considerable investment. It would unreasonable to expect rates to be done under every possible condition, and not feasible to do for every study a regulatory agency, risk management group, or laboratory undergoes. Models to predict hydroxyl generation rate under differing conditions can be used as an assessment tool. Two models were created, one without a NOM component and one with an NOM component, to help understand the importance of NOM in radical

rate prediction. The stochastic models produced from the data is an excellent start towards an overarching predictive equation goal. As produced, the models accurately predict radical generation under the range of experimental conditions, accounting for close to 95% of experimental effects. The models were applied to literature data, in an effort to test the soundness of the model, and limitations based on bounds. Although the models deviate outside of experimental bounds, most noticeably under higher intensities of light, they behave well within bounds, accurately predicting literature measured values. The model is also unable to predict changes in radical generation as nanoparticle size changes. The model with NOM ultimately preforms better, as it includes the influence of DOC radical attenuation.

The importance of understanding how the rate of hydroxyl generation is affected by environmental conditional changes is underlined in the final chapter, wherein *D. magna* were exposed to TiO_2 concentration gradients under changing conditions. TiO_2 nanoparticle toxicity measurements was successfully translate to hydroxyl radical measurements, inherently describing toxicity in a more accurate metric. TiO_2 nanoparticles are merely the vector producing the toxicant. Toxicity was demonstrated to be driven by the rate at which hydroxyl radicals are produced. This demonstrates importance of an organism's oxidant defense system. An overworked defense system will result in decreased health, and reproductive fitness. Further, younger organisms and organisms with less developed anti-oxidant responses are more at risk. These organisms sit at lower levels of food chains, so implications of effects on secondary and tertiary consumers is entirely within the realm of possibility.

To conclude, the assessments made in this dissertation add to the pool of knowledge concerning TiO_2 nanoparticle toxicity and the interactions of nanoparticles in complex aquatic environment. Hydroxyl radical generation rate was measured under interacting, environmentally relevant conditions and built a model from these rates to aid in regulatory and risk assessment decisions. Finally, TiO_2 nanoparticle toxicity was correlated with hydroxyl radicals, linking organism toxicity to the rate of radical generation.

FUTURE DIRECTIONS

There are a number of reasonable directions that this project could be expanded. Looking from the top, down, the importance of understanding the flow of nanoparticles to the environment has been identified. Although it was outside the scope of this dissertation, the estimations/measurements of actual concentrations of nanoparticles moving to the aquatic compartment is paramount to effective and correct assessment of the true risk of TiO_2 NPs. Work to continue identifying sources and means of movement is of high importance. Further, investigating the duality between world regions that use these enabled products vs those that have the infrastructure to handle product disposal represents an interesting avenue of product lifecycle research. The ability of wastewater treatment plants to remove TiO_2 NPs (and NPs in general) plays a role in hazard mitigation that cannot be understated. A footrace between nanoparticle usage and the development of WWTP technology, and improvement of infrastructure within less developed countries is occurring, and the results will have direct impact on TiO_2 NPs risk assessment.

The expansive nature of an environmental compartment makes an encompassing model difficult to produce. For example, the Biotic Ligand Model is the result of thousands of data points across a multitude of studies from many labs over many years. The models produced in this dissertation are a slight scratch on the surface, working to explain some basic interactions between a small number of conditions. Model expansion is the most obvious route of direction. Physical characteristics of the NP itself will play an important role in hydroxyl radical generation and toxicity. This current model

represents an upper bound measurement of radical production, as all the crystallinity of the nanoparticles was completely anatase. Mixes of nanoparticles will result in different generation rates, as UV-A wavelengths are not energetic enough to excite electrons in rutile nanoparticles enough to generate radicals. Further, this model only assesses effects of anatase nanoparticles of a particular size, 21 nm. Smaller nanoparticles have been shown to increase generation. Water quality changes such as alkalinity, and hardness will slightly modify interactions at the surface of nanoparticles, resulting in changes in radical generation rates, and need to be accounted for as well. Entire dissertations could be dedicated to dissecting a single of these components.

Further, bounds can always be expanded, particularly in the case of UV-A intensity. Future studies should use a more representative simulation of sunlight, rather than just low intensity BLB bulbs, to better account for the complete sunlight spectrum. Likewise, NOM component variation can also play a role in effects. Differing concentrations of the constitutional components of NOM can affect NP surface interactions and must be accounted for. Additional focus on the specific interactions of NOM and TiO_2 NPs is important as well. The mechanisms of NOM absorption to TiO_2 nanoparticles, and how changes in water chemistry affects this interaction would be an important improvement to the model as well.

Irradiated titanium dioxide has been shown to degrade NOM. As such, the interactions between the changing NOM components and TiO_2 must be better understood. This is certainly a complex question, and has many questions nested within. Studies observing the changes in radical generation as the aliphatic/aromatic ratio of NOM

changes under photocatalytic oxidation, as well as observations of whole NOM molecule changes using C_{13} NMP techniques may provide additional insight. One aspect that may have specific toxicological impact is determining the propensity for NOM breakdown to release bound metal ions. Copper ions bound to humic aids within NOM can be released during advanced oxidation of functionalities resulting in humic acid breakdown[172]. An increased concentration of bioavailable copper ions in water as a result of this break down can result in additional injury stress to organisms [173], compounding the oxidative stress damages from hydroxyl radical exposure. and if this will result in increased injury to organisms.

Based on the conclusions drawn from the 5th chapter, toxicity occurs as a result of oxidative damage. Although the risk for mortal toxicity is certainly present, the chronic exposure to TiO_2 is a more realistic bigger picture concern. Consistent energy and organism resources dedicated to system detoxification will result in less-fit organisms, reduced sexual reproduction, few offspring, and possible genetic mutations as a result of DNA adducts or mutations. An in-depth, multigenerational study about an organism's energetic, and genetic response to chronic TiO_2 exposure would be of significant use to helping explain the impacts of TiO_2 nanoparticle exposure. Morphological changes to gill epithelia caused by TiO_2-generated hydroxyl radical would be of a particular interest, as this area seems likely to be one of the more sensitive to exposure.

APPENDICES

Appendix A

Model Iteration Comparisons

Models with No Dissolved Organic Carbon

*Table A1.1 Through Zero, No Rules Backwards. The top selected model, produced using no-rules backward step AICc linear regression techniques. Model was forced through 0 to account for no radical generation under null conditions. Model equation is obtained from the sum of all Terms multiplied by their associated Estimate. (T_1*E_1) + (T_2E_2)…(T_n*E_n).*

Summary of Fit

R^2	0.973
R^2_{Adj}	0.964
RMSE	0.0743
Mean of Response	0.2708
Observations	30

AICc
-64.3645

Analysis of Variance

Source	DF	Sum of Squares	Mean Square	F Ratio
Model	3	7.4964	2.499	452.0591
Error	27	0.1492	0.006	**Prob > F**
C. Total	30	7.6457		<.0001*
Tested against reduced model: Y=0				

Parameter Estimates

Term	Estimate	Std Error	t Ratio	Prob>|t|	Lower 95%	Upper 95%	Variance
TiO_2*Light	0.07219	0.01214	5.95	<.0001*	0.0472766	0.0970967	0.00015
TiO_2*$Light^2$	-0.03701	0.006317	-5.86	<.0001*	-0.049967	-0.024045	3.990E-05
TiO_2*$Light^3$	0.00537	0.000785	6.84	<.0001*	0.0037592	0.0069808	6.162E-07

Effect Tests

Source	Nparm	DF	Sum of Squares	F Ratio	Prob > F
TiO_2*Light	1	1	0.1954	35.3547	<.0001*
TiO_2*$Light^2$	1	1	0.1897	34.3212	<.0001*
TiO_2*$Light^3$	1	1	0.2586	46.7906	<.0001*

Table A1.2 Through Zero, No Rules, Forwards. Produced using no-rules forward step AICc linear regression techniques. Model was forced through 0 to account for no radical generation under null conditions

Summary of Fit

R^2	0.981
R^2_{Adj}	0.972
RMSE	0.074548
Mean of Response	0.270813
Observations	30

AICc

-62.4357

Analysis of Variance

Source	DF	Sum of Squares	Mean Square	F Ratio
Model	4	7.5012	1.8753	337.4441
Error	26	0.1445	0.0055	**Prob > F**
C. Total	30	7.6457		<.0001*
Tested against reduced model: Y=0				

Parameter Estimates

Term	Estimate	Std Error	t Ratio	Prob>|t|	Lower 95%	Upper 95%	Variance
TiO_2*Light	0.0721	0.0122	5.93	<.0001*	0.0471	0.097151	0.00015
TiO_2*$Light^2$	-0.0370	0.0063	-5.84	<.0001*	-0.0500	-0.023962	4.01E-05
$Light^3$	0.0002	0.0003	0.92	0.3635	-0.0003	0.000746	6.25E-08
TiO_2*$Light^3$	0.0053	0.0008	6.79	<.0001*	0.0038	0.006964	6.21E-07

Effect Tests

Source	Nparm	DF	Sum of Squares	F Ratio	Prob > F
TiO_2*Light	1	1	0.1951	35.1085	<.0001*
TiO_2*$Light^2$	1	1	0.1895	34.0918	<.0001*
$Light^3$	1	1	0.0048	0.8555	0.3635
TiO_2*$Light^3$	1	1	0.2559	46.0432	<.0001*

Table A1.3 All Parameters, No Rules. Produced using no-rules, all parameters considered AICc linear regression techniques. Model was forced through 0 to account for no radical generation under null conditions

Summary of Fit

R^2	0.982
R^2_{Adj}	0.976
RMSE	0.078072
Mean of Response	0.270813
Observations	30

AICc

-62.4357

Analysis of Variance

Source	DF	Sum of Squares	Mean Square	F Ratio
Model	7	7.5055	1.07221	175.9118
Error	23	0.1402	0.0061	**Prob > F**
C. Total	30	7.6457		<.0001*

Tested against reduced model: Y=0

Parameter Estimates

Term	Estimate	Std Error	t Ratio	Prob>|t|	Lower 95%	Upper 95%	Variance
TiO_2	0.00016	0.0039	0.04	0.9682	-0.0080	0.0083	1.548E-05
Light	0.11015	0.1330	0.83	0.4159	-0.1649	0.3852	0.017675
TiO_2*Light	0.06088	0.0188	3.23	0.0037*	0.0219	0.0998	0.000354
$Light^2$	-0.05805	0.0692	-0.84	0.4101	-0.2011	0.0851	0.004787
TiO_2*$Light^2$	-0.03111	0.0097	-3.22	0.0038*	-0.0511	-0.0112	9.312E-05
$Light^3$	0.00742	0.0086	0.86	0.3969	-0.0104	0.0252	7.394E-05
TiO_2*$Light^3$	0.00462	0.0012	3.87	0.0008*	0.0021	0.0071	1.426E-06

Effect Tests

Source	Nparm	DF	Sum of Squares	F Ratio	Prob > F
TiO_2	1	1	0.00001	0.0016	0.9682
Light	1	1	0.00418	0.6865	0.4159
TiO_2*Light	1	1	0.06367	10.4466	0.0037*
$Light^2$	1	1	0.00429	0.704	0.4101
TiO_2*$Light^2$	1	1	0.06329	10.384	0.0038*
$Light^3$	1	1	0.00454	0.7453	0.3969
TiO_2*$Light^3$	1	1	0.09118	14.959	0.0008*

Table A1.4 Through Zero, Nonlinear, Bounded. Non-linear AICc linear regression bounded per parameter by expected interactions. Model was forced through 0 to account for no radical generation under null conditions. This was one of the weakest models produced.

Summary of Fit					
SSE	**DFE**	**MSE**	**RMSE**	$\mathbf{R^2}$	$\mathbf{R^2_{adj}}$
0.333818593	23	0.014514	0.1204734	0.9563	0.9493
AIC	**AICc**	**RSS**	**Likelihood**		
-45.011	-43.411	0.8078	-54.220		
Parameter Estimates					
Term	**Estimate**	**Std Error**			
TiO_2	0	0.0061			
Light	0.0028	0.2052			
TiO_2*Light	0.0015	0.0291			
$Light^2$	0	0.1067			
TiO_2* $Light^3$	0	0.0149			
$Light^3$	0.0001	0.0133			
TiO_2*$Light^3$	0.0008	0.0018			
Solved By: Analytic Gauss-Newton					

Table A1.5 Through Zero No Rules Backward. Model produced using no-rules backward step AICc linear regression techniques. Regression allowed to fit natural data (not forced through 0).

Summary of Fit

R^2	0.9730
R^2_{Adj}	0.9699
RMSE	0.0752
Mean of Response	0.2708
Observations	30

AICc	BICc
-61.94	-57.43

Analysis of Variance

Source	DF	Sum of Squares	Mean Square	F Ratio
Model	3	5.299	1.766	312.611
Error	26	0.147	0.006	**Prob > F**
C. Total	29	5.445		<.0001*

Tested against reduced model: Y=0

Parameter Estimates

Term	Estimate	Std Error	t Ratio	Prob>|t|	Lower 95%	Upper 95%	Variance
Intercept	0.01130	0.0175	0.65	0.5246	-0.0247	0.0473	0.0003
TiO_2*Light	0.07114	0.0124	5.75	<.0001*	0.0457	0.0966	0.0002
TiO_2*$Light^2$	-0.03672	0.0064	-5.73	<.0001*	-0.0499	-0.0236	4.098E-05
TiO_2*$Light^3$	0.00535	0.0008	6.73	<.0001*	0.0037	0.0070	6.320E-07

Effect Tests

Source	Nparm	DF	Sum of Squares	F Ratio	Prob > F
TiO_2*Light	1	1	0.1866	33.026	<.0001*
TiO_2*$Light^2$	1	1	0.1858	32.889	<.0001*
TiO_2*$Light^3$	1	1	0.2556	45.236	<.0001*

Table A1.5 Through Zero, No Rules, All Parameters. Model produced using no-rules all parameters included AICc linear regression techniques. Regression allowed to fit natural data (not forced through 0).

Summary of Fit

R^2	0.9743
R^2_{Adj}	0.9661
RMSE	0.0798
Mean of Response	0.2708
Observations	30

AICc	BICc
-61.9407	-57.4347

Analysis of Variance

Source	DF	Sum of Squares	Mean Square	F Ratio
Model	7	5.3053	0.7579	118.938
Error	22	0.1402	0.0064	**Prob > F**
C. Total	29	5.4455		<.0001*

Tested against reduced model: Y=0

Parameter Estimates

Term	Estimate	Std Error	t Ratio	Prob>|t|	Lower 95%	Upper 95%	Variance
Intercept	0.0001	0.0419	0	0.9973	-0.0868	0.0871	0.0018
TiO_2	0.0001	0.0060	0.02	0.9811	-0.0123	0.0125	3.57E-05
Light	0.1100	0.1400	0.79	0.4403	-0.1803	0.4004	0.0196
TiO_2*Light	0.0609	0.0196	3.11	0.0051*	0.0203	0.1015	0.0004
$Light^2$	-0.0580	0.0713	-0.81	0.4242	-0.2058	0.0898	0.0051
TiO_2* $Light^2$	-0.0311	0.0099	-3.14	0.0048*	-0.0517	-0.0106	9.83E-05
$Light^3$	0.0074	0.0088	0.84	0.4092	-0.0109	0.0257	7.78E-05
TiO_2* $Light^3$	0.0046	0.0012	3.78	0.0010*	0.0021	0.0072	1.50E-06

Effect Tests

Source	Nparm	DF	Sum of Squares	F Ratio	Prob > F
TiO_2	1	1	0.0000	0.00	0.9811
Light	1	1	0.0039	0.62	0.4403
TiO_2*Light	1	1	0.0616	9.67	0.0051*
$Light^2$	1	1	0.0042	0.66	0.4242
TiO_2* $Light^2$	1	1	0.0628	9.85	0.0048*
$Light^3$	1	1	0.0045	0.71	0.4092
TiO_2* $Light^3$	1	1	0.0909	14.26	0.0010*

Table A2.10 Not Through Zero, Nonlinear, Bounded. Non-linear AICc linear regression bounded per parameter by expected interactions. Model was allowed to fit the natural data (not forced through 0).

Summary of Fit					
SSE	**DFE**	**MSE**	**RMSE**	R^2	R^2_{adj}
0.20405761	22	0.0093	0.0963086	0.9733	0.9663
AIC	**AICc**	**RSS**	**Likelihood**		
-49.8177	-48.22	0.6882	-56.623		
Parameter Estimates					
Term	**Estimate**	**Std Error**			
Intercept	0.0009	0.0506			
TiO_2	0	0.0072			
Light	0.4191	0.1689			
TiO_2*Light	0.0015	0.0236			
$Light^2$	-0.2200	0.0860			
TiO_2*$Light^2$	0	0.0120			
$Light^3$	0.0274	0.0106			
TiO_2*$Light^3$	0.0008	0.0015			
Solved By: Analytic Gauss-Newton					

Models with Dissolved Organic Carbon (Appendix A2)

*Table A2.1 Through Zero, No Rules, Backward. The top selected model, produced using no-rules backward step AICc linear regression techniques. Model was forced through 0 to account for no radical generation under null conditions. Model equation is obtained from the sum of all Terms multiplied by their associated Estimate. (T_1*E_1) + (T_2E_2)…(T_n*E_n).*

Summary of Fit

R^2	0.9476
R^2_{Adj}	0.9458
RMSE	0.0658
Mean of Response	0.1622
Observations	155

AICc	BICc
-396.253	-378.56

Analysis of Variance

Source	DF	Sum of Squares	Mean Square	F Ratio
Model	5	15.8168	3.1634	730.9005
Error	150	0.6492	0.0043	Prob > F
C. Total	155	16.4660		<.0001*
Tested against reduced model: Y=0				

Parameter Estimates

Term	Estimate	Std Error	t Ratio	Prob>|t|	Lower 95%	Upper 95%	Variance
TiO_2*UV_i	0.0477	0.0047	10.06	<.0001*	0.0383	0.0570	2.243E-05
TiO_2*UV_i^2	-0.0230	0.0025	-9.36	<.0001*	-0.0279	-0.0181	6.032E-06
TiO_2*UV_i^3	0.0035	0.0003	11.36	<.0001*	0.0029	0.0041	9.303E-08
DOC*UV_i^3	-0.00013	2.93E-05	-4.44	<.0001*	-0.0002	-7.235e-5	8.585E-10
TiO_2*DOC*UV_i^3	-7.832e-5	5.58E-06	-14.04	<.0001*	-8.935e-5	-6.73e-5	3.1136E-11

Effect Tests

Source	Nparm	DF	Sum of Squares	F Ratio	Prob > F
TiO_2*UV_i	1	1	0.43828431	101.2663	<.0001*
TiO_2*UV_i^2	1	1	0.37941878	87.6654	<.0001*
TiO_2*UV_i^3	1	1	0.55832939	129.003	<.0001*
DOC*UV_i^3	1	1	0.08544253	19.7416	<.0001*
TiO_2*DOC*UV_i^3	1	1	0.85278695	197.0379	<.0001*

Table A2.2 Through Zero, No Rules, Forwards. Produced using no-rules forward step AICc linear regression techniques. Model was forced through 0 to account for no radical generation under null conditions.

Summary of Fit

R^2	0.9488
R^2_{Adj}	0.9464
RMSE	0.0654
Mean of Response	0.1622
Observations	155

AICc	BICc
-395.55	-372.189

Analysis of Variance

Source	DF	Sum of Squares	Mean Square	F Ratio
Model	7	15.8321	2.2617	528.1203
Error	148	0.6338	0.0042	Prob > F
C. Total	155	16.4660		<.0001*
Tested against reduced model: Y=0				

Parameter Estimates

Term	Estimate	Std Error	t Ratio	Prob>|t|	Lower 95%	Upper 95%	Variance
TiO_2*UV_i	0.06148	0.00836	7.35	<.0001*	0.044947	0.078005	6.9956E-05
TiO_2*UV_i*DOC	-0.00472	0.00236	-2.00	0.0476*	-0.009392	-0.000052	5.5838E-06
TiO_2*UV_i^2	-0.03007	0.00435	-6.92	<.0001*	-0.038652	-0.021479	1.8879E-05
TiO_2* UV_i^3	0.00432	0.00054	8.01	<.0001*	0.003256	0.005389	2.9160E-07
DOC*UV_i^2	-0.00062	0.00014	-4.42	<.0001*	-0.000902	-0.000345	1.9881E-08
TiO_2*DOC*UV_i^2	0.00248	0.00123	2.02	0.0451*	0.000055	0.004903	1.5055E-06
TiO_2*DOC* UV_i^3	-0.00039	0.00015	-2.53	0.0125*	-0.000686	-0.000084	2.3104E-08

Effect Tests

Source	Nparm	DF	Sum of Squares	F Ratio	Prob > F
TiO_2*UV_i	1	1	0.23134616	54.0197	<.0001*
TiO_2*UV_i*DOC	1	1	0.017096	3.9919	0.0476*
TiO_2*UV_i^2	1	1	0.20504336	47.878	<.0001*
TiO_2* UV_i^3	1	1	0.27487837	64.1845	<.0001*
DOC*UV_i^2	1	1	0.08369796	19.5436	<.0001*
TiO_2*DOC*UV_i^2	1	1	0.01748437	4.0826	0.0451*
TiO_2*DOC* UV_i^3	1	1	0.0273818	6.3937	0.0125*

Table A2.3 Through Zero, Combined Rules, Forward/Backward. Produced using combined rules forward step AICc linear regression. Model was forced through 0 to account for no radical generation under null condition

Summary of Fit

R^2	0.949
R^2_{Adj}	0.9443
RMSE	0.0667
Mean of Response	0.1622
Observations	155

AICc	BICc
-395.55	-372.189

Analysis of Variance

Source	DF	Sum of Squares	Mean Square	F Ratio
Model	13	15.8342	1.21802	273.7544
Error	142	0.63180	0.00445	**Prob > F**
C. Total	155	16.4660		<.0001*

Tested against reduced model: Y=0

Parameter Estimates

Term	Estimate	Std Error	t Ratio	Prob>|t|	Lower 95%	Upper 95%	Variance
TiO_2	-0.0006	0.0025	-0.22	0.8249	-0.0054620	0.0043608	6.17523E-06
UV_i	0.1051	0.0717	1.47	0.1446	-0.0365500	0.2468316	0.005137592
TiO_2* UV_i	0.0487	0.0074	6.63	<.0001*	0.0341904	0.0632514	5.40225E-05
DOC	-0.0009	0.0043	-0.21	0.8324	-0.0093870	0.0075691	1.83955E-05
TiO_2*DOC	0.0003	0.0008	0.44	0.6618	-0.0011820	0.0018561	5.91361E-07
UV_i *DOC	-0.0395	0.0176	-2.24	0.0267*	-0.0743890	-0.0046350	0.000311275
UV_i^2	-0.0598	0.0371	-1.61	0.1092	-0.1331640	0.0135442	0.001376929
TiO_2*UV_i^2	-0.0225	0.0038	-5.99	<.0001*	-0.0299150	-0.0150730	1.40925E-05
UV_i^3	0.0078	0.0046	1.69	0.0926	-0.0013040	0.0168876	2.11692E-05
TiO_2*UV_i^3	0.0033	0.0005	7.15	<.0001*	0.0024002	0.0042333	2.15296E-07
DOC* UV_i^2	0.0224	0.0091	2.47	0.0147*	0.0044737	0.0404112	8.26281E-05
TiO_2*DOC* UV_i^2	-0.0004	0.0001	-7.81	<.0001*	-0.0004910	-0.0002930	2.51502E-09
DOC* UV_i^3	-0.0030	0.0011	-2.70	0.0078*	-0.0052700	-0.0008130	1.27013E-06

Effect Tests

Source	Nparm	DF	Sum of Squares	F Ratio	Prob > F
TiO_2	1	1	0.0002185	0.0491	0.8249
UV_i	1	1	0.00957368	2.1517	0.1446
TiO_2* UV_i	1	1	0.19547591	43.934	<.0001*
DOC	1	1	0.00019991	0.0449	0.8324
TiO_2*DOC	1	1	0.00085495	0.1922	0.6618
UV_i *DOC	1	1	0.02231543	5.0155	0.0267*
UV_i^2	1	1	0.01155901	2.5979	0.1092
TiO_2*UV_i^2	1	1	0.15974537	35.9034	<.0001*
UV_i^3	1	1	0.01276030	2.8679	0.0926
TiO_2*UV_i^3	1	1	0.22769200	51.1747	<.0001*
DOC* UV_i^2	1	1	0.02712244	6.0959	0.0147*
TiO_2*DOC* UV_i^2	1	1	0.27137622	60.9929	<.0001*
DOC* UV_i^3	1	1	0.03239140	7.2801	0.0078*

Table A2.4 Through Zero, No Rules, All Parameters. Produced using no-rules, all parameters AICc linear regression. Model was forced through 0 to account for no radical generation under null conditions

Summary of Fit

R^2	0.9495
R^2_{Adj}	0.9440
RMSE	0.0669
Mean of Response	0.1622
Observations	155.0000

AICc	BICc
-395.55	-372.189

Analysis of Variance

Source	DF	Sum of Squares	Mean Square	F Ratio
Model	15	15.8400	1.0560	236.1655
Error	140	0.6260	0.0045	**Prob > F**
C. Total	155	16.4660		<.0001*

Tested against reduced model:
Y=0

Parameter Estimates

Term	Estimate	Std Error	t Ratio	Prob>|t|	Lower 95%	Upper 95%	Variance
TiO_2	0.0001761	0.002657	0.07	0.9472	-0.005076	0.0054283	7.05965E-06
UV_i	0.0755237	0.089807	0.84	0.4018	-0.102029	0.2530766	0.008065297
TiO_2* UV_i	0.0535876	0.012765	4.2	<.0001*	0.0283504	0.0788248	0.000162945
DOC	0.0000132	0.004457	0	0.9976	-0.008798	0.008824	1.98648E-05
TiO_2*DOC	-1.072e-5	0.000888	-0.01	0.9904	-0.001767	0.0017453	7.88544E-07
UV_i*DOC	-0.029197	0.02637	-1.11	0.2701	-0.081331	0.0229382	0.000695377
TiO_2* UV_i*DOC	-0.00169	0.003701	-0.46	0.6486	-0.009007	0.0056268	1.36974E-05
UV_i^2	-0.04088	0.046737	-0.87	0.3832	-0.133281	0.0515212	0.002184347
TiO_2* UV_i^2	-0.025843	0.006549	-3.95	0.0001*	-0.038791	-0.012896	4.28894E-05
UV_i^3	0.005164	0.005809	0.89	0.3755	-0.00632	0.0166482	3.37445E-05
TiO_2* UV_i^3	0.0037912	0.000811	4.68	<.0001*	0.0021884	0.0053941	6.57721E-07
DOC* UV_i^2	0.0156183	0.013699	1.14	0.2562	-0.011466	0.0427028	0.000187663
TiO_2*DOC* UV_i^2	0.0007953	0.001899	0.42	0.676	-0.002959	0.0045496	3.6062E-06
DOC* UV_i^3	-0.002087	0.001706	-1.22	0.2232	-0.005459	0.0012854	2.91044E-06
TiO_2*DOC* UV_i^3	-0.000169	0.000235	-0.72	0.4746	-0.000634	0.0002967	5.5225E-08

Effect Tests

Source	Nparm	DF	Sum of Squares	F Ratio	Prob > F
TiO_2	1	1	0.000019	0.0044	0.9472
UV_i	1	1	0.003162	0.7072	0.4018
TiO_2* UV_i	1	1	0.078801	17.6232	<.0001*
DOC	1	1	3.92E-08	0	0.9976
TiO_2*DOC	1	1	6.50E-7	0.0001	0.9904
UV_i*DOC	1	1	0.005481	1.2259	0.2701
TiO_2* UV_i*DOC	1	1	0.000933	0.2086	0.6486
UV_i^2	1	1	0.003421	0.7651	0.3832
TiO_2* UV_i^2	1	1	0.069633	15.5728	0.0001*
UV_i^3	1	1	0.003534	0.7903	0.3755
TiO_2* UV_i^3	1	1	0.097780	21.8676	<.0001*
DOC* UV_i^2	1	1	0.005812	1.2998	0.2562
TiO_2*DOC* UV_i^2	1	1	0.000784	0.1754	0.676

Table A2.5 Through Zero, Nonlinear, Bounded. Non-linear AICc linear regression bounded per parameter by expected interactions. Model was forced through 0 to account for no radical generation under null conditions. This was one of the two weakest models produced.

Summary of Fit

SSE	DFE	MSE	RMSE	R^2	R^2_{adj}
0.78131	140	0.00558	0.0747	0.93693	0.9316

AIC	AICc	RSS	Likelihood
-191.95	-189.753	1.1101	-382.77

Parameter Estimates

Term	Estimate	Std Error
TiO2	0.00176	0.002968
Light	0.14965	0.100330
TiO2*Light	0.00335	0.014261
DOC	-0.00137	0.004979
TiO2*DOC	-0.00024	0.000992
TiO2*Light*DOC	0.00516	0.004134
Light^2	-0.07820	0.052213
Light*Light^2	0.00965	0.006489
TiO2*Light*Light^2	0.00063	0.000905
TiO2*DOC*Light^2	-0.00269	0.002121
Light*DOC*Light^2	-0.00012	0.001906
TiO2*Light*DOC*Light^2	0.00025	0.000263

Solved By: Analytic Gauss-Newton

Table A2.6 Not Through Zero, No Rules, Backwards. No rule, backwards stepping AICc linear regression allowed to fit natural data (not forced through 0).

Summary of Fit

R^2	0.9476
R^2_{Adj}	0.9458
RMSE	0.0660
Mean of Response	0.1622
Observations	155

AICc	BICc
-394.06	-373.517

Analysis of Variance

Source	DF	Sum of Squares	Mean Square	F Ratio
Model	5	11.7381	2.34762	538.8075
Error	149	0.64920	0.00436	**Prob > F**
C. Total	154	12.3873		<.0001*
Tested against reduced model: Y=0				

Parameter Estimates

Term	Estimate	Std Error	t Ratio	Prob>|t|	Lower 95%	Upper 95%	Variance
Intercept	0.00018	0.008086	0.02	0.9823	-0.01579	0.0161578	6.53834E-05
TiO_2*UV_i	0.04764	0.004804	9.92	<.0001*	0.038153	0.0571392	2.30784E-05
$TiO_2*UV_i^2$	-0.02300	0.002472	-9.30	<.0001*	-0.02788	-0.018112	6.11078E-06
$TiO_2*UV_i^3$	0.00346	0.000306	11.3	<.0001*	0.002858	0.0040695	9.3636E-08
$DOC*UV_i^3$	-0.00013	3.45E-05	-3.79	0.0002*	-0.000199	-6.256e-5	1.19025E-09
$TiO_2*DOC*UV_i^3$	-7.828e-5	5.89E-06	-13.29	<.0001*	-0.00009	-6.664e-5	3.46921E-11

Effect Tests

Source	Nparm	DF	Sum of Squares	F Ratio	Prob > F
TiO_2*UV_i	1	1	0.42859743	98.3683	<.0001*
$TiO_2*UV_i^2$	1	1	0.3771321	86.5564	<.0001*
$TiO_2*UV_i^3$	1	1	0.55677518	127.7867	<.0001*
$DOC*UV_i^3$	1	1	0.06260031	14.3675	0.0002*
$TiO_2*DOC*UV_i^3$	1	1	0.76938388	176.5829	<.0001*

Table A2.7 Not Through Zero, No Rules, Forward. No rule, forward stepping AICc linear regression allowed to fit natural data (not forced through 0).

Summary of Fit

R^2	0.9488
R^2_{Adj}	0.9464
RMSE	0.0657
Mean of Response	0.1622
Observations	155

AICc	**BICc**
-393.332	-367.182

Analysis of Variance

Source	DF	Sum of Squares	Mean Square	F Ratio
Model	7	11.7536	1.67909	389.5135
Error	147	0.63368	0.00431	**Prob > F**
C. Total	154	12.3873		<.0001*
Tested against reduced model: Y=0				

Parameter Estimates

Term	Estimate	Std Error	t Ratio	Prob>|t|	Lower 95%	Upper 95%	Variance
Intercept	0.001547	0.008277	0.19	0.8521	-0.01481	0.01790	6.85087E-05
TiO_2*UV_i	0.061336	0.008425	7.28	<.0001*	0.04469	0.07799	7.09806E-05
TiO_2*UV_i *DOC	-0.004720	0.002371	-1.99	0.0484*	-0.00941	-3.434e-5	5.62164E-06
TiO_2*UV_i^2	-0.030027	0.004364	-6.88	<.0001*	-0.03865	-0.02140	1.90445E-05
TiO_2*UV_i^3	0.004319	0.000542	7.98	<.0001*	0.00325	0.00539	2.93764E-07
DOC* UV_i^2	-0.000641	0.000171	-3.76	0.0002*	-0.00098	-0.00030	2.9241E-08
TiO_2*DOC*UV_i^2	0.002480	0.001231	2.01	0.0458*	0.00005	0.00491	1.51536E-06
TiO_2*DOC*UV_i^3	-0.000385	0.000153	-2.52	0.0128*	-0.00069	-0.00008	2.3409E-08

Effect Tests

Source	Nparm	DF	Sum of Squares	F Ratio	Prob > F
TiO_2*UV_i	1	1	0.22849689	53.0065	<.0001*
TiO_2*UV_i *DOC	1	1	0.01708319	3.9629	0.0484*
TiO_2*UV_i^2	1	1	0.20407848	47.3419	<.0001*
TiO_2*UV_i^3	1	1	0.27417018	63.6017	<.0001*
DOC* UV_i^2	1	1	0.0608773	14.1223	0.0002*
TiO_2*DOC*UV_i^2	1	1	0.01749748	4.059	0.0458*
TiO_2*DOC*UV_i^3	1	1	0.0273666	6.3485	0.0128*

Table A2.8 Not Through Zero, Combined Rules. Combined rules AICc linear regression allowed to fit natural data (not forced through 0).

Summary of Fit

R^2	0.9490
R^2_{Adj}	0.9443
RMSE	0.0669
Mean of Response	0.1622
Observations	155

AICc	BICc
-379.666	-337.468

Analysis of Variance

Source	DF	Sum of Squares	Mean Square	F Ratio
Model	13	11.7559	0.904297	201.9257
Error	141	0.63145	0.004478	**Prob > F**
C. Total	154	12.3873		<.0001*
Tested against reduced model: Y=0				

Parameter Estimates

Term	Estimate	Std Error	t Ratio	Prob>|t|	Lower 95%	Upper 95%	Variance
Intercept	0.00726	0.02588	0.28	0.7796	-0.043908	0.058419	0.000670
TiO_2	-0.00122	0.00346	-0.35	0.7242	-0.008060	0.005615	0.000012
UV_i	0.10096	0.07344	1.37	0.1714	-0.044233	0.246147	0.005394
TiO_2*UV_i	0.04894	0.00742	6.6	<.0001*	0.034280	0.063599	0.000055
DOC	-0.00249	0.00709	-0.35	0.7261	-0.016494	0.011520	0.000050
TiO_2*DOC	0.00047	0.00091	0.52	0.6045	-0.001324	0.002266	0.000001
UV_i*DOC	-0.03879	0.01789	-2.17	0.0318*	-0.074151	-0.003419	0.000320
UV_i^2	-0.05884	0.03739	-1.57	0.1178	-0.132755	0.015078	0.001398
TiO_2* UV_i^2	-0.02253	0.00377	-5.98	<.0001*	-0.029978	-0.015079	0.000014
UV_i^3	0.00770	0.00463	1.67	0.0981	-0.001443	0.016851	0.000021
TiO_2* UV_i^3	0.00332	0.00047	7.14	<.0001*	0.002401	0.004241	0.000000
DOC* UV_i^2	0.02228	0.00914	2.44	0.0160*	0.004219	0.040346	0.000083
TiO_2*DOC* UV_i^2	-0.00040	0.00006	-7.21	<.0001*	-0.000507	-0.000289	0.000000
DOC* UV_i^3	-0.00303	0.00113	-2.67	0.0084*	-0.005264	-0.000786	0.000001

Effect Tests

Source	Nparm	DF	Sum of Squares	F Ratio	Prob > F
TiO_2	1	1	0.00055976	0.125	0.7242
UV_i	1	1	0.00846258	1.8897	0.1714
TiO_2*UV_i	1	1	0.1950546	43.5549	<.0001*
DOC	1	1	0.00055186	0.1232	0.7261
TiO_2*DOC	1	1	0.00120669	0.2694	0.6045
UV_i*DOC	1	1	0.02105054	4.7005	0.0318*
UV_i^2	1	1	0.01109038	2.4764	0.1178
TiO_2* UV_i^2	1	1	0.16006679	35.7422	<.0001*
UV_i^3	1	1	0.01241725	2.7727	0.0981
TiO_2* UV_i^3	1	1	0.22803181	50.9186	<.0001*
DOC* UV_i^2	1	1	0.02663316	5.9471	0.0160*
TiO_2*DOC* UV_i^2	1	1	0.23288122	52.0014	<.0001*
DOC* UV_i^3	1	1	0.03195221	7.1348	0.0084*

Table A2.9 Not Through Zero, Combined Rules, All Parameters. Combined rules AICc linear regression allowed to fit natural data (not forced through 0).

Summary of Fit	
R^2	0.9495
R^2_{Adj}	0.9440
RMSE	0.0671
Mean of Response	0.1622
Observations	155

AICc	**BICc**
-375.995	-328.724

Analysis of Variance

Source	DF	Sum of Squares	Mean Square	F Ratio
Model	15	11.7613	0.7841	174.1017
Error	139	0.62600	0.0045	**Prob > F**
C. Total	154	12.3873		<.0001*

Tested against reduced model: Y=0

Parameter Estimates

Term	Estimate	Std Error	t Ratio	Prob>|t|	Lower 95%	Upper 95%	Variance
Intercept	-0.000002	0.027783	0.000000	0.9999	-0.054933	0.054929	0.000772
TiO_2	0.000176	0.003960	0.040000	0.9646	-0.007654	0.008006	0.000016
UV_i	0.075525	0.092827	0.810000	0.4173	-0.108010	0.259061	0.008617
TiO_2*UV_i	0.053587	0.013023	4.110000	<.0001*	0.027838	0.079336	0.000170
DOC	0.000014	0.007884	0.000000	0.9986	-0.015574	0.015602	0.000062
TiO_2*DOC	-0.000011	0.001124	-0.010000	0.9924	-0.002233	0.002211	0.000001
Light*DOC	-0.029197	0.026969	-1.080000	0.2809	-0.082520	0.024126	0.000727
TiO_2*UV_i*DOC	-0.001690	0.003754	-0.450000	0.6533	-0.009113	0.005733	0.000014
UV_i^2	-0.040880	0.047246	-0.870000	0.3884	-0.134294	0.052533	0.002232
TiO_2*UV_i^2	-0.025843	0.006599	-3.920000	0.0001*	-0.038892	-0.012795	0.000044
UV_i^3	0.005164	0.005848	0.880000	0.3788	-0.006399	0.016727	0.000034
TiO_2*UV_i^3	0.003791	0.000815	4.650000	<.0001*	0.002180	0.005403	0.000001
DOC*UV_i^2	0.015618	0.013812	1.130000	0.2601	-0.011691	0.042928	0.000191
TiO2*DOC*UV_i^2	0.000795	0.001911	0.420000	0.6779	-0.002983	0.004573	0.000004
DOC*UV_i^2	-0.002087	0.001715	-1.220000	0.2258	-0.005478	0.001305	0.000003
TiO_2*DOC*UV_i^3	-0.000169	0.000237	-0.710000	0.4767	-0.000636	0.000299	0.000000

Effect Tests

Source	Nparm	DF	Sum of Squares	F Ratio	Prob > F
TiO_2	1	1	0.0000089	0.002	0.9646
UV_i	1	1	0.0029813	0.662	0.4173
TiO_2*UV_i	1	1	0.0762532	16.9316	<.0001*
DOC	1	1	1.36E-08	0	0.9986
TiO_2*DOC	1	1	0.0000004	0.0001	0.9924
Light*DOC	1	1	0.0052784	1.172	0.2809
TiO_2*UV_i*DOC	1	1	0.0009128	0.2027	0.6533
UV_i^2	1	1	0.0033718	0.7487	0.3884
TiO_2*UV_i^2	1	1	0.0690620	15.3348	0.0001*
UV_i^3	1	1	0.0035115	0.7797	0.3788
TiO_2*UV_i^3	1	1	0.0974243	21.6325	<.0001*
DOC*UV_i^2	1	1	0.0057584	1.2786	0.2601
TiO2*DOC*UV_i^3	1	1	0.0007802	0.1732	0.6779

Table A2.10 Not Through Zero, Nonlinear: Bounded. Non-linear AICc linear regression bounded per parameter by expected interactions. Model was allowed to fit the natural data (not forced through 0). This was one of the two weakest models produced

Summary of Fit					
SSE	**DFE**	**MSE**	**RMSE**	R^2	R^2_{adj}
AIC	**AICc**	**RSS**	**Likelihood**		
-184.885	-182.688	1.1101	-379.238		
Parameter Estimates					
Term	**Estimate**	**Std Error**			
Intercept	-0.061086	0.030980			
Light	0.075525	0.000000			
TiO_2*UV_i	0.004414	0.010153			
DOC	-0.001699	0.008877			
TiO_2*DOC	-0.000145	0.001277			
TiO_2* UV_i *DOC	0.008575	0.003421			
UV_i^2	-0.004288	0.009964			
UV_i^3	0.000763	0.001883			
TiO_2*UV_i^3	0.000596	0.000663			
TiO_2*DOC*UV_i^2	-0.004494	0.001758			
DOC*UV_i^3	-0.000118	0.001222			
TiO_2*DOC*UV_i^3	0.000478	0.000220			
Solved By: Analytic Gauss-Newton					

Appendix B

Generation Rates from Literature Compared to Predicted Generation Rates

Table B1.1: *Comparisons of Literature Measured Values versus Predicted Values of Hydroxyl Radical Generation Comparisons of measured hydroxyl radicals from literature sources to model predicted hydroxyl radicals considering the interactions between TiO_2 and UV-A intensity. Assumptions are noted on the table.*

Author	Organism/ Indicator	Nanoparticle (mg/L)	Nanoparticle Size	DOC mg/L	UV Intensity (µW/cm2/nm)	Degradation Rate	_	Predicted Hydroxyl Radicals (µM/h)	Total Radicals (µM)
Ba-Abbad et al., 2012	Chlorophenol Degradation	2000	10-50 nm	0	23W/m2	% Removal after X minutes	*Rate Con*		
		2000		0	**1.638 µW/cm2/nm**	50 mg/L: 100%; 60 m	3.69x10-2	85.10805297	85.10805297
		2000		0	assuming 6% UV across 320-400 nm	100 mg/L: 90%; 120 m	2.19x10-2	85.10805297	85.10805297
		2000				150 mg/L: 79%; 120 m	1.65x10-2	85.10805297	85.10805297
						2,4 DCP			
		2000		0		50 mg/L: 89.6%; 60 m	3.28x10-2	85.10805297	85.10805297
		2000		0		100mg/L: 75%; 120 m	1.71x10-2	85.10805297	85.10805297
		2000		0		150 mg/L: 71.6%; 120 m	1.37x10-2	85.10805297	85.10805297
						2,4,6 TCP			
		2000		0		50 mg: 82.4%; 120 m	2.41x10-2	85.10805297	85.10805297
		2000		0		100mg/L: 64%; 120 m	1.36x10-2	85.10805297	85.10805297
		2000		0		150 mg/L: 53.6%; 120 m	1.29x10-2	85.10805297	85.10805297

He et al., 2016	*E. coli*	*mg/L TiO2*	*Size Anatase*	*DOC*	*Light*	*Rate Decrease (rel)*			
						Compared to 0 [DOC]			
		1000	25.1 nm	0	0.18mW/cm2	0%		36.23667188	36.23667188
		1000	31.4	50	**2.25**	30%		36.23667188	36.23667188
		1000	22.4	200	**µW/cm2/nm**	27%		36.23667188	36.23667188
					assuming 320-400 nm				
			Size Rutile			Compared to 0 DOC			
		1000	34.5	0		0%		36.23667188	36.23667188
		1000	28.1	50		43%		36.23667188	36.23667188
		1000	30.6	200		3%		36.23667188	36.23667188
Hu et al., 2007	*Antimicrobial agents*	*TiO2 mg/L*	*Deguassa P25*			*initial rate µM/min*			*Per Minute*
	initial conc of sulfox 98 µM	100		0		3.9		2.462563917	0.041042732
	99 µM	0		0	*9x10-5 Einstein/min*	0.2		0	0
	98 µM	100		0	assuming across 320-400 nm	5.4		2.462563917	0.041042732
	85 µM	100		0	**0.43**	nr		2.462563917	0.041042732
	98 µM	100		0	**µW/cm2/nm**	nr		2.462563917	0.041042732
	5 µM	100		0		1.2		2.462563917	0.041042732
	9 µM	100		0		2.2		2.462563917	0.041042732
	47 µM	100		0		5.1		2.462563917	0.041042732
	90 µM	100		0		5.8		2.462563917	0.041042732
	230 µM	100		0		6.9		2.462563917	0.041042732
	480 µM	100		0		7.3		2.462563917	0.041042732
	93 µM	100		0		1.5		2.462563917	0.041042732
	92 µM	50		0		3.1		1.231281958	0.020521366
	92 µM	100		0		3.7		2.462563917	0.041042732
	87 µM	500		0		5.2		12.31281958	0.20521366
	81 µM	1000		0		6.9		24.62563917	0.410427319
	99 µM	100		0		4.2		2.462563917	0.041042732
	99 µM	100		0		5.1		2.462563917	0.041042732
	100 µM	100		0		5.4		2.462563917	0.041042732
	21 µM	100		0		2.7		2.462563917	0.041042732
	21 µM	100		0	HCO3-: 0.5 mM	3.2		2.462563917	0.041042732
	19 µM	100		0	HCO3-: 10 mM	4.3		2.462563917	0.041042732

	18 µM	100		0	HCO3-: 20 mM	6.7		2.462563917	0.041042732
	19 µM	100		0	HCO3-: 100 mM	6.2		2.462563917	0.041042732
	20 µM	100		0		4.2		2.462563917	0.041042732
	20 µM	100		2		0.76		2.462563917	0.041042732
	20 µM	100		10		0.54		2.462563917	0.041042732
	20 µM	100		20		0.54		2.462563917	0.041042732
	20 µM	100		0		3		2.462563917	0.041042732
	20 µM	100		2		5		2.462563917	0.041042732
	20 µM	100		10		3.6		2.462563917	0.041042732
	20 µM	100		20		2.4		2.462563917	0.041042732
	94 µM	100		0		3.8		2.462563917	0.041042732
Huang et al., 2008	*NOM*		*21 nm*		*8 W (helois Italquartz*	*Rate x mg/L /min*			
		100		10	**2.5**	0.0054		3.3070625	0.055117708
		300		10	**µW/cm/nm**	0.0154		9.9211875	0.165353125
		500		10		0.0156		16.5353125	0.275588542
		1000		10	assume 320-400 nm	0.0163		33.070625	0.551177083
Jassby et al., 2009	*terephthalic acid*		*P25 nm*		*1min@ 4.0E-5 W/cm2/s*	*reaction rate decrease*			
		5		0	**0.5**	0%		0.137570625	0.002292844
		5		0.5	**µW/cm2**	28%		0.137570625	0.002292844
		5		5		32%		0.137570625	0.002292844
		5		20		52%		0.137570625	0.002292844
Ma et al., 2012	3'[p-amiophenyl]-fluorescein		25 nm			**ROS Generation**			
		0.1		0	(320-400 nm)	~1 µM OCl^-		2.858418842	2.858418842
		0.5		0	No Filter	~4 µM OCl^-		14.29209421	14.29209421
		1		0	**19.8**	~12 µM OCl^- (ROS)		28.58418842	28.58418842
		0.1		0	Silica Window Glass	<1 µM		0.334117013	0.334117013
		0.5		0	**10.9**	~3.5 µM		1.670585067	1.670585067
		1		0		12 µM		3.341170133	3.341170133
		0.1		0	Petri Dish Glass	< 1 µM		0.893144046	0.893144046
		0.5		0	**14.2**	~4 µM		4.465720228	4.465720228
		1		0		12 µM		8.931440456	8.931440456

		0.1		0	Microscope Slide Glass	< 1 µM		1.061475657	1.061475657
		0.5		0	**14.9**	~4 µM		5.307378287	5.307378287
		1		0		12 µM		10.61475657	10.61475657
		0.1		0	Acrylic Glass	<1 µM		0.012348725	0.012348725
		0.5		0	**5.15**	< 1 µM		0.061743627	0.061743627
		1		0		< 1 µM		0.123487254	0.123487254
		0.1		0	345 nm cutoff (no wavelengths below)	< 1		0.423584347	0.423584347
		0.5		0	**11.6**	3.5 µM		2.117921736	2.117921736
		1		0		~11.5 µM		4.235843472	4.235843472
		0.1		0	360 nm cutoff	< 1µM		0.113603621	0.113603621
		0.5		0	**8.33**	2 µM		0.568018103	0.568018103
		1		0		8 µM		1.136036206	1.136036206
		0.1		0	400 nm cutoff	<1 µM		0	0
		0.5		0	**0**	<1 µM OCl-		0	0
		1		0		< 1 µM		0	0
Nagaveni et l., 2004			Deguassa p25		Driect sunlight 0.753 kW/m2	initial Degradation rates			
		0						0	0
	phenol	1000		0		0.012 µM/L/s		726154.9071	726154.9071
	p-nitrophenol	1000		0		0.37 µM/L/s		726154.9071	726154.9071
	salicyclic acid	1000		0	**53.65**	0.028 µM/L/s		726154.9071	726154.9071
					µW/cm2/s				
			Combustion synthesized		assuming 6% UV-A across 320-400 nm				
	phenol	1000		0		0.023 µM/L/s		726154.9071	726154.9071
	p-nitrophenol	1000		0		1.64 µM/L/s		726154.9071	726154.9071
	salicyclic acid	1000		0		0.75 µM/L/s		726154.9071	726154.9071

Sanders et al., 2012	TBARS	mg/L	22nm (a/r)		3.75 J/cm2 for 2 hours	relative to control			
		0		0		all NPs saw		0	0
		100		0	**13.02**	significant increase		651.3254568	1302.650914
					µW/cm2/nm	in ROS generation			
		mg/L	25 nm (A)		assuming across 320-400 nm	except 25nm Anatase **Relative assessment**			
		0		0				0	0
		100		0				651.3254568	1302.650914
		mg/L	31 nm (a/r)						
		0		0				0	0
		100		0				651.3254568	1302.650914
		mg/L	59 nm (a/r)						
		0		0				0	0
		100		0				651.3254568	1302.650914
		mg/L	142 nm (a)						
		0		0				0	0
		100		0				651.3254568	1302.650914
		mg/L	214 nm (r)						
		0		0				0	0
		100		0				651.3254568	1302.650914
Wormington et al., 2007	Fluorescein		< 25 nm			Actual $OH^{\bullet}$ µM/h			
		0		0	0	0		0	0
		0		3	µW/cm/nm	0		0	0
		0		6		0		0	0
		0		12		0		0	0
		0		0	52	~1.5		0	0
		0		3		~2		0	0
		0		6		~1.5		0	0
		0		12		~1.5		0	0
		4.5		0	0	0		0	0
		4.5		3		0		0	0
		4.5		6		0		0	0
		4.5		12		0		0	0

		4.5		0	52	~4		2962.557702	2962.557702
		4.5		3		~3.5		2962.557702	2962.557702
		4.5		6		~3.0		2962.557702	2962.557702
		4.5		12		~2.5		2962.557702	2962.557702
Wywroll et al., 2006	TFA	1000	7 to 10	0	2.36 mW/cm^2 UV-A	12.5		107713.0329	26928.25822
		1000	15 to 25	0	**29.5**	9		107713.0329	26928.25822
		1000	200 to 220	0	**µW/cm^2/nm**	3		107713.0329	26928.25822
					assuming 320-400 nm	**Relative Generation**			
					15 min IRT				
Yin et al., 2012	MTS Assay						**2.48 µW/cm^2/nm**	**4.96 µW/cm^2/nm**	**9.92 µW/cm^2/nm**
		0	A25 (25 nm	0	UV-A Doses assuming 320-390 nm	**Relative Generation**	0	0	0
		50		0	2.5 J/cm^2 => 173.61 µW/cm^2	P25>A25>A325>R100	1.665780883	5.133309146	115.7089775
		100		0	**2.48**		3.331561766	10.26661829	231.417955
			A325 (325 nm		**µW/cm^2/nm**				
		0		0			0	0	0
		50		0	5.0 J/cm^2 => 347.22 µW/cm^2		1.665780883	5.133309146	115.7089775
		100		0	**4.96**		3.331561766	10.26661829	231.417955
					µW/cm^2/nm				
		0	p25 (25 nm)	0			0	0	0
		50		0	10 J/cm^2 => 694.44 µW/cm^2		1.665780883	5.133309146	115.7089775
		100		0	**9.92**		3.331561766	10.26661829	231.417955
			R100 (100nm)		**µW/cm^2/nm**				
		0		0			0	0	0
		50		0			1.665780883	5.133309146	115.7089775
		100		0			2.958386117	10.26661829	231.417955

Table B1.2: Comparisons of measured hydroxyl radicals from literature sources to model predicted hydroxyl radicals, based on the interactions of TiO_2, UV-A intensity and DOC. Assumptions are noted on the table.

Author	**Organism/ Indicator**	**Nanoparticle (mg/L)**	**Nanoparticle Size**	**DOC mg/L**	**UV Intensity (µW/cm²/nm)**	**Degradation Rate**	**.**	**Predicted Hydroxyl Radicals (µM/ 1 hr)**	**Total Radicals (µM)**
Ba-Abbad et al., 2012	Chlorophenol Degradation	2000	10-50 nm	0	23W/m²	% Removal after X minutes	*Rate Con*		
		2000		0	**1.638 µW/cm²/nm**	50 mg/L: 100%; 60 m	3.69x10-2	63.1712	63.1712
		2000		0	assuming 6% UV across 320-400 nm	100 mg/L: 90%; 120 m	2.19x10-2	63.1712	63.1712
		2000				150 mg/L: 79%; 120 m	1.65x10-2	63.17112	63.17112
						2,4 DCP			
		2000		0		50 mg/L: 89.6%; 60 m	3.28x10-2	63.17112	63.17112
		2000		0		100mg/L: 75%; 120 m	1.71x10-2	63.17112	63.17112
		2000		0		150 mg/L: 71.6%; 120 m	1.37x10-2	63.17112	63.17112
						2,4,6 TCP			
		2000		0		50 mg: 82.4%; 120 m	2.41x10-2	63.17112	63.17112
		2000		0		100mg/L: 64%; 120 m	1.36x10-2	63.17112	63.17112
		2000		0		150 mg/L: 53.6%; 120 m	1.29x10-2	63.17112	63.17112
He et al., 2016	*E. coli*	*mg/L TiO_2*	*Size Anatase*	*DOC*	*Light*	*Rate Decrease (rel)*			
						Compared to 0 [DOC]			
		1000	25.1 nm	0	0.18mW/cm²	0%		30.2629	30.2629
		1000	31.4	50	**2.25**	30%		-14.4176	-14.4176
		1000	22.4	200	**µW/cm²/nm**	27%		-148.4589	-148.4589
					assuming 320-400 nm				
			Size Rutile			Compared to 0 DOC			

		1000	34.5	0		0%		30.2629	30.2629
		1000	28.1	50		43%		-14.4176	-14.4176
		1000	30.6	200		3%		-148.4600	-148.4600
Hu et al., 2007	*Antimicrobial agents*	*TiO_2 mg/L*	*Deguassa P25*			*initial rate µM/min*			*Per Minute*
	initial conc of sulfox 98 µM	100		0		3.9		1.6518	0.027529095
	99 µM	0		0	*9x10-5 Einstein/min*	0.2		0	0
	98 µM	100		0	assuming across 320-400 nm	5.4		1.65174569	0.027529095
	85 µM	100		0	**0.43**	nr		1.65174569	0.027529095
	98 µM	100		0	**µW/cm^2/nm**	nr		1.65174569	0.027529095
	5 µM	100		0		1.2		1.65174569	0.027529095
	9 µM	100		0		2.2		1.65174569	0.027529095
	47 µM	100		0		5.1		1.65174569	0.027529095
	90 µM	100		0		5.8		1.65174569	0.027529095
	230 µM	100		0		6.9		1.65174569	0.027529095
	480 µM	100		0		7.3		1.65174569	0.027529095
	93 µM	100		0		1.5		1.65174569	0.027529095
	92 µM	50		0		3.1		0.825872845	0.013764547
	92 µM	100		0		3.7		1.65174569	0.027529095
	87 µM	500		0		5.2		8.258728449	0.137645474
	81 µM	1000		0		6.9		16.5174569	0.275290948
	99 µM	100		0		4.2		1.65174569	0.027529095
	99 µM	100		0		5.1		1.65174569	0.027529095
	100 µM	100		0		5.4		1.65174569	0.027529095
	21 µM	100		0		2.7		1.65174569	0.027529095
	21 µM	100		0	HCO_3^-: 0.5 mM	3.2		1.65174569	0.027529095
	19 µM	100		0	HCO_3^-: 10 mM	4.3		1.65174569	0.027529095
	18 µM	100		0	HCO_3^-: 20 mM	6.7		1.65174569	0.027529095
	19 µM	100		0	HCO_3^-: 100 mM	6.2		1.65174569	0.027529095
	20 µM	100		0		4.2		1.65174569	0.027529095
	20 µM	100		2		0.76		1.650479557	0.027507993
	20 µM	100		10		0.54		1.645415025	0.027423584
	20 µM	100		20		0.54		1.639084361	0.027318073
	20 µM	100		0		3		1.65174569	0.027529095
	20 µM	100		2		5		1.650479557	0.027507993
	20 µM	100		10		3.6		1.645415025	0.027423584
	20 µM	100		20		2.4		1.639084361	0.027318073
	94 µM	100		0		3.8		1.65174569	0.027529095

Huang et al., 2008	*NOM*		*21 nm*		*8 W (helois Italquartz*	*Rate x mg/L /min*			
		100		10	**2.5**	0.0054		1.709380256	0.028489671
		300		10	**µW/cm²/nm**	0.0154		5.168859206	0.086147653
		500		10		0.0156		8.628338156	0.143805636
		1000		10	assume 320-400 nm	0.0163		17.27703553	0.287950592
Jassby et al., 2009	*terephthalic acid*		*P25*		*1min@ 4.0E-5 W/cm²/s*	*reaction rate decrease*			
		5		0	**0.5**	0%		0.092570543	0.001542842
		5		0.5	**µW/cm²**	28%		0.092537924	0.001542299
		5		5		32%		0.092244353	0.001537406
		5		20		52%		0.091265783	0.001521096
Ma et al., 2012	3'[p-amiophenyl]-fluorescein		25 nm			**ROS Generation**			
		0.1		0	(320-400 nm)	~1 µM OCl^-		1.88180139	1.88180139
		0.5		0	No Filter	~4 µM OCl^-		9.40900695	9.40900695
		1		0	**19.8**	~12 µM OCl^- (ROS)		18.8180139	18.8180139
		0.1		0	Silica Window Glass	<1 µM		0.227325193	0.227325193
		0.5		0	**10.9**	~3.5 µM		1.136625963	1.136625963
		1		0		12 µM		2.273251925	2.273251925
		0.1		0	Petri Dish Glass	< 1 µM		0.595836042	0.595836042
		0.5		0	**14.2**	~4 µM		2.979180212	2.979180212
		1		0		12 µM		5.958360424	5.958360424
		0.1		0	Microscope Slide Glass	< 1µM		0.706365121	0.706365121
		0.5		0	**14.9**	~4 µM		3.531825606	3.531825606
		1		0		12 µM		7.063651212	7.063651212
		0.1		0	Acrylic Glass	<1 µM		0.010863403	0.010863403
		0.5		0	**5.15**	< 1 µM		0.054317017	0.054317017
		1		0		< 1 µM		0.108634034	0.108634034
		0.1		0	345 nm cutoff (no wavelengths	< 1		0.286540744	0.286540744

					below)				
		0.5		0	**11.6**	3.5 µM		1.432703722	1.432703722
		1		0		~11.5 µM		2.865407444	2.865407444
		0.1		0	360 nm cutoff	< 1µM		0.08009761	0.08009761
		0.5		0	**8.33**	2 µM		0.400488049	0.400488049
		1		0		8 µM		0.800976098	0.800976098
		0.1		0	400 nm cutoff	<1 µM		0	0
		0.5		0	**0**	<1 µM OCl-		0	0
		1		0		< 1 µM		0	0
Nagaveni et l., 2004			Deguassa p25		Direct sunlight 0.753 kW/m^2	Initial Degradation Rates			
		0						0	
	phenol	1000		0		0.012 µM/L/s		471319.1029	130.921973
	p-nitrophenol	1000		0		0.37 µM/L/s		471319.1029	130.921973
	salicyclic acid	1000		0	**53.65**	0.028 µM/L/s		471319.1029	130.921973
					µW/cm^2/s				
			Combustion synthesized		assuming 6% UV-A across 320-400 nm				
	phenol	1000		0		0.023 µM/L/s		471319.1029	130.921973
	p-nitrophenol	1000		0		1.64 µM/L/s		471319.1029	130.921973
	salicyclic acid	1000		0		0.75 µM/L/s		471319.1029	130.921973
Sanders et al., 2012	TBARS	mg/L	22nm (a/r)		3.75 J/cm^2 for 2 hours	relative to control all NPs saw significant increase in ROS generation except 25nm Anatase **Relative assessment**			
		0		0				0	
		100		0	**13.02**			436.7833094	
					µW/cm^2/nm				
		mg/L	25 nm (A)		assuming across 320-400 nm				
		0		0				0	
		100		0				436.7833094	
		mg/L	31 nm (a/r)						
		0		0				0	
		100		0				436.7833094	

		mg/L	59 nm (a/r)						
		0		0				0	
		100		0				436.7833094	
		mg/L	142 nm (a)						
		0		0				0	
		100		0				436.7833094	
		mg/L	214 nm (r)						
		0		0				0	
		100		0				436.7833094	
Wormington et al., 2007	Fluorescein		< 25 nm			Actual $OH^{\bullet}$ µM/h			
		0		0	0	0		0	0
		0		3	µW/cm^2/nm	0		0	0
		0		6		0		0	0
		0		12		0		0	0
		0		0	52	~1.5		0	0
		0		3		~2		-54.96324538	-54.96324538
		0		6		~1.5		-109.9264908	-109.9264908
		0		12		~1.5		-219.8529815	-219.8529815
		4.5		0	0	0		0	0
		4.5		3		0		0	0
		4.5		6		0		0	0
		4.5		12		0		0	0
		4.5		0	52	~4		1920.555	1920.555
		4.5		3		~3.5		1732.84332	1732.84332
		4.5		6		~3.0		1545.13164	1545.13164
		4.5		12		~2.5		1169.70828	1169.70828
Wywroll et al., 2006	TFA	1000	7 to 10	0	2.36 mW/cm^2 UV-A	12.5		70326.9824	17581.7456
		1000	15 to 25	0	**29.5**	9		70326.9824	17581.7456
		1000	200 to 220	0	**µW/cm^2/nm**	3		70326.9824	17581.7456
					assuming 320-400 nm	**Relative Generation**			
					15 min IRT				

Yin et al., 2012	MTS Assay						**2.48 µW/cm²/nm**	**4.96 µW/cm²/nm**	**9.92 µW/cm²/nm**
		0	A25 (25 nm	0	UV-A Doses assuming 320-390 nm	**Relative Generation**	0	0	0
		50		0	2.5 J/cm² => 173.61 µW/cm2	P25>A25>A325>R100	1.479193058	4.664736049	79.56391219
		100		0	**2.48**		2.958386117	9.329472098	159.1278244
			A325 (325 nm		**µW/cm²/nm**				
		0		0			0	0	0
		50		0	5.0 J/cm² => 347.22 µW/cm²		1.479193058	4.664736049	79.56391219
		100		0	**4.96**		2.958386117	9.329472098	159.1278244
					µW/cm²/nm				
		0	p25 (25 nm)	0			0	0	0
		50		0	10 J/cm² => 694.44 µW/cm²		1.479193058	4.664736049	79.56391219
		100		0	**9.92**		2.958386117	9.329472098	159.1278244
			R100 (100nm)		**µW/cm²/nm**				
		0		0			0	0	0
		50		0			1.479193058	4.664736049	79.56391219
		100		0			2.958386117	9.329472098	159.1278244

Appendix C

Changes in Aggregation Sizes under UV light Over Time

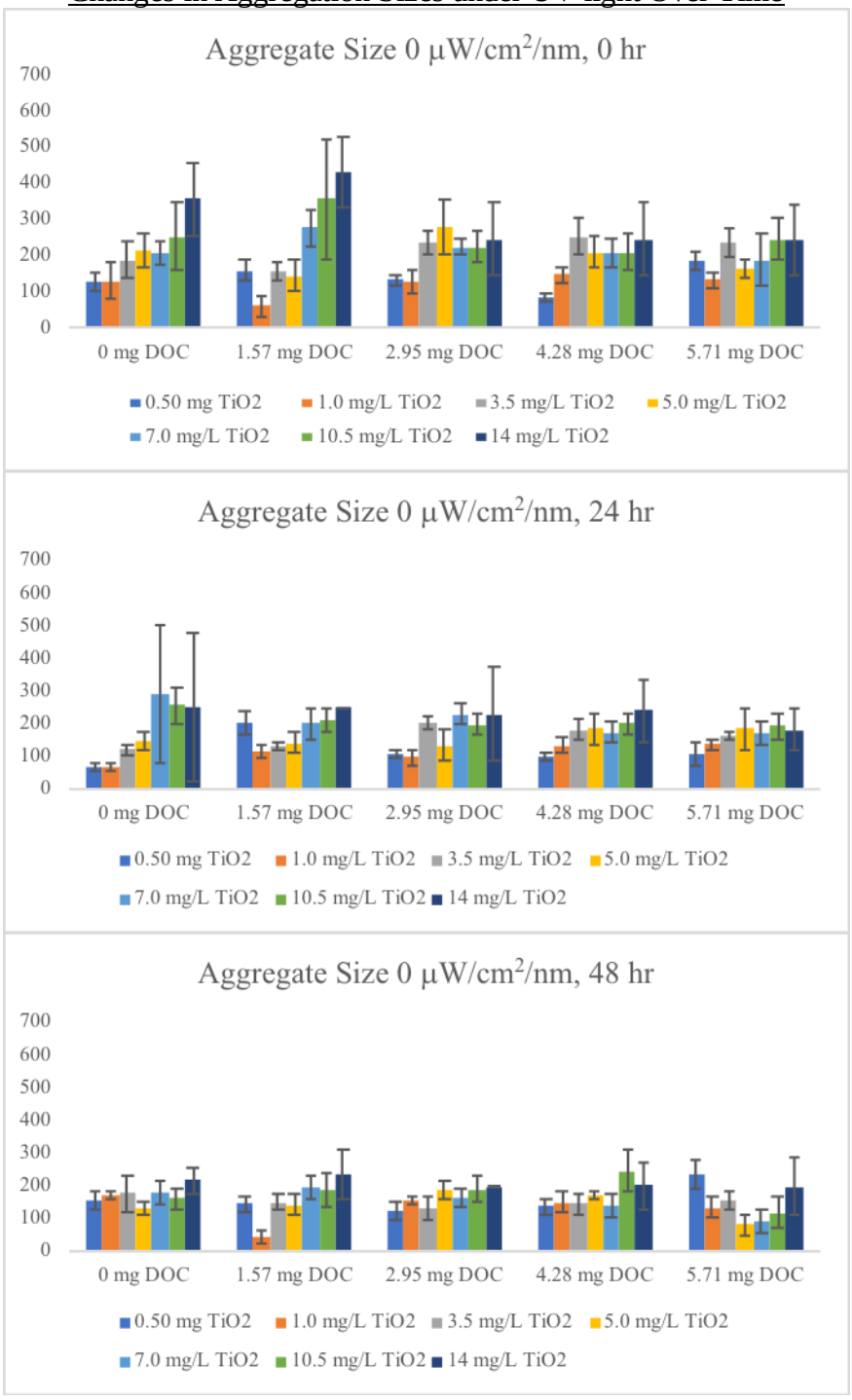

Figure C1.1 Size of TiO_2 + NOM aggregates under 0 µW/cm2/nm UV-A intensity across 48 hours

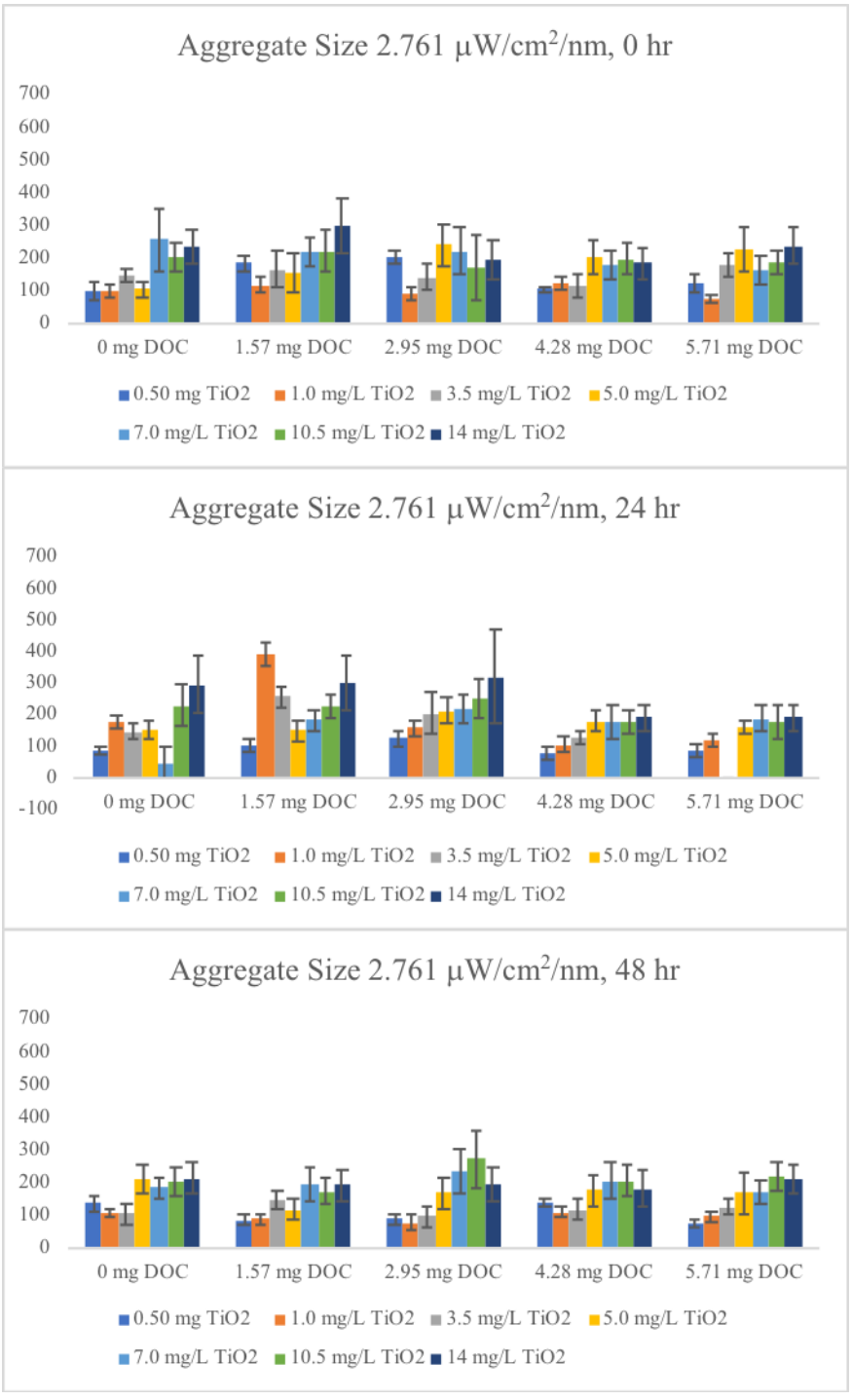

Figure C1.2 Size of TiO_2 + NOM aggregates under 2.671 µW/cm2/nm UV-A intensity across 48 hours

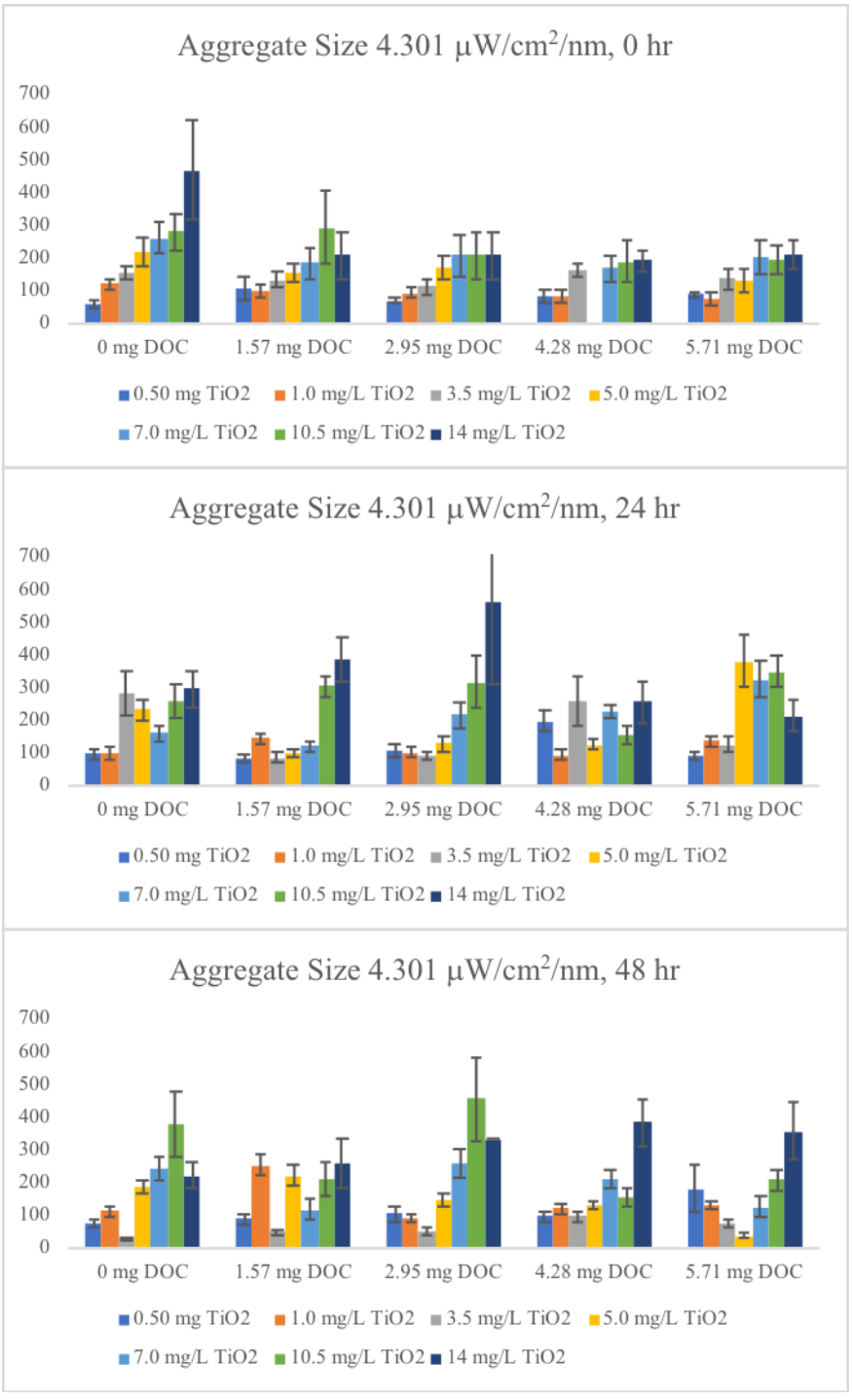

Figure C1.3 Size of TiO_2 + NOM aggregates under 4.301 µW/cm2/nm UV-A intensity across 48 hours

Figure C1.4 Size of TiO_2 + NOM aggregates under 5.177 µW/cm2/nm UV-A intensity across 48 hours

Appendix D

Daphnia magna LC_{50} Information

TiO2 Concentration; mg/L	DOC; mg/L	UV µW/cm2/nm	0 hr Alive	24 hr Alive	48 hr Alive	% Dead	Predicted uM OH/hr	At 32 hr (10/01)	Measured Hydroxyls
0	4.28	**0**	20	20	20	0	0	0	0
0.5	4.28	**0**	20	20	20	0	0	0	0
1	4.28	**0**	20	20	20	0	0	0	0
5	4.28	**0**	20	20	20	0	0	0	0
10.5	4.28	**0**	20	20	20	0	0	0	0.064
14	4.28	**0**	20	20	20	0	0	0	0.0832
TiO2 Concentration; mg/L	**DOC; mg/L**	**UV µW/cm2/nm**	**0 hr Alive**	**24 hr Alive**	**48 hr Alive**	**% Dead**	**Predicted uM OH/hr**	**At 32 hr (10/01)**	**Actual Hydroxyls**
0	4.28	**5.188**	20	19	18	10	-0.077872614	0	0
0.5	4.28	**5.188**	20	20	13	35	-0.045295909	0	0.2848
1	4.28	**5.188**	20	20	6	70	-0.012719204	-0.407014515	0.5152
5	4.28	**5.188**	20	4	0	100	0.247894439	7.932622032	4.0224
10.5	4.28	**5.188**	20	0	0	100	0.606238196	19.39962229	16.7648
14	4.28	**5.188**	20	0	0	100	0.834275133	26.69680426	27.4368
TiO2 Concentration; mg/L	**DOC; mg/L**	**UV µW/cm2/nm**	**0 hr Alive**	**24 hr Alive**	**48 hr Alive**	**% Dead**	**Predicted uM OH/hr**	**At 32 hr (10/01)**	**Actual Hydroxyls**
0	4.28	**2.167**	20	20	20	0	-0.005674944	-0.18159821	0
0.5	4.28	**2.167**	20	20	20	0	0.007885008	0.252320248	0.1088
1	4.28	**2.167**	20	19	19	5	0.02144496	0.686238706	0.2464
5	4.28	**2.167**	20	20	19	5	0.129924574	4.157586371	1.7312
10.5	4.28	**2.167**	20	19	13	35	0.279084044	8.930689411	6.8736
14	4.28	**2.167**	20	20	4	80	0.374003707	11.96811862	10.0992
TiO2 Concentration; mg/L	**DOC; mg/L**	**UV µW/cm2/nm**	**0 hr Alive**	**24 hr Alive**	**48 hr Alive**	**% Dead**	**Predicted uM OH/hr**	**At 32 hr (10/01)**	**Actual Hydroxyls**
0	1.57	**2.167**	20	20	20	0	-0.002081697	0	0
0.5	1.57	**2.167**	20	20	20	0	0.012558182	0.401861814	0.2272
1	1.57	**2.167**	20	20	19	5	0.02719806	0.870337924	0.5216
5	1.57	**2.167**	20	19	5	75	0.144317088	4.618146808	4.1792
10.5	1.57	**2.167**	20	9	0	100	0.305355751	9.771384024	9.6416
14	1.57	**2.167**	20	14	0	100	0.4078349	13.0507168	12.8352
TiO2 Concentration; mg/L	**DOC; mg/L**	**UV µW/cm2/nm**	**0 hr Alive**	**24 hr Alive**	**48 hr Alive**	**% Dead**	**Predicted uM OH/hr**	**At 32 hr (10/01)**	**Actual Hydroxyls**
0	2.95	**4.301**	20	19	19	5	-0.03058239	-0.978636489	0
0.5	2.95	**4.301**	20	20	20	0	-0.012196178	-0.39027771	0.112
1	2.95	**4.301**	20	20	20	0	0.006190033	0.198081069	0.4576
5	2.95	**4.301**	20	20	16	20	0.153279728	4.9049513	4.0864
10.5	2.95	**4.301**	20	16	1	95	0.355528058	11.37689787	11.9136
14	2.95	**4.301**	20	16	0	100	0.484231541	15.49540932	18.4224
TiO2 Concentration;	**DOC;**	**UV**	**0 hr Alive**	**24 hr Alive**	**48 hr Alive**	**% Dead**	**Predicted uM**	**At 32 hr (10/01)**	**Actual**

mg/L	mg/L	µW/cm2/nm					OH/hr		Hydroxyls
0	0	**2.671**	20	20	20	0	0	0	0
0.5	0	**2.671**	20	20	16	20	0.014616059	0.467713878	0.9184
1	0	**2.671**	20	20	1	95	0.029232117	0.935427756	2.1728
5	0	**2.671**	20	19	0	100	0.146160587	4.677138778	6.6016
10.5	0	**2.671**	20	18	0	100	0.306937232	9.821991433	10.368
14	0	**2.671**	20	15	0	100	0.409249643	13.09598858	13.5136
TiO2 Concentration; mg/L	**DOC; mg/L**	**UV µW/cm2/nm**	**0 hr Alive**	**24 hr Alive**	**48 hr Alive**	**% Dead**	**Predicted uM OH/hr**	**At 32 hr (10/01)**	**Actual Hydroxyls**
0	0	**4.301**	20	20	20	0	0	0	0
0.5	0	**4.301**	20	20	15	25	0.027577546	0.882481483	0.8768
1	0	**4.301**	20	20	6	70	0.055155093	1.764962966	1.9008
5	0	**4.301**	20	20	0	100	0.275775463	8.824814831	9.504
10.5	0	**4.301**	20	20	0	100	0.579128473	18.53211114	18.7808
14	0	**4.301**	20	20	0	100	0.772171298	24.70948153	24.1248
TiO2 Concentration; mg/L	**DOC; mg/L**	**UV µW/cm2/nm**	**0 hr Alive**	**24 hr Alive**	**48 hr Alive**	**% Dead**	**Predicted uM OH/hr**	**At 32 hr (10/01)**	**Actual Hydroxyls**
0	0	**0**	20	20	20	0	0	0	0
0.5	0	**0**	20	20	20	0	0	0	0.0288
1	0	**0**	20	20	20	0	0	0	0
5	0	**0**	20	20	20	0	0	0	0
10.5	0	**0**	20	20	20	0	0	0	0.016
14	0	**0**	20	20	20	0	0	0	0.0864
TiO2 Concentration; mg/L	**DOC; mg/L**	**UV µW/cm2/nm**	**0 hr Alive**	**24 hr Alive**	**48 hr Alive**	**% Dead**	**Predicted uM OH/hr**	**At 32 hr (10/01)**	**Actual Hydroxyls**
0	5.71	4.301	20	19	19	5	-0.059195067	-1.894242153	0
0.5	5.71	4.301	20	20	20	0	-0.049408206	-1.581062582	0.0896
1	5.71	4.301	20	20	20	0	-0.039621344	-1.267883011	0.1696
5	5.71	4.301	20	20	11	45	0.038673549	1.237553557	1.136
10.5	5.71	4.301	20	20	11	45	0.146329026	4.682528837	4.672
14	5.71	4.301	20	20	0	100	0.214837057	6.874785834	7.9872
TiO2 Concentration; mg/L	**DOC; mg/L**	**UV µW/cm2/nm**	**0 hr Alive**	**24 hr Alive**	**48 hr Alive**	**% Dead**	**Predicted uM OH/hr**	**At 32 hr (10/01)**	**Actual Hydroxyls**
0	0	5.188	20	20	20	0	0	0	0
0.5	0	5.188	20	20	14	30	0.055980803	1.79138569	1.0144
1	0	5.188	20	18	1	95	0.111961606	3.58277138	2.2176
5	0	5.188	20	7	0	100	0.559808028	17.9138569	11.088
10.5	0	5.188	20	5	0	100	1.175596859	37.61909949	46.5664
14	0	5.188	20	7	0	100	1.567462479	50.15879932	50.2432

0 mg/L DOC 2.671 µW/cm^2/nm UV

XLSTAT 2018.2.50628 - Dose effect analysis - Start time: 4/24/18 at 12:23:07 AM / End time: 4/24/18 at 12:23:17 AM
Observation weights: Workbook = Book1 / Sheet = Sheet1 / Range = Sheet1!$B$1:$B$6 / 5 rw and 1 clm
Response variable(s): Workbook = Book1 / Sheet = Sheet1 / Range = Sheet1!$C$1:$C$6 / 5 rw and 1 clm
Quantitative: Workbook = Book1 / Sheet = Sheet1 / Range = Sheet1!$A$1:$A$6 / 5 rw and 1 clm
Model: Probit
Confidence interval (%): 95
Stop conditions: Iterations = 1000 / Convergence = 1E-06
Maximization of the likelihood function using the Newton-Raphson algorithm

Summary statistics:

Variable	Observations	Obs. with missing data	Obs. without missing data	Minimum	Maximum	Mean	Std. deviation
Dead	5	0	5	4.000	20.000	16.600	6.344
Log(Dose/Conc.)	5	0	5	-0.745	1.131	0.512	0.688

Regression of Variable Dead:

Goodness of fit statistics (Variable Dead):

Statistic	Independent	Full
Observations	100	100
Sum of weights	100.000	100.000
DF	99	98
-2 Log(Likelihood)	91.177	28.087
R²(McFadden)	0.000	0.692
R²(Cox and Snell)	0.000	0.468
R²(Nagelkerke)	0.000	0.782
AIC	93.177	32.087
SBC	95.782	37.297
Iterations	0	6

Model parameters (Variable Dead):

Source	Value	Standard error	Wald Chi-Square	Pr > Chi²
Intercept	0.912	0.317	8.256	0.004
Log(Dose/Conc.)	2.367	0.481	24.257	< 0.0001

Source	Wald Lower bound (95%)	Wald Upper bound (95%)	Odds ratio	Odds ratio Lower bound (95%)	Odds ratio Upper bound (95%)
Intercept	0.290	1.534			
Log(Dose/Conc.	1.425	3.309	10.664	4.158	27.350

)

Equation of the model (Variable Dead):
Dead = 0+1*(XLSTAT_CDFNormal(0.911694625105838+2.3668356350036*Log(Dose/Conc.)))

Predictions and residuals (Variable Dead):

Observation	Total	Log(Dose/Conc.)	Dose	Dead	Dead/Weigh t	Percent Mort	Std Dev	% STDEV
Obs1	20	-0.7447275	0.18	4.000	0.200	20.000	0.816	4.082
Obs2	20	0.33645973	2.17	19.000	0.950	95.000	0.500	2.500
Obs3	20	0.81954394	6.60	20.000	1.000	100.000	0.000	0.000
Obs4	20	1.01577876	10.37	20.000	1.000	100.000	0.000	0.000
Obs5	20	1.13065535	13.51	20.000	1.000	100.000	0.000	0.000

Probability analysis with the fitted model (Variable Dead):

Probability	Dose/Conc.	Lower bound 95%	Upper bound 95%
0.01	0.043	0.008	0.094
0.05	0.083	0.024	0.157
0.10	0.118	0.041	0.210
0.20	0.182	0.078	0.305
0.30	0.247	0.122	0.408
0.40	0.322	0.174	0.536
0.50	0.412	0.237	0.707
0.60	0.527	0.315	0.956
0.70	0.686	0.416	1.354
0.80	0.934	0.560	2.095
0.90	1.433	0.816	3.974
0.95	2.041	1.092	6.877
0.99	3.960	1.838	19.745

TiO2 LC

Probability analysis with the fitted model (Variable Dead):

Probability	TiO2	Lower bound 95%	Upper bound 95%
0.01	0.331	0.191	0.416
0.05	0.400	0.266	0.481
0.10	0.442	0.316	0.521

Model Point	Log Dose	Dead	Percet Mort	Dose
-14	-1.379	0.009	0.934	0.042
-13	-1.354	0.011	1.096	0.044
-12	-1.328	0.013	1.280	0.047
-11	-1.303	0.015	1.491	0.050
-10	-1.278	0.017	1.732	0.053
-9	-1.253	0.020	2.004	0.056
-8	-1.227	0.023	2.313	0.059
-7	-1.202	0.027	2.660	0.063
-6	-1.177	0.030	3.050	0.067
-5	-1.152	0.035	3.486	0.071
-4	-1.126	0.040	3.972	0.075
-3	-1.101	0.045	4.511	0.079
-2	-1.076	0.051	5.108	0.084
-1	-1.051	0.058	5.767	0.089
0	-1.025	0.065	6.490	0.094
1	-1.000	0.073	7.282	0.100
2	-0.975	0.081	8.145	0.106
3	-0.949	0.091	9.084	0.112
4	-0.924	0.101	10.101	0.119
5	-0.899	0.112	11.198	0.126
6	-0.874	0.124	12.378	0.134
7	-0.848	0.136	13.642	0.142
8	-0.823	0.150	14.992	0.150
9	-0.798	0.164	16.429	0.159
10	-0.773	0.180	17.951	0.169
11	-0.747	0.196	19.560	0.179
12	-0.722	0.213	21.253	0.190
13	-0.697	0.230	23.028	0.201
14	-0.672	0.249	24.884	0.213
15	-0.646	0.268	26.816	0.226

0.20	0.500	0.386	0.580
0.30	0.546	0.443	0.631
0.40	0.589	0.493	0.685
0.50	0.632	0.540	0.747
0.60	0.678	0.586	0.822
0.70	0.732	0.633	0.919
0.80	0.799	0.687	1.057
0.90	0.904	0.762	1.296
0.95	1.000	0.825	1.543
0.99	1.209	0.951	2.154

Pred OH

Probability	Pred OH	Lower bound 95%	Upper bound 95%
0.01	0.309	0.178	0.390
0.05	0.374	0.248	0.450
0.10	0.414	0.295	0.488
0.20	0.468	0.361	0.542
0.30	0.511	0.414	0.591
0.40	0.551	0.461	0.641
0.50	0.591	0.505	0.699
0.60	0.635	0.548	0.769
0.70	0.684	0.592	0.859
0.80	0.748	0.643	0.988
0.90	0.845	0.712	1.213
0.95	0.935	0.772	1.443
0.99	1.131	0.890	2.015

16	-0.621	0.288	28.821	0.239
17	-0.596	0.309	30.894	0.254
18	-0.571	0.330	33.030	0.269
19	-0.545	0.352	35.223	0.285
20	-0.520	0.375	37.466	0.302
21	-0.495	0.398	39.752	0.320
22	-0.470	0.421	42.074	0.339
23	-0.444	0.444	44.424	0.359
24	-0.419	0.468	46.793	0.381
25	-0.394	0.492	49.174	0.404
26	-0.369	0.516	51.558	0.428
27	-0.343	0.539	53.937	0.453
28	-0.318	0.563	56.301	0.481
29	-0.293	0.586	58.643	0.509
30	-0.268	0.610	60.955	0.540
31	-0.242	0.632	63.229	0.572
32	-0.217	0.655	65.457	0.606
33	-0.192	0.676	67.633	0.643
34	-0.167	0.697	69.750	0.681
35	-0.141	0.718	71.803	0.722
36	-0.116	0.738	73.786	0.765
37	-0.091	0.757	75.695	0.811
38	-0.066	0.775	77.526	0.860
39	-0.040	0.793	79.277	0.911
40	-0.015	0.809	80.944	0.966
41	0.010	0.825	82.526	1.024
42	0.035	0.840	84.022	1.085
43	0.061	0.854	85.432	1.150
44	0.086	0.868	86.756	1.219
45	0.111	0.880	87.994	1.292
46	0.136	0.891	89.148	1.369
47	0.162	0.902	90.220	1.451
48	0.187	0.912	91.213	1.538
49	0.212	0.921	92.128	1.630
50	0.237	0.930	92.969	1.727
51	0.263	0.937	93.740	1.831
52	0.288	0.944	94.443	1.940
53	0.313	0.951	95.082	2.057
54	0.338	0.957	95.661	2.180
55	0.364	0.962	96.183	2.310
56	0.389	0.967	96.653	2.448
57	0.414	0.971	97.075	2.595
58	0.439	0.975	97.451	2.750
59	0.465	0.978	97.786	2.915
60	0.490	0.981	98.083	3.090

61	0.515	0.983	98.345	3.275
62	0.540	0.986	98.576	3.471
63	0.566	0.988	98.779	3.678
64	0.591	0.990	98.956	3.899
65	0.616	0.991	99.111	4.132
66	0.641	0.992	99.245	4.379
67	0.667	0.994	99.361	4.642
68	0.692	0.995	99.460	4.919
69	0.717	0.995	99.546	5.214
70	0.742	0.996	99.619	5.526
71	0.768	0.997	99.682	5.857
72	0.793	0.997	99.735	6.208
73	0.818	0.998	99.780	6.579
74	0.843	0.998	99.818	6.973
75	0.869	0.998	99.850	7.391
76	0.894	0.999	99.877	7.833
77	0.919	0.999	99.899	8.302
78	0.944	0.999	99.918	8.799
79	0.970	0.999	99.933	9.326
80	0.995	0.999	99.946	9.884
81	1.020	1.000	99.956	10.476
82	1.045	1.000	99.965	11.103
83	1.071	1.000	99.972	11.768
84	1.096	1.000	99.977	12.473
85	1.121	1.000	99.982	13.219
86	1.146	1.000	99.986	14.011
87	1.172	1.000	99.989	14.850
88	1.197	1.000	99.991	15.739
89	1.222	1.000	99.993	16.681
90	1.247	1.000	99.994	17.680
91	1.273	1.000	99.996	18.738
92	1.298	1.000	99.997	19.860
93	1.323	1.000	99.997	21.049
94	1.348	1.000	99.998	22.309
95	1.374	1.000	99.998	23.645
96	1.399	1.000	99.999	25.061
97	1.424	1.000	99.999	26.561
98	1.449	1.000	99.999	28.151
99	1.475	1.000	99.999	29.836
100	1.500	1.000	100.000	31.623
101	1.525	1.000	100.000	33.516
102	1.551	1.000	100.000	35.523
103	1.576	1.000	100.000	37.649
104	1.601	1.000	100.000	39.903
105	1.626	1.000	100.000	42.292
106	1.652	1.000	100.000	44.824

107	1.677	1.000	100.000	47.508
108	1.702	1.000	100.000	50.352
109	1.727	1.000	100.000	53.367
110	1.753	1.000	100.000	56.562
111	1.778	1.000	100.000	59.948
112	1.803	1.000	100.000	63.538
113	1.828	1.000	100.000	67.342
98	1.449	1.000	99.999	28.151
99	1.475	1.000	99.999	29.836
100	1.500	1.000	100.000	31.623
101	1.525	1.000	100.000	33.516
102	1.551	1.000	100.000	35.523
103	1.576	1.000	100.000	37.649
104	1.601	1.000	100.000	39.903
105	1.626	1.000	100.000	42.292
106	1.652	1.000	100.000	44.824
107	1.677	1.000	100.000	47.508
108	1.702	1.000	100.000	50.352
109	1.727	1.000	100.000	53.367
110	1.753	1.000	100.000	56.562
111	1.778	1.000	100.000	59.948
112	1.803	1.000	100.000	63.538
113	1.828	1.000	100.000	67.342

1.57 mg/L DOC 2.671 μW/cm^2/nm UV

XLSTAT 2018.2.50628 - Dose effect analysis - Start time: 4/24/18 at 12:33:02 AM / End time: 4/24/18 at 12:33:12 AM
Observation weights: Workbook = Book1 / Sheet = Sheet1 / Range = 'Sheet1'!$B$1:$B$6 / 5 rw and 1 clm
Response variable(s): Workbook = Book1 / Sheet = Sheet1 / Range = 'Sheet1'!$C$1:$C$6 / 5 rw and 1 clm
Quantitative: Workbook = Book1 / Sheet = Sheet1 / Range = 'Sheet1'!$A$1:$A$6 / 5 rw and 1 clm
Model: Probit
Confidence interval (%): 95
Stop conditions: Iterations = 1000 / Convergence = 1E-06
Maximization of the likelihood function using the Newton-Raphson algorithm

Summary statistics:

Variable	Observations	Obs. with missing data	Obs. without missing data	Minimum	Maximum	Mean	Std. deviation
Dead	5	0	5	0.000	20.000	11.200	8.976
Log(Dose/Conc.)	5	0	5	-0.638	1.109	0.358	0.701

Regression of variable Dead:

Goodness of fit statistics (Variable Dead):

Statistic	Independent	Full
Observations	100	100
Sum of weights	100.000	100.000
DF	99	98
-2 Log(Likelihood)	137.186	32.474
R^2(McFadden)	0.000	0.763
R^2(Cox and Snell)	0.000	0.649
R^2(Nagelkerke)	0.000	0.870
AIC	139.186	36.474
SBC	141.791	41.684
Iterations	0	6

Model parameters (Variable Dead):

Source	Value	Standard error	Wald Chi-Square	Pr > Chi²	Wald Lower bound (95%)	Wald Upper bound (95%)	Odds ratio	Odds ratio Lower bound (95%)	Odds ratio Upper bound (95%)
Intercept	-0.992	0.350	8.013	0.005	-1.679	-0.305			
Log(Dose/Conc.)	3.042	0.519	34.300	< 0.0001	2.024	4.060	20.946	7.568	57.971

Dead = 0+1*(XLSTAT_CDFNormal(-0.991872483824682+3.04192837456428*Log(Dose/Conc.)))

Predictions and residuals (Variable Dead):

Observation	Weight	Log(Dose/Conc.)	Dose	Dead	Dead/Weight	% Mortaliy	Std Dev	STD DEV%	Pred(Dead)/Weight
Obs1	20	-0.6382722	0.22999998	0.000	0.000	0.000	0.000	0.000	0.002

Obs2	20	-0.2839967	0.51999995	1.000	0.050	5.000	0.500	2.500	0.032
Obs3	20	0.62117628	4.17999998	15.000	0.750	75.000	0.957	4.787	0.815
Obs4	20	0.98407703	9.63999991	20.000	1.000	100.000	0.000	0.000	0.977
Obs5	20	1.10856502	12.8399999	20.000	1.000	100.000	0.000	0.000	0.991

Probability analysis with the fitted model (Variable Dead):

Probability	Dose/Conc.	Lower bound 95%	Upper bound 95%
0.01	0.364	0.114	0.678
0.05	0.610	0.242	1.021
0.10	0.803	0.359	1.277
0.20	1.120	0.575	1.689
0.30	1.425	0.801	2.085
0.40	1.749	1.053	2.516
0.50	2.119	1.347	3.029
0.60	2.567	1.705	3.686
0.70	3.151	2.162	4.615
0.80	4.006	2.799	6.123
0.90	5.589	3.879	9.351
0.95	7.359	4.976	13.542
0.99	12.326	7.703	27.958

TiO2

Probability analysis with the fitted model (Variable Dead):

Probability	TiO2	Lower bound 95%	Upper bound 95%
0.01	0.741	0.293	1.211
0.05	1.116	0.535	1.674
0.10	1.388	0.734	2.000
0.20	1.808	1.069	2.498
0.30	2.187	1.391	2.956
0.40	2.573	1.729	3.438
0.50	2.996	2.101	3.993
0.60	3.488	2.529	4.683
0.70	4.105	3.046	5.621
0.80	4.966	3.726	7.075
0.90	6.467	4.807	9.976
0.95	8.043	5.840	13.459
0.99	12.108	8.226	24.142

Model Point	Log Dose	Dead	% Mortality	Dose
1	-1.000	0.000	0.003	0.100
2	-0.975	0.000	0.004	0.106
3	-0.949	0.000	0.005	0.112
4	-0.924	0.000	0.007	0.119
5	-0.899	0.000	0.010	0.126
6	-0.874	0.000	0.013	0.134
7	-0.848	0.000	0.018	0.142
8	-0.823	0.000	0.024	0.150
9	-0.798	0.000	0.031	0.159
10	-0.773	0.000	0.042	0.169
11	-0.747	0.001	0.055	0.179
12	-0.722	0.001	0.071	0.190
13	-0.697	0.001	0.093	0.201
14	-0.672	0.001	0.120	0.213
15	-0.646	0.002	0.155	0.226
16	-0.621	0.002	0.198	0.239
17	-0.596	0.003	0.252	0.254
18	-0.571	0.003	0.319	0.269
19	-0.545	0.004	0.401	0.285
20	-0.520	0.005	0.502	0.302
21	-0.495	0.006	0.625	0.320
22	-0.470	0.008	0.775	0.339
23	-0.444	0.010	0.954	0.359
24	-0.419	0.012	1.169	0.381
25	-0.394	0.014	1.425	0.404
26	-0.369	0.017	1.728	0.428
27	-0.343	0.021	2.085	0.453
28	-0.318	0.025	2.501	0.481
29	-0.293	0.030	2.985	0.509
30	-0.268	0.035	3.545	0.540
31	-0.242	0.042	4.188	0.572
32	-0.217	0.049	4.922	0.606
33	-0.192	0.058	5.755	0.643
34	-0.167	0.067	6.695	0.681
35	-0.141	0.078	7.751	0.722
36	-0.116	0.089	8.928	0.765
37	-0.091	0.102	10.233	0.811

Pred OH

Probability	Pred OH	Lower bound 95%	Upper bound 95%
0.01	0.638	0.241	1.063
0.05	0.974	0.450	1.486
0.10	1.220	0.625	1.785
0.20	1.604	0.924	2.246
0.30	1.953	1.215	2.670
0.40	2.311	1.523	3.120
0.50	2.705	1.866	3.639
0.60	3.166	2.264	4.286
0.70	3.746	2.748	5.173
0.80	4.562	3.390	6.556
0.90	5.996	4.418	9.350
0.95	7.514	5.407	12.745
0.99	11.473	7.711	23.345

38	-0.066	0.117	11.671	0.860
39	-0.040	0.132	13.247	0.911
40	-0.015	0.150	14.964	0.966
41	0.010	0.168	16.824	1.024
42	0.035	0.188	18.826	1.085
43	0.061	0.210	20.969	1.150
44	0.086	0.232	23.248	1.219
45	0.111	0.257	25.659	1.292
46	0.136	0.282	28.195	1.369
47	0.162	0.308	30.845	1.451
48	0.187	0.336	33.599	1.538
49	0.212	0.364	36.444	1.630
50	0.237	0.394	39.366	1.727
51	0.263	0.423	42.349	1.831
52	0.288	0.454	45.376	1.940
53	0.313	0.484	48.431	2.057
54	0.338	0.515	51.494	2.180
55	0.364	0.545	54.549	2.310
56	0.389	0.576	57.578	2.448
57	0.414	0.606	60.562	2.595
58	0.439	0.635	63.485	2.750
59	0.465	0.663	66.332	2.915
60	0.490	0.691	69.089	3.090
61	0.515	0.717	71.742	3.275
62	0.540	0.743	74.280	3.471
63	0.566	0.767	76.694	3.678
64	0.591	0.790	78.977	3.899
65	0.616	0.811	81.123	4.132
66	0.641	0.831	83.129	4.379
67	0.667	0.850	84.992	4.642
68	0.692	0.867	86.712	4.919
69	0.717	0.883	88.292	5.214
70	0.742	0.897	89.734	5.526
71	0.768	0.910	91.042	5.857
72	0.793	0.922	92.222	6.208
73	0.818	0.933	93.280	6.579
74	0.843	0.942	94.223	6.973
75	0.869	0.951	95.059	7.391
76	0.894	0.958	95.795	7.833
77	0.919	0.964	96.440	8.302
78	0.944	0.970	97.002	8.799
79	0.970	0.975	97.488	9.326
80	0.995	0.979	97.906	9.884

81	1.020	0.983	98.264	10.476
82	1.045	0.986	98.568	11.103
83	1.071	0.988	98.825	11.768
84	1.096	0.990	99.041	12.473
85	1.121	0.992	99.221	13.219
86	1.146	0.994	99.371	14.011
87	1.172	0.995	99.495	14.850
88	1.197	0.996	99.597	15.739
89	1.222	0.997	99.680	16.681
90	1.247	0.997	99.747	17.680
91	1.273	0.998	99.801	18.738
92	1.298	0.998	99.844	19.860
93	1.323	0.999	99.879	21.049
94	1.348	0.999	99.906	22.309
95	1.374	0.999	99.928	23.645
96	1.399	0.999	99.945	25.061
97	1.424	1.000	99.958	26.561
98	1.449	1.000	99.968	28.151
99	1.475	1.000	99.976	29.836
100	1.500	1.000	99.982	31.623

4.28 mg/L DOC 2.671 μW/cm^2/nm UV

XLSTAT 2018.2.50628 - Dose effect analysis - Start time: 4/24/18 at 12:38:15 AM / End time: 4/24/18 at 12:38:16 AM
Observation weights: Workbook = Book1 / Sheet = Sheet1 / Range = Sheet1!$B$1:$B$7 / 6 rw and 1 clm
Response variable(s): Workbook = Book1 / Sheet = Sheet1 / Range = Sheet1!$C$1:$C$7 / 6 rw and 1 clm
Quantitative: Workbook = Book1 / Sheet = Sheet1 / Range = Sheet1!$A$1:$A$7 / 6 rw and 1 clm
Model: Probit
Confidence interval (%): 95
Stop conditions: Iterations = 1000 / Convergence = 1E-06
Maximization of the likelihood function using the Newton-Raphson algorithm

Summary statistics:

Variable	Observations	Obs. with missing data	Obs. without missing data	Minimum	Maximum	Mean	Std. deviation
Dead	6	0	6	0.000	20.000	7.500	7.880
Log(Dose/Conc.)	6	0	6	-0.959	1.477	0.333	0.876

Regression of variable Dead:

Goodness of fit statistics (Variable Dead):

Statistic	Independent	Full
Observations	120	120
Sum of weights	120.000	120.000
DF	119	118
-2 Log(Likelihood)	158.775	75.403
R^2(McFadden)	0.000	0.525
R^2(Cox and Snell)	0.000	0.501
R^2(Nagelkerke)	0.000	0.683
AIC	160.775	79.403
SBC	163.563	84.978
Iterations	0	6

Model parameters (Variable Dead):

Source	Value	Standard error	Wald Chi-Square	Pr > Chi²	Wald Lower bound (95%)	Wald Upper bound (95%)	Odds ratio	Odds ratio Lower bound (95%)	Odds ratio Upper bound (95%)
Intercept	-1.608	0.334	23.241	< 0.000	-2.261	-0.954			

				1 < 0.000					
Log(Dose/Conc.)	2.085	0.363	32.971	1	1.374	2.797	8.048	3.950	16.400

Equation of the model (Variable Dead):
Dead = 0+1*(XLSTAT_CDFNormal(-1.60778205363983+2.08543555933366*Log(Dose/Conc.)))

Predictions and residuals (Variable Dead):

Observation	Weight	Log(Dose/Conc.)	Dose	Dead	Dead/Weight	Precent Mort	Std Dev	STD DEV%	Pred(Dead)/Weight
Obs1	20	-0.9586073	0.11	0.000	0.000	0.000	0.000	0.000	0.000
Obs2	20	-0.60206	0.25	1.000	0.050	5.000	0.500	2.500	0.002
Obs3	20	0.2380461	1.72999999	1.000	0.050	5.000	0.500	2.500	0.133
Obs4	20	0.83695674	6.87000005	7.000	0.350	35.000	0.500	2.500	0.555
Obs5	20	1.00432137	10.0999999	16.00 0	0.800	80.000	1.414	7.071	0.687
Obs6	20	1.47712125	29.9999997	20.00 0	1.000	100.000	0.000	0.000	0.930

Probability analysis with the fitted model (Variable Dead):

Probability	Dose/Conc.	Lower bound 95%	Upper bound 95%
0.01	0.452	0.108	0.946
0.05	0.960	0.330	1.699
0.10	1.434	0.594	2.340
0.20	2.330	1.192	3.502
0.30	3.307	1.933	4.773
0.40	4.461	2.857	6.358
0.50	5.901	4.009	8.534
0.60	7.806	5.459	11.806
0.70	10.530	7.361	17.240
0.80	14.946	10.127	27.690
0.90	24.293	15.259	55.186
0.95	36.282	21.079	99.053
0.99	76.998	37.954	302.158

TiO2

Probability	TiO2	Lower bound 95%	Upper bound 95%
0.01	1.206	0.181	2.405
0.05	2.318	0.630	3.824
0.10	3.282	1.209	4.951
0.20	5.003	2.590	6.964

Model Point	Log Dose	Dead	Dose	% Mort
0	-1.535	0.000	0.029	0.000
1	-1.500	0.000	0.032	0.000
2	-1.465	0.000	0.034	0.000
3	-1.429	0.000	0.037	0.000
4	-1.394	0.000	0.040	0.000
5	-1.359	0.000	0.044	0.000
6	-1.323	0.000	0.048	0.001
7	-1.288	0.000	0.052	0.001
8	-1.253	0.000	0.056	0.001
9	-1.217	0.000	0.061	0.002
10	-1.182	0.000	0.066	0.002
11	-1.146	0.000	0.071	0.003
12	-1.111	0.000	0.077	0.004
13	-1.076	0.000	0.084	0.006
14	-1.040	0.000	0.091	0.008
15	-1.005	0.000	0.099	0.011
16	-0.970	0.000	0.107	0.014
17	-0.934	0.000	0.116	0.019
18	-0.899	0.000	0.126	0.025
19	-0.864	0.000	0.137	0.033
20	-0.828	0.000	0.148	0.043
21	-0.793	0.001	0.161	0.055
22	-0.758	0.001	0.175	0.072

0.30	6.779	4.282	9.330
0.40	8.789	6.180	12.756
0.50	11.203	8.161	18.230
0.60	14.280	10.274	27.328
0.70	18.514	12.757	43.424
0.80	25.089	16.110	76.163
0.90	38.238	21.896	168.835
0.95	54.156	28.006	328.194
0.99	104.031	44.063	1151.574

Pred OH

Probability	Pred OH	Lower bound 95%	Upper bound 95%
0.01	0.833	0.089	1.805
0.05	1.706	0.369	2.984
0.10	2.501	0.777	3.948
0.20	3.974	1.856	5.717
0.30	5.549	3.298	7.872
0.40	7.381	4.999	11.155
0.50	9.637	6.812	16.725
0.60	12.583	8.766	26.554
0.70	16.738	11.092	45.073
0.80	23.373	14.289	85.602
0.90	37.140	19.930	212.226
0.95	54.442	26.028	452.736
0.99	111.555	42.560	1892.332

23	-0.722	0.001	0.190	0.092
24	-0.687	0.001	0.206	0.118
25	-0.652	0.002	0.223	0.151
26	-0.616	0.002	0.242	0.191
27	-0.581	0.002	0.263	0.241
28	-0.545	0.003	0.285	0.302
29	-0.510	0.004	0.309	0.377
30	-0.475	0.005	0.335	0.469
31	-0.439	0.006	0.364	0.580
32	-0.404	0.007	0.394	0.714
33	-0.369	0.009	0.428	0.874
34	-0.333	0.011	0.464	1.064
35	-0.298	0.013	0.504	1.290
36	-0.263	0.016	0.546	1.556
37	-0.227	0.019	0.593	1.868
38	-0.192	0.022	0.643	2.232
39	-0.157	0.027	0.697	2.654
40	-0.121	0.031	0.756	3.140
41	-0.086	0.037	0.821	3.698
42	-0.051	0.043	0.890	4.335
43	-0.015	0.051	0.966	5.057
44	0.020	0.059	1.048	5.872
45	0.056	0.068	1.136	6.786
46	0.091	0.078	1.233	7.807
47	0.126	0.089	1.337	8.940
48	0.162	0.102	1.451	10.191
49	0.197	0.116	1.574	11.565
50	0.232	0.131	1.707	13.066
51	0.268	0.147	1.852	14.696
52	0.303	0.165	2.009	16.457
53	0.338	0.184	2.180	18.350
54	0.374	0.204	2.364	20.373
55	0.409	0.225	2.565	22.523
56	0.444	0.248	2.783	24.796
57	0.480	0.272	3.019	27.186
58	0.515	0.297	3.275	29.686
59	0.551	0.323	3.552	32.285
60	0.586	0.350	3.854	34.974
61	0.621	0.377	4.180	37.741
62	0.657	0.406	4.535	40.572
63	0.692	0.435	4.919	43.454
64	0.727	0.464	5.337	46.371

65	0.763	0.493	5.789	49.307
66	0.798	0.522	6.280	52.247
67	0.833	0.552	6.813	55.175
68	0.869	0.581	7.391	58.075
69	0.904	0.609	8.018	60.932
70	0.939	0.637	8.697	63.730
71	0.975	0.665	9.435	66.458
72	1.010	0.691	10.235	69.101
73	1.045	0.716	11.103	71.649
74	1.081	0.741	12.045	74.092
75	1.116	0.764	13.067	76.421
76	1.152	0.786	14.175	78.629
77	1.187	0.807	15.377	80.713
78	1.222	0.827	16.681	82.667
79	1.258	0.845	18.096	84.490
80	1.293	0.862	19.630	86.182
81	1.328	0.877	21.295	87.744
82	1.364	0.892	23.101	89.177
83	1.399	0.905	25.061	90.485
84	1.434	0.917	27.186	91.674
85	1.470	0.927	29.492	92.747
86	1.505	0.937	31.993	93.710
87	1.540	0.946	34.706	94.571
88	1.576	0.953	37.649	95.336
89	1.611	0.960	40.842	96.012
90	1.646	0.966	44.306	96.606
91	1.682	0.971	48.064	97.125
92	1.717	0.976	52.140	97.577
93	1.753	0.980	56.562	97.967
94	1.788	0.983	61.359	98.303
95	1.823	0.986	66.563	98.590
96	1.859	0.988	72.208	98.834
97	1.894	0.990	78.332	99.041
98	1.929	0.992	84.975	99.215
99	1.965	0.994	92.182	99.360
100	2.000	0.995	100.000	99.481

0 mg/L DOC 4.301 μW/cm^2/nm UV

XLSTAT 2018.2.50628 - Dose effect analysis - Start time: 4/24/18 at 12:44:54 AM / End time: 4/24/18 at 12:44:56 AM
Observation weights: Workbook = Book1 / Sheet = Sheet1 / Range = Sheet1!$B$1:$B$6 / 5 rw and 1 clm
Response variable(s): Workbook = Book1 / Sheet = Sheet1 / Range = Sheet1!$C$1:$C$6 / 5 rw and 1 clm
Quantitative: Workbook = Book1 / Sheet = Sheet1 / Range = Sheet1!$A$1:$A$6 / 5 rw and 1 clm
Model: Probit
Confidence interval (%): 95
Stop conditions: Iterations = 1000 / Convergence = 1E-06
Maximization of the likelihood function using the Newton-Raphson algorithm
Summary statistics:

Variable	Observations	Obs. with missing data	Obs. without missing data	Minimum	Maximum	Mean	Std. deviation
Dead	5	0	5	5.000	20.000	15.800	5.908
Log(Dose/Conc.)	5	0	5	-0.056	1.382	0.771	0.568

Regression of variable Dead:
Goodness of fit statistics (Variable Dead):

Statistic	Independent	Full
Observations	100	100
Sum of weights	100.000	100.000
DF	99	98
-2 Log(Likelihood)	102.791	46.971
R^2(McFadden)	0.000	0.543
R^2(Cox and Snell)	0.000	0.428
R^2(Nagelkerke)	0.000	0.666
AIC	104.791	50.971
SBC	107.397	56.181
Iterations	0	7

Model parameters (Variable Dead):

Source	Value	Standard error	Wald Chi-Square	Pr > Chi²	Wald Lower bound (95%)	Wald Upper bound (95%)	Odds ratio	Odds ratio Lower bound (95%)	Odds ratio Upper bound (95%)
Intercept	-0.483	0.255	3.594	0.058	-0.982	0.016			
Log(Dose/Conc.)	3.677	1.139	10.427	0.001	1.445	5.908	39.514	4.242	368.063

Equation of the model (Variable Dead):

Dead = 0+1*(XLSTAT_CDFNormal(-0.483028065572815+3.6766507069787*Log(Dose/Conc.)))

Predictions and residuals (Variable Dead):

Observation	Weight	Log(Dose/Conc.)	Dose	Dead	Dead/Weight	Percent Mortality	Std Dev	STD DEV%	Pred(Dead)/Weight
Obs1	20	-0.0555173	0.88000006	5.000	0.250	25	0.957427	4.78713554	0.246
Obs2	20	0.2787536	1.9	14.00	0.700	70	0.577350	2.88675135	0.706
Obs3	20	0.97772361	9.5000001	20.00	1.000	100	0	0	0.999
Obs4	20	1.27369559	18.7800001	20.00	1.000	100	0	0	1.000
Obs5	20	1.3823773	24.1199998	20.00	1.000	100	0	0	1.000

Probability analysis with the fitted model (Variable Dead):

Probability	Dose/Conc.	Lower bound 95%	Upper bound 95%
0.01	0.315	0.033	0.565
0.05	0.483	0.095	0.748
0.10	0.606	0.168	0.874
0.20	0.799	0.328	1.070
0.30	0.974	0.520	1.265
0.40	1.155	0.745	1.513
0.50	1.353	0.984	1.892
0.60	1.586	1.216	2.531
0.70	1.879	1.444	3.651
0.80	2.292	1.701	5.813
0.90	3.020	2.078	11.385
0.95	3.791	2.426	20.041
0.99	5.809	3.211	58.508

TiO2

Probability	TiO2	Lower bound 95%	Upper bound 95%
0.01	0.195	0.018	0.337
0.05	0.288	0.053	0.432
0.10	0.355	0.094	0.497
0.20	0.456	0.184	0.596
0.30	0.547	0.292	0.694
0.40	0.638	0.418	0.820
0.50	0.738	0.550	1.021
0.60	0.852	0.669	1.371
0.70	0.995	0.781	1.990
0.80	1.193	0.904	3.185
0.90	1.534	1.080	6.265
0.95	1.887	1.239	11.054
0.99	2.785	1.591	32.363

Model Point	Log Con	Dead	Dose	% Mortality
0	-0.218	0.099	0.605	9.936
1	-0.200	0.112	0.631	11.154
2	-0.182	0.125	0.658	12.476
3	-0.164	0.139	0.686	13.904
4	-0.145	0.154	0.715	15.438
5	-0.127	0.171	0.746	17.081
6	-0.109	0.188	0.778	18.832
7	-0.091	0.207	0.811	20.689
8	-0.073	0.227	0.846	22.650
9	-0.055	0.247	0.882	24.712
10	-0.036	0.269	0.920	26.871
11	-0.018	0.291	0.959	29.120
12	0.000	0.315	1.000	31.454
13	0.018	0.339	1.043	33.864
14	0.036	0.363	1.087	36.342
15	0.055	0.389	1.134	38.879
16	0.073	0.415	1.182	41.464
17	0.091	0.441	1.233	44.086
18	0.109	0.467	1.286	46.735
19	0.127	0.494	1.341	49.398
20	0.145	0.521	1.398	52.064
21	0.164	0.547	1.458	54.721
22	0.182	0.574	1.520	57.356
23	0.200	0.600	1.585	59.960
24	0.218	0.625	1.653	62.519
25	0.236	0.650	1.723	65.025
26	0.255	0.675	1.797	67.467
27	0.273	0.698	1.874	69.836
28	0.291	0.721	1.954	72.124
29	0.309	0.743	2.037	74.325
30	0.327	0.764	2.125	76.431
31	0.345	0.784	2.215	78.438

Pred OH

Probability	Pred OH	Lower bound 95%	Upper bound 95%
0.01	0.345	0.032	0.594
0.05	0.509	0.094	0.763
0.10	0.626	0.165	0.877
0.20	0.805	0.324	1.051
0.30	0.965	0.516	1.224
0.40	1.127	0.738	1.447
0.50	1.302	0.970	1.802
0.60	1.505	1.182	2.420
0.70	1.756	1.379	3.512
0.80	2.105	1.595	5.621
0.90	2.707	1.906	11.058
0.95	3.331	2.188	19.510
0.99	4.916	2.808	57.120

32	0.364	0.803	2.310	80.343
33	0.382	0.821	2.409	82.142
34	0.400	0.838	2.512	83.833
35	0.418	0.854	2.619	85.417
36	0.436	0.869	2.731	86.893
37	0.455	0.883	2.848	88.262
38	0.473	0.895	2.970	89.527
39	0.491	0.907	3.097	90.689
40	0.509	0.918	3.229	91.754
41	0.527	0.927	3.367	92.724
42	0.545	0.936	3.511	93.605
43	0.564	0.944	3.661	94.400
44	0.582	0.951	3.818	95.115
45	0.600	0.958	3.981	95.755
46	0.618	0.963	4.151	96.326
47	0.636	0.968	4.329	96.832
48	0.655	0.973	4.514	97.279
49	0.673	0.977	4.707	97.672
50	0.691	0.980	4.908	98.017
51	0.709	0.983	5.118	98.317
52	0.727	0.986	5.337	98.577
53	0.745	0.988	5.565	98.802
54	0.764	0.990	5.803	98.995
55	0.782	0.992	6.051	99.161
56	0.800	0.993	6.310	99.302
57	0.818	0.994	6.579	99.422
58	0.836	0.995	6.861	99.523
59	0.855	0.996	7.154	99.608
60	0.873	0.997	7.460	99.679
61	0.891	0.997	7.779	99.739
62	0.909	0.998	8.111	99.788
63	0.927	0.998	8.458	99.828
64	0.945	0.999	8.820	99.862
65	0.964	0.999	9.197	99.889
66	0.982	0.999	9.590	99.912
67	1.000	0.999	10.000	99.930
68	1.018	0.999	10.428	99.944
69	1.036	1.000	10.873	99.956
70	1.055	1.000	11.338	99.966
71	1.073	1.000	11.823	99.973
72	1.091	1.000	12.328	99.979
73	1.109	1.000	12.856	99.984
74	1.127	1.000	13.405	99.987
75	1.145	1.000	13.978	99.990
76	1.164	1.000	14.576	99.993

77	1.182	1.000	15.199	99.994
78	1.200	1.000	15.849	99.996
79	1.218	1.000	16.527	99.997
80	1.236	1.000	17.233	99.998
81	1.255	1.000	17.970	99.998
82	1.273	1.000	18.738	99.999
83	1.291	1.000	19.539	99.999
84	1.309	1.000	20.375	99.999
85	1.327	1.000	21.246	99.999
86	1.345	1.000	22.154	100.000
87	1.364	1.000	23.101	100.000
88	1.382	1.000	24.089	100.000
89	1.400	1.000	25.119	100.000
90	1.418	1.000	26.193	100.000
91	1.436	1.000	27.313	100.000
92	1.455	1.000	28.480	100.000
93	1.473	1.000	29.698	100.000
94	1.491	1.000	30.968	100.000
95	1.509	1.000	32.292	100.000
96	1.527	1.000	33.672	100.000
97	1.545	1.000	35.112	100.000
98	1.564	1.000	36.613	100.000
99	1.582	1.000	38.178	100.000
100	1.600	1.000	39.811	100.000

2.95 mg/L DOC 4.301 μW/cm^2/nm UV

XLSTAT 2018.2.50628 - Dose effect analysis - Start time: 4/24/18 at 11:56:57 AM / End time: 4/24/18 at 11:57:11 AM
Observation weights: Workbook = Book1 / Sheet = Sheet1 / Range = 'Sheet1'!$B$1:$B$6 / 5 rw and 1 clm
Response variable(s): Workbook = Book1 / Sheet = Sheet1 / Range = 'Sheet1'!$C$1:$C$6 / 5 rw and 1 clm
Quantitative: Workbook = Book1 / Sheet = Sheet1 / Range = 'Sheet1'!$A$1:$A$6 / 5 rw and 1 clm
Model: Probit
Confidence interval (%): 95
Stop conditions: Iterations = 1000 / Convergence = 1E-06
Maximization of the likelihood function using the Newton-Raphson algorithm
Summary statistics:

Variable	Observations	Obs. with missing data	Obs. without missing data	Minimum	Maximum	Mean	Std. deviation
Dead	5	0	5	0.000	20.000	8.600	9.070
Log(Dose/Conc.)	5	0	5	-0.959	1.265	0.347	0.860

Regression of variable Dead:
Goodness of fit statistics (Variable Dead):

Statistic	Independent	Full
Observations	100	100
Sum of weights	100.000	100.000
DF	99	98
-2 Log(Likelihood)	136.663	28.033
R^2(McFadden)	0.000	0.795
R^2(Cox and Snell)	0.000	0.663
R^2(Nagelkerke)	0.000	0.889
AIC	138.663	32.033
SBC	141.268	37.243
Iterations	0	8

Model parameters (Variable Dead):

Source	Value	Standard error	Wald Chi-Square	Pr > Chi²	Wald Lower bound (95%)	Wald Upper bound (95%)	Odds ratio	Odds ratio Lower bound (95%)	Odds ratio Upper bound (95%)
Intercept	-5.358	1.171	20.934	< 0.0001	-7.654	-3.063			
Log(Dose/Conc.)	6.544	1.395	22.005	< 0.0001	3.810	9.278	695.194	45.147	10704.828

Equation of the model (Variable Dead):
Dead = 0+1*(XLSTAT_CDFNormal(-5.35818817794232+6.54419161610856*Log(Dose/Conc.)))
Predictions and residuals (Variable Dead):

Observation	Weight	Log(Dose/Conc.)	Dose	Dead	Dead/Weight	Percent Mort	Std Dev	STD DEV%	Pred(Dead)/Weight
Obs1	20	-0.9586073	0.11	0.000	0.000	0.000	0.000	0.000	0.000

Obs2	20	-0.3372422	0.45999997	0.000	0.000	0.000	0.000	0.000		0.000
Obs3	20	0.68930886	4.89000001	4.000	0.200	20.000	0.816	4.082		0.198
Obs4	20	1.07591176	11.91	19.000	0.950	95.000	0.500	2.500		0.954
Obs5	20	1.26528963	18.4200002	20.000	1.000	100.000	0.000	0.000		0.998

Probability analysis with the fitted model (Variable Dead):

Probability	Dose/Conc.	Lower bound 95%	Upper bound 95%
0.01	2.906	1.545	3.870
0.05	3.693	2.295	4.657
0.10	4.197	2.820	5.166
0.20	4.900	3.588	5.908
0.30	5.478	4.229	6.570
0.40	6.026	4.821	7.261
0.50	6.588	5.396	8.050
0.60	7.203	5.980	9.015
0.70	7.923	6.607	10.281
0.80	8.859	7.345	12.121
0.90	10.342	8.396	15.427
0.95	11.752	9.312	18.960
0.99	14.937	11.206	28.170

TiO2

Probability analysis with the fitted model (Variable Dead):

Probability	TiO2	Lower bound 95%	Upper bound 95%
0.01	3.260	1.972	4.122
0.05	3.971	2.713	4.806
0.10	4.412	3.204	5.236
0.20	5.012	3.892	5.847
0.30	5.494	4.446	6.378
0.40	5.943	4.946	6.918
0.50	6.396	5.425	7.518
0.60	6.883	5.905	8.233
0.70	7.445	6.414	9.147
0.80	8.162	7.005	10.436
0.90	9.271	7.832	12.663
0.95	10.300	8.537	14.943
0.99	12.549	9.960	20.545

Pred OH

Model Point	Log Dose	Dead	Dose	% Mortl
1	-1.500	0.000	0.032	0.000
2	-1.470	0.000	0.034	0.000
3	-1.439	0.000	0.036	0.000
4	-1.409	0.000	0.039	0.000
5	-1.379	0.000	0.042	0.000
6	-1.348	0.000	0.045	0.000
7	-1.318	0.000	0.048	0.000
8	-1.288	0.000	0.052	0.000
9	-1.258	0.000	0.055	0.000
10	-1.227	0.000	0.059	0.000
11	-1.197	0.000	0.064	0.000
12	-1.167	0.000	0.068	0.000
13	-1.136	0.000	0.073	0.000
14	-1.106	0.000	0.078	0.000
15	-1.076	0.000	0.084	0.000
16	-1.045	0.000	0.090	0.000
17	-1.015	0.000	0.097	0.000
18	-0.985	0.000	0.104	0.000
19	-0.955	0.000	0.111	0.000
20	-0.924	0.000	0.119	0.000
21	-0.894	0.000	0.128	0.000
22	-0.864	0.000	0.137	0.000
23	-0.833	0.000	0.147	0.000
24	-0.803	0.000	0.157	0.000
25	-0.773	0.000	0.169	0.000
26	-0.742	0.000	0.181	0.000
27	-0.712	0.000	0.194	0.000
28	-0.682	0.000	0.208	0.000
29	-0.652	0.000	0.223	0.000
30	-0.621	0.000	0.239	0.000
31	-0.591	0.000	0.257	0.000
32	-0.561	0.000	0.275	0.000
33	-0.530	0.000	0.295	0.000
34	-0.500	0.000	0.316	0.000
35	-0.470	0.000	0.339	0.000
36	-0.439	0.000	0.364	0.000
37	-0.409	0.000	0.390	0.000
38	-0.379	0.000	0.418	0.000

Probability	Pred OH	Lower bound 95%	Upper bound 95%
0.01	3.025	1.721	3.942
0.05	3.781	2.464	4.691
0.10	4.259	2.970	5.168
0.20	4.919	3.698	5.856
0.30	5.458	4.297	6.459
0.40	5.964	4.846	7.078
0.50	6.480	5.380	7.774
0.60	7.041	5.921	8.610
0.70	7.695	6.502	9.692
0.80	8.537	7.185	11.240
0.90	9.860	8.153	13.971
0.95	11.106	8.991	16.831
0.99	13.884	10.707	24.081

39	-0.348	0.000	0.448	0.000
40	-0.318	0.000	0.481	0.000
41	-0.288	0.000	0.515	0.000
42	-0.258	0.000	0.553	0.000
43	-0.227	0.000	0.593	0.000
44	-0.197	0.000	0.635	0.000
45	-0.167	0.000	0.681	0.000
46	-0.136	0.000	0.731	0.000
47	-0.106	0.000	0.783	0.000
48	-0.076	0.000	0.840	0.000
49	-0.045	0.000	0.901	0.000
50	-0.015	0.000	0.966	0.000
51	0.015	0.000	1.036	0.000
52	0.045	0.000	1.110	0.000
53	0.076	0.000	1.191	0.000
54	0.106	0.000	1.277	0.000
55	0.136	0.000	1.369	0.000
56	0.167	0.000	1.468	0.001
57	0.197	0.000	1.574	0.002
58	0.227	0.000	1.688	0.005
59	0.258	0.000	1.810	0.012
60	0.288	0.000	1.940	0.026
61	0.318	0.001	2.081	0.053
62	0.348	0.001	2.231	0.104
63	0.379	0.002	2.392	0.199
64	0.409	0.004	2.565	0.367
65	0.439	0.007	2.750	0.652
66	0.470	0.011	2.949	1.117
67	0.500	0.018	3.162	1.849
68	0.530	0.030	3.391	2.953
69	0.561	0.046	3.636	4.556
70	0.591	0.068	3.899	6.796
71	0.621	0.098	4.180	9.803
72	0.652	0.137	4.482	13.686
73	0.682	0.185	4.806	18.506
74	0.712	0.243	5.154	24.261
75	0.742	0.309	5.526	30.867
76	0.773	0.382	5.926	38.159
77	0.803	0.459	6.354	45.898
78	0.833	0.538	6.813	53.796
79	0.864	0.615	7.305	61.547
80	0.894	0.689	7.833	68.861
81	0.924	0.755	8.399	75.498
82	0.955	0.813	9.006	81.287
83	0.985	0.861	9.657	86.145

84	1.015	0.901	10.355	90.063
85	1.045	0.931	11.103	93.102
86	1.076	0.954	11.906	95.369
87	1.106	0.970	12.766	96.995
88	1.136	0.981	13.689	98.116
89	1.167	0.989	14.678	98.860
90	1.197	0.993	15.739	99.334
91	1.227	0.996	16.876	99.624
92	1.258	0.998	18.096	99.796
93	1.288	0.999	19.403	99.893
94	1.318	0.999	20.806	99.946
95	1.348	1.000	22.309	99.974
96	1.379	1.000	23.921	99.988
97	1.409	1.000	25.650	99.994
98	1.439	1.000	27.504	99.998
99	1.470	1.000	29.492	99.999
100	1.500	1.000	31.623	100.000

4.28 mg/L DOC 4.301 μW/cm^2/nm UV

XLSTAT 2018.2.50628 - Dose effect analysis - Start time: 4/25/18 at 2:24:53 PM / End time: 4/25/18 at 2:24:54 PM
Observation weights: Workbook = Book1 / Sheet = DOC / Range = DOC!$P$1:$P$8 / 7 rw and 1 clm
Response variable(s): Workbook = Book1 / Sheet = DOC / Range = DOC!$Q$1:$Q$8 / 7 rw and 1 clm
Quantitative: Workbook = Book1 / Sheet = DOC / Range = DOC!$O$1:$O$8 / 7 rw and 1 clm
Model: Probit
Confidence interval (%): 95
Stop conditions: Iterations = 100 / Convergence = 1E-06
Maximization of the likelihood function using the Newton-Raphson algorithm
Summary statistics:

Variable	Observations	Obs. with missing data	Obs. without missing data	Minimum	Maximum	Mean	Std. deviation
Dead	7	0	7	0.000	30.000	12.286	10.806
Log(Measured OH)	7	0	7	0.318	1.012	0.708	0.225

Regression of variable Dead:
Goodness of fit statistics (Variable Dead):

Statistic	Independent	Full
Observations	210	210
Sum of weights	210.000	210.000
DF	209	208
-2 Log(Likelihood)	284.208	154.625
R^2(McFadden)	0.000	0.456
R^2(Cox and Snell)	0.000	0.460
R^2(Nagelkerke)	0.000	0.621
AIC	286.208	158.625
SBC	289.555	165.319
Iterations	0	6

Model parameters (Variable Dead):

Source	Value	Standard error	Wald Chi-Square	Pr > Chi²	Wald Lower bound (95%)	Wald Upper bound (95%)	Odds ratio	Odds ratio Lower bound (95%)	Odds ratio Upper bound (95%)
Intercept	-5.769	0.767	56.640	< 0.0001	-7.271	-4.267			
Log(Measured OH)	7.270	0.953	58.246	< 0.0001	5.403	9.137	1436.460	222.056	9292.328

Equation of the model (Variable Dead):

Dead = 0+1*(XLSTAT_CDFNormal(-5.76898326227484+7.2699368028867*Log(Measured OH)))

Predictions and residuals (Variable Dead):

Observation	Weight	Log(Measured OH)	Dose	Dead	Dead/Weight	% Mortality	Pred(Dead)/Weight
Obs1	30	0.31806333	2.08	0.000	0.000	0.000	0.000
Obs2	30	0.47596159	2.992	2.000	0.067	6.667	0.010
Obs3	30	0.66860953	4.6624	2.000	0.067	6.667	0.182
Obs4	30	0.75532593	5.6928	12.000	0.400	40.000	0.391
Obs5	30	0.83148584	6.784	17.000	0.567	56.667	0.609
Obs6	30	0.89679068	7.8848	23.000	0.767	76.667	0.774
Obs7	30	1.01219585	10.2848	30.000	1.000	100.000	0.944

Probability analysis with the fitted model (Variable Dead):

Probability	Measured OH	Lower bound 95%	Upper bound 95%
0.01	2.975	2.273	3.507
0.05	3.692	3.025	4.185
0.10	4.142	3.516	4.605
0.20	4.762	4.206	5.189
0.30	5.265	4.766	5.678
0.40	5.737	5.277	6.162
0.50	6.216	5.771	6.691
0.60	6.736	6.271	7.312
0.70	7.340	6.810	8.092
0.80	8.115	7.456	9.165
0.90	9.329	8.403	10.960
0.95	10.466	9.250	12.739
0.99	12.988	11.037	16.948

Model Point	log Dose	Dead	Dose	% Mortl
1	0.000	0.000	1.000	0.000
2	0.012	0.000	1.028	0.000
3	0.024	0.000	1.057	0.000
4	0.036	0.000	1.087	0.000
5	0.048	0.000	1.118	0.000
6	0.061	0.000	1.150	0.000
7	0.073	0.000	1.182	0.000
8	0.085	0.000	1.216	0.000
9	0.097	0.000	1.250	0.000
10	0.109	0.000	1.286	0.000
11	0.121	0.000	1.322	0.000
12	0.133	0.000	1.359	0.000
13	0.145	0.000	1.398	0.000
14	0.158	0.000	1.437	0.000
15	0.170	0.000	1.478	0.000
16	0.182	0.000	1.520	0.000
17	0.194	0.000	1.563	0.001
18	0.206	0.000	1.607	0.001
19	0.218	0.000	1.653	0.001
20	0.230	0.000	1.699	0.002
21	0.242	0.000	1.748	0.003
22	0.255	0.000	1.797	0.004
23	0.267	0.000	1.848	0.006
24	0.279	0.000	1.900	0.009
25	0.291	0.000	1.954	0.013
26	0.303	0.000	2.009	0.018
27	0.315	0.000	2.066	0.025
28	0.327	0.000	2.125	0.035
29	0.339	0.000	2.185	0.048
30	0.352	0.001	2.247	0.066

31	0.364	0.001	2.310	0.089
32	0.376	0.001	2.376	0.119
33	0.388	0.002	2.443	0.159
34	0.400	0.002	2.512	0.211
35	0.412	0.003	2.583	0.278
36	0.424	0.004	2.656	0.363
37	0.436	0.005	2.731	0.471
38	0.448	0.006	2.809	0.606
39	0.461	0.008	2.888	0.775
40	0.473	0.010	2.970	0.984
41	0.485	0.012	3.054	1.241
42	0.497	0.016	3.140	1.554
43	0.509	0.019	3.229	1.932
44	0.521	0.024	3.321	2.386
45	0.533	0.029	3.415	2.927
46	0.545	0.036	3.511	3.565
47	0.558	0.043	3.611	4.313
48	0.570	0.052	3.713	5.183
49	0.582	0.062	3.818	6.188
50	0.594	0.073	3.926	7.338
51	0.606	0.086	4.037	8.645
52	0.618	0.101	4.151	10.118
53	0.630	0.118	4.269	11.767
54	0.642	0.136	4.390	13.597
55	0.655	0.156	4.514	15.613
56	0.667	0.178	4.642	17.817
57	0.679	0.202	4.773	20.207
58	0.691	0.228	4.908	22.780
59	0.703	0.255	5.047	25.527
60	0.715	0.284	5.190	28.438
61	0.727	0.315	5.337	31.499
62	0.739	0.347	5.488	34.692
63	0.752	0.380	5.643	37.999
64	0.764	0.414	5.803	41.395
65	0.776	0.449	5.967	44.857
66	0.788	0.484	6.136	48.359
67	0.800	0.519	6.310	51.873
68	0.812	0.554	6.488	55.373
69	0.824	0.588	6.672	58.831
70	0.836	0.622	6.861	62.222
71	0.848	0.655	7.055	65.522
72	0.861	0.687	7.254	68.707
73	0.873	0.718	7.460	71.759
74	0.885	0.747	7.671	74.659

75	0.897	0.774	7.888	77.395
76	0.909	0.800	8.111	79.956
77	0.921	0.823	8.341	82.334
78	0.933	0.845	8.577	84.525
79	0.945	0.865	8.820	86.529
80	0.958	0.883	9.069	88.347
81	0.970	0.900	9.326	89.984
82	0.982	0.914	9.590	91.446
83	0.994	0.927	9.861	92.743
84	1.006	0.939	10.141	93.883
85	1.018	0.949	10.428	94.878
86	1.030	0.957	10.723	95.740
87	1.042	0.965	11.026	96.480
88	1.055	0.971	11.338	97.112
89	1.067	0.976	11.659	97.646
90	1.079	0.981	11.989	98.095
91	1.091	0.985	12.328	98.469
92	1.103	0.988	12.677	98.777
93	1.115	0.990	13.036	99.031
94	1.127	0.992	13.405	99.237
95	1.139	0.994	13.785	99.404
96	1.152	0.995	14.175	99.537
97	1.164	0.996	14.576	99.643
98	1.176	0.997	14.988	99.727
99	1.188	0.998	15.413	99.793
100	1.200	0.998	15.849	99.844

5.71 mg/L DOC 4.301 μW/cm²/nm UV

XLSTAT 2018.2.50628 - Dose effect analysis - Start time: 4/24/18 at 1:11:59 AM / End time: 4/24/18 at 1:12:01 AM
Observation weights: Workbook = Book1 / Sheet = Sheet1 / Range = 'Sheet1'!$B$1:$B$6 / 5 rw and 1 clm
Response variable(s): Workbook = Book1 / Sheet = Sheet1 / Range = 'Sheet1'!$C$1:$C$6 / 5 rw and 1 clm
Quantitative: Workbook = Book1 / Sheet = Sheet1 / Range = 'Sheet1'!$A$1:$A$6 / 5 rw and 1 clm
Model: Probit
Confidence interval (%): 95
Stop conditions: Iterations = 1000 / Convergence = 1E-06
Maximization of the likelihood function using the Newton-Raphson algorithm
Summary statistics:

Variable	Observations	Obs. with missing data	Obs. without missing data	Minimum	Maximum	Mean	Std. deviation
Dead	5	0	5	0.000	20.000	7.600	7.429
Log(Dose/Conc.)	5	0	5	-1.046	0.903	-0.037	0.771

Regression of variable Dead:
Goodness of fit statistics (Variable Dead):

Statistic	Independent	Full
Observations	100	100
Sum of weights	100.000	100.000
DF	99	98
-2 Log(Likelihood)	134.391	78.616
R²(McFadden)	0.000	0.415
R²(Cox and Snell)	0.000	0.428
R²(Nagelkerke)	0.000	0.578
AIC	136.391	82.616
SBC	138.996	87.826
Iterations	0	6

Model parameters (Variable Dead):

Source	Value	Standard error	Wald Chi-Square	Pr > Chi²	Wald Lower bound (95%)	Wald Upper bound (95%)	Odds ratio	Odds ratio Lower bound (95%)	Odds ratio Upper bound (95%)
Intercept	-0.837	0.289	8.410	0.004	-1.403	-0.271			
Log(Dose/Conc.)	1.973	0.431	20.999	< 0.0001	1.129	2.817	7.195	3.094	16.733

Equation of the model (Variable Dead):
Dead = 0.1+0.9*(XLSTAT_CDFNormal(-0.83716370710242+1.9733517030089*Log(Dose/Conc.)))
Predictions and residuals (Variable Dead):

Observation	Weight	Log(Dose/Conc.)	Dose	Dead	Dead/Weight	% Mort	Std Dev	STD DEV%
Obs1	20	-1.0457575	0.089999998	0.000	0.000	0.000	0.000	0.000

Obs2	20	-0.7695511	0.169999992	0.000	0.000	0.000	0.000	0.000	
Obs3	20	0.05690485	1.139999996	9.000	0.450	45.000	0.500	2.500	
Obs4	20	0.66931688	4.669999994	9.000	0.450	45.000	1.500	7.500	
Obs5	20	0.90254678	7.990000013	20.000	1.000	100.000	0.000	0.000	

Probability analysis with the fitted model (Variable Dead):

Probability	Dose/Conc.	Lower bound 95%	Upper bound 95%
0.01	0.124	0.021	0.296
0.05	0.289	0.078	0.564
0.10	0.453	0.154	0.803
0.20	0.780	0.344	1.254
0.30	1.154	0.603	1.768
0.40	1.613	0.947	2.435
0.50	2.207	1.398	3.390
0.60	3.018	1.988	4.902
0.70	4.219	2.787	7.563
0.80	6.245	3.984	13.053
0.90	10.757	6.282	28.950
0.95	16.854	8.983	56.934
0.99	39.132	17.199	206.823

Model Point	Log Dose	Dead	Dose	% Mortality
1	-1.500	0.000	0.032	0.030
2	-1.475	0.000	0.034	0.035
3	-1.449	0.000	0.036	0.042
4	-1.424	0.000	0.038	0.049
5	-1.399	0.001	0.040	0.058
6	-1.374	0.001	0.042	0.069
7	-1.348	0.001	0.045	0.081
8	-1.323	0.001	0.048	0.095
9	-1.298	0.001	0.050	0.111
10	-1.273	0.001	0.053	0.130
11	-1.247	0.002	0.057	0.152
12	-1.222	0.002	0.060	0.177
13	-1.197	0.002	0.064	0.205
14	-1.172	0.002	0.067	0.238
15	-1.146	0.003	0.071	0.275
16	-1.121	0.003	0.076	0.318
17	-1.096	0.004	0.080	0.366
18	-1.071	0.004	0.085	0.421
19	-1.045	0.005	0.090	0.483
20	-1.020	0.006	0.095	0.553
21	-0.995	0.006	0.101	0.632
22	-0.970	0.007	0.107	0.721
23	-0.944	0.008	0.114	0.820
24	-0.919	0.009	0.120	0.932
25	-0.894	0.011	0.128	1.056
26	-0.869	0.012	0.135	1.195
27	-0.843	0.013	0.143	1.350
28	-0.818	0.015	0.152	1.521
29	-0.793	0.017	0.161	1.711
30	-0.768	0.019	0.171	1.920
31	-0.742	0.022	0.181	2.151
32	-0.717	0.024	0.192	2.405
33	-0.692	0.027	0.203	2.684
34	-0.667	0.030	0.215	2.990
35	-0.641	0.033	0.228	3.323
36	-0.616	0.037	0.242	3.687
37	-0.591	0.041	0.257	4.082
38	-0.566	0.045	0.272	4.512
39	-0.540	0.050	0.288	4.977
40	-0.515	0.055	0.305	5.479

41	-0.490	0.060	0.324	6.021
42	-0.465	0.066	0.343	6.603
43	-0.439	0.072	0.364	7.229
44	-0.414	0.079	0.385	7.899
45	-0.389	0.086	0.408	8.615
46	-0.364	0.094	0.433	9.378
47	-0.338	0.102	0.459	10.190
48	-0.313	0.111	0.486	11.053
49	-0.288	0.120	0.515	11.966
50	-0.263	0.129	0.546	12.931
51	-0.237	0.139	0.579	13.949
52	-0.212	0.150	0.614	15.020
53	-0.187	0.161	0.650	16.145
54	-0.162	0.173	0.689	17.323
55	-0.136	0.186	0.731	18.554
56	-0.111	0.198	0.774	19.839
57	-0.086	0.212	0.821	21.175
58	-0.061	0.226	0.870	22.563
59	-0.035	0.240	0.922	24.001
60	-0.010	0.255	0.977	25.488
61	0.015	0.270	1.036	27.021
62	0.040	0.286	1.097	28.599
63	0.066	0.302	1.163	30.220
64	0.091	0.319	1.233	31.880
65	0.116	0.336	1.307	33.578
66	0.141	0.353	1.385	35.310
67	0.167	0.371	1.468	37.073
68	0.192	0.389	1.556	38.864
69	0.217	0.407	1.649	40.678
70	0.242	0.425	1.748	42.513
71	0.268	0.444	1.852	44.364
72	0.293	0.462	1.963	46.228
73	0.318	0.481	2.081	48.099
74	0.343	0.500	2.205	49.975
75	0.369	0.519	2.337	51.852
76	0.394	0.537	2.477	53.724
77	0.419	0.556	2.625	55.587
78	0.444	0.574	2.783	57.439
79	0.470	0.593	2.949	59.274
80	0.495	0.611	3.126	61.089
81	0.520	0.629	3.313	62.880
82	0.545	0.646	3.511	64.644
83	0.571	0.664	3.721	66.377
84	0.596	0.681	3.944	68.076
85	0.621	0.697	4.180	69.737
86	0.646	0.714	4.431	71.359

87	0.672	0.729	4.696	72.938
88	0.697	0.745	4.977	74.473
89	0.722	0.760	5.275	75.960
90	0.747	0.774	5.591	77.400
91	0.773	0.788	5.926	78.789
92	0.798	0.801	6.280	80.127
93	0.823	0.814	6.656	81.413
94	0.848	0.826	7.055	82.645
95	0.874	0.838	7.477	83.825
96	0.899	0.850	7.925	84.951
97	0.924	0.860	8.399	86.024
98	0.949	0.870	8.902	87.043
99	0.975	0.880	9.435	88.010
100	1.000	0.889	10.000	88.924

0 mg/L DOC 5.188 µW/cm^2/nm UV

XLSTAT 2018.2.50628 - Dose effect analysis - Start time: 4/24/18 at 1:13:56 AM / End time: 4/24/18 at 1:13:58 AM
Observation weights: Workbook = Book1 / Sheet = Sheet1 / Range = 'Sheet1'!$B$1:$B$6 / 5 rw and 1 clm
Response variable(s): Workbook = Book1 / Sheet = Sheet1 / Range = 'Sheet1'!$C$1:$C$6 / 5 rw and 1 clm
Quantitative: Workbook = Book1 / Sheet = Sheet1 / Range = 'Sheet1'!$A$1:$A$6 / 5 rw and 1 clm
Model: Probit
Confidence interval (%): 95
Stop conditions: Iterations = 1000 / Convergence = 1E-06
Maximization of the likelihood function using the Newton-Raphson algorithm
Summary statistics:

Variable	Observations	Obs. with missing data	Obs. without missing data	Minimum	Maximum	Mean	Std. deviation
Dead	5	0	5	6.000	20.000	17.000	5.541
Log(Dose/Conc.)	5	0	5	0.004	1.701	0.953	0.689

Regression of variable Dead:
Goodness of fit statistics (Variable Dead):

Statistic	Independent	Full
Observations	100	100
Sum of weights	100.000	100.000
DF	99	98
-2 Log(Likelihood)	84.542	32.375
R²(McFadden)	0.000	0.617
R²(Cox and Snell)	0.000	0.406
R²(Nagelkerke)	0.000	0.712
AIC	86.542	36.375
SBC	89.147	41.586
Iterations	0	8

Model parameters (Variable Dead):

Source	Value	Standard error	Wald Chi-Square	Pr > Chi²	Wald Lower bound (95%)	Wald Upper bound (95%)	Odds ratio	Odds ratio Lower bound (95%)	Odds ratio Upper bound (95%)
Intercept	-0.552	0.298	3.417	0.065	-1.137	0.033			
Log(Dose/Conc.)	6.342	1.628	15.173	< 0.0001	3.151	9.533	568.080	23.361	13814.558

Equation of the model (Variable Dead):
Dead = 0+1*(XLSTAT_CDFNormal(-0.551807813407823+6.34226253195223*Log(Dose/Conc.)))
Predictions and residuals (Variable Dead):

Observation	Weight	Log(Dose/Conc.)	Dose	Dead	Dead/Weight	% Mortality	Std Dev	STD DEV%
Obs1	20	0.00432137	1.00999999	6.000	0.300	30.000	0.577	2.887
Obs2	20	0.34635297	2.21999998	19.000	0.950	95.000	0.500	2.500
Obs3	20	1.04493155	11.0900001	20.000	1.000	100.000	0.000	0.000
Obs4	20	1.66810624	46.5700002	20.000	1.000	100.000	0.000	0.000

Obs5	20	1.70104963	50.2399999	20.000	1.000	100.000	0.000	0.000

Probability analysis with the fitted model (Variable Dead):

Probability	Dose/Conc.	Lower bound 95%	Upper bound 95%
0.01	0.525	0.209	0.729
0.05	0.672	0.340	0.870
0.10	0.767	0.438	0.960
0.20	0.900	0.592	1.091
0.30	1.010	0.727	1.208
0.40	1.114	0.857	1.335
0.50	1.222	0.983	1.487
0.60	1.340	1.109	1.688
0.70	1.478	1.237	1.969
0.80	1.658	1.380	2.402
0.90	1.946	1.576	3.226
0.95	2.220	1.743	4.152
0.99	2.843	2.085	6.733

Model Point	Log Dose	Dead	Dose	% Mortality
0	-0.018	0.252	0.959	25.235
1	0.000	0.291	1.000	29.054
2	0.018	0.331	1.043	33.124
3	0.036	0.374	1.087	37.404
4	0.055	0.418	1.134	41.845
5	0.073	0.464	1.182	46.392
6	0.091	0.510	1.233	50.988
7	0.109	0.556	1.286	55.570
8	0.127	0.601	1.341	60.079
9	0.145	0.645	1.398	64.457
10	0.164	0.687	1.458	68.652
11	0.182	0.726	1.520	72.619
12	0.200	0.763	1.585	76.320
13	0.218	0.797	1.653	79.728
14	0.236	0.828	1.723	82.825
15	0.255	0.856	1.797	85.602
16	0.273	0.881	1.874	88.058
17	0.291	0.902	1.954	90.203
18	0.309	0.921	2.037	92.051
19	0.327	0.936	2.125	93.623
20	0.345	0.949	2.215	94.941
21	0.364	0.960	2.310	96.032
22	0.382	0.969	2.409	96.924
23	0.400	0.976	2.512	97.643
24	0.418	0.982	2.619	98.215
25	0.436	0.987	2.731	98.664
26	0.455	0.990	2.848	99.012
27	0.473	0.993	2.970	99.278
28	0.491	0.995	3.097	99.479
29	0.509	0.996	3.229	99.629
30	0.527	0.997	3.367	99.738
31	0.545	0.998	3.511	99.818
32	0.564	0.999	3.661	99.875
33	0.582	0.999	3.818	99.915
34	0.600	0.999	3.981	99.943
35	0.618	1.000	4.151	99.962
36	0.636	1.000	4.329	99.975
37	0.655	1.000	4.514	99.984
38	0.673	1.000	4.707	99.990
39	0.691	1.000	4.908	99.994
40	0.709	1.000	5.118	99.996
41	0.727	1.000	5.337	99.998
42	0.745	1.000	5.565	99.999

43	0.764	1.000	5.803	99.999
44	0.782	1.000	6.051	99.999
45	0.800	1.000	6.310	100.000
46	0.818	1.000	6.579	100.000
47	0.836	1.000	6.861	100.000
48	0.855	1.000	7.154	100.000
49	0.873	1.000	7.460	100.000
50	0.891	1.000	7.779	100.000
51	0.909	1.000	8.111	100.000
52	0.927	1.000	8.458	100.000
53	0.945	1.000	8.820	100.000
54	0.964	1.000	9.197	100.000
55	0.982	1.000	9.590	100.000
56	1.000	1.000	10.000	100.000
57	1.018	1.000	10.428	100.000
58	1.036	1.000	10.873	100.000
59	1.055	1.000	11.338	100.000
60	1.073	1.000	11.823	100.000
61	1.091	1.000	12.328	100.000
62	1.109	1.000	12.856	100.000
63	1.127	1.000	13.405	100.000
64	1.145	1.000	13.978	100.000
65	1.164	1.000	14.576	100.000
66	1.182	1.000	15.199	100.000
67	1.200	1.000	15.849	100.000
68	1.218	1.000	16.527	100.000
69	1.236	1.000	17.233	100.000
70	1.255	1.000	17.970	100.000
71	1.273	1.000	18.738	100.000
72	1.291	1.000	19.539	100.000
73	1.309	1.000	20.375	100.000
74	1.327	1.000	21.246	100.000
75	1.345	1.000	22.154	100.000
76	1.364	1.000	23.101	100.000
77	1.382	1.000	24.089	100.000
78	1.400	1.000	25.119	100.000
79	1.418	1.000	26.193	100.000
80	1.436	1.000	27.313	100.000
81	1.455	1.000	28.480	100.000
82	1.473	1.000	29.698	100.000
83	1.491	1.000	30.968	100.000
84	1.509	1.000	32.292	100.000
85	1.527	1.000	33.672	100.000
86	1.545	1.000	35.112	100.000
87	1.564	1.000	36.613	100.000
88	1.582	1.000	38.178	100.000

89	1.600	1.000	39.811	100.000
90	1.618	1.000	41.513	100.000
91	1.636	1.000	43.288	100.000
92	1.655	1.000	45.138	100.000
93	1.673	1.000	47.068	100.000
94	1.691	1.000	49.081	100.000
95	1.709	1.000	51.179	100.000
96	1.727	1.000	53.367	100.000
97	1.745	1.000	55.649	100.000
98	1.764	1.000	58.028	100.000
99	1.782	1.000	60.509	100.000
100	1.800	1.000	63.096	100.000
86	1.545	1.000	35.112	100.000
87	1.564	1.000	36.613	100.000
88	1.582	1.000	38.178	100.000
89	1.600	1.000	39.811	100.000
90	1.618	1.000	41.513	100.000
91	1.636	1.000	43.288	100.000
92	1.655	1.000	45.138	100.000
93	1.673	1.000	47.068	100.000
94	1.691	1.000	49.081	100.000
95	1.709	1.000	51.179	100.000
96	1.727	1.000	53.367	100.000
97	1.745	1.000	55.649	100.000
98	1.764	1.000	58.028	100.000
99	1.782	1.000	60.509	100.000
100	1.800	1.000	63.096	100.000

4.28 mg/L DOC 5.188 μW/cm^2/nm UV

XLSTAT 2018.2.50628 - Dose effect analysis - Start time: 4/24/18 at 1:19:15 AM / End time: 4/24/18 at 1:19:17 AM
Observation weights: Workbook = Book1 / Sheet = Sheet1 / Range = 'Sheet1'!$B$1:$B$6 / 5 rw and 1 clm
Response variable(s): Workbook = Book1 / Sheet = Sheet1 / Range = 'Sheet1'!$C$1:$C$6 / 5 rw and 1 clm
Quantitative: Workbook = Book1 / Sheet = Sheet1 / Range = 'Sheet1'!$A$1:$A$6 / 5 rw and 1 clm
Model: Probit
Confidence interval (%): 95
Stop conditions: Iterations = 1000 / Convergence = 1E-06
Maximization of the likelihood function using the Newton-Raphson algorithm
Summary statistics:

Variable	Observations	Obs. with missing data	Obs. without missing data	Minimum	Maximum	Mean	Std. deviation
Dead	5	0	5	7.000	20.000	16.200	5.180
Log(Dose/Conc.)	5	0	5	-0.553	1.438	0.486	0.796

Regression of variable Dead:
Goodness of fit statistics (Variable Dead):

Statistic	Independent	Full
Observations	100	100
Sum of weights	100.000	100.000
DF	99	98
-2 Log(Likelihood)	97.245	50.340
R²(McFadden)	0.000	0.482
R²(Cox and Snell)	0.000	0.374
R²(Nagelkerke)	0.000	0.602
AIC	99.245	54.340
SBC	101.850	59.551
Iterations	0	8

Model parameters (Variable Dead):

Source	Value	Standard error	Wald Chi-Square	Pr > Chi²	Wald Lower bound (95%)	Wald Upper bound (95%)	Odds ratio	Odds ratio Lower bound (95%)
Intercept	1.500	0.641	5.476	0.019	0.244	2.757		
Log(Dose/Conc.)	3.417	1.447	5.574	0.018	0.580	6.254	30.486	1.787

Equation of the model (Variable Dead):
Dead = 0+1*(XLSTAT_CDFNormal(1.50008694249099+3.41727195468116*Log(Dose/Conc.))
)
Predictions and residuals (Variable Dead):

Observation	Weight	Log(Dose/Conc.)	Dose	Dead	Dead/Weight	Percent Mortaltiy	Std Dev	STD DEV%
Obs1	20	-0.552842	0.27999998	7.000	0.350	35.000	1.258	6.292
Obs2	20	-0.2839967	0.519999948	14.000	0.700	70.000	1.000	5.000
Obs3	20	0.60422605	4.019999971	20.000	1.000	100.000	0.000	0.000
Obs4	20	1.22427401	16.75999983	20.000	1.000	100.000	0.000	0.000
Obs5	20	1.43838411	27.44000019	20.000	1.000	100.000	0.000	0.000

Probability analysis with the fitted model (Variable Dead):

Measured Hydroxyl Radical

Probability	Dose/Conc.	Lower bound 95%	Upper bound 95%
0.01	0.076	0.000	0.162
0.05	0.120	0.000	0.211
0.10	0.153	0.002	0.243
0.20	0.206	0.010	0.293
0.30	0.256	0.033	0.341
0.40	0.307	0.089	0.405
0.50	0.364	0.199	0.544
0.60	0.432	0.316	1.031
0.70	0.518	0.394	2.674
0.80	0.642	0.466	8.947
0.90	0.863	0.564	49.786
0.95	1.102	0.653	207.895
0.99	1.745	0.850	3067.233

Model Point	Log Dose	Dead	Dose	% Mortality
0	-1.030	0.022	0.093	2.165
1	-1.000	0.028	0.100	2.761
2	-0.970	0.035	0.107	3.487
3	-0.939	0.044	0.115	4.363
4	-0.909	0.054	0.123	5.408
5	-0.879	0.066	0.132	6.642
6	-0.848	0.081	0.142	8.084
7	-0.818	0.098	0.152	9.751
8	-0.788	0.117	0.163	11.657
9	-0.758	0.138	0.175	13.813
10	-0.727	0.162	0.187	16.226
11	-0.697	0.189	0.201	18.898
12	-0.667	0.218	0.215	21.826
13	-0.636	0.250	0.231	24.998
14	-0.606	0.284	0.248	28.400
15	-0.576	0.320	0.266	32.009
16	-0.545	0.358	0.285	35.797
17	-0.515	0.397	0.305	39.731
18	-0.485	0.438	0.327	43.771
19	-0.455	0.479	0.351	47.878
20	-0.424	0.520	0.376	52.007
21	-0.394	0.561	0.404	56.115
22	-0.364	0.602	0.433	60.158
23	-0.333	0.641	0.464	64.095
24	-0.303	0.679	0.498	67.887
25	-0.273	0.715	0.534	71.502
26	-0.242	0.749	0.572	74.910
27	-0.212	0.781	0.614	78.089
28	-0.182	0.810	0.658	81.024
29	-0.152	0.837	0.705	83.703
30	-0.121	0.861	0.756	86.123
31	-0.091	0.883	0.811	88.286
32	-0.061	0.902	0.870	90.199
33	-0.030	0.919	0.933	91.872
34	0.000	0.933	1.000	93.320

35	0.030	0.946	1.072	94.560
36	0.061	0.956	1.150	95.611
37	0.091	0.965	1.233	96.491
38	0.121	0.972	1.322	97.221
39	0.152	0.978	1.417	97.820
40	0.182	0.983	1.520	98.306
41	0.212	0.987	1.630	98.696
42	0.242	0.990	1.748	99.006
43	0.273	0.992	1.874	99.249
44	0.303	0.994	2.009	99.439
45	0.333	0.996	2.154	99.584
46	0.364	0.997	2.310	99.695
47	0.394	0.998	2.477	99.779
48	0.424	0.998	2.656	99.841
49	0.455	0.999	2.848	99.887
50	0.485	0.999	3.054	99.920
51	0.515	0.999	3.275	99.944
52	0.545	1.000	3.511	99.962
53	0.576	1.000	3.765	99.974
54	0.606	1.000	4.037	99.982
55	0.636	1.000	4.329	99.988
56	0.667	1.000	4.642	99.992
57	0.697	1.000	4.977	99.995
58	0.727	1.000	5.337	99.997
59	0.758	1.000	5.722	99.998
60	0.788	1.000	6.136	99.999
61	0.818	1.000	6.579	99.999
62	0.848	1.000	7.055	99.999
63	0.879	1.000	7.565	100.000
64	0.909	1.000	8.111	100.000
65	0.939	1.000	8.697	100.000
66	0.970	1.000	9.326	100.000
67	1.000	1.000	10.000	100.000
68	1.030	1.000	10.723	100.000
69	1.061	1.000	11.498	100.000
70	1.091	1.000	12.328	100.000
71	1.121	1.000	13.219	100.000
72	1.152	1.000	14.175	100.000
73	1.182	1.000	15.199	100.000
74	1.212	1.000	16.298	100.000
75	1.242	1.000	17.475	100.000
76	1.273	1.000	18.738	100.000
77	1.303	1.000	20.092	100.000
78	1.333	1.000	21.544	100.000
79	1.364	1.000	23.101	100.000
80	1.394	1.000	24.771	100.000

81	1.424	1.000	26.561	100.000
82	1.455	1.000	28.480	100.000
83	1.485	1.000	30.539	100.000
84	1.515	1.000	32.745	100.000
85	1.545	1.000	35.112	100.000
86	1.576	1.000	37.649	100.000
87	1.606	1.000	40.370	100.000
88	1.636	1.000	43.288	100.000
89	1.667	1.000	46.416	100.000
90	1.697	1.000	49.770	100.000
91	1.727	1.000	53.367	100.000
92	1.758	1.000	57.224	100.000
93	1.788	1.000	61.359	100.000
94	1.818	1.000	65.793	100.000
95	1.848	1.000	70.548	100.000
96	1.879	1.000	75.646	100.000
97	1.909	1.000	81.113	100.000
98	1.939	1.000	86.975	100.000
99	1.970	1.000	93.260	100.000
100	2.000	1.000	100.000	100.000

References:

1. Klaine SJ, Alvarez PJJ, Batley GE, Fernandes TF, Handy RD, Lyon DY, Mahendra S, McLaughlin MJ, Lead JR. 2008. Nanomaterials in the environment: behavior, fate, bioavailability, and effects. *Environ. Toxicol. Chem.* 27:1825–1851.
2. Chen X, Mao SS. 2007. Titanium Dioxide Nanomaterials: Synthesis, Properties, Modifications, and Applications. *Chem. Rev.* 107:2891–2959.
3. Guo M-Z, Maury-Ramirez A, Poon CS. 2016. Self-cleaning ability of titanium dioxide clear paint coated architectural mortar and its potential in field application. *Journal of Cleaner Production*. 112:3583–3588.
4. Johnson AC, Bowes MJ, Crossley A, Jarvie HP, Jurkschat K, Jürgens MD, Lawlor AJ, Park B, Rowland P, Spurgeon D, Svendsen C, Thompson IP, Barnes RJ, Williams RJ, Xu N. 2011. An assessment of the fate, behavior and environmental risk associated with sunscreen TiO_2 nanoparticles in UK field scenarios. *Science of the Total Environment, The*. 409:2503–2510.
5. Folli A, Pade C, Hansen TB, De Marco T, Macphee DE. 2012. TiO_2 photocatalysis in cementitious systems: Insights into self-cleaning and depollution chemistry. *Cement and Concrete Research*. 42:539–548.
6. Graziani L, Quagliarini E, Osimani A, Aquilanti L, Clementi F, Yéprémian C, Lariccia V, Amoroso S, D'Orazio M. 2013. Evaluation of inhibitory effect of TiO_2 nanocoatings against microalgal growth on clay brick facades under weak UV exposure conditions. *Building and Environment*. 64:38–45.
7. Huang X, Leal M, Li Q. 2008. Degradation of natural organic matter by TiO_2 photocatalytic oxidation and its effect on fouling of low-pressure membranes. *Water Research*. 42:1142–1150.
8. Kwon S, Fan M, Cooper AT, Yang H. 2008. Photocatalytic Applications of Micro- and Nano-TiO 2in Environmental Engineering. *Critical Reviews in Environmental Science and Technology*. 38:197–226.
9. Boonen E, Beeldens A. 2014. Recent Photocatalytic Applications for Air Purification in Belgium. *Coatings*. 4:553–573.
10. Fujishima A, Zhang X. 2006. Titanium dioxide photocatalysis: present situation and future approaches. *Comptes Rendus Chimie*. 9:750–760.
11. Chen X. 2009. Titanium Dioxide Nanomaterials and Their Energy Applications. *Chinese Journal of Catalysis*. 30:839–851.
12. Linsebigler AL, Lu G, Yates JT. 1995. Photocatalysis on TiO_2 Surfaces: Principles, Mechanisms, and Selected Results. *Chem. Rev.* 95:735–758.
13. Fujishima A. 2008. TiO_2 photocatalysis and related surface phenomena. *Surface Science Reports*. 63:515–582.
14. Amiano I, Olabarrieta J, Vitorica J, Zorita S. 2012. Acute toxicity of nanosized TiO_2 to Daphnia magnaunder UVA irradiation. *Environmental Toxicology and Chemistry*. 31:2564–2566.

15. Mansfield CM, Alloy MM, Hamilton J, Verbeck GF, Newton K, Klaine SJ, Roberts AP. 2015. Photo-induced toxicity of titanium dioxide nanoparticles to Daphnia magna under natural sunlight. *Chemosphere*. 120:206–210.
16. Li Z, Cong S, Xu Y. 2014. Brookite vs Anatase TiO_2 in the Photocatalytic Activity for Organic Degradation in Water. *ACS Catal.* 4:3273–3280.
17. Ma H, Brennan A, Diamond SA. 2012. Phototoxicity of TiO_2 nanoparticles under solar radiation to two aquatic species: Daphnia magna and Japanese medaka. *Environmental Toxicology and Chemistry*. 31:1621–1629.
18. Schneider J, Matsuoka M, Takeuchi M, Zhang J, Horiuchi Y, Anpo M, Bahnemann DW. 2014. Understanding TiO2 Photocatalysis: Mechanisms and Materials. *Chem. Rev.* 114:9919–9986.
19. Hirakawa T, Nosaka Y. 2002. Properties of $O_2^{\bullet-}$ and $OH^{\bullet}$ Formed in TiO_2 Aqueous Suspensions by Photocatalytic Reaction and the Influence of H_2O_2 and Some Ions. *Langmuir*. 18:3247–3254.
20. Newton GL, Milligan JR. 2006. Fluorescence detection of hydroxyl radicals. *Radiation Physics and Chemistry*. 75:473–478.
21. Nosaka Y, Komori S, Yawata K, Hirakawa T, Nosaka AY. 2003. Photocatalytic $OH^{\bullet}$ radical formation in TiO_2 aqueous suspension studied by several detection methods. *Phys. Chem. Chem. Phys.* 5:4731–4735.
22. Daimon T, Hirakawa T, Kitazawa M, Suetake J, Nosaka Y. 2008. Formation of singlet molecular oxygen associated with the formation of superoxide radicals in aqueous suspensions of TiO2 photocatalysts. *Applied Catalysis A: General*. 340:169–175.
23. Konaka R, Kasahara E, Dunlap WC, Yamamoto Y, Chien KC, Inoue M. 1999. Irradiation of titanium dioxide generates both singlet oxygen and superoxide anion. *Free Radic. Biol. Med.* 27:294–300.
24. Leytner S, Hupp JT. 2000. Evaluation of the energetics of electron trap states at the nanocrystalline titanium dioxide/aqueous solution interface via time-resolved photoacoustic spectroscopy. *Chemical Physics Letters*. 330:231–236.
25. Knorr FJ, Mercado CC, McHale JL. 2008. Trap-State Distributions and Carrier Transport in Pure and Mixed-Phase TiO 2: Influence of Contacting Solvent and Interphasial Electron Transfer. *J. Phys. Chem. C*. 112:12786–12794.
26. Forman HJ, Augusto O, Brigelius-Flohe R, Dennery PA, Kalyanaraman B, Ischiropoulos H, Mann GE, Radi R, Roberts LJ, Vina J, Davies KJA. 2015. Even free radicals should follow some rules_ A Guide to free radical research terminology and methodology. *Free Radic. Biol. Med.* 78:233–235.
27. Bruker Biospin. 2008. *What is EPR?*:1–2.
28. Junk MJN. 2012. Electron Paramagnetic Resonance Theory. *Assessing the Functional Structure of Molecular Transporters by EPR Spectroscopy*. Springer Berlin Heidelberg, Berlin, Heidelberg, pp 7–52.
29. Li M, Yin J-J, Wamer WG, Lo YM. 2014. Mechanistic characterization of titanium dioxide nanoparticle-induced toxicity using electron spin resonance. *Journal of Food and Drug Analysis*. 22:76–85.

30. Brezova V, Dvoranova D, Stasko A. 2007. Characterization of titanium dioxide photoactivity following the formation of radicals by EPR spectroscopy. *Research on Chemical Intermediates*. 33:251–268.
31. Schwarz PF, Turro NJ, Bossmann SH, Braun AM, Wahab AA, Durr H. 1997. A New Method To Determine the Generation of Hydroxyl Radicals in Illuminated TiO_2 Suspensions. *The Journal of Physical Chemistry*. 101:7127–7134.
32. Shibata H, Ogura Y, Sawa Y, Kono Y. 1998. Hydroxyl Radical Generation Depending on O2or H2O by a Photocatalyzed Reaction in an Aqueous Suspension of Titanium Dioxide. *Bioscience, Biotechnology, and Biochemistry*. 62:2306–2311.
33. Saure M, Hofkens J, Enderlein J. 2011. Handbook of Fluorescence Spectroscopy and Imaging. *Basic Principles of Fluorescence Spectroscopy*. pp 1–30.
34. Skoog D, Holler FJ, Crouch SR. 2007. *Principles of Instrumental Analysis*. Thomson Brookes/Cole, Belmont :399–425.
35. Ma H, Brennan A, Diamond SA. 2012. Photocatalytic reactive oxygen species production and phototoxicity of titanium dioxide nanoparticles are dependent on the solar ultraviolet radiation spectrum. *Environmental Toxicology and Chemistry*. 31:2099–2107.
36. Cohn CA, Simon SR, Schoonen MA. 2008. Comparison of fluorescence-based techniques for the quantification of particle-induced hydroxyl radicals. *Part Fibre Toxicol*. 5:2–9.
37. Ishibashi K-I, Fujishima A, Watanabe T, Hashimoto K. 2000. Detection of active oxidative species in TiO2 photocatalysis using the fluorescence technique. *Electrochemistry Communications*. 2:207–210.
38. Gomes SIL, Caputo G, Pinna N, Scott-Fordsmand JJ, Amorim MJB. 2015. Effect of 10 different TiO_2 and ZrO_2 (nano)materials on the soil invertebrate Enchytraeus crypticus. *Environmental Toxicology and Chemistry*. 34:2409–2416.
39. Turchi CS, Ollis DF. 1990. Photocatalytic degradation of organic water contaminants: Mechanisms involving hydroxyl radical attack. *Journal of Catalysis*. 122:178–192.
40. McCullagh C, Robertson JMC, Bahnemann DW, Robertson PKJ. 2007. The application of TiO_2 photocatalysis for disinfection of water contaminated with pathogenic micro-organisms: a review. *Research on Chemical Intermediates*. 33:359–375.
41. Robichaud CO, Uyar AE, Darby MR, Zucker LG, Wiesner MR. 2009. Estimates of Upper Bounds and Trends in Nano- TiO_2 Production As a Basis for Exposure Assessment. *Environ. Sci. Technol.* 43:4227–4233.
42. Keller AA, McFerran S, Lazareva A, Suh S. 2013. Global life cycle releases of engineered nanomaterials. *J Nanopart Res*. 15:S230–17.
43. Lazareva A, Keller AA. 2014. Estimating Potential Life Cycle Releases of Engineered Nanomaterials from Wastewater Treatment Plants. *ACS Sustainable Chem. Eng.* 2:1656–1665.

44. Sun TY, Gottschalk F, Hungerbühler K, Nowack B. 2014. Comprehensive probabilistic modelling of environmental emissions of engineered nanomaterials. *Environmental Pollution*. 185:69–76.
45. Gottschalk F, Sonderer T, Scholz RW, Nowack B. 2009. Modeled Environmental Concentrations of Engineered Nanomaterials (TiO_2, ZnO, Ag, CNT, Fullerenes) for Different Regions. *Environ. Sci. Technol.* 43:9216–9222.
46. Keller AA, Lazareva A. 2014. Predicted Releases of Engineered Nanomaterials: From Global to Regional to Local. *Environ. Sci. Technol. Lett.* 1:65–70.
47. Westerhoff P, Song G, Hristovski K, Kiser MA. 2011. Occurrence and removal of titanium at full scale wastewater treatment plants: implications for TiO_2 nanomaterials. *J. Environ. Monit.* 13:1195–10.
48. Keller AA, Wang H, Zhou D, Lenihan HS, Cherr G, Cardinale BJ, Miller R, Ji Z. 2010. Stability and Aggregation of Metal Oxide Nanoparticles in Natural Aqueous Matrices. *Environ. Sci. Technol.* 44:1962–1967.
49. Sillanpää M, Paunu T-M, Sainio P. 2011. Aggregation and deposition of engineered TiO_2 nanoparticles in natural fresh and brackish waters. *J. Phys.: Conf. Ser.* 304:012018–9.
50. Loosli F, Le Coustumer P, Stoll S. 2013. TiO_2 nanoparticles aggregation and disaggregation in presence of alginate and Suwannee River humic acids. pH and concentration effects on nanoparticle stability. *Water Research*. 47:6052–6063.
51. Swietlik J, Sikorska E. Characterization of natural organic matter fractions by high pressure size-exclusion chromatography, specific UV absorbance and total luminescence. *Polish Journal of Environmental Studies*. 15:145–153.
52. Filella M. 2010. Quantifying 'humics' in freshwaters: purpose and methods. *Chemistry and Ecology*. 26:177–186.
53. Sillanpää M, Paunu T-M, Sainio P. 2011. Aggregation and deposition of engineered TiO_2 nanoparticles in natural fresh and brackish waters. *J. Phys.: Conf. Ser.* 304:012018–9.
54. Hund-Rinke K, Simon M. 2006. Ecotoxic Effect of Photocatalytic Active Nanoparticles (TiO_2) on Algae and Daphnids (8 pp). *Environ Sci Pollut Res*. 13:225–232.
55. Wormington AM, Coral J, Alloy MM, Delmarè CL, Mansfield CM, Klaine SJ, Bisesi JH, Roberts AP. 2017. Effect of natural organic matter on the photo-induced toxicity of titanium dioxide nanoparticles. *Environmental Toxicology and Chemistry*. 36:1661–1666.
56. Xiong S, George S, Ji Z, Lin S, Yu H, Damoiseaux R, France B, Ng KW, Loo SCJ. 2012. Size of TiO_2 nanoparticles influences their phototoxicity: an in vitro investigation. *Arch Toxicol*. 87:99–109.
57. Wyrwoll AJ, Lautenschläger P, Bach A, Hellack B, Dybowska A, Kuhlbusch TAJ, Hollert H, Schäffer A, Maes HM. 2016. Size matters – The phototoxicity of TiO2 nanomaterials. *Environmental Pollution*. 208:859–867.
58. Petersen EJ, Reipa V, Watson SS, Stanley DL, Rabb SA, Nelson BC. 2014. DNA Damaging Potential of Photoactivated P25 Titanium Dioxide Nanoparticles. *Chem. Res. Toxicol.* 27:1877–1884.

59. Wamer WG, Yin JJ, Wei RR. 1997. Oxidative Damage to Nucleic Acids Photosensitized by Titanium Dioxide. *Free Radic. Biol. Med.* 23:851–858.
60. Johnston HJ, Hutchison GR, Christensen FM, Peters S, Hankin S, Stone V. 2009. Identification of the mechanisms that drive the toxicity of TiO_2 particulates: the contribution of physicochemical characteristics. *Part Fibre Toxicol*. 6:33–27.
61. Sharma VK. 2009. Aggregation and toxicity of titanium dioxide nanoparticles in aquatic environment—A Review. *Journal of Environmental Science and Health, Part A*. 44:1485–1495.
62. Li S, Erickson RJ, Wallis LK, Diamond SA, Hoff DJ. 2015. Modeling TiO_2 nanoparticle phototoxicity: The importance of chemical concentration, ultraviolet radiation intensity, and time. *Environmental Pollution*. 205:327–332.
63. Sanders K, Degn LL, Mundy WR, Zucker RM, Dreher K, Zhao B, Roberts JE, Boyes WK. 2012. In Vitro Phototoxicity and Hazard Identification of Nano-scale Titanium Dioxide. *Toxicology and Applied Pharmacology*. 258:226–236.
64. Kim KT, Klaine SJ, Cho J, Kim S-H, Kim SD. 2010. Oxidative stress responses of Daphnia magna exposed to TiO_2 nanoparticles according to size fraction. *Science of the Total Environment, The*. 408:2268–2272.
65. Jassby D, Farner Budarz J, Wiesner M. 2012. Impact of Aggregate Size and Structure on the Photocatalytic Properties of TiO_2 and ZnO Nanoparticles. *Environ. Sci. Technol.* 46:6934–6941.
66. Clemente Z, Castro VLSS, Moura MAM, Jonsson CM, Fraceto LF. 2014. Toxicity assessment of TiO_2 nanoparticles in zebrafish embryos under different exposure conditions. *Aquatic Toxicology*. 147:129–139.
67. Fu PP, Xia Q, Hwang H-M, Ray PC, Yu H. 2014. Mechanisms of nanotoxicity: Generation of reactive oxygen species. *Journal of Food and Drug Analysis*. 22:64–75.
68. Ma H, Wallis LK, Diamond S, Li S, Canas-Carrell J, Parra A. 2014. Impact of solar UV radiation on toxicity of ZnO nanoparticles through photocatalytic reactive oxygen species (ROS) generation and photo- induced dissolution. *Environmental Pollution*. 193:165–172.
69. Lin D, Ji J, Long Z, Yang K, Wu F. 2012. The influence of dissolved and surface-bound humic acid on the toxicity of TiO_2 nanoparticles to Chlorella sp. *Water Research*. 46:4477–4487.
70. Konstantinou IK, Albanis TA. 2004. TiO2-assisted photocatalytic degradation of azo dyes in aqueous solution: kinetic and mechanistic investigations. *'Applied Catalysis B, Environmental'*. 49:1–14.
71. Gupta SM, Tripathi M. 2011. A review of TiO2 nanoparticles. *Chin. Sci. Bull.* 56:1639–1657.
72. Turchi CS, Ollis DF. 1990. Photocatalytic Degradation of Organic-Water Contaminants - Mechanisms Involving Hydroxyl Radical Attack. *Journal of Catalysis*. 122:178–192.
73. Nosaka Y, Komori S, Yawata K, Hirakawa T, Nosaka AY. 2003. Photocatalytic $^{\cdot}OH$ radical formation in TiO_2 aqueous suspension studied by several detection methods. *Phys. Chem. Chem. Phys.* 5:4731–4735.

74. Fujishima A, Zhang X, Tryk DA. 2008. TiO_2 photocatalysis and related surface phenomena. *Surface Science Reports*. 63:515–582.
75. Uchino T, Tokunaga H, Ando M, Utsumi H. 2002. Quantitative determination of OH radical generation and its cytotoxicity induced by TiO_2-UVA treatment. *Toxicol In Vitro*. 16:629–635.
76. Brezova V, Dvoranova D, Stasko A. 2007. Characterization of titanium dioxide photoactivity following the formation of radicals by EPR spectroscopy. *Research on Chemical Intermediates*. 33:251–268.
77. Dvoranová D, Barbieriková Z, Brezová V. 2014. Radical Intermediates in Photoinduced Reactions on TiO_2 (An EPR Spin Trapping Study). *Molecules*. 19:17279–17304.
78. Haynes VN, Ward JE, Russell BJ, Agrios AG. 2017. Photocatalytic effects of titanium dioxide nanoparticles on aquatic organisms − current knowledge and suggestions for future research. *Aquatic Toxicology*.:1–38. doi:10.1016/j.aquatox.2017.02.012.
79. Kim J, Lee S, Kim C-M, Seo J, Park Y, Kwon D, Lee S-H, Yoon T-H, Choi K. 2014. Non-monotonic concentration–response relationship of TiO_2 nanoparticles in freshwater cladocerans under environmentally relevant UV-A light. *Ecotoxicology and Environmental Safety*. 101:240–247.
80. Jovanović B. 2015. Review of titanium dioxide nanoparticle phototoxicity: Developing a phototoxicity ratio to correct the endpoint values of toxicity tests. *Environmental Toxicology and Chemistry*. 34:1070–1077.
81. He X, Sanders S, Aker WG, Lin Y, Douglas J, Hwang H-M. 2015. Assessing the effects of surface-bound humic acid on the phototoxicity of anatase and rutile TiO2 nanoparticles in vitro. *JES*. 42:50–60.
82. Al-Abed SR, Virkutyte J, Ortenzio JNR, McCarrick RM, Degn LL, Zucker R, Coates NH, Childs K, Ma H, Diamond S, Dreher K, Boyes WK. 2016. Environmental aging alters $Al(OH)_3$ coating of TiO_2 nanoparticles enhancing their photocatalytic and phototoxic activities. *Environmental Science: Nano*. 3:593–601.
83. Bunsen R, Roscoe H. 1859. Photochemische Untersuchungen. *Annalen der Physik und Chemie*. 184:193–273.
84. Oris JT, Giesy JP. 1986. Photoinduced toxicity of anthracene to juvenile bluegill sunfish (Lepomis Macrochirus Rafinesque): Photoperiod effects and predictive hazard evaluation. *Environmental Toxicology and Chemistry*. 5:761–768.
85. Ankley GT, Erickson RJ, Phipps GL, Mattson VR, Kosian PA, Sheedy BR, Cox JS. 1995. Effects of light intensity on the phototoxicity of fluoranthene to a benthic macroinvertebrate. *Environ. Sci. Technol.* 29:2828–2833.
86. Diem S, Rohr von MR, Hering JG, Kohler H-PE, Schirmer M, Gunten von U. 2013. NOM degradation during river infiltration: Effects of the climate variables temperature and discharge. *Water Research*. 47:6585–6595.
87. Drosos M, Ren M, Frimmel FH. 2015. The effect of NOM to TiO_2: interactions and photocatalytic behavior. *'Applied Catalysis B, Environmental'*. 165:328–334.

88. Aiken GR, Hsu-Kim H, Ryan JN. 2011. Influence of Dissolved Organic Matter on the Environmental Fate of Metals, Nanoparticles, and Colloids. *Environ. Sci. Technol.* 45:3196–3201.
89. USEPA. 2007. Whole Effluent Toxicity Training Video Series, Freshwater Series.:1–63.
90. Ou B, Hampsch-Woodill M, Flanagan J, Deemer EK, Prior RL, Huang D. 2002. Novel Fluorometric Assay for Hydroxyl Radical Prevention Capacity Using Fluorescein as the Probe. *J. Agric. Food Chem.* 50:2772–2777.
91. US EPA. 1991. *Compendium of ERT Toxicity Testing Procedures*. U.S. Environmental Protection Agency; Office of Solid Waste and Emergency Response, Washington, DC :17–20.
92. Finney DJ. 1952. Probit Analysis (2nd Ed). *Journal of the Institute of Actuaries*. 78:388–390.
93. Liu S, Lim M, Fabris R, Chow C, Drikas M, Amal R. 2010. Comparison of photocatalytic degradation of natural organic matter in two Australian surface waters using multiple analytical techniques. *Organic Geochemistry*. 41:124–129.
94. Dvoranová D, Barbieriková Z, Brezová V. 2014. Radical Intermediates in Photoinduced Reactions on TiO_2 (An EPR Spin Trapping Study). *Molecules*. 19:17279–17304.
95. Miller RJ, Bennett S, Keller AA, Pease S, Lenihan HS. 2012. TiO_2 Nanoparticles Are Phototoxic to Marine Phytoplankton. In Gilbert, JA, ed., *PLoS ONE*. 7:e30321–8.
96. Zhang J, Nosaka Y. 2013. Quantitative Detection of OH Radicals for Investigating the Reaction Mechanism of Various Visible-Light TiO_2 Photocatalysts in Aqueous Suspension. *J. Phys. Chem. C*. 117:1383–1391.
97. Ishibashi K, Fujishima A, Watanabe T, Hashimoto K. 2000. Detection of active oxidative species in TiO_2 photocatalysis using the fluorescence technique. *Electrochemistry Communications*. 2:207–210.
98. Rao MV, Rajeshwar K, Verneker VRP, DuBow J. 1980. Photosynthetic production of hydrogen and hydrogen peroxide on semiconducting oxide grains in aqueous solutions. *The Journal of Physical Chemistry*. 84:1987–1991.
99. Harbour JR, Tromp J, Hair ML. 1985. Photogeneration of hydrogen peroxide in aqueous TiO_2 dispersions. *Canadian Journal of Chemistry*. 63:204–208.
100. Cadet J, Davies KJA, Medeiros MH, Di Mascio P, Wagner JR. 2017. Formation and repair of oxidatively generated damage in cellular DNA. *Free Radic. Biol. Med.* 107:13–34.
101. Evans MD, Dizdaroglu M, Cooke MS. 2004. Oxidative DNA damage and disease: induction, repair and significance. *Mutation Research/Reviews in Mutation Research*. 567:1–61.
102. Yin J-J, Liu J, Ehrenshaft M, Roberts JE, Fu PP, Mason RP, Zhao B. 2012. Phototoxicity of nano titanium dioxides in HaCaT keratinocytes—Generation of reactive oxygen species and cell damage. *Toxicology and Applied Pharmacology*. 263:81–88.

103. Uchino T, Tokunaga H, Ando M, Utsumi H. 2002. Quantitative determination of OH radical generation and its cytotoxicity induced by TiO_2-UVA treatment. *Toxicol In Vitro*. 16:629–635.
104. Williamson CE. 1996. Effects of UV radiation on freshwater ecosystems. *International Journal of Environmental Studies*. 51:245–256.
105. Uyguner CS, Bekbolet M. 2005. Evaluation of humic acid photocatalytic degradation by UV–vis and fluorescence spectroscopy. *Catalysis Today*. 101:267–274.
106. Yan ND, Keller W, Scully NM, Lean DRS, Dillon PJ. 1996. Increased UV-B penetration in a lake owing to drought-induced acidification. *Nature*. 381:141–143.
107. Dimitroula H, Daskalaki VM, Frontistis Z, Kondarides DI, Panagiotopoulou P, Xekoukoulotakis NP, Mantzavinos D. 2012. Solar photocatalysis for the abatement of emerging micro-contaminants in wastewater: Synthesis, characterization and testing of various TiO_2 samples. *'Applied Catalysis B, Environmental'*. 117-118:283–291.
108. Gaya UI, Abdullah AH. 2008. Heterogeneous photocatalytic degradation of organic contaminants over titanium dioxide: A review of fundamentals, progress and problems. *Journal of Photochemistry and Photobiology C: Photochemistry Reviews*. 9:1–12.
109. Shibata H, Ogura Y, Sawa Y. 1998. Hydroxyl radical generation depending on O2 or H2O by a photocatalyzed reaction in an aqueous suspension of titanium dioxide. *Bioscience*.
110. Nagaveni K, Sivalingam G, Hegde MS, Madras G. 2004. Photocatalytic Degradation of Organic Compounds over Combustion-Synthesized Nano-TiO 2. *Environ. Sci. Technol.* 38:1600–1604.
111. Brezova V, Stasko A, Biskupic S, Blazkova A, Havlinova B. 1994. Kinetics of Hydroxyl Radical Spin Trapping in Photoactivated Homogeneous (H2O2) and Heterogeneous (TiO_2, O_2) Aqueous Systems. *The Journal of Physical Chemistry*. 98:8977–8984.
112. Drescher M, Jeschke G. 2012. EPR Spectroscopy. *Topics in Current Chemistry*.:1–247.
113. Sun L, Bolton JR. 1996. Determination of the Quantum Yield for the Photochemical Generation of Hydroxyl Radicals in TiO_2 Suspensions. *The Journal of Physical Chemistry*. 100:4127–4134.
114. Hirakawa T, Nosaka Y. 2002. Properties of $O_2^{\bullet-}$ and $OH^{\bullet}$ Formed in TiO_2 Aqueous Suspensions by Photocatalytic Reaction and the Influence of H_2O_2 and Some Ions. *Langmuir*. 18:3247–3254.
115. Eremia S, Chevalierlucia D, Radu G, Marty J. 2008. Optimization of hydroxyl radical formation using TiO_2 as photocatalyst by response surface methodology. *Talanta*. 77:858–862.
116. Tiede K, Hassellöv M, Breitbarth E, Chaudhry Q, Boxall ABA. 2009. Considerations for environmental fate and ecotoxicity testing to support

environmental risk assessments for engineered nanoparticles. *Journal of Chromatography A*. 1216:503–509.
117. Bondarenko O, Juganson K, Ivask A, Kasemets K, Mortimer M, Kahru A. 2013. Toxicity of Ag, CuO and ZnO nanoparticles to selected environmentally relevant test organisms and mammalian cells in vitro: a critical review. *Arch Toxicol*. 87:1181–1200.
118. Burnham KP, Anderson DR. 2016. Multimodel Inference. *Sociological Methods & Research*. 33:261–304.
119. Mazerolle M. 2004. *Making sense out of Akaike's Information Criterion (AIC): its use and interpretation in model selection and inference from ecological data In: Mazzarolle, M.J. (Ed.), Mouvements et reproduction des amphibiens en tourbières perturbées. PhD Thesis*. Available from http://www.theses.ulaval.ca/2004/21842/apa.html#d0e5831.
120. Symonds MRE, Moussalli A. 2011. A brief guide to model selection, multimodel inference and model averaging in behavioural ecology using Akaike's information criterion. *Behav Ecol Sociobiol*. 65:13–21.
121. Burnham KP, Anderson DR. 2016. Multimodel Inference. *Sociological Methods & Research*. 33:261–304.
122. Gomes A, Fernandes E, Lima JLFC. 2005. Fluorescence probes used for detection of reactive oxygen species. *Journal of Biochemical and Biophysical Methods*. 65:45–80.
123. Daneshvar N, Rabbani M, Modirshahla N, Behnajady MA. 2004. Kinetic modeling of photocatalytic degradation of Acid Red 27 in UV/ TiO_2 process. *Journal of Photochemistry and Photobiology A: Chemistry*. 168:39–45.
124. Ba-Abbad MM, Kadhum A, Mohamad AB, Takriff MS, Sopian K. 2012. Synthesis and catalytic activity of TiO_2 nanoparticles for photochemical oxidation of concentrated chlorophenols under direct solar radiation. *International Journal of Electochemcial Science*.:4872–4888.
125. Diamond SA, Trenham PC, Adams MJ, Hossack BR, Knapp RA, Stark SL, Bradford D, Corn PS, Czarnowski K, Brooks PD, Fagre D, Breen B, Detenbeck NE, Tonnessen K. 2005. Estimated Ultraviolet Radiation Doses in Wetlands in Six National Parks. *Ecosystems*. 8:462–477.
126. Haynes VN, Ward JE, Russell BJ, Agrios AG. 2017. Photocatalytic effects of titanium dioxide nanoparticles on aquatic organisms − current knowledge and suggestions for future research. *Aquatic Toxicology*.:1–38.
127. Eremia S, Chevalierlucia D, Radu G, Marty J. 2008. Optimization of hydroxyl radical formation using TiO_2 as photocatalyst by response surface methodology. *Talanta*. 77:858–862.
128. Rana S, Kalaichelvan PT. 2013. Ecotoxicity of Nanoparticles. *ISRN Toxicology*. 2013:1–11.
129. Menard A, Drobne D, Jemec A. 2011. Ecotoxicity of nanosized TiO_2. Review of in vivo data. *Environmental Pollution*. 159:677–684.
130. Kammer von der F, Ottofuelling S, Hofmann T. 2010. Assessment of the physico-chemical behavior of titanium dioxide nanoparticles in aquatic

environments using multi-dimensional parameter testing. *Environmental Pollution*. 158:3472–3481.
131. He X, Sanders S, Aker WG, Lin Y, Douglas J, Hwang H-M. 2016. Assessing the effects of surface-bound humic acid on the phototoxicity of anatase and rutile TiO_2 nanoparticles in vitro. *JES*. 42:50–60.
132. Uyguner CS, Bekbolet M. 2010. TiO_2-assisted photocatalytic degradation of humic acids: effect of copper ions. *Water Science & Technology*. 61:2581–12.
133. Chen W, Qian C, Liu X-Y, Yu H-Q. 2014. Two-Dimensional Correlation Spectroscopic Analysis on the Interaction between Humic Acids and TiO_2 Nanoparticles. *Environ. Sci. Technol.* 48:11119–11126.
134. Yang K, Lin D, Xing B. 2009. Interactions of Humic Acid with Nanosized Inorganic Oxides. *Langmuir*. 25:3571–3576.
135. Symonds MRE, Moussalli A. 2010. A brief guide to model selection, multimodel inference and model averaging in behavioral ecology using Akaike's information criterion. *Behav Ecol Sociobiol*. 65:13–21.
136. Mazerolle MJ. 2007. APPENDIX 1: Making sense out of Akaike's Information Criterion (AIC): its use and interpretation in model selection and inference from ecological data.:1–13.
137. Carlotti ME, Ugazio E, Sapino S, Vione D, Fubini B. 2011. Lipid Peroxidation Processes Photoinduced by Titanium Dioxide in Emulsion Systems, Representative of Sunscreen Formulations. *Journal of Dispersion Science and Technology*. 32:913–922.
138. Luttrell T, Halpegamage S, Tao J, Kramer A, Sutter E, Batzill M. 2014. Why is anatase a better photocatalyst than rutile? - Model studies on epitaxial TiO_2 films. *Sci. Rep.* 4:515–8.
139. Chowdhury I, Cwiertny DM, Walker SL. 2012. Combined Factors Influencing the Aggregation and Deposition of nano- TiO_2 in the Presence of Humic Acid and Bacteria. *Environ. Sci. Technol.* 46:6968–6976.
140. Xiang C, Yang F, Li M, Jaridi M, Wu N. 2012. Experimental and statistical analysis of surface charge, aggregation and adsorption behaviors of surface-functionalized titanium dioxide nanoparticles in aquatic system. *J Nanopart Res*. 15:7621–12.
141. Yigit Z, Inan H. 2009. A Study of the Photocatalytic Oxidation of Humic Acid on Anatase and Mixed-phase Anatase–Rutile TiO_2 Nanoparticles. *Water Air Soil Pollut: Focus*. 9:237–243.
142. Weir A, Westerhoff P, Fabricius L, Hristovski K, Goetz von N. 2012. Titanium Dioxide Nanoparticles in Food and Personal Care Products. *Environ. Sci. Technol.* 46:2242–2250.
143. Pietrzak A, Adamus J, Langier B. 2016. Application of Titanium Dioxide in Cement and Concrete Technology. *KEM*. 687:243–249.
144. Guo M-Z, Maury-Ramirez A, Poon CS. 2015. Photocatalytic activities of titanium dioxide incorporated architectural mortars: Effects of weathering and activation light. *Building and Environment*. 94:395–402.

145. Botta C, Labille J, Auffan M, Borschneck D, Miche H, Cabié M, Masion A, Rose J, Bottero J-Y. 2011. TiO_2-based nanoparticles released in water from commercialized sunscreens in a life-cycle perspective: Structures and quantities. *Environmental Pollution*. 159:1543–1550.
146. Praetorius A, Scheringer M, Hungerbühler K. 2012. Development of Environmental Fate Models for Engineered Nanoparticles—A Case Study of TiO_2 Nanoparticles in the Rhine River. *Environ. Sci. Technol.* 46:6705–6713.
147. Lin D, Tian X, Wu F, Xing B. 2010. Fate and Transport of Engineered Nanomaterials in the Environment. *Journal of Environment Quality*. 39:1896–13.
148. Al-Kattan A, Wichser A, Vonbank R, Brunner S, Ulrich A, Zuin S, Nowack B. 2013. Release of TiO_2 from paints containing pigment- TiO_2 or nano-TiO_2 by weathering. *Environ. Sci.: Processes Impacts*. 15:2186–9.
149. Gutierrez ER, Kamens RM, Tolocka M, Sexton K, Jaspers I. 2015. A comparison of three dispersion media on the physicochemical and toxicological behavior of TiO_2 and NiO nanoparticles. *Chemico-Biological Interactions*.:1–8.
150. Buxton GV, Greenstock CL, Helman WP, Ross AB. 1988. Critical Review of rate constants for reactions of hydrated electrons, hydrogen atoms and hydroxyl radicals ($OH^{\bullet}/O^{\bullet-}$ in Aqueous Solution. *Journal of Physical and Chemical Reference Data*. 17:513–886.
151. Liochev SI. 2013. Reactive oxygen species and the free radical theory of aging. *Free Radic. Biol. Med.* 60:1–4.
152. Apel K, Hirt H. 2004. Reactive Oxygen Species: Metabolism, Oxidative Stress, and Signal Transduction. *Annu. Rev. Plant Biol.* 55:373–399.
153. Winterbourn CC. 2008. Reconciling the chemistry and biology of reactive oxygen species. *Nat Chem Biol*. 4:278–286.
154. Dickinson BC, Chang CJ. 2011. Chemistry and biology of reactive oxygen species in signaling or stress responses. *Nat Chem Biol*. 7:504–511.
155. Gerrity D, Mayer B, Ryu H, Crittenden J, Abbaszadegan M. 2009. A comparison of pilot-scale photocatalysis and enhanced coagulation for disinfection byproduct mitigation. *Water Research*. 43:1597–1610.
156. Liu S, Lim M, Fabris R, Chow C, Chiang K, Drikas M, Amal R. 2008. Removal of humic acid using TiO_2 photocatalytic process – Fractionation and molecular weight characterisation studies. *Chemosphere*. 72:263–271.
157. Brunelli A, Pojana G, Callegaro S, Marcomini A. 2013. Agglomeration and sedimentation of titanium dioxide nanoparticles (n-TiO_2) in synthetic and real waters. *J Nanopart Res*. 15:2742–11.
158. Lin X, Li J, Ma S, Liu G, Yang K, Tong M, Lin D. 2014. Toxicity of TiO_2 Nanoparticles to Escherichia coli: Effects of Particle Size, Crystal Phase and Water Chemistry. In Rozhkova, EA, ed., *PLoS ONE*. 9:e110247–8.
159. Yang SP, Bar-Ilan O, Peterson RE, Heideman W, Hamers RJ, Pedersen JA. 2013. Influence of Humic Acid on Titanium Dioxide Nanoparticle Toxicity to Developing Zebrafish. *Environ. Sci. Technol.* 47:4718–4725.

160. Xiong D, Fang T, Yu L, Sima X, Zhu W. 2011. Effects of nano-scale TiO_2, ZnO and their bulk counterparts on zebrafish: Acute toxicity, oxidative stress and oxidative damage. *Science of the Total Environment, The*. 409:1444–1452.
161. Federici G, Shaw B, Handy R. 2007. Toxicity of titanium dioxide nanoparticles to rainbow trout (*Oncorhynchus mykiss*): Gill injury, oxidative stress, and other physiological effects. *Aquatic Toxicology*. 84:415–430.
162. Ma H, Diamond SA. 2013. Phototoxicity of TiO_2 nanoparticles to zebrafish (*Danio rerio*) is dependent on life stage. *Environmental Toxicology and Chemistry*. 32:2139–2143.
163. Dawidowicz P, Loose CJ. 1992. Metabolic Costs During Predator-Induced Diel Vertical Migration of Daphnia. *Limnology and Oceanography*. 37:1589–1595.
164. Dodson S. 1990. Prediciting deil vertical migration of zooplankton. *Limnology and Oceanography*. 25:1195–1200.
165. Stich H-B, Lampert W. 1981. Predator evasion as an explanation of diurnal vertical migration by zooplankton. *Nature*. 293:396–398.
166. Lee S-W, Kim S-M, Choi J. 2009. Genotoxicity and ecotoxicity assays using the freshwater crustacean Daphnia magna and the larva of the aquatic midge Chironomus riparius to screen the ecological risks of nanoparticle exposure. *Environmental Toxicology and Pharmacology*. 28:86–91.
167. Tong T, Shereef A, Wu J, Binh CTT, Kelly JJ, Gaillard J-F, Gray KA. 2013. Effects of Material Morphology on the Phototoxicity of Nano-TiO_2 to Bacteria. *Environ. Sci. Technol.* 47:12486–12495.
168. Pavasupree S, Ngamsinlapasathian S, Nakajima M, Suzuki Y, Yoshikawa S. 2006. Synthesis, characterization, photocatalytic activity and dye-sensitized solar cell performance of nanorods/nanoparticles TiO_2 with mesoporous structure. *Journal of Photochemistry and Photobiology A: Chemistry*. 184:163–169.
169. Li S, Pan X, Wallis LK, Fan Z, Chen Z, Diamond SA. 2014. Comparison of TiO_2 nanoparticle and graphene-TiO2 nanoparticle composite phototoxicity to *Daphnia magna* and *Oryzias latipes*. *Chemosphere*. 112:62–69.
170. Janus M, Kusiak E, Morawski AW. 2009. Carbon Modified TiO2 Photocatalyst with Enhanced Adsorptivity for Dyes from Water. *Catal Lett*. 131:506–511.
171. Wallis LK, Diamond SA, Ma H, Hoff DJ, Al-Abed SR, Li S. 2014. Chronic TiO_2 nanoparticle exposure to a benthic organism, *Hyalella azteca*: impact of solar UV radiation and material surface coatings on toxicity. *Science of the Total Environment*. 499:1–8.
172. Wengel M, Kothe E, Schmidt CM, Heide K, Gleixner G. 2006. Degradation of organic matter from black shales and charcoal by the wood-rotting fungus Schizophyllum commune and release of DOC and heavy metals in the aqueous phase. *Science of The Total Environment*. 367:383–393.
173. Kim KT, Edgington AJ, Klaine SJ, Cho J-W, Kim SD. 2009. Influence of Multiwalled Carbon Nanotubes Dispersed in Natural Organic Matter on Speciation and Bioavailability of Copper. *Environ. Sci. Technol.* 43:8979–8984.